Manufacturing and characterization of self-healing polymer materials intended for the electrical insulation of future power modules

Baptiste Arati

Université Fédérale
Toulouse Midi-Pyrénées

THÈSE

En vue de l'obtention du
DOCTORAT DE L'UNIVERSITÉ DE TOULOUSE

Délivré par l'Université Toulouse 3 - Paul Sabatier

Présentée et soutenue par

Baptiste ARATI

Le 21 février 2023

Mise en oeuvre et caractérisation de matériaux polymères autocicatrisants pour assurer les fonctions d'isolation électrique des futurs modules de puissance

---

Ecole doctorale : **GEETS - Génie Electrique Electronique,Télécommunications et Santé : du système au nanosystème**

Spécialité : **Génie Electrique**

Unité de recherche :
LAPLACE - Laboratoire PLAsma et Conversion d'Énergie

Thèse dirigée par
Gilbert TEYSSEDRE et Vincent BLEY

Jury

M. Rint SIJBESMA, Rapporteur
M. Cyril BUTTAY, Rapporteur
M. Pierre-Yves PICHON, Examinateur
Mme Lara PERRIN, Examinatrice
M. Gilbert TEYSSEDRE, Directeur de thèse
Mme Corinne ALONSO, Présidente

Manufacturing and characterization of self-healing polymers intended for the electrical insulation of future power modules

Abstract

Power Modules (PM) are devices that convert electrical energy for many applications, making them a crucial part of the new concerns surrounding electrification of a large part of human operations (power generation and distribution, electrical transports, home appliances etc…). Conventional power modules are electrically insulated with soft silicone gel, that surrounds the power components and their connective wire bonds. But with the growing need for higher power densities, faster switching frequencies and longer operational times, new power module architectures that can satisfy the reliability requirements are now being developed.

One of the most promising concepts for new PM packages is the PCB (Printed Circuit Board)-embedded design, where the power components are buried inside a thermoset composite substrate. However, confining the active component raises technical challenges and thermo-mechanical failure is a major reliability concern for these designs. Therefore, designing a new material answering the specifications of PCB-embedded power semiconductors while preventing the occurrence of damage is desirable for a high reliability architectures.

With the recent change of paradigm in thermosetting materials covalent adaptable networks cross the gap between thermosetting and thermoplastic and offer new properties for the dielectric material (intrinsic self-healing, tuneable thermomechanical profile, recycling…). Usually intended for mechanical applications, the development of dynamic networks is promising for repairing mechanical damages caused during thermal cycles and prevent the subsequent electrical degradation of the PCBs. The objective of this thesis is therefore to develop a new self-healing polymer, compatible with the requirements of the next generation of PM and that can answer their reliability needs.

Vitrimers have especially echoed in the scientific community as a promising self-healing solution compatible with industrial applications. By directly reacting industrial epoxy resins used in the PCB field with carboxylic acids, it is possible to create a transesterification-based vitrimer to produce self-healing PCBs. With the ability to tune properties with carboxylic acid blends and catalyst content, vitrimers are offering a flexible base to explore new self-healing power module concepts. Based on the most used epoxy resin in the PCB manufacturing industry, the main vitrimer of this study is produced from bulk polymerization of diglycidyl ether of bisphenol A (DGEBA) resin and sebacic acid, in the presence of 1-methylimidazole as catalyst.

Unlike reprocessing demonstrations shown in the literature, a critical study of the healing capabilities of the material within the application frame is proposed. By removing the use of constant external pressure for the healing process, healing conditions are closer to what can be encountered in operation. To promote high mobility without the added pressure work, shape-memory is used to assist the healing process, yielding excellent joining ability and healing efficiency, demonstrated both on mechanical and electrical indicators.

The applicability of such a material to the power field is also demonstrated. The very high dielectric strength and thermal stability of the material is shown, validating its use for high-power applications. Manufacturing of a complete self-healing vitrimeric PCB compatible with high-density interconnection processes is shown, demonstrating that these materials are valuable for the future power module packaging trends.

Finally, a study of the main conduction mechanism of vitrimers in regard to their mobility is proposed. Conduction in polymers is often based on relaxation modes in polymeric chains, allowing the diffusion of conductive species in the network. In addition of the glass transition, vitrimers also

exhibit a vitrimeric transition, driven by the trans-esterification exchange reaction in the network. In that regard, it is possible to express a link between conductivity and viscosity at high temperatures, that may be useful to design efficient vitrimers for electrical insulation applications.

Regardless of the specific materials used in this study, vitrimers are now closer to the application state than ever before. With the fast-growing understanding of those networks, many new formulations from bio-sourced to catalyst-free materials are proposed. With today's imperative to decrease the impact of industrial operations on the environment, using vitrimers may be a great initiative to produce high-reliability, long-lasting and recyclable power modules for the future.

GENERAL SUMMARY

List of figures

List of Tables

List of equations

List of abbreviations

0-9

1-MI	1-Methyl Imidazole

A

Al	Aluminium
Al_2O_3	Alumina
AlN	Aluminium Nitride
ATR	Attenuated Total Reflectance

C

CAN	Covalent Adaptable Network
CCL	Copper Clad Laminate
CHDA	CycloHexane DiAcid
CTE	Coefficient of Thermal Expansion
Cu	Copper

D

DA	Diels-Alder
DB	Dielectric Breakdown
DBC	Direct Bonded Copper
DGEBA	DiGlycidyl Ether of Bisphenol A
DMA	Dynamic Mechanical Analysis
DSC	Differential Scanning Calorimetry
DTA	Differential Thermal Analysis

E

EMC	Epoxy Molding Compound

F

FPGA	Field-Programmable Gate Array
FR4	Flame Retardant 4 (norm)
FTIR	Fourier Transformed InfraRed

G

GaN	Gallium Nitride

H

H	Hydrogen
HDI	High Density Interconnection

I

IGBT	Insulated-Gate Bipolar Transistor

P

Pb	Lead
PC	Phosphate Cement
PCB	Printed Circuit Board
PD	Partial Discharge
PDIV	Partial Discharge Initiation Voltage
PM	Power Modules

PTFE	Poly Tetra Fluoro Ethylene

R

RCC	Resin Coated Copper
RMS	Root Mean Square
ROMP	Ring-Opening Metathesis Polymerization
RT	Room Temperature

S

SA	Sebacic Acid
Si	Silicon
SiC	Silicon Carbide
Si-gel	Silicone gel
SiO_2	Silicon Dioxide (silica)
Sn	Tin
SR	Solder Resist

T

TBD	Triaza BicycloDecene
TIM	Thermal Interface Material
Tg	Glass Transition temperature
TGA	ThermoGravimetric Analysis
Tj	Junction temperature (semiconductor)
TMA	ThermoMechanical Analysis
Tv	Vitrimeric temperature

V

VFT	Vogel-Fulcher-Tammann

W

WBG	Wide Band Gap
WLF	William-Landel-Ferry

General Introduction

Power Modules (PM) are electronic devices that allow the conversion of electrical energy for a wide variety of sectors. By modulating the input electrical power waveform through the commutation of several power semiconductors acting like switches, PMs can output the appropriate power waveform required in a designated application. Typically insulated with silicone-gel, the power chips must manage high voltages and receive large amounts of current, generating heat losses leading to the aging of the system.

With the need for cleaner and more abundant energy sources being at the heart of the problematics of this century, the ever-increasing electrification of human operations (renewables, automotive, aerospace etc…) is driving research on energy harnessing and storage alongside with the need for more efficient, more compact, more reliable power modules to achieve efficient and safe power conversion for the future.

In order to increase the capabilities of nowadays power modules, new devices are being developed with architectures increasing the overall power density or using wide bang gap (WBG) components capable of operating healthily with faster switching speeds at higher voltages and temperatures. One of the most studied designs is the Printed Circuit Board (PCB) embedded module, that internalizes the chips within a composite substrate that is playing the role of mechanical support, electrical insulation and housing of the connection path in the form of copper tracks and vias. This solution also offers other optimizations, such as lowering overall parasitic inductances for more efficient switching and offering new cooling options decreasing thermomechanical stress. Another research line is to change the conventional soft silicone-gel used for encapsulation of commercial devices with harder materials that can help to increase the reliability of the current state of the art architectures.

Despite being interesting prospects, such big changes come with technical challenges that need to be tackled before consistently reaching better performances with new modules. In these cases, it is expected that the insulation material maintains a high degree of electrical insulation while also providing new thermal and mechanical improvements to the system. Relying more and more on the encapsulation material therefore means that the reliability of the device will be more and more dependent on the health status of the dielectric material.

For such a task, conventional hard insulating materials are often not quite suitable, although they often improve the thermal conduction. Indeed, using harder materials increases the risk of generating stresses, cracks and delamination during electrothermal cycling, which can decrease thermal dissipation capabilities and increase the risk of electrical failure. In this regard, providing a more reliable encapsulation solution is key to create new long-lasting devices, capable of bearing the improvements necessary to the power electronics field.

The goal of this work is therefore to develop a reliable embedding material, that can be used either as a replacement for silicone gel or to assist in the development of new architectures like the PCB-embedded ones. Ideally, the material should be able to answer the specification of the applications while also being able to recover from possible damages or prevent further degradations associated with aging. This research therefore focuses on developing a new dielectric material that can be used in the power electronics field and exhibiting self-healing properties, relevant to this applicative environment.

To date, many self-healing concepts have been uncovered and studied in the literature but only a few have been presented with applications in mind, even less so for non-structural usage. Given the

unforgiving target environment, using self-healing materials with electrical insulation function as the main objective remains challenging. With the recent discovery of new Covalent Adaptable Networks (CANs), thermosetting materials can be modified to become repairable and reprocessible with the appropriate stimuli. These modified polymeric networks can exhibit sufficient mobility to exhibit dynamic properties such as stress-relaxation and self-healing while also conserving their overall crosslink density, making them promising options for the development of new electrical insulation materials.

Overall, several benefits can be expected in terms of reliability with the mending of normally critical damages and the prevention of aggravation cascades leading to the destruction of the device. Repair cycles at key points in the life of the device become possible and prediction/triggering of those repairs could be used to manage the day-to-day endurance of the insulating organ.

As the primary objective for this thesis, the development of these new self-healing materials for the electrical insulation of future high-power devices is explored. A critical evaluation of their applicability is proposed, focusing on their intrinsic properties in regard to the specification of the domain and the recreation of relatable damages for the applicative frame. The production of several demonstrators is used to illustrate the manufacturing possibilities and to showcase the healing properties of these new systems on electrical parameters, again in configurations closest to the final application.

Secondly, this work proposes methods for the formulation, the elaboration and the manufacturing of these promising materials. As the research community is vastly growing around self-healing concepts, guidance is provided for new formulators and insulation designers interested in implementing these new materials into new electrical insulation applications.

The first chapter of this thesis presents typical and new power module packaging architectures and proposes new strategies to increase their reliability, with an emphasis on the use of new self-healing polymers.

The second chapter shows in detail the selection and formulation of precursors intended for the elaboration of self-healing polymers, focusing on the manufacturing of transesterification-based vitrimers.

The third chapter demonstrates the PCB manufacturing capabilities and is dedicated to the critical evaluation of the applicability of these new materials to the power electronics field, both in conventional and new module architectures.

Finally, the fourth chapter explores the stress-relaxation properties of formulated vitrimers and proposes an empirical relationship between the electrical conductivity and the viscosity associated with the dynamic network of these materials.

Chapter I – Power modules packaging and new strategies to increase reliability

Chapter I – Power modules packaging and new strategies to increase reliability

Introduction

Depending on their field of application, Power Modules (PM) have been manufactured and distributed under many types of packaging. However, most power modules share the same type of architecture, including a power chip (or die), soldered on a Direct Bonded Copper (DBC) substrate and connected by several wire-bonds from the top. The whole assembly is usually attached over a metallic baseplate and surrounded by a hard plastic shell before being encapsulated in silicone gel for electrical insulation and to prevent environmental pollution.

During their lifetime, power modules endure many power cycles and several integrity degradations can occur, leading to partial or most likely catastrophic failure of the device. This is especially true for high power, high temperature applications where the different phenomena leading to failure are increased. Among the most common failure sources, thermomechanical stress and dielectric aging are the most harmful events. Indeed, layering different materials with different Coefficients of Thermal Expansion (CTE) result in strong interfacial stresses that can damage solder layers and wire bonds, degrading thermal dissipation and increasing electrical currents until failure. Alternatively, working under high voltage also requires high insulating properties, that can degrade during aging and allow partial discharge formation and erosion of the dielectric, leading to dielectric breakdown and short circuits.

Failures are difficult to predict and to avoid, especially with the wide variety of designs and applications that has been developed. Therefore, several improvements have been sought for and demonstrated to reduce the occurrence of these damages and in return increase the lifetime, reliability and performances of power modules.

- Solder layers tend to be replaced by diffusion bonding or sintering, with higher adhesion between the die and its support
- Removal and replacement of bond-wires has been quite prolific and designs are blooming from planar top connection and press-packs to vias in embedded packages.
- Silicone-gel also tend to be replaced, as harder encapsulation materials appear to play an important role in the thermomechanical stabilisation of the encapsulated components.

Such new developments give rise to entirely new architectures that can endure harsher conditions and root the development of more powerful, more reliable technologies. Nowadays, Printed circuit board (PCB) embedded devices are at the heart of many new designs, with easier manufacturing processes, smaller overall volumes and better thermal and electrical performances.

With the growing importance of the dielectric materials in power module reliability, the development of smarter, high reliability dielectric materials is more and more desirable. Indeed, materials are ever more confined in a harder matrix and insulation distances have been reduced considerably. Cracking of the PCB dielectric layers occur during aging, compromising the healthy operation of the system. In that regard, developing a self-healing dielectric material, capable of closing cracks and recover electrical insulation properties might be a suitable solution to extend the life expectancy of these systems.

1. Conventional power modules and their associated failure modes

1. Power module healthy working conditions and typical architecture

a. Inside of a working power module

Power modules (PM) are complex assemblies developed for the conversion of electrical energy. As main parts of power converters, they hold a critical role in modulating electrical signals to be used in the most appropriate way for their designated applications. As examples, the input/output of high voltages from the main power-grid, the energy supply to motors for the transport sector or the matching needs for home electrical appliances, are all permitted by the use of power modules.

In order to accomplish these tasks, power modules rely on power components, also called "*power switches*", that can be controlled to allow or prevent the flow of current inside of the component. Those components are often arranged in a grouped structure called "*commutation cell*" and are the building blocks of power conversion.

Depending on the intended use, power devices will experience very different working conditions, but it is common for converters to experience thousands of volts and hundreds of amps during normal operation, thus managing a rather large amount of electrical energy.

With each commutation, the flow of energy is allowed or prevented depending on the state of each power switch, and every switching comes with small power losses that will be expressed as heat, raising the overall temperature of the switching components. Monitoring this temperature rise is very important as it is a witness of the healthy working condition for a given module. This temperature is typically measured at the component level as the junction temperature Tj, which can be as high as 150°C or even higher depending on the type of component.

b. Typical power module packaging

In order to function properly, power chips require a supportive housing, designed to accommodate for power supply and output, electrical insulation and cooling. This collection of operational requirements are ensured by what can be called "the packaging" of the power component and is generally adapted for each type of power module, depending on the routing and expected function of the device. For convenience, the whole package is contained in a protective outer shell bearing other secondary functions, such as shock and light protection.

The typical PM packaging is composed of several organs that perform critical functions, dedicated to the efficient and safe operation of the power dies. A typical architecture for die packaging in conventional power module designs is presented in **Figure 1**.

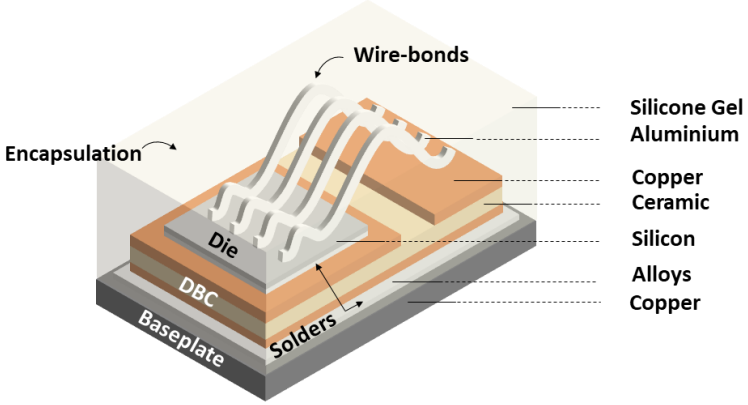

Figure 1 – Representation of a typical die package in conventional power module architectures.

From bottom to top, one can find the following elements in most power module architectures:

- The baseplate is the foundation of the power module. It is accessible from outside of the package and is the main thermal interface between the power module and the external cooling system dedicated to the device (radiator, air cooling, liquid cooling etc…). It is often made of copper or other high thermal conductivity materials. The baseplate is usually coupled with an outer plastic shell to create a receptacle for the delicate components inside.

- The Direct Bonded Copper (DBC) is the main support for the power chips. It is made of a layered arrangement of metal and ceramic and is directly soldered to the baseplate. The DBC plays the role of an electrical deck for the power dies in surface, providing large conductive areas for bottom connections. Additionally, it acts as an insulated thermal drain from below, guiding the generated heat through the insulating ceramic and towards the baseplate and cooling system.

- The power chip is the main active component, responsible for the electrical commutations necessary to signal modulation and the main provider of the heat drained through the DBC. These dies are usually made of silicon and receive a top metallization before being soldered (bottom connection) on top of the DBC.

- The wire-bonds are the top connection of the dies. They are almost exclusively made of pure aluminium or copper and are arranged into arrays of several wires per die, providing multiple paths for the current to flow through.

- Encapsulation of the electrically active components (Wire bonds, Si-chips, DBC) is achieved by filling the whole package with silicone gel. The gel will act as an insulator between conductive paths that do not share the same voltage and will also protect the delicate wire bonds and chips from contacts with the exterior.

Such assemblies can withstand stress to great extents for a rather long time, but the end of life of the device will be reached inevitably. Gathered under the term of reliability, the study of the life cycle and aging of devices can help to understand the root causes of power module failures and guide their improvement for future energy needs.

2. Concept of reliability

Reliability is a vast topic surrounding the entire life cycle of a system. It represents a probability of performing without failure accordingly to its intended function, intended usage time and operating working conditions. It is akin to how long the system can fulfil its mission before failure. However, it is important to distinguish between the reliability and the life-expectancy, as reliability relates to a population rather than an individual. The classical representation of a life cycle for a population of power modules can be represented by a "*bathtub*" curve (see **Figure 2**).

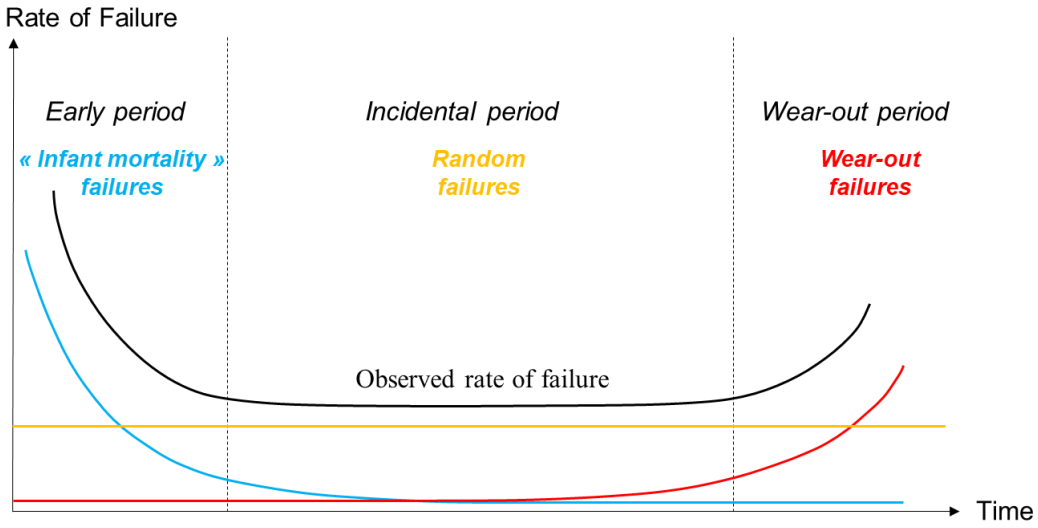

Figure 2 – "Bathtub" curve representing the different phases of a system reliability

Reliability plays out right after the manufacturing, also called "*early period*", when defects from flawed processes can prevent the item from achieving its mission properly. During this first period, many kinds of "*infant mortality*" failures can occur in a rather short time, resulting in a high failure rate.

When most of the innately defective devices have been ruled out, there is an "*incidental period*" where damages are less likely to happen and are more dependent on specific events that individual devices can experience. This includes misuse or exceptional degradations in operation as well as less critical defects remaining from the early life and aggravating with time. It is more of a stochastic process where damages are difficult to predict but are also much less common. This is the useful time for an item, or usable life period.

Finally, for devices that ran their whole intended lifetime without catastrophic failures, then comes the "*wear-out period*" where the accumulated damage shows an effect on failure rate of the system, developing characteristic failures. This period is driving the end of life of the devices and the damages extent will only go up past that point, showing an ever-increasing rate of failure. Knowing the beginning of this period helps to determine the acceptable time before a device must be replaced, preventing the occurrence of those wear-out failures in operating conditions.

In order to improve reliability, one can statistically lower the failure rate at any stage during the life of the studied system. However, early and incidental periods are more related to uncontrolled production processes or usage outside of the safe operating zone respectively. Module design is not to be blamed in itself, thus these are not relevant topics for the module designer. On the other hand, the wear-out period is rather tied to the system itself and its specific mission, which can be reproduced and studied by designers in order to improve the useful healthy operating time.

Therefore, the goal of reliability studies for designer is to reproduce, identify, and classify failure modes attributed to the end-of-life of power modules in order to better predict their occurrence and reduce the failure rate attributed to them.

3. Typical failure modes of conventional power modules

a. *Thermomechanical failure*

Failure modes in power modules are almost exclusively related to the temperature variations within the device. Expansion and contraction of the materials caused by mismatches in their Coefficient of Thermal Expansion (CTE) (see **Table 1**) will cause a periodic stress in the bulk and at interfaces, resulting in fatigue and failure of several key parts of the system.

Indeed, by bonding two materials together, the interface between them acts as a confined space where every portion needs to expand and contract at the same rate to remain stress-free. When this condition is not met, a reciprocal force is imparted on both materials which will be expressed as thermal stress (cf. **Figure 3**). The material that expands more with temperature is prevented to do so by the other material, resulting in a compressive stress at the interface, and reciprocally the material that expands less experiences a tensile force at the interface.

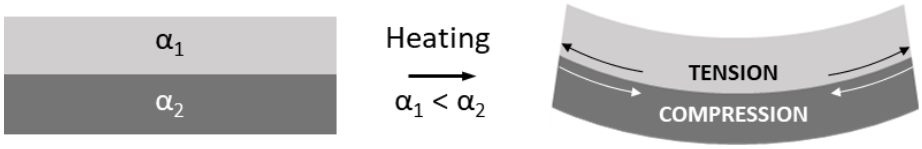

Figure 3 – Representation of reciprocal thermal stress experienced by bonded surfaces with mismatched CTE (α) during a temperature increase. Left) Stress-free assembly at manufacturing temperature. Right) Stressed assembly during heating.

In a static type of failure, the stress either exceeds the cohesion limit of one material, breaking it in the process, or exceeds the adhesion limit, resulting in the separation of both materials. In both cases, the result is the removal of the confinement for at least one part of the bonded materials. In a fatigue type of failure however, the stress will not exceed the cohesive or adhesive strength of the bonded materials. But the accumulated internal stress can be sufficient to seed and propagate defects, effectively damaging the materials at every cycle.

Table 1 – Conventional materials used in PM and their associated Coefficient of Thermal Expansion (CTE)

Component	Material	CTE (ppm/°C)
DBC	Copper	16-17
	Ceramics (Al_2O_3)	6-8
Solder	Alloys	Variable
Chip	Silicium, SiC, GaN	3-5
Wire Bond	Aluminium	22-23
Encapsulation	Silicone gel	250-450

(i) Solder fatigue

The solder is connecting the active power chip to the DBC underneath. Acting as a stress buffer, the solder accommodates for the difference of thermal expansion between both components, and therefore will experience significant plastic strain accumulation during power cycles.

This periodic plastic strain favours crack propagation and decreases the solder joint thermal contact, resulting in an increase of the local temperature due to the difficulty to transfer heat from the chip to the DBC [1]–[3]. This increase in temperature also exacerbates the expansion difference between the chip and the DBC, creating even higher stresses as a positive feedback loop until destruction of the bottom connection.

While being a serious issue in practical applications, complete solder degradation is a slow process that is less likely to be encountered in the accelerated tests with short cycle times (seconds), where the thermal stress is more concentrated at the wirebonds. Smet et al. (2011) [4] have shown that no thermal resistance (Rth) variation could be measured following ageing of power modules after several stress-inducing protocols, despite showing clear signs of cracking at the edges of the solder bonds (cf. **Figure 4**). These results are supported by other authors [3], indicating that solder fatigue might only become relevant when sufficient damage has been done (larger voids, centred under the chip) in a way that significantly decreases the thermal conductivity of the contact. This phenomenon is therefore best regarded as an aggravating factor becoming more and more prevalent with longer aging of the module.

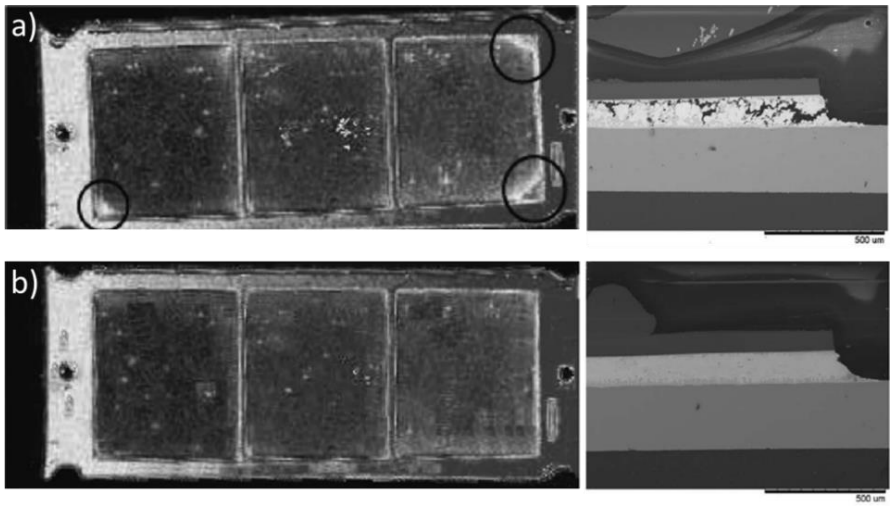

Figure 4 – Crack propagation in the solder layer for a) low stress amplitudes (207k cycles – ΔTj = 60°C, Tj,max = 150°C, Cycle duration = 45s) and b) high stress amplitudes (60k cycles – ΔTj = 80°C, Tjmax = 170°C , Cycle duration = 30s) [4].

(ii) Wire bonds degradation

During power cycling, wire bonds also experience stress attributed to CTE mismatches. Depending on the position along the wire, several types of failures have been described (cf. **Figure 5**).

Similarly to the solder fatigue, the aluminium wire directly in contact with the top of the silicon die pad will experience an interfacial stress due to the difference of CTE between the two materials. This failure mode is referred to as "*bond-wire lift-off*" and was described as a crack growth between fine and coarse grains within the aluminium bond foot, finally lifting the bond foot off of the die pad [2]. This theory is consistent with the lack of lift-offs when the wire is in contact with copper tracks with a better matching CTE [3].

Wire bonds were also reported to fail away from the die pad. Indeed, the wire is a rather long component, that can be subjected to large linear deformations during heat cycles. Since it is bonded to the silicon die in multiple places, the free loops formed in between bond feet can experience severe shear stress both from their own extension but also through the dilation of the encapsulation (silicone gel) material surrounding it. These failure modes are called "*wire fatigue*" or "*heel cracking*" and are generally considered less common than typical lift-off [3].

Despite having the same root causes as solder fatigue, wire bond degradation is often described as the most damaging event encountered in power module aging. Indeed, when one wire is destroyed, the overall current density quickly increases in the remaining ones. This sudden increase of current will heat up the rest of the top connections and expose them to even more detrimental effects until complete failure happens.

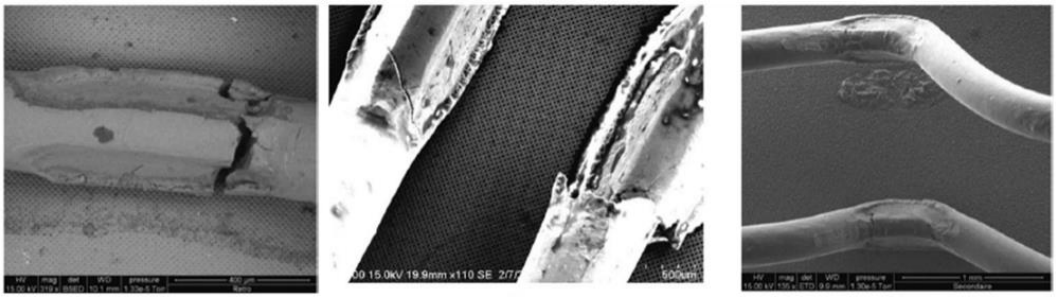

Figure 5 – Thermomechanical damages of wire-bonds. Left) Heel cracking, Middle) Fatigue induced fracture, Right) Bond lift-off [4]

b. Dielectric failure

Either from the nominal operating voltages or during transient overvoltages generated during switching, materials used for electrical insulation can endure several degradations that decrease the reliability of a power module. The most obvious way in which a dielectric could fail is by complete dielectric breakdown, which is a case where the designed insulator cannot withstand the applied electrical field and starts behaving as a conductor, failing completely at its intended purpose. Not many studies are centred around this specific failure mode for power modules, as careful design can almost eliminate the risk for a total breakdown. However, several degradation mechanisms can enhance the probability of a breakdown to happen, making the study of these events very valuable.

(i) Partial discharges (PDs)

Dielectric breakdown can be triggered when the thickness of the designed insulation is reduced during electrical aging under partial discharges regime.

Partial discharges are small dielectric breakdowns events occurring outside of the main dielectric matrix when the electric field is high enough, but not sufficient for a proper breakdown of the whole insulation. Most often happening in the air around the dielectric like in inductor coils or cables, discharges can also be triggered within the volume of the dielectric, in voids and other non-insulating defects where the field can be sufficiently concentrated. These electrical discharges damage the dielectric surface, causing erosion, gas formation and an increase of local temperature and can eventually lead to a proper dielectric breakdown [5].

In the case of power modules, PDs trigger around defects of the substrate, the rim of copper metallization, or at the interface between silicone and metallised ceramic where imperfect etching is found (cf. **Figure 6**).

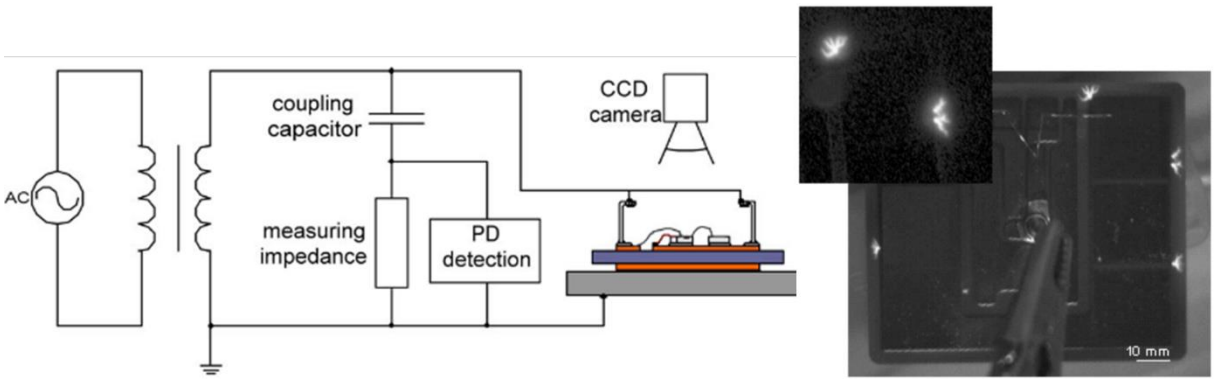

Figure 6 – Left) Experimental setup using electrical an optical PD detection. Partial discharges on the outer edges of the etched metallization on an AlN substrate embedded in silicone gel. (9.5 kV – PD level ≈ 500pC) [6]

The field-enhancing geometry of the defects greatly impacts the occurrence of PDs, with metallisation defects being considered as the first cause of partial discharge initiation in power modules. Interfacial defects like delaminations are the next most probable cause of partial discharge initiation directly concerning the dielectric material [7].

Working under a partial discharge regime also plays a key role in the formation of electrical trees, named after their typical branching geometry. Electrical treeing can be observed as the partial discharges degrade the dielectric, generating a more conductive path at every discharge. Eventually the electrical tree will reach a copper track and cause a short circuit or will decrease the thickness of the dielectric, enough for a real breakdown to happen. The exact mechanism for the formation of electrical trees remains unknown, but several hypothesis have been proposed, referencing Joule heating, UV generation, impact ionization or Maxwell stresses as possible roots for trees propagation [6].

(ii) Water uptake

Depending on the domain of application, a significant amount of water can accumulate in polymeric materials, changing their electrical properties and condensing in empty cavities.

Water uptake is not always considered when referring to silicone gels, however these polymers can exhibit a significant loss of breakdown voltage after exposition to water. Silicone gel can be described as a soft matrix containing unreacted silicone fluids that swell the elastomeric network, remaining inside it via osmotic pressure. When exposed to humidity, unreacted fluids dissolve water into the material, drastically lowering its dielectric breakdown strength (cf. **Figure 7**). However, the process of water diffusion could be reversible through slow heating to draw the moisture out of the material [8].

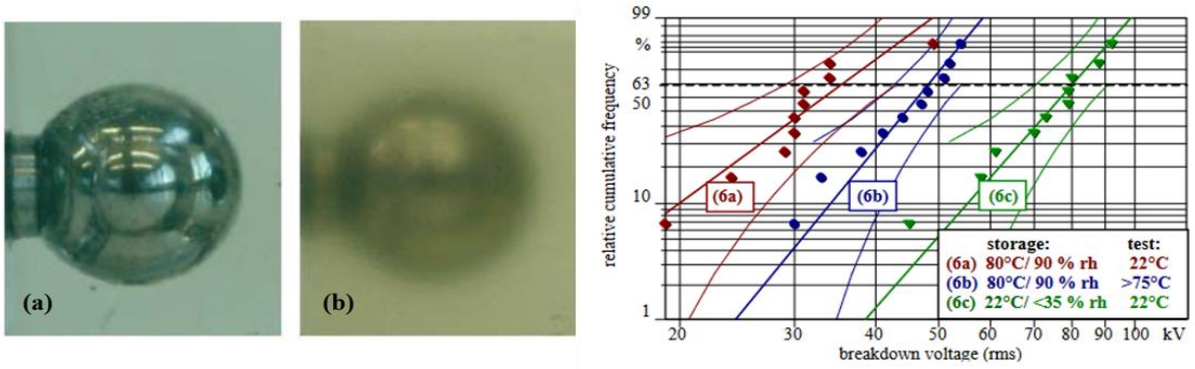

Figure 7 – Left) Phase separation of water dissolved in silicone gel a after exposure to humidity, at 75°C (a) and after cooling to 22°C (b). Right) Weibull plots of breakdown voltages, (green) references, (blue) humid silicone gel at 75°C, (red) humid silicone gel at 22°C [8].

Water uptake will also fill voids and cracks, or even electrical trees to form water trees, and follow the evolution of other defects during aging. These defects can also be the siege for partial discharges, coupling electrical damages with water spread, potentially causing insulation issues with time [6].

To summarize, partial discharges are the biggest threat for dielectric materials, occurring mainly around other defects and reducing the overall designed insulation thickness until breakdown. Similarly to thermomechanical damages, partial discharges occurrence increases when coupled with other defects, such as thermomechanical stress or water uptake in the bulk insulation. Water penetrating in the insulation can lower its electrical endurance, fill up and aggravate small defects and be the siege for further partial discharges, making it an aggravating factor for dielectric failure.

2. New trends in power module packaging

1. Wide Band Gap (WBG) components

While not directly considered as packaging, one of the biggest changes in power module architecture is coming from the growing use of wide band gap materials for the main active chip material.

The WBG denomination comes from the energy band theory, that describe the interaction of electron orbitals depending on their energy level and distance to other orbitals in a solid-like structure. In a solid material, the electrons are grouped in a resting energy level called the valence band, at which they are mobilized for the cohesion of the material and are not available for conduction. Higher energy states are represented by the conduction band in which electrons are freed from the valence state and are able to move, participating to the conduction. The gap between those two energy bands is called the band gap (or forbidden band) and represents the amount of energy required to free a bound electron from its valence state to the conduction state.

For conductors, the two bands aren't really separated and electrons are able to hop from one energy state to the other very easily. In the case of semi-conductors and insulators, the bands are separated by a variable energy requirement, increasing with the insulating character of the given material (cf. **Figure 8**).

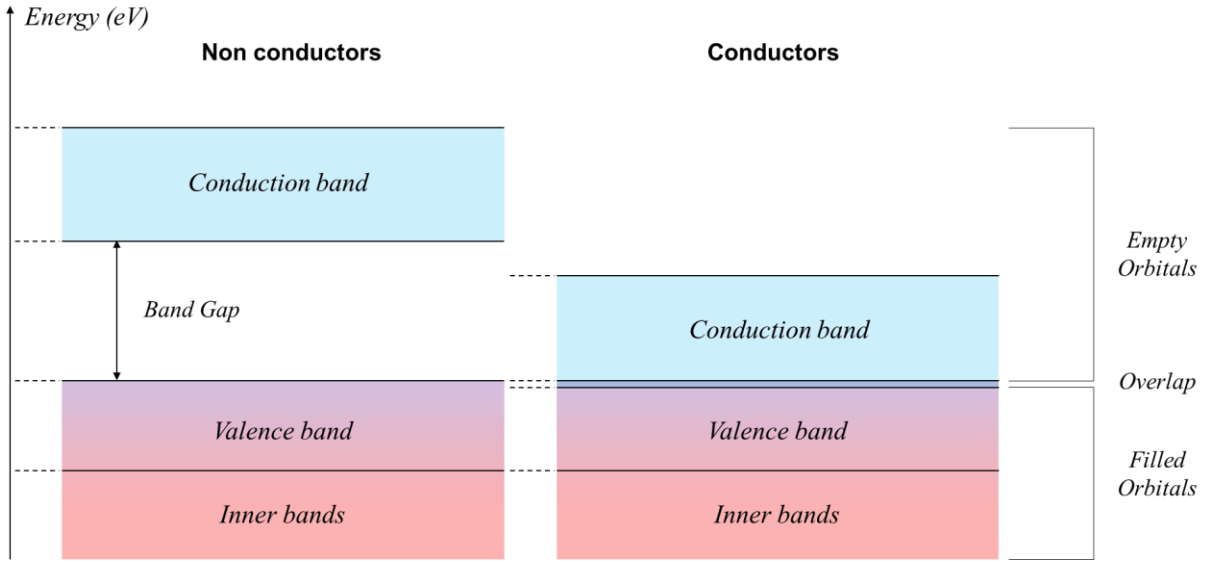

Figure 8 – Energy band theory simple representation for non-conducting and conducting materials.

Silicon based chips are physically limited to lower voltages due to the risk of breakdown and cannot run above 200°C without becoming conductive, since increasing the temperature helps electrons to reach the conduction band more easily, while also reducing the band gap [9]. These components are also less efficient with the increase of switching frequency [10]. By using WBG materials (SiC, GaN) it is possible to increase the dielectric strength of the component by a factor of 10, increase switching frequencies and operating temperatures significantly. WBG components also experience less power losses, requiring lower cooling capabilities for the same operating conditions as conventional Si-chips [10]–[12]. This allows to make modules with even higher energy densities while also increasing the overall efficiency of the device.

However, conventional packaging is not designed for such high electrical fields and temperatures. As a requirement for future power module technology, new packaging must be developed and encapsulation materials are also required to increase in performance, reaching higher breakdown strength and remaining stable at higher temperatures while keeping a high degree of reliability.

2. Interconnection improvements

a. Bottom connection

As identified previously, solder layers are an important part of thermomechanical cascade failures, most often ending up with a top connection failure due to the increase in overall temperatures. By improving the bottom connection technology, one can expect to reduce the rate of failure at the end of life of a device.

Silver sintering of the die onto its substrate has been thoroughly studied and is now identified as a potentially new dominant approach for thermomechanical improvements of the bottom connection. This process consists in the application of a silver particle layer onto the substrate, where the future chip will be attached, followed by careful chip placement and subsequent sintering. The latter is performed at moderate temperatures (250°C) but under rather high pressures (tens of MPa). At the end of this process, a solid silver layer is obtained, very strongly bonding the chip to its substrate [13], [14].

Stockmeier et al. (2008) [13] presented a power cycling test comparison between soldered and sintered modules (cf. **Figure 9**). When looking at the failure mechanism of a soldered device, there is a clear increase in junction temperature with each power cycle, resulting in the lift-off of wire-bonds as expected for accelerated tests. With sintered devices however, it is found that the junction temperature stays rather constant throughout the entirety of the test, suggesting that the thermal drain from the bottom connection is not impaired, and the final failure mode is attributed to heel cracking in the bond wires. As such, sintered modules can approximately triple their number of cycles before complete failure.

This result is somewhat explainable, due to the fact that lift-offs are originating from a CTE difference between the wire and the chip, resulting in more stress with higher temperatures, whereas the heel crack phenomenon is rather attributed to the expansion on the wire upon itself, increasing the damages in the bent heel with the number of cycles. This shows that by changing the solder component, mostly deemed as an aggravating factor for bond-wire failures, one can change the way failure is encountered in the module.

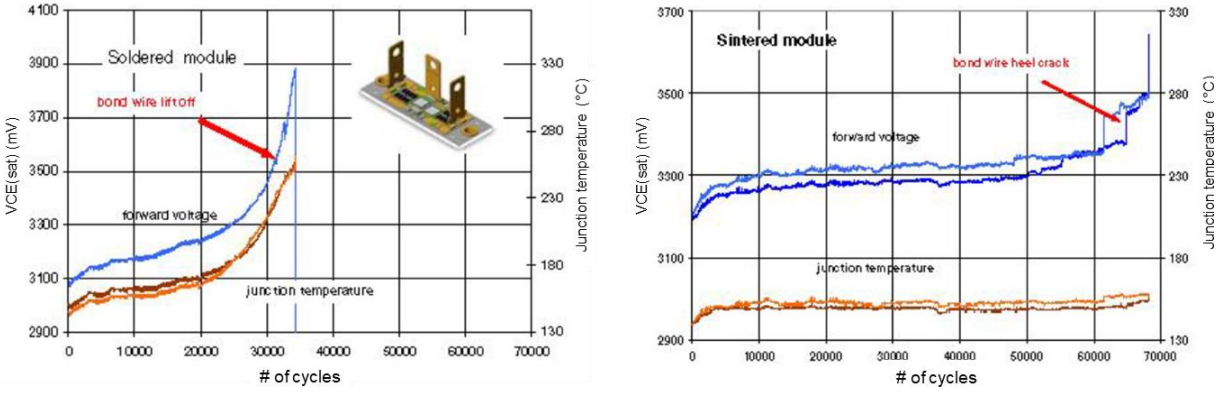

Figure 9 – Left) Change of V_{CE} during power cycling of a soldered module with the number of cycles. The failure mode is attributed to wire lift-off. Right) Similar test on a sintered module showing bond wire heel-crack [13].

Such results also suggest that even with vast improvements in reliability of the die-attach process, bond wire damage is still the ultimate failure mode of the device. As sintering technology becomes more widespread, top connection technology also needs to be improved in order to keep increasing life expectancies in normal operating stress conditions.

b. Top connection improvements

Optimizing the top connection seems vital to increase the lifetime and reliability of power modules. Fortunately, numerous new designs have been proposed in order to improve this part of the system and several review of designs and interconnection schemes can be found in the literature [10], [13], [15].

The main new technologies for connecting the power components can be classified as three large approaches: planar, press-packs and embedded packages. The common characteristic of these solutions is the complete removal of the wire-bonds, thus removing the associated failure modes entirely. Another positive effect of wire-bond removal is the reduction of the length of the top connection, drastically reducing the parasitic inductance and resistance of the entire circuit. In addition, most of those new packages offer better thermal management solutions with lower thermal resistance of the package, inducing less overall thermomechanical stress. More than simply changing the way power chips are connected, these concepts represent a large turn in power module design and manufacturing.

(i) Planar interconnection

For a time, very thick wire-bonds called "*ribbons*" were developed in an effort to increase the reliability without changing the architecture too deeply. While reliability gains may have been obtained in this way, the development of wide connecting surface areas have quickly been extended to a more generalized version of planar connection.

Planar interconnection removes the individual contacts of a die and replaces them with a shared conductive plane running through the whole package. Some designs propose to use a copper layer to distribute the power to each die, while other may entirely copy the bottom structure by placing another DBC on the top of the package, allowing for dual-sided cooling and tackling many thermomechanical issues that would come from the difficulty to drain heat from the package (cf. **Figure 10**).

One of the challenges of this approach is the need for high planarity between the power components. This is paramount for reliability since some chips might end-up being only loosely connected while others might be pressed too harshly against the conductive track. Spacers have been proposed to allow more versatility in the designs, but stress management during power cycling still looks challenging.

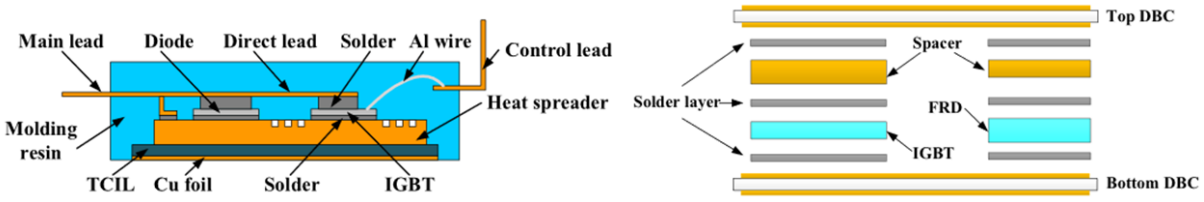

Figure 10 – Example of planar top connections. Left) Direct Lead Bonding technology. Right) Sandwich structure with spacers [15]

(ii) Press-packs technology

Press-packs technology is another way to take on the challenges of aging top connections, by removing the need for a constant and solid contact altogether. Instead of trying to accommodate stress in a constrained interface of two bonded materials, press-packs use springs to enter into contact with the die, using external pressure (cf. **Figure 11**). That way an electrical connection is made but the mechanical stress is significantly reduced compared to a bonded interconnection. In theory, this could also solve the challenges of having components of different sizes.

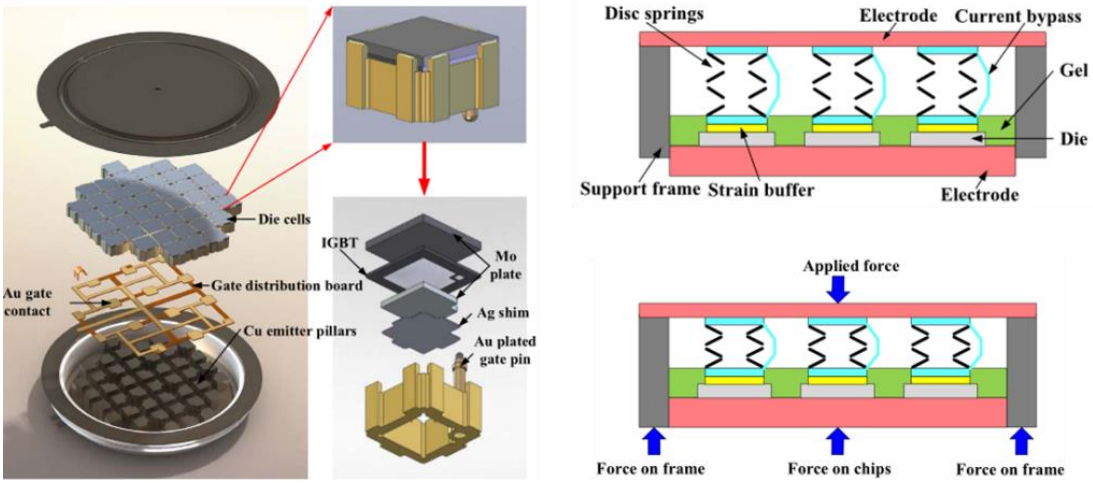

Figure 11 – Press-pack concept for a die cell array. Schematics of the pressing motion onto the dies [15].

In practice however, silicon chips do need to be protected by some sort of mechanical buffer, usually a molybdenum layer, capable of spreading the applied pressure from the spring onto the whole die pad. Another challenge is to apply the connecting pressure uniformly on a whole array of cells, ensuring the proper connection of all components. Finally, an un-bonded contact may be less efficient at transporting power and heat since the effective contacting surface is probably inferior to the full intended surface of the electrode. At the moment, it looks like components with large surface areas cannot be reliably implemented without experiencing some bending stress. [15], [16]

(iii) Embedded packaging

Embedded packages are at the limit of what can still be called an *interconnection improvement*. It does bring a new way to connect the chip but also embodies a whole new manufacturing concept. The main idea is to relocate the power chips from above to inside of their substrate, and to drill specifically where the connection is required, filling up the gap by electro deposition of copper to make a blind via. In a way, the embedded chip benefits from a planar approach with a top electrical deck spreading the power to each individual component, but at the same time enables the individual components to have different heights and still be suitably connected.

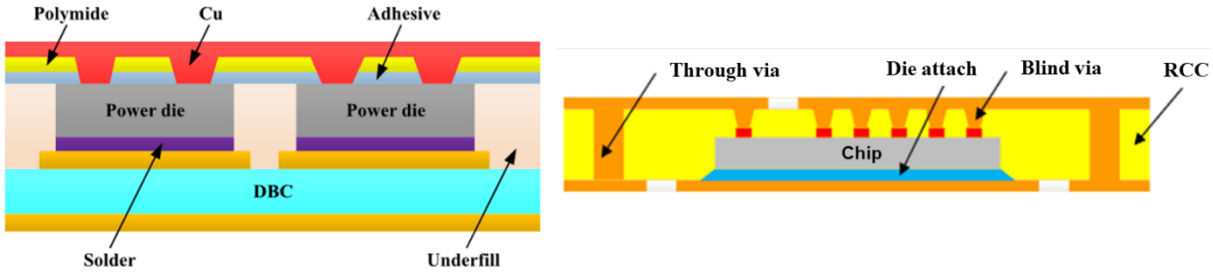

Figure 12 – Left) Conventional DBC mounted chip with via top connections. Right) Entirely embedded chip in Resin Coated Copper (RCC) with through vias and blind vias [15].

This also allows for easier manufacturing of multi-layer systems since through-vias can reach other embedded power tracks underneath, spreading the power to other part of the system. Most of these packages also exhibit quasi-flat architectures, making them eligible for double-sided cooling and die stacking, both being critical aspects for future power module technologies.

3. Printed Circuit Board embedded designs

a. Anatomy of Printed Circuit Boards (PCBs)

Printed Circuit Boards (PCBs) are integrated structures used in the electronic field, that were originally developed as a way to increase the compacity of complex "*2D*" circuits. Their use has since risen exponentially with the computer era and democratization of many portable electronic devices.

Nowadays, PCBs are most often made from a layering of glass fibre reinforced epoxy composites, acting as both the substrate and the electrical insulation, and copper sheets of about 18 to 35µm in thickness, that can be selectively etched in order to create the "*printed*" desired conductive path. According to this definition, the simplest PCB would therefore be composed of a single layer of dielectric material supporting a single layer of etched copper tracks. However, PCBs are often much more complex than that, with many interconnected layers and several designated processes in order to improve their performances. A more realistic view of a PCB for typical electronics can be seen in **Figure 13**.

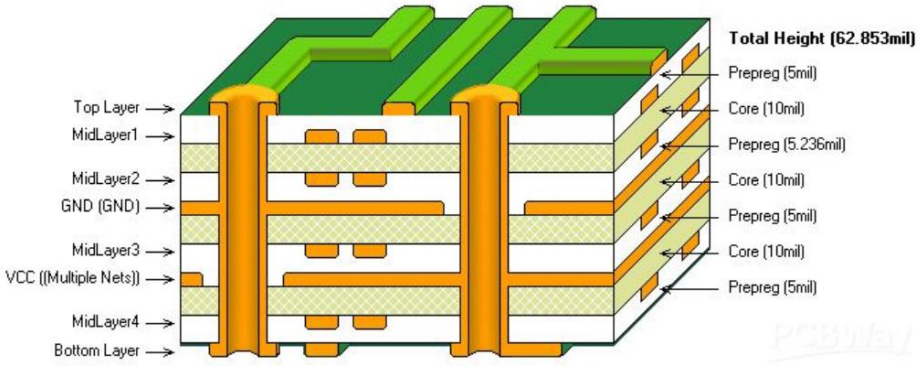

Figure 13 – Multi-layer PCB architecture used in the electronic field showing several copper layers and vias (orange) separated by insulation materials (white and light green).

Given the high level of control previously attained in the industry for the manufacturing of regular electronic boards, PCB-embedding rapidly became one of the most studied technology to produce new embedded power electronic packaging.

While PCB technology is well-studied and widely used for low power applications, it was bound to change drastically to make it applicable for high power devices. The insulation thicknesses and copper cross-sections have been increased and dimensioned to the expected higher voltages and currents, and the number of layers was decreased to match the lower complexity and higher reliability needs of high-power circuitry.

However, incremental changes with topological adaptations are not sufficient to shift from low power to high power applications. Innovation regarding PCB power devices is still wildly ongoing, and supposedly many materials and processes will be explored to draw the best out of these architectures.

b. Combined architecture improvements

As presented in the previous section 2.b(iii), embedded interconnection structures are very interesting to minimize the parasitic inductances and improve thermal management of the package.

With the large interest for new PCB-embedded power electronics, several studies have shown the improvements that such a change can bring. Indeed, PCB packages offer very interesting opportunities for manufacturing complex high-end converters, integrating more components within the power board and allowing routing in three dimensions. Not only do they offer new interconnection capabilities (top and bottom), but they also benefit from new encapsulation materials and an overall completely different manufacturing process.

Hou et al. [17], [18] presented a 3D-PCB-embedded design with dual-sided cooling (cf. **Figure 14**) and both active and passive embedded components situated on two separate levels. The maximum registered temperature was around 85°C with no heat spreader and 71°C with both above and underneath heat spreaders. In order to guarantee reliable operating conditions, a high-Tg, low-CTE polymer was chosen as the insulator.

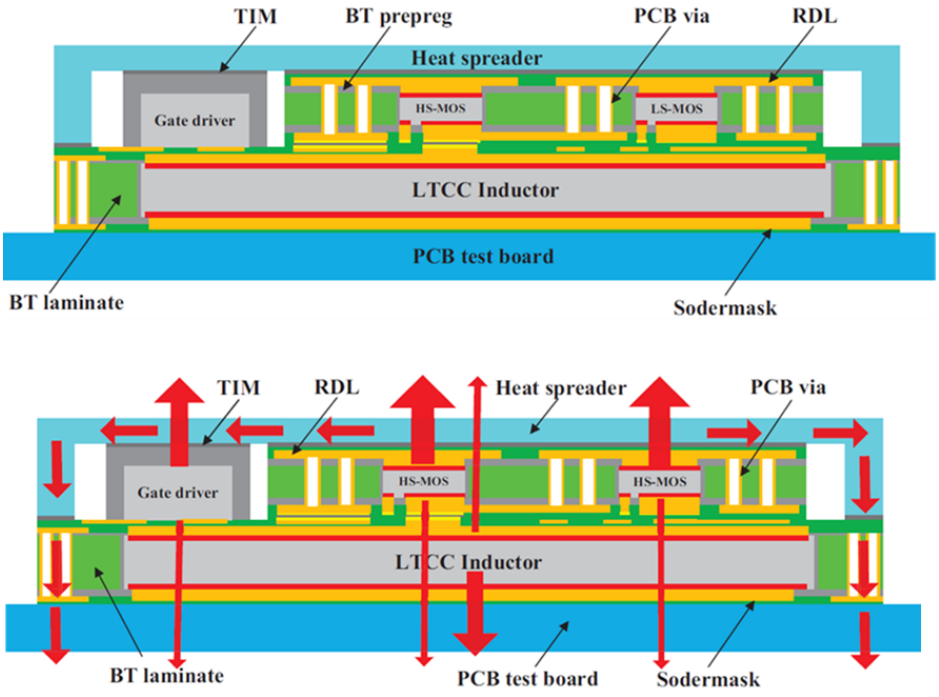

Figure 14 – Top) 3D-PCB-embedded dual-sided cooling design. Bottom) Main heat dissipation path of the proposed architecture [17]

In 2020, they proposed a symmetrical PCB-embedded design for SiC MOSFETs that provides equal cooling capability on both sides and drastically simplifies manufacturing processes. As wire bonds and DBC are replaced by the circuit board, die attachments and encapsulation processes were also not required anymore since the embedding in the polymer acts both as a confinement space for later external connection and as a primary electrical insulation (cf. **Figure 15**). Vias can be precisely drilled at the designated position using a laser and connection is achieved by subsequent copper metallization until a blind via is formed. This collection of techniques can be performed at a panel-level using batch processing and can be used as part of the High-Density Interconnection (HDI) technologies to the benefit of high-power devices.

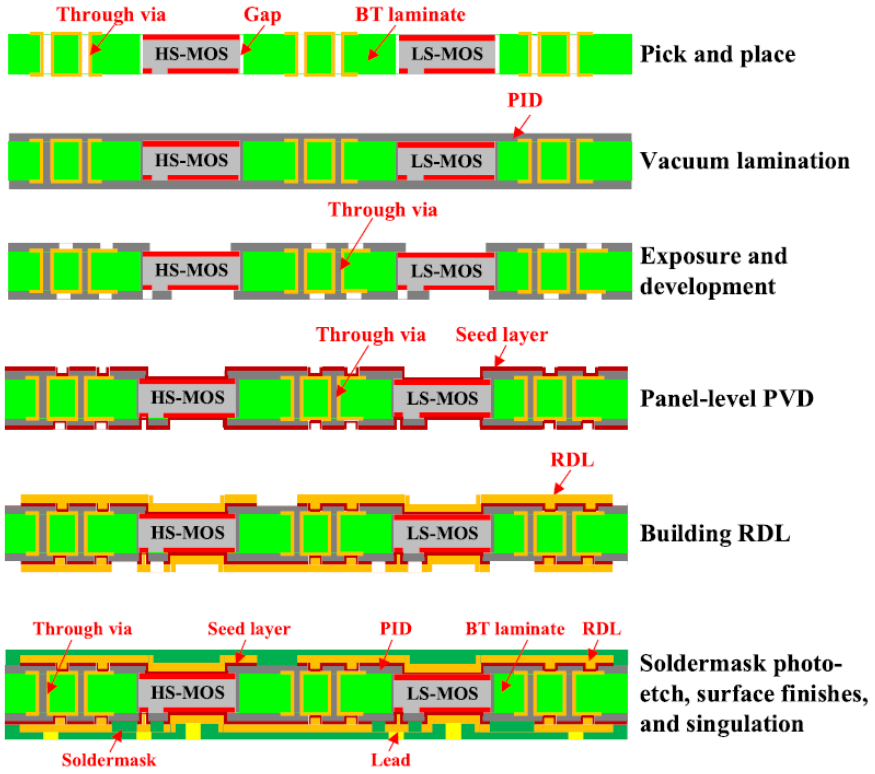

Figure 15 – Manufacturing process for a PCB-embedded MOSFET power module. [18]

Not only the manufacturing process is simpler, but vast performances improvement was demonstrated using such architecture, with the highest parasitic inductance evaluated at 1.24 nH at 100 kHz which equals to an 87% decrease from conventional wire-bonded packages and on the high-side of new packaging improvements. By replacing blind vias with “blind blocks” (square surface area) thermal dissipation paths, they simulated a decrease of 26% in thermal resistance of the package and a decrease of 45% of von Mises stresses on the SiC MOSFETs (less warpage due to less thermomechanical stress), which is advantageous in conjunction with a dual-sided cooling solution.

However, designing regular electronics is different from the workflow followed in the manufacturing of high-power electronic devices. Design toolkits encompassing several physical domains and design rules directed towards manufacturability are still lacking for now [19]. Most likely, new processes must emerge before these solutions can be produced at a larger scale consistently and become economically more affordable.

In conclusion, PCB embedded architectures demonstrate promising results and propose several advantages in terms of efficiency (low parasitic inductances), thermal management (lower thermal resistance and new cooling options), compacity (achievable 3D design) and overall reliability (decreased thermomechanical stress, higher dielectric strength). But, as part of any new technology advancement, high-power PCBs also come with new challenges that need to be tackled in order to ensure a robust and reliable base for the power electronics industry to thrive on.

3. Specification of reliable encapsulation materials for new power modules

1. Limitations of conventional insulation materials for future packages

a. Silicone gel

(i) Dielectric limitation

Understanding the roles and limitations of materials that were tested and approved on older designs is paramount to select an appropriate solution that can fit the requirements of new modules. As discussed before, silicone gel is the reference material when it comes to encapsulation of conventional modules designs. As part of this task, silicone gel is primarily expected to have high electrical insulation properties.

However, with technological advancements leading to the use of WBG semiconductors (SiC, GaN, Diamond) as an alternative to the usual Si chips, the maximum operational voltages tend to increase dramatically (from 6.5 to 10kV and above), with electrical fields up to 3 or more times higher in new designs using WBG components depending on the geometry [10], [20]. Silicone gel exhibits a typical breakdown strength of 15 to 20 kV/mm. Thus, with the growing risk of actual intrinsic breakdowns, the silicone gel might be reaching a limit in terms of reliability for electrical insulation of future packages.

Even though direct breakdowns are pretty rare when dielectric stresses are properly dimensioned, they are mostly occurring subsequently to aging under partial discharges, as mentioned in **1.3.b.** Avoiding partial discharges altogether is a much more difficult challenge, since metallization defects can be present from the early life of the devices (field concentrating geometry), and cracks or delaminations can occur in the most stressed areas where the electric field is likely to be very high. These two mechanisms do not really depend on the intrinsic dielectric properties but rather, are the consequence of the design, the manufacturing process and the aging of the system.

So, instead of trying to prevent the inevitable initiation of PDs, authors have tried to increase the erosion and breakdown resistance of polymer insulation under PD regime. And the easiest way to increase the erosion resistance of a polymer is adding inorganic fillers to the polymer matrix. Indeed, by physically shielding organic matter using an inorganic filler, it is possible to greatly reduce the amount of material vaporized by the plasma generated during a discharge. Li et al. (2010) [21] have compared the dielectric performances of several epoxy compounds using different size of inorganic fillers (micro and nanoscopic). Using a rod-to-plate setup, they measured the erosion depth generated by PDs onto the elaborated composites. They also investigated the breakdown strength and time-to-breakdown for each samples using a sphere-to-plan setup.

When using micro-sized fillers, the erosion depth can be divided by two compared to the unfilled matrix, as expected. However, dielectric breakdown (DB) happened after 1h30min under PD regime, exemplifying a typical way to escalate from discharges to breakdown (see **Figure 16**). When actually measuring the time before breakdown and the DB field, micro-filled composites show half the breakdown time and less than half the breakdown field of the neat polymer matrix. Overall, it was found that micro sized fillers drastically decrease the electrical performance of a dielectric compared to the polymer matrix alone.

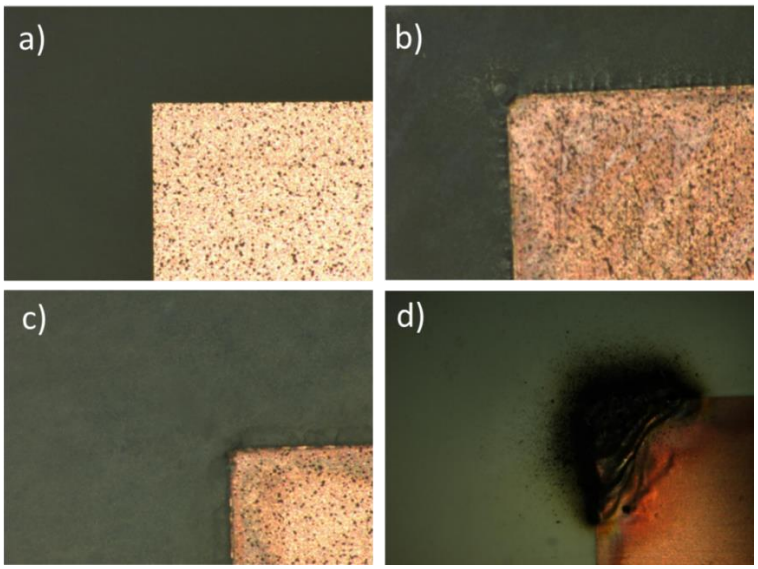

Figure 16 – Erosion damages on dielectric samples subjected to 4.8kV$_{RMS}$ 60Hz sine stress. a) Neat epoxy before erosion, b) Neat epoxy after 2h, c) with Al_2O_3 nano-fillers after 2h d) with Al_2O_3 micro-fillers after 1h30 [21]

On the contrary, when using nano-fillers, a very long time-to-breakdown could be registered, with a dielectric strength comparable to the matrix alone. The erosion depth was also among the lowest values, only beaten by a mix of micro and nano-sized fillers, as nanoparticles can provide additional shielding of the matrix in between the micro-sized ones, effectively increasing the total coverage.

Those results are explained by the fact that micro-fillers add a lot of defects that can be the initiation point for PDs, damaging the polymer step by step and leading to an early breakdown. DB strength is also decreased as defects around the micro-fillers could act as relays for the current, lowering the effective dielectric thickness on which the voltage is applied (cf. **Figure 17**).

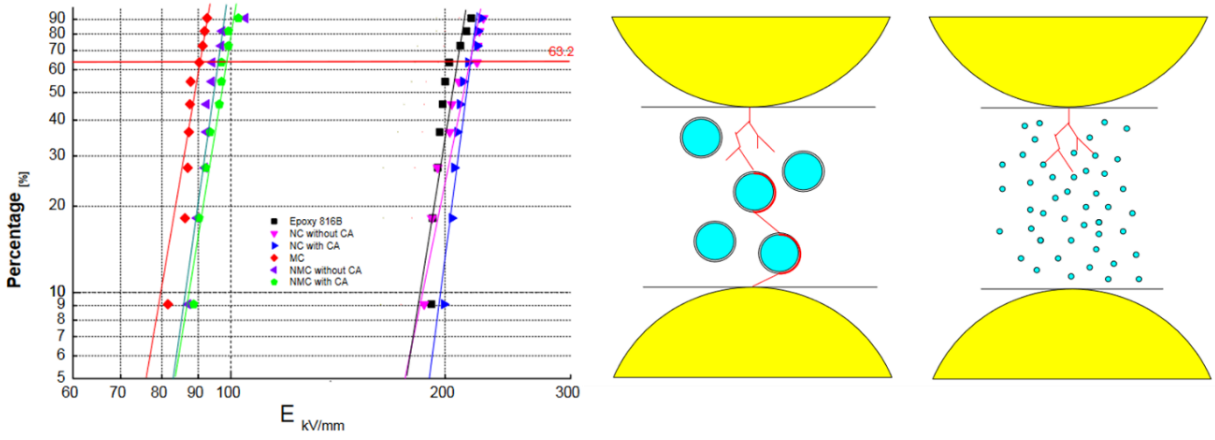

Figure 17 – Left) Weibull's plot of dielectric breakdown probability on neat epoxy (black), nanocomposite (pink/blue), micro-composite (red), nano-micro-composite (purple/green). Right) Role of filler size on breakdown path propagation [21]

Regardless of the exact mechanism, it seems like inorganic nano-fillers can be of great value to counteract the ill effects of PDs and increasing the electrical performance of polymer materials.

(ii) Thermomechanical limitation

As a secondary requirement, having an effective insulation role means that the silicone gel must also exhibit a very good conformation to the embedded components. This means having a sufficiently low viscosity during casting to easily fill all the gaps created by complex geometry, but

also to remain bonded in all situations throughout the life of the power device, which implies a good management of thermomechanical stresses.

Thermal stress (σ) experienced by a single ideal material confined and submitted to a temperature change can easily be expressed as a function of the elastic modulus (E) and the CTE (α) from Hooke's law, as shown in **Equation (1)**. While being much more complicated to express when two non-ideal materials are confined by a common interface, the main parameters of elastic modulus and thermal expansion remain relevant.

$$\Delta\sigma_{thermal} = E.\alpha.\Delta T \qquad (1)$$

Mechanical compliancy is therefore a true concern when it comes to designing a silicone encapsulant, since typical gels exhibit huge expansions with temperature, with expected CTEs of several hundred ppm/°C and because the actual amount of stress received by a bonded joint in fact depends on the elastic modulus and CTE of both contacting materials.

In order to prevent high thermomechanical stresses, commercial silicone gel used for encapsulation is extremely soft and was designed to have no significant mechanical impact on the assembly. Intentional optimization pushed towards the most linear and low mechanical profile possible, lowering glass transitions far below -50°C and trying to attain the lowest available elastic modulus (as low as a few kPa) and hardness, even after aging [22], [23]. By being so compliant, the gel does not generate large stresses during its own expansion, making it a good solution for encapsulation of delicate structures like bond wires.

The question of the role of the encapsulant in the reliability is a rather recent concept. Previously, the encapsulation was simply considered as a way to prevent arcing in between two charged components, as well as a protection from dust and other contaminants that could lead to electrical failures. However, this high mechanical compliance could be one of the reasons for bond wire failure mechanisms, as wires can move extensively and experience strain fatigue within the dielectric during power cycles, which led to the development of the new interconnection technologies in the first place.

More recently, authors developed encapsulation materials that could help with the typical failure modes of power modules The general strategy was to reduce thermomechanical stresses by better matching the CTE of the encapsulant with the rest of the module. Additionally, having a stiffer encapsulation could mechanically stabilize the wire-bonds and prevent too much deformation. In addition, harder encapsulants often provide better thermal conduction, reducing the immediate increase of temperature and the overall thermal gradient.

Simulations showed the evolutions of the directional stress components at the bond foot for different encapsulation materials, from no encapsulation to hard ceramic encapsulation (cf. **Figure 18**). In-plane stresses (σ_X, σ_Y) were found to increase as well as being more homogeneous with harder encapsulation materials, while the out-of-plane stress (σ_Z) was found to change from a tensile (positive) loading to a compressive (negative) loading, removing the tensile force lifting the bond of the chip and equalizing with the in-plane stress with the hardest materials. This means that the bond foot would be subjected to a quasi-hydrostatic pressure when encapsulated with harder materials [24].

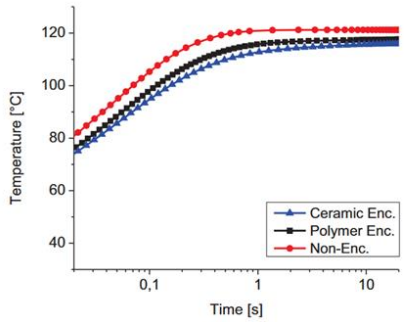

	Von Mises stress σ_{eq} [MPa]	Max. Normal stress σ_x [MPa]	Max. Normal stress σ_y [MPa]	Max Normal stress σ_z [MPa]
Variant I	45,5	-36	-48	15
Variant II	43,8	-73	-72,5	-34
Variant III	42,4	-110	-110	-86,5

Figure 18 – Left) Simulated thermal stabilization for different encapsulation materials. Right) Simulated directional stress profile for each encapsulant (I – No Encapsulant, II – Polymer, III – Ceramic) [24]

An experimental study was conducted and confirmed simulation results, with the replacement of silicone gel with a stiff cement-based materials [25]. Power modules were subjected to stress conditions at the limit of typical datasheet values (see **Figure 19**) until end of life and the probability of failure was represented using a Weibull plot, showing and increase in expected lifetimes by more than a factor 3.

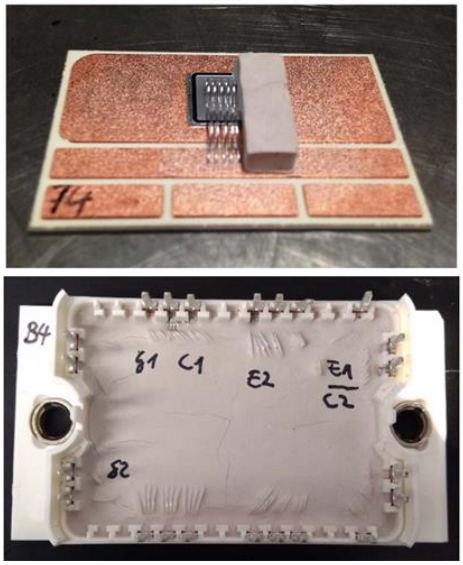

t_{on} [s]	t_{off} [s]	I_{pulse} [A]	$T_{j,min}$ [°C]	$T_{j,max}$ [°C]	ΔT [K]	T_m [°C]
1	8	100	20	150	130	85

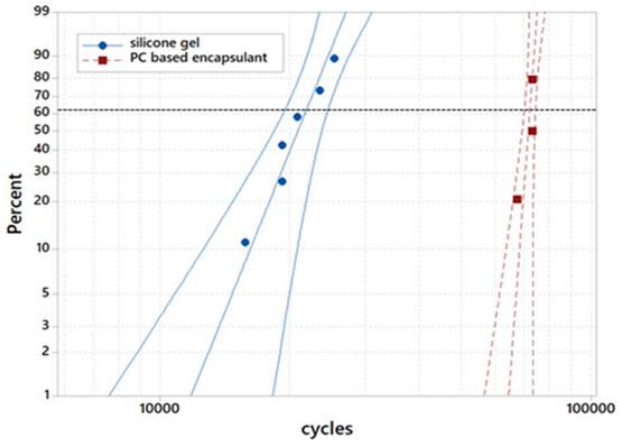

Figure 19 – Left) Phosphate Cement (PC) encapsulated module. Right) Power cycling parameters and failure probability with silicone gel (blue) and PC (red) encapsulants [25].

Failure analysis showed that the PMs encapsulated in silicone gel experienced many lift-offs, with low solder degradations, which is consistent with previously reported results for high stress cycles (cf. **Figure 20**). With cement encapsulation however, the main failure mode shifted to chip metallization damage as a result of corrosion induced by reactive compounds in the cement. Solder degradation was found and could be attributed to the higher number of cycles endured by these modules compared to the silicone reference, since this failure mode typically appears with longer testing times.

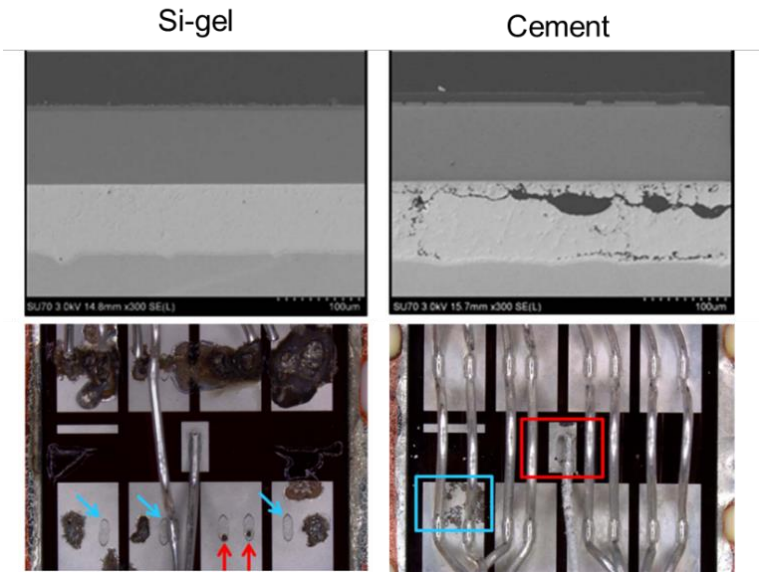

Figure 20 – Failure analysis of power modules depending on the encapsulation material. Left) Blue arrows indicate lift-offs, red arrows indicate thermal damages. Right) Blue and red squares indicate different corrosion damages. [25]

The same research team continued to investigate cement-based encapsulation with Naumann's work (2020) [26]. The volumetric thermomechanical simulations revealed that hard encapsulation could alleviate part of the stress received by the die and the solder, representing a von Mises stress decrease of 17 and 8% respectively. Although these results are promising, the maximum stress on the bond wire increased by 10% and shear/normal forces on the interface between the bond and the die also showed a significant increase (not quantified). Carefully managing the mechanical properties of the encapsulate is therefore very important in order to optimize the stress profile near the active components.

And as was shown previously, using the appropriate inorganic fillers can also decrease erosion from partial discharges, while preserving most if not all of the breakdown resistance from the polymer matrix, making filled epoxy and other hard encapsulation materials promising solutions for future high-power devices.

b. *Epoxy composites*

(i) Thermomechanical limitations

As mentioned before, PCB-embedded designs get a lot of attraction in the power engineering field as a very promising solution for new packaging.

FR4 materials (Fire Resistant 4 norm) are standard composite materials used in most PCB related applications and are most often manufactured from epoxy resin and E-rated glass fibers (E-Glass). Usually manufactured from layering several fiberglass cloth impregnated with pre-cured resin (Stage B material), FR4 materials are usually cured in a heating press under high pressures (tens of MPa) to remove most of the air and ensure a high cohesion between layers.

But as with any layered multi-material composites, thermomechanical stress and adhesion strength are major concerns when it comes to thermal cycling and aging. PCB materials are no exceptions, and furthermore, the reinforced polymeric matrix used for PCBs can exhibit delamination modes with its own reinforcing fibers, as well as with the embedded copper tracks which may become detrimental for high-power devices where aging of the board can be largely accelerated in operation.

Randoll et al. (2014, 2015) [27], [28] demonstrated that following thermal shocks testing (-40 to +125°C for 2000 cycles), the reinforced epoxy exhibits significant damages near the copper interface. This can be considered as a mixed failure, meaning that delamination (in between materials) and cracking (inside a given material) both occur. As shown in **Figure 21**, part of the damage shows a rather clean adhesive failure, mainly around glass fibers, while the damage near the copper interface is best described as a cohesive failure within the matrix.

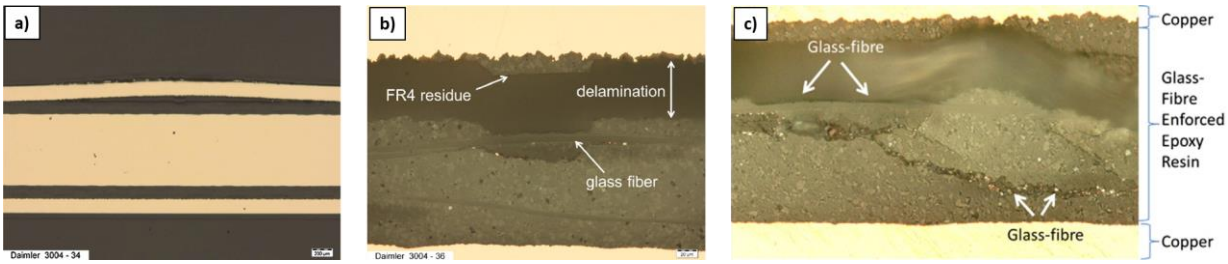

Figure 21 – a) Cross-section image of a delaminated copper track inside a PCB dummy sample. b, c) Cohesive failures of the reinforced epoxy near a copper track [27], [28]

Such failure modes have also been observed with other electronic components embedded in a hard matrix, as with ceramic capacitors, where cracking was observed between the copper and the polymeric matrix, which is consistent with a CTE induced failure mode [29].

This is highly problematic for highly integrated, high-voltage power converters, where such damages are likely to give rise to other electrical issues. In their chapter on the "*Selection criteria for Multichip Dielectrics*" Feger and Feger (1993) [30] directly relate mechanical damages to electrical failures, making this a crucial challenge for future PCB-embedded devices.

(ii) Humidity related damages

Similarly to silicone-gel, epoxy compounds are known for their ability to store water in their network and can experience similar degradations. (Degraded dielectric properties, water treeing etc…).

But unlike with silicone gel as soft encapsulant, in hard encapsulation materials, water accumulated inside the material cannot diffuse as easily and escape. The high heating rates encountered during power cycling can generate high pressures, as evaporation takes place inside of a confined space. This can lead to another type of mechanical failure, referred to as the "pop-corn" effect, where the water pressure bursts the encapsulation material, generating many damages in the process [31] (cf. **Figure 22**).

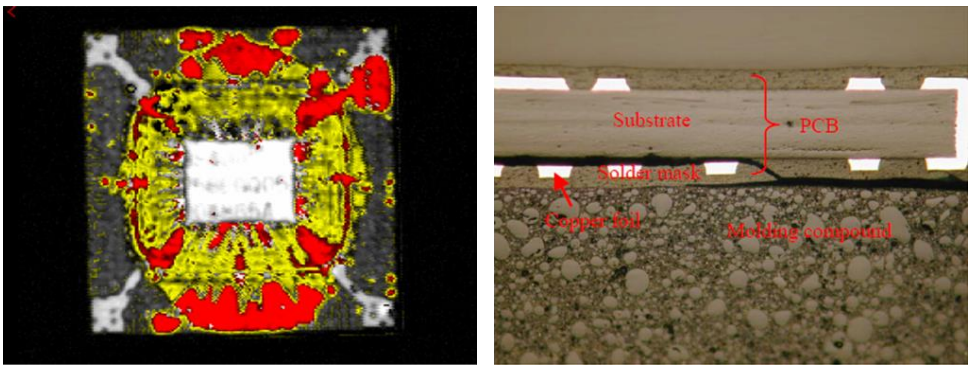

Figure 22 – Left) Acoustic image of failed FPGA (red is delaminated). Right) Cross-section image of cracking around the PCB [31].

While cracking or delamination caused by water uptake is a problem in itself, delamination induced by CTE mismatch can also be an entry point for water, creating a new positive feedback loop between thermomechanical failure and water uptake.

Dong Kil Shin et al. (2010) [32] proposed a PCB-mounted 3D chip package, embedded in filled epoxy resin. Their goal was to enhance adhesion of the epoxy molding compound (EMC) to the solder resist (SR) layer to increase the reliability of the package in humid environment (cf. **Figure 23**). By soaking PCB boards in water before applying the molding compound, delamination could be observed, showing that accumulation of water can create adhesive defects during encapsulation, that can later trigger crack initiation and propagation.

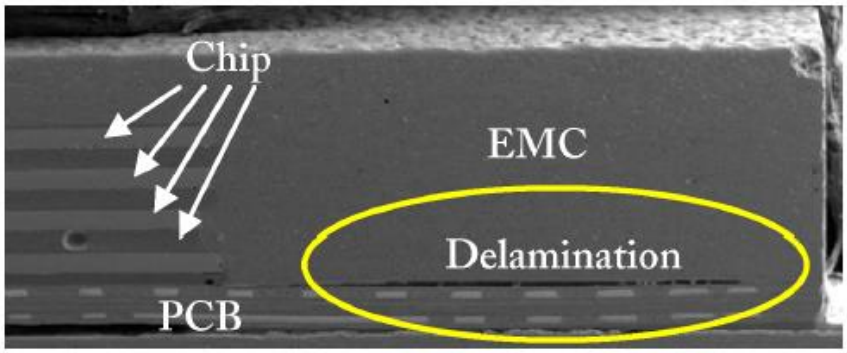

Figure 23 – Delamination between the PCB and the epoxy molding compound (EMC) [32]

c. Conclusion on conventional materials limitations

To summarize the current state of encapsulation/embedding materials, silicone gel is not a satisfying solution for current architectures where other harder solutions seem more desirable and does not fit the new requirements in terms of wide band-gap components due to its low breakdown strength. Additionally, silicone gel also cannot fit in new integrated architectures such as embedded or multichip due to its lack of structural stability, making it unsuitable as a substrate material.

Epoxy compounds have been used previously for encapsulation of power components in discrete packages and could be the solution for silicone gel shortcomings in terms of dielectric strength and mechanical stability. But the use of a harder, reinforced epoxy in high-power applications still suffers from thermomechanical stresses, exhibiting cracks and delamination within the insulation material, making the package unreliable especially in humid environments [33].

2. *Ideal encapsulation material for PCB packages*

a. *Intended functions for the dielectric material*

In order to set the requirements for an improved dielectric solution for PCB packages, it is important to specify the roles and expected properties intended for this new material.

First of all, an ideal dielectric must be compatible with PCB manufacturing and generally high-density interconnection technologies processes, that are intended for new high-power converters. Namely, compatibility should be ensured with hot-press manufacturing, selective etching, laser drilling, metal plating and sintering or soldering.

It is also required to at least provide the same improvements that typical FR4 material offers compared to silicone gel for high voltage integrated structures. This means an improved dielectric strength as well as higher mechanical stability.

Additionally, it should propose a solution to the FR4 failure mechanisms that prevent its reliable use in new power module architectures. Thus, the ideal dielectric should prevent cracking and delamination, as well as water uptake altogether.

b. Properties required for integrated PCB manufacturing

Manufacturing of a PCB is a rather complex process, involving several steps. Without going into the specifics of this field, the key material requirements necessary for PCB manufacturing can be underlined.

(i) Thermal stability

Thermal stability is one of the most important properties for a PCB material. Indeed, in addition of the curing process and operational temperatures, the polymeric material can be exposed to very high temperatures during solder operations, that can easily degrade the material. With the generalization of lead-free processes, polymers used in PCBs will need to endure from 240 to 270°C, against 210 to 245°C previously needed for tin-lead (Sn-Pb) solders.

Thermal degradation can also lead to outgassing and pressure build up, delaminating the layers of the now defective board. Reactive radicals can also be generated during thermal degradation, usually crosslinking the polymer further and therefore changing its intrinsic properties [30], [34]. Thermogravimetric tests are used to assess the mass loss of a given amount of material with rising temperatures. In normalized tests, most FR4 materials exhibit a mass loss of 5% between 320 and 350°C (cf. **Figure 24**) [35].

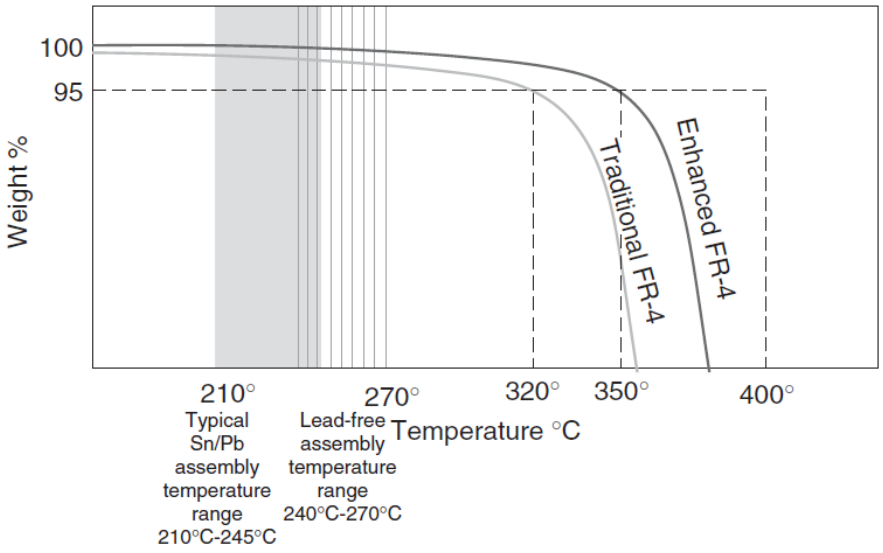

Figure 24 – Illustration of decomposition curves compared to temperature ranges of assembly processes [35].

(ii) Chemical properties

In order to obtain the desired conductive tracks, PCB's copper layers are chemically etched. Electro-plating is also used to fill blind vias and metallize through vias. Chemical resistance is therefore very important to withstand the different chemical treatments (such as strong acids and bases, oxidative solutions and solvents) used during this manufacturing process. That is why crosslinked materials such as epoxy compounds are favored when making PCBs, as their gelled network is quite strong against most chemical attacks.

Additionally, an ideal material would be able to be cut and processed using a laser, capable of precise etching and drilling of the polymer layers to reveal the connective areas of power chips before the metallization.

c. Comparison between FR4 and Silicone gel

(i) Dielectric properties

From the previous reported data, it is clear that having a high dielectric strength is a necessary condition for a reliable insulation material. Decades ago, Garrou [34] was already proposing several high performances materials that could be used for innovative multichip packages. Extremely high dielectric strength was proposed, with breakdown field values up in the hundreds of kV/mm, aligned with the expected concentration of electrical stresses that comes with highly integrated architectures. However, more recent evaluations take into account that most insulator typically do not exhibit such high dielectric strength values when rated at conventional thicknesses (100µm range) due to the increased probability of defects in the tested volume. In that regard, a dielectric strength superior to 50kV/mm should be within the range of what is acceptable for new insulation materials [33].

FR-4 materials used conventionally for PCB manufacturing display a dielectric strength around 50kV/mm which is why those materials are favored for high voltage applications. Silicone gel usually exhibit a lower dielectric strength of about 15 to 20kV/mm [36].

Another important consideration is the proper electrical insulation of the power component. A high volumic resistivity is required to avoid current leakage between the emitter and the collector of the power die, reducing the blocking power of the component or even shorting it altogether. Acceptable resistivity values should range from 10^{13} to 10^{16} Ω.cm [35]–[38].

(i) Mechanical strength

During the manufacturing of a PCB, several pressing, lamination and other manipulations are required. Having a high mechanical strength guarantees a good resistance to plastic deformation and a high elastic modulus provides lower elongation for a given applied stress [34]. Flexural strength is also important to resist the bending stress put on the thin power board when mounting components or when experiencing uneven heating.

Reinforced epoxy resin is notorious for its good mechanical properties and is widely available for a range of application requiring actual mechanical support. Its tensile strength is above 240 MPa and its flexural strength is near 400-500MPa. Its elastic modulus is around 21 to 24 GPa, with maximum elongation at break close to a few percent [37]–[39]. However, most of these properties can be directly related to the reinforcing fabric inside of the material, as unfilled epoxy resin usually exhibits much lower elastic modulus (a few Gigapascals) and strength (tens of Megapascals).

In comparison, silicone gel is almost impossible to rate mechanically with conventional setups and requires rheometric measurements and other methods specific to soft gels or liquids in order to determine their mechanical properties. The elastic modulus of silicone gel should be expected within 100 to 500kPa range (sometimes even below), which is several orders of magnitude below the elastic modulus of typical epoxy matrixes used in FR4 composites. In summary, silicone gel cannot be used as a structural material.

d. Approaches to prevent FR4 typical failure modes

(i) Management of thermomechanical stress

In order to prevent FR4 typical failure modes (cracking and delamination), one must lower the periodic thermomechanical stress experienced within the material. As explained in 1.a(ii),

thermomechanical stress is a function of the temperature change, the CTE difference between neighbouring materials and their elastic modulus. In the case of power modules, the general strategy is to match the CTE of materials in contact in order to reduce thermal stresses. In the case of PCB-embedded modules, the polymer CTE should be in between the CTE of copper (16ppm/°C) and silicon (3ppm/°C). However, polymers can experience changes of CTE depending on their glass transition temperature (Tg).

The glass transition temperature is a notorious indicator for polymer processing and usage. Above this temperature, mechanical properties are severely lowered and the polymer will adopt a rubber-like set of properties [34]. At Tg, a polymer is expected to have an increase of CTE, generating an increase of stress that could lead to delamination if the material cannot relax during the dimensional change (cf. **Figure 25**) [30], [34]. This is why most polymers used in electronics boards are selected for their high Tg in order to remain below this transition, ensuring high mechanical properties in operation. In the sixth edition of the *Printed Circuit Handbook* (2008) [35], Coombs evaluated the ideal Tg of FR-4 materials between 140 and 175°C, as it is the temperature limit for most electronic components.

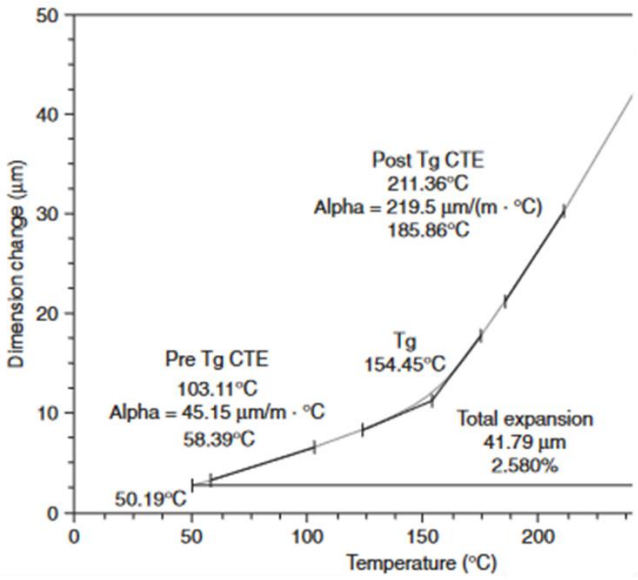

Figure 25 – Thermomechanical Analysis (TMA) showing the CTE change during the glass transition [35]

However, the PCB reliability is not directly related to the Tg being high, but more to the variation of thermal stress generated during the transition. FR-4 materials show a CTE of 50-70ppm/°C below Tg and a CTE of 250-350ppm/°C above Tg, which justifies the conventional attempt to remain below Tg at all times, keeping the glass transition temperature above of the application range and preventing the related increase of thermal stress [35], [37], [38].

On the other hand, silicone gel has a constant high CTE evaluated around 335ppm/°C, due to the fact that its glass transition temperature is always far below usage temperatures [36], [40]. But silicone gel can still be used in power cycling devices without cracking, due to the fact that it is compliant enough to accommodate the large expansion, without causing a significant reciprocal stress onto other components.

Lall et al. (2018) [41] showed that having a more compliant epoxy compound can provide a higher toughness and demonstrated that peak fracture toughness was obtained when materials were cured right below their expected final glass transition, which prevents the mobility of unreacted compounds leading to a slightly less reticulated material (slightly more compliant). This is an

interesting lead towards the development of an epoxy matrix that is less subject to cracking during thermal stresses.

In conclusion, there is a complex interdependence between Tg, mechanical properties and CTE variations for a given couple of bonded materials. Thus, selecting the right thermomechanical properties requires to have a good understanding of the heating profile and mechanical needs for an assembly (cohesion, adhesion strengths), which is highly dependent on the system architecture (heat generation, cooling, buffer layers, thickness etc…) and the mission profile.

(ii) Lowering operating temperatures

Another possible route to lower thermal stress is to lower the maximum temperature experienced during power cycles, regardless of the CTE-mechanical stiffness trade-off.

When looking at new PCB packages, polymer layers are the worst heat conductors in the stack, leading to an increase of global thermal resistance and accumulation of heat inside the package [42]. To improve the thermal conductivity of PCB materials, Randoll et al. (2014-2015) [27], [28] proposed epoxy composites that exhibit up to six times the heat conductivity of conventional PCBs (6 W/m.K against 1W/m.K).

Looking at **Figure 26**, it is clear that the use of inorganic fillers is the main strategy to increase thermal conductivity. Size and concentration of fillers controls the conductivity of such materials, and a multimodal size distribution allow for maximum packing efficiency of fillers inside the polymeric matrix, leading to the creation of an unconnected network of ceramic relays for heat to dissipate more easily.

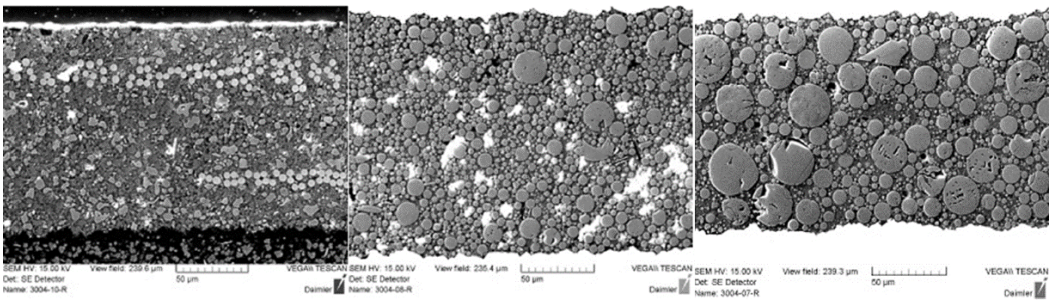

Figure 26 – Standard PCB material with 1.5W/m.K (left), PCB material with 3W/m.K (middle), PCB material with 5W/m.K (right). Same scale is used. [28]

Conveniently, using large amounts of fillers also helps to reduce the CTE down to the desired levels, lowering thermal stress two folds. As seducing as this may seem, using such a large concentration of fillers may cause difficulties with the manufacturing process as well as resulting in a probably lower dielectric strength, as more relays and defects are available for arc propagation [21].

Another approach is to consider the polymer, not as a heat conductor, but rather as a heat capacity supplying enough thermal drains. By using a low thermally conductive underfill (0.9 W/m.K – similar to classical FR4 materials) in their simulations, Fan et al. (2008) [43] showed that thermal dissipation can be improved. As shown in **Figure 27**, an area covered with underfill and solder balls competes with a surface that would be totally covered with only solder balls, achieving the same thermal dissipation. Even when using a very low number of thermal contacts (2x2), the simulation shows an even heat dissipation, leading to the conclusion that sufficient area of contact combined with a few highly conductive heat sinks can provide an efficient cooling solution, provided that the underfill can act as a heat capacity and is conductive enough to meet the draining capabilities of the thermal vias.

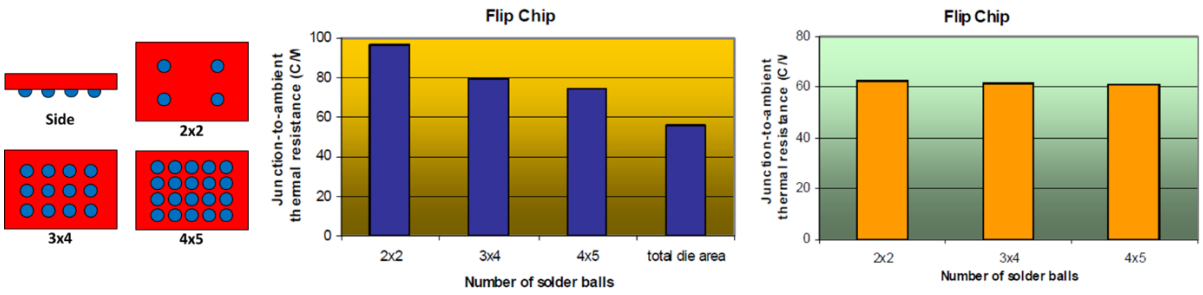

Figure 27 – Influence of Flip Chip number of solder ball contacts on simulated thermal resistance of the associated packages. Middle) No underfill is used. Right) Underfill is used. [43]

Similarly to the tailoring of the CTE and mechanical properties, the thermal resistance of the package is not solely a question of having a dielectric with a given thermal conductivity, but rather heavily depends on the type of architecture and the design of vias supposed to drain the heat generated by the semiconductor.

(iii) Reduction of water uptake related degradations

Preventing the damages caused by water is an important goal for epoxy embedded power modules. While not being the main damaging factor, water can degrade electrical properties, as well as preventing proper adhesion and even cause pressure build up leading to delamination.

Soles et Yee (2000) [44], [45] studied water uptake at a molecular level in epoxy networks. They propose the theory of a nano void interconnected structure within the epoxy chains, where water could penetrate. According to these studies, a maximum amount of water could be reached for the maximum number of voids available for storage. This would be the case for completely reticulated rigid networks where the polymeric structure is entirely fixed. In that regard, having a higher flexibility network could mean that nanovoids get closed from time to time, being unavailable for maximum water uptake. On the other hand, it seems like having a more polar network would lead to more water uptake, as each polar group could be an adsorption site for water molecules. But at the same time having polar groups could lead to a decrease of the rate of water uptake due to the interactions of water with the polar material, slowing down their diffusion.

In that regard, the physical structure of a rigid polymer network may be related to a water capacity whereas the chemistry of the polymer backbone could be used to tailor the rate of diffusion and possibly provide additional storage capacity.

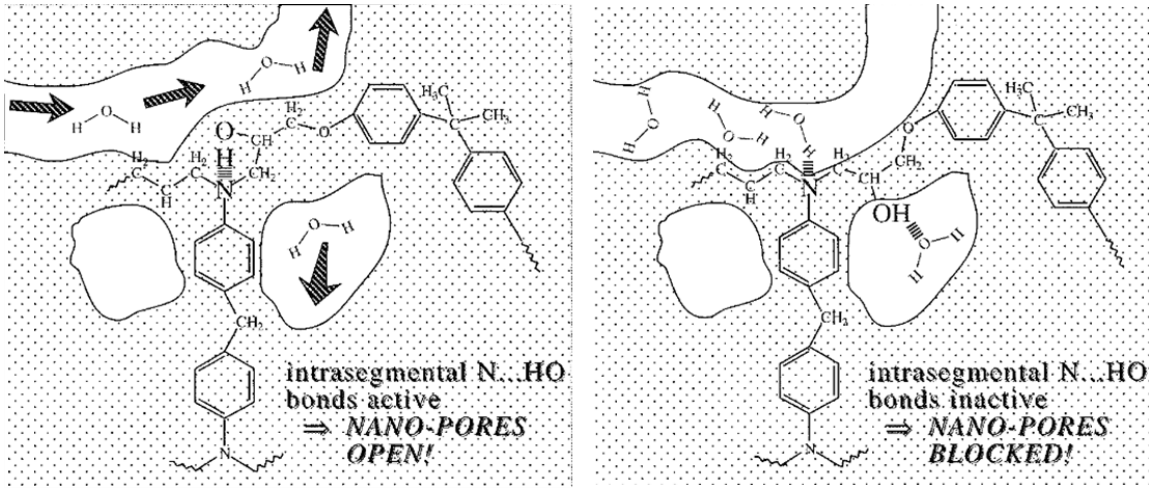

Figure 28 – Polar interactions between epoxy chains and water. Left) Intra-chain interaction cannot block water diffusion. Right) H-bond interaction between chains and water molecules slows the diffusion rate.

Overall, these are interesting studies but are quite hard to generalize as a guideline for an ideal material. Another take on these issues would be to reduce the consequences of water uptake in order to prevent delamination. A classical strategy is to improve the bonding strength to decrease the adhesive failures caused by humidity. Several effects can promote the adhesion between materials and in 1987, Kinloch proposed four main theories ruling the adhesion strength: mechanical interlocking, adsorption, diffusion and electrostatic forces [46].

Ferguson and Qu (2006) [47] experimentally tested adhesion of a mirror polished pure copper to an unfilled epoxy (minimal interlocking). After hydrothermal aging (85°C, 85%RH for 168h), the adhesion strength of the epoxy was only a third of that of the reference samples (9 J/m² for control samples to 3.76 J/m² for the worst result). Based on Kinloch's equations, they calculated that the work of adhesion between copper and epoxy, for an "adsorption only" interface would reach 260.7 mJ/m² in a dry state and -270.4 mJ/m² when water is present at the interface. This means that delamination can occur spontaneously at such a clean and smooth interface instead of requiring work when water is adsorbed on the surface of those two materials. In comparison with the experimental values however, it is clear that despite trying to prevent interlocking, this effect is still at play (roughness is non null) and still makes the largest part of adhesion (9 J/m² for experimental values compared to 260 mJ/m² for the calculated part of adsorption) as diffusion and electrostatic interactions should indeed be minimal (clean, unoxidized smooth metal surface).

Mechanical interlocking is a very powerful interaction that can represent a large portion of the adhesion strength, provided that the polymer resin shows good wettability with the rough surface, creating a wide anchor effect and increasing the surface area available for the other adhesion forces. Cho and Cho (2000) rated the highest adhesion of epoxy resins onto oxidized copper at 200N/m, compared to approximately 50N/m for un-oxidized copper. The oxidation was achieved by etching of the natural thin oxide of the copper in a dilute solution of sulphuric acid solution followed by baking in air at 175°C, resulting in a rough and oxidized surface suitable for interlocking and chemical interaction with the resin [48]. This process emulates several commercial solutions that are sold as adhesion promoter for copper surface treatment in the field of PCB.

As a conclusion, preventing water uptake at a material level through formulation is quite a challenge, especially given the number of other specifications an ideal dielectric must have. Developing water barriers seems more beneficial as a system-level improvement for the overall reliability of new packages, preventing water uptake entirely. If the water barrier is ever breached however, providing the highest adhesion strength with mechanical interlocking can help mitigate the occurrence of delamination that could occur. Trying to slowly bake the moisture out of the package could be a valid solution before going into more aggressive power cycles [8], [32].

e. Summary of specifications for the ideal PCB material

From the afore mentioned required properties, it is possible to summarize the ideal specifications for a polymer intended for PCB embedded design of new high-power converters. Overall, the entire set of properties required cannot be solely defined by the polymer matrix, but rather are a product of the matrix properties, the composite nature of the final material as well as a clear definition of the system operating conditions and expected life-cycle. In order to propose the best embedding material, one should look at all of these considerations and tune the final material accordingly.

As a general note, it seems like using inorganic nanofillers is a promising approach to improve the thermomechanical performances (lower CTE, higher thermal conductivity) and increase the resistance to partial discharges without sacrificing on dielectric strength. Apart from the process related properties like adhesion strength, determining the glass transition temperature and the

acceptable level of water uptake is also necessary to consider the final system design. A tuneable Tg and the use of water barriers would be valuable concepts to counter most problematics.

Table 2 summarizes the properties range of both reference materials (silicone gel and FR4 composites) and the ideal specification a new dielectric could have. For each rated property, a qualitative indication is used to mark if the given property in predominantly dependant on the dielectric matrix, if it is more related to a composite nature with inorganic fillers or if it is rather a result of the system architecture and processes.

Table 2 – Dielectric materials ideal properties for a PCB embedded design

Properties	Silicone gel	FR4 composites	Ideal dielectric	Matrix dependant
Dielectric Strength (kV/mm)	15-20	50	> 50	Yes
Volumic Resistivity (Ω.cm)	10^{14} - 10^{16}	10^{13} - 10^{15}	10^{13} - 10^{16}	Yes
Thermal Stability (%wt)	N/A	5 at 320°C	< 5 at 320°C	Yes
Chemical resistance	High	High	Highest possible	Yes
Glass transition Temperature (°C)	Below the application range	Above the application range	Tuned to lower thermal stress	System level
Thermal Conductivity (W/m.K)	N/A	0.9 - 1	> 1	Mostly Composite
Tensile Strength (MPa)	N/A	> 240	Comparable to FR4	Mostly Composite
Flexural Strength (MPa)	N/A	≥ 400	Comparable to FR4	Mostly Composite
Elastic Modulus (GPa)	10^{-4} to 10^{-3}	> 21	Stiffer than Si-gel Softer than FR4	Mostly Composite
CTE (ppm/°C)	>300	50-70	3 < CTE < 16	Mostly Composite
Compliant with HDI	No	Yes	As much as possible	System level
Adhesion	Moderate	High	Highest possible	System level
Water Absorption	Moderate	High	Lowest possible	System level

4. Self-healing concepts as innovative approaches to reliability

1. Concept of self-healing for improved reliability

Despite the selection of an ideal material, it is clear that thermomechanical failures of highly stressed PCBs cannot be solved solely by aggregating the best available properties on one material. With the need to guarantee safe operation for an ever-increasing amount of time, the question of the reliability of dielectrics still remains.

Preventing all mechanical damages during the whole aging of these highly stressed systems seems like an impossible task, as it may depend too profoundly on the architecture, processes and the intended mission of the device. However, new materials are being actively researched, with the intent to provide them with robust healing capabilities.

While these materials are most often developed with structural applications in mind, but having an insulator capable of filling holes or even recovering its structure entirely following a mechanical damage seems also very valuable for electrical applications suffering from thermomechanical damages that favour electrical failure modes.

With this in mind, developing a material that can recover its mechanical integrity could not only help to extend its lifespan by preventing catastrophic damages, but could also decrease the prevalence of failures by reducing the risk of aggravation of non-critical defects (damage prevention approach). **Figure 29** shows the ideal self-healing behaviour in relation to the end of life and therefore reliability of a system [49]. As such, self-healing concepts will be reviewed in this work with a focus on high-end electrical application and the intent to use self-healing properties as a way to improve the reliability of electrical systems.

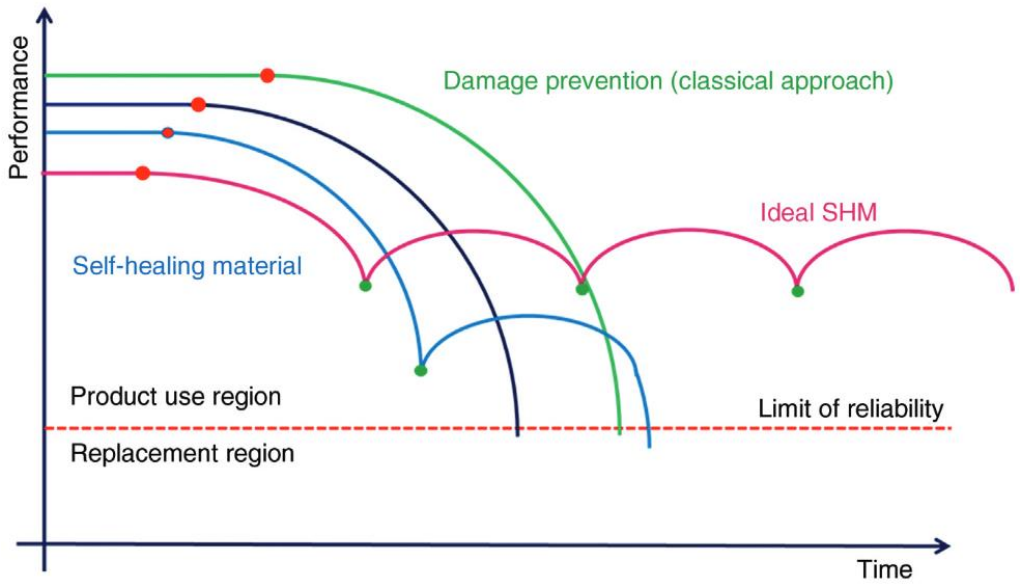

Figure 29 – Different approaches to material-based reliability. Typical material (dark blue), Damage prevention approach (green), one-shot material healing (light blue), ideal self-healing material (pink) [49].

2. Definitions of self-healing

a. Repairing functions not materials

Self-healing is a broad and general term that does not clearly points towards a material property. When heard for the first time, this term might be evocative of science-fiction novels, as it seems

almost inconceivable for a real material to be able to revert its aging process, repairing the critical damages it received and becoming healthy anew. That is because this is not what self-healing is. Reverting aging and recovering a material as new as the first day it was created is not possible with the technology available today. When a damage occurs, the system changes forever, atom placement will be different, and the subsequent properties of the material will most likely change.

This change of properties is where self-healing actually matters, as the measurement of a set of properties is related to the macroscopic use of the material, that is intended for a designated function. Damage can be present and still the related property might not be affected on a given observation time, resulting in a functional material. Alternatively, damages can be recovered while some of its initial properties remains deteriorated, making the material less effective at its originally intended function.

This means that the determination of the healing capabilities of a material is related to the evaluation of a function of a material. In that regard, the damaging mechanism does not have to be directly related to the recovered property, but rather simply needs to impact said property in order to be evaluated. In order to rate the efficiency of the healing process, one must define the properties related to the function and assess if those properties are indeed recovered after the healing process. In that sense, healing efficiencies can be superior to 100%, as the healed material could even outperform the original one.

Figure 30 shows different materials that were mechanically damaged. In the case of the broken pole, it is clear that the intended function to be recovered is mechanical integrity, albeit with a very low efficiency since this amount of duct tape is nowhere close to the rigidity of a new wooden pole. However, in the case of the broken bowl, the *kintsukuroi* or "*golden repair*" satisfies both the mechanical integrity function, as well as an aesthetic function. In that regard, one could argue that the aesthetics of such a repaired bowl is superior to its unbroken and unrepaired counterpart. Finally, biological systems are known for their incredible healing capabilities. In this last example, a leaf has been damaged and its own healing mechanisms helped closing the injury and repaired many different functions. The shape factor, the protection against the environment, the reinforcement of weaker spots could be invoked as many functions that could be repaired with great efficiency. However, one could argue that the color inherently associated with the photosynthesis function has not been recovered at all.

In this thesis, the healing efficiency will therefore be evaluated based on a set of initial properties relevant for the electrical insulation function, that can be degraded in a meaningful way resembling failure modes encountered in the application frame, in comparison to their recovered value that can be measured after the healing process.

Figure 30 – Example of healing of mechanical damages for the recovery of different intended functions.

b. Classification of self-healing mechanisms

(i) Autonomicity

A self-healing reaction always needs a trigger to begin the recovery process. Either this trigger can be the damage itself, in which case the healing will be described as autonomic, or it can be activated through a variety of conditions set from the outside, in which case the healing will be described as non-autonomic.

Most of the time when referring to "self-healing", it is implied that the mechanism is autonomic which means that the conditions in which damage occurs are sufficient for significant recovery, in that case, the process will start as soon as the damage has been dealt. Very few materials show true autonomic behaviours, as self-healing requires a mobile phase in order to bring new reagents/molecules near the damage site or even physically closing a gap. This process is most often activated by heat or other energetic stimuli in order to achieve recovery in a decent amount of time (kinetics and thermodynamics involved). In that case, the healing process is referred to as non-autonomic.

It may be difficult to determine either a material is autonomously healing or not in some situations. Materials that experience very different conditions during their lifetimes can adopt autonomic and non-autonomic behaviours alternatively. As an example, in heat cycling devices such as power modules, the materials can experience a wide range of temperature that can activate or inactivate the self-healing phenomenon without external intervention.

Skin reconstruction is often cited as a comprehensive example for autonomic self-healing; as an autonomic mechanism, the mobile phase (blood) automatically starts flowing towards the damaged region as soon as the damage has been dealt without requiring external action (bleeding). Though is it reasonable to expect a slowed or disrupted recovery in drastically cold environments, as blood may not flow properly to the wound and heat will be needed in order to ensure recovery, therefore showing a non-autonomic behaviour.

(ii) Extrinsicity or Intrinsicity

Alternatively, re-establishing continuity of a set of properties most often requires a physico-chemical change in the material. As stated before, the healing process always involves a mobile phase that can intervene in the damaged section of the material to repair it. This can be achieved in many ways, but the overall process can be classified into two sub-categories: extrinsic and intrinsic healing.

Indeed, a material could inherently possess the ability to reorganize parts of itself, either by physically changing its geometry as it can occur with shape-memory, or by chemically altering its structure to create a new atom arrangement. In that case, the healing process is called "*intrinsic*". Or the material may require an external force or an additional supply of chemical reagents in order to do so. In that case, the healing is called "*extrinsic*". Following this definition, the melting of a broken gold piece could be considered a physical intrinsic healing process, although non-autonomic is most situations. On the opposite side, the use of melted solder to repair a defective contact on a power board could be considered an extrinsic, and also non-autonomic process.

Again, it might be difficult to use this classification is some cases. Following with the skin analogy, it is not actually skin that reorganize itself on a physico-chemical level to close a wound. The blood (mobile phase) will carry inflammatory compounds and new building blocks for conjunctive tissues that will slowly degrade into skin material as the wound heal and age. It that regard skin healing would be and autonomous extrinsic process at the start (closing of the wound) and an autonomous intrinsic mechanism at the end (refining of scar tissue). It is worth noting than even in this case, the

resulting scared material will exhibit different properties from the previously intact skin, still leading to aging.

3. State of the art of self-healing strategies

Polymers are the most versatile materials for self-healing. In order to produce a mobile phase, polymeric materials do not need excessive amounts of energy as it may be required in metals and ceramics. The wide variety of chemistries available allows infinite design and tuning of every aspect of polymeric matter. This flexibility in the elaboration process motivated countless studies developing self-healing over a huge field of applications. But due to the large development of organic composite materials, they can also accommodate many physical means of recovery such as expanding phase composites or shape memory [49].

a. *Extrinsic approach: composite healing*

(i) *Microcapsules*

Microcapsules are a simple way to grant self-healing properties to a polymer. The healing agent is encapsulated within a thin membraned capsule that can be ruptured by a crack, releasing its content that can react on site to fill damaged area with a newly formed material.

White et al. (2001) are considered as pioneers of this method, as they were the first to show efficient healing through micro-encapsulation of monomer within a matrix containing the catalyst required for the polymerization. After damaging the sample, the ring-opening metathesis polymerization (ROMP) process was identified by infrared spectroscopy and confirmed that actual polymerization had been achieved [50]. The chemical reagent contained within the capsule is not always a precursor of the polymer supposed to react to a catalyst; Hager et al. (2017) reported some attempts using pure solvents or two reagent systems for example. In fact, several authors went down this path and presented similar solutions for self-healing polymers. Hillewaere and Du Prez (2015) summarized the most promising chemistries used for such concepts [51].

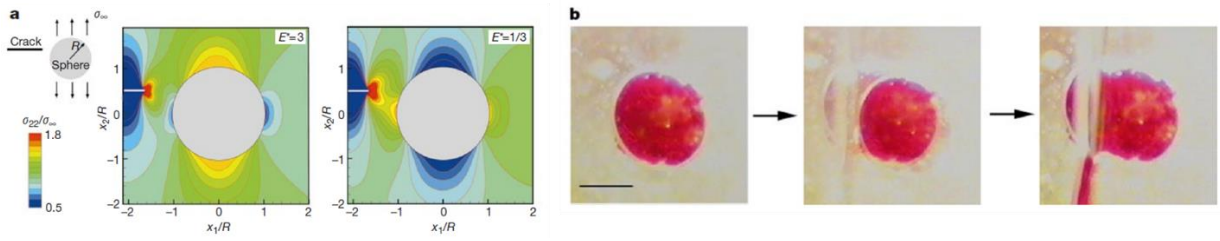

Figure 31 – a) Stress profile near a spherical inclusion embedded in a linearly elastic matrix and subjected to tensile loading perpendicular to the fracture plane. Difference of stress channelling between equally compliant (E*=3) and a three times more compliant (E*=1/3) inclusions compared to the matrix. b) Observation of the release process (scale bar = 0,25mm). [50]

Unfortunately, it is known that capsules tend to break during manufacturing processes, which greatly reduce the healing capabilities of such solutions. Protective outer-shells have been developed to try to counteract this effect, but harder, less compliant capsules tend to deflect the cracks instead of channelling them, resulting in a less effective recovery as less cracks will be filled. White et al. found that the capsule should appear 3 times more compliant than the matrix to demonstrate a channelling effect [50] (cf. **Figure 31a**). In addition, the use of capsules is limited to small damages as it is difficult to fill bigger voids with a small volume of reagent, very small cracks could also be a challenge as the unreacted monomers might not flow properly inside of tiny gaps. This solution also relies on the fact that damage will not happen twice on the same position which makes them unreliable for applications where stress is likely to concentrate at the same spot.

All of these issues make microcapsules difficult to use with a PCB application in mind, where pressure and lamination will be regularly used. Additionally, it is likely that cracking will occur several times in the same area as power module concentrate most stresses around the active components.

(ii) Vascular networks

In order to ensure more healing cycles, vascular-like networks have been developed. With the ability to carry fluxes of healing agents coupled with highly networked structure, these systems seem to resolve some of the issues encountered with microcapsules.

White's team (2007) have since worked on these new architectures to enhance the healing capabilities of their extrinsic concept. A microvascular system was designed around the same chemistry but this time the system was able to recover properties over 7 cycles (between 30 and 70% efficiency on facture toughness) [52] (cf. **Figure 32**). While this is certainly a big step forward, the restricted cycling ability combined with the low recovery efficiency might not be worth the technical challenge of implementing such a network into a complex assembly like power modules. Authors recognize that resupplying the network and dealing with catalyst depletion is challenging and advise to investigate dual component networks in order to gain more healing cycles. This means having two intertwined networks with all the technological challenges it presents.

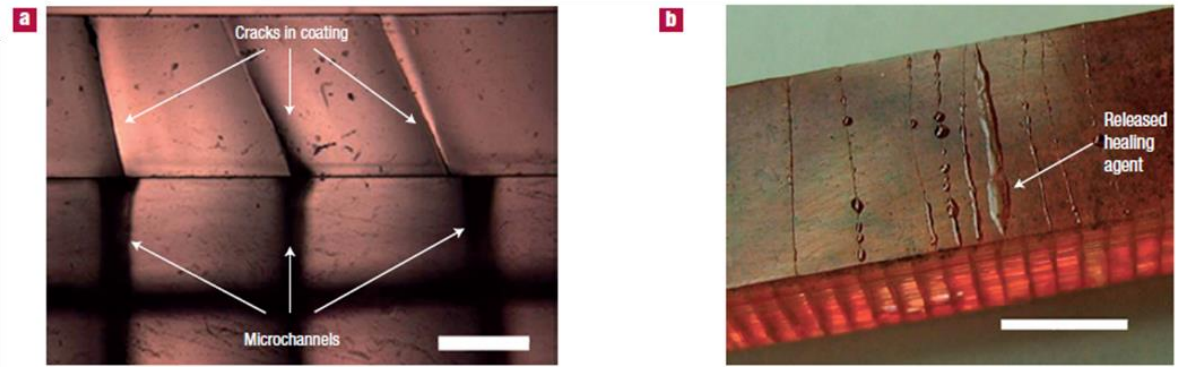

Figure 32 – a) Cross-sectional image of the coating showing that cracks initiating at the surface and propagating towards the microchannel openings at the interface (scale bar=0.5 mm). b) Optical image of self-healing structure after cracking, revealing the excess of healing fluid (scale bar=5 mm). [52]

The best attempt is described as a dual vascular network containing epoxy resin and an amine hardener, where the healing efficiency is comprised between 40 and 80% and cycling capabilities around 30 cycles. These micro-channelled systems seem promising even for large scale damages but viscosity of the precursors remain a technical challenge for filling big voids. High viscosity is desirable in order for the reaction to trigger near the damage site, but low viscosity allow further penetration of the healing agent into bigger cracks [49].

Although these methods show promising results, they are very complex to implement and introduce additional potential damage sources such as adhesion between the vascular network and the matrix, channelling of cracks alongside it or even heat expansion or phase change of the reagents inside the network. Being able to interact with the network seems very important and might not be compatible with an enclosed implementation within a power module or other technical parts of a power electronic assembly.

In conclusion, there is no extrinsic solution that can currently fit the needs for high power electronics applications, requiring a high level of reliability to work in stressful environments.

b. Intrinsic approach: Chemistry of healing

(i) Non-covalent bonding

All intrinsic self-healing concepts are related to the ability of a material to create and break chemical bonds in order to build a dynamic molecular network. This way, the network is able to flow and provide the necessary mobility required for rebinding. This way, after a damage event, the material will flow and enter back into contact with the other side of the crack, rebinding the network on a molecular level. Therefore, by imparting a dynamic network to a material, one can effectively grant intrinsic self-healing properties to the resulting material. Interestingly, since this healing behaviour is a macroscopic reflection of a microscopic dynamic effect, the more bonds that are subjected to this dynamic network, the easier the healing process can be observed.

Despite being considered much weaker than covalent bonds, non-covalent bonds represent a larger portion of the total bonding energy that is contained within most organic systems, simply by their sheer number and variety. In fact, most of intermolecular interactions are related to non-covalent bonds, including ionic bonds, hydrogen bonds, Van der Waals forces and other electrostatic or hydrophobic effects. Due to their inherently weak nature, non-covalent bonds are reversible, meaning that the link they provide for cohesion can be easily broken and reformed dynamically. These exchanges can happen rather quickly, weakly binding the participating molecules into a rather cohesive solid called a supramolecular network.

Hydrogen bonds are very common and are considered as the most stable non-covalent bonds. A common proton will be shared between a hydrogen donor group and an acceptor group, in a very fast exchange. In this dynamic reaction, the proton can be considered as "*part of both groups*", even though the interaction is considered mostly electrostatic, making it harder to separate the two molecules. Chen et al. (2012, 2014) [53], [54] tried to elaborate a polymer network, driven by hydrogen bonds in order to grant it self-healing properties. In both attempts, the resulting polymer could be healed after mechanical damage at moderate temperatures (25°C and 60°C) over the course of 24 hours (see **Figure 33**). Healing efficiency was rated on the extensibility of the material, which could recover between 92 and 100% of the original value. In both cases however, the polymers showed low glass transition temperatures (from 2 to 5°C) and overall weak mechanical properties. Indeed, hydrogen bonds have mostly been used to design very soft rubbers and hydrogels for low temperature applications with low mechanical strength and high deformability requirements [55]–[59].

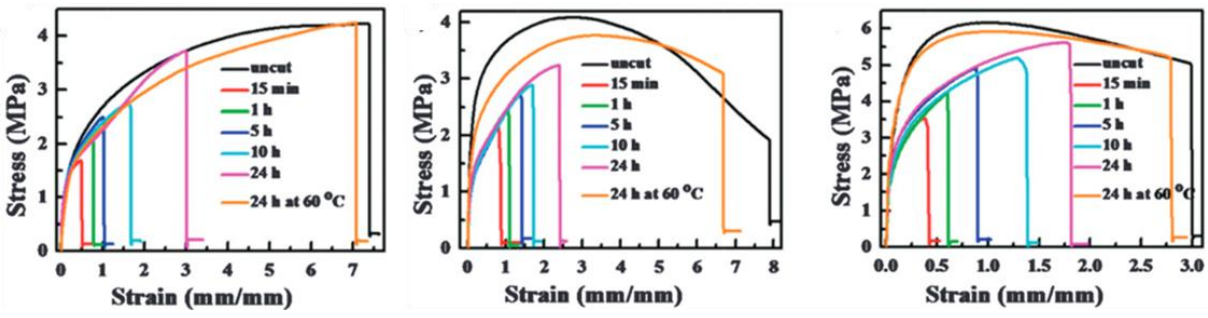

Figure 33 –Tensile tests evaluating the self-healing efficiency of three block copolymers with multiple H-bonds (Cut, pressed for 1min, healed at 60°C for 24h) [54].

Several other solutions have been investigated for non-covalent self-healing. Ionomers (polymers with discrete ionic charges) rely on ionic electrostatic bonds to generate cohesive forces within the network [60]. Pi-Pi stacking rely on the stabilisation between π orbital systems of two molecules (usually aromatic rings) to assume a lower energy state, therefore softly bonding the molecules

together [61]. And host-guest interactions often involve chelating molecules that bond to metals and form a coordination complex [62].

Still, each of these solutions relies on very weak energy bonds that would result in a low cohesive material, unsuitable for high temperature applications.

(ii) Reversible covalent bonding

Covalent bonds are known for their exceptional stability. They are the main bonds that organize most of solid matter and covalently bonded solids usually exhibit high mechanical properties due to the high stability of their molecular network. Covalent bonds are generally considered to be the result of irreversible reactions as the energy required to break them will also be high enough to degrade the whole molecular structure.

Still, there are covalent bonds that are less stable than others and that can be broken with lower amounts of energy, effectively leading to a reversible covalent bonding reaction. By designing a network that relies on such reversible covalent bonds, one can make an intrinsic self-healing material that should exhibit much higher mechanical properties than its non-covalent counterparts. This peculiar covalent yet reversible networks are called Covalent Adaptable networks (CANs) and are the subject of many recent studies [63].

CANs can be separated into two subcategories: Dissociative CANs and Associative CANs. Dissociative networks are almost entirely based on the Diels-Alder (DA) chemistry, or "*click chemistry*" where the bond is entirely reversible, meaning that chains can exist in the two linked or unlinked state (cf. **Figure 34**). This type of chemistry is very diverse and regroup several reactions that can be used for reversible covalent bonding. Among these solutions, several chemistries are available and applicable to a wide variety of materials, even for the most technical applications. As an example, several modifications of epoxy resins have been performed, using different reversible covalent bonds in order to prepare high stiffness healing epoxy compounds, with elastic moduli in the gigaPascal range [64], [65]. Another attempt focussed on the possibility of making self-healing epoxy composites using Diels-Alder chemistry [66].

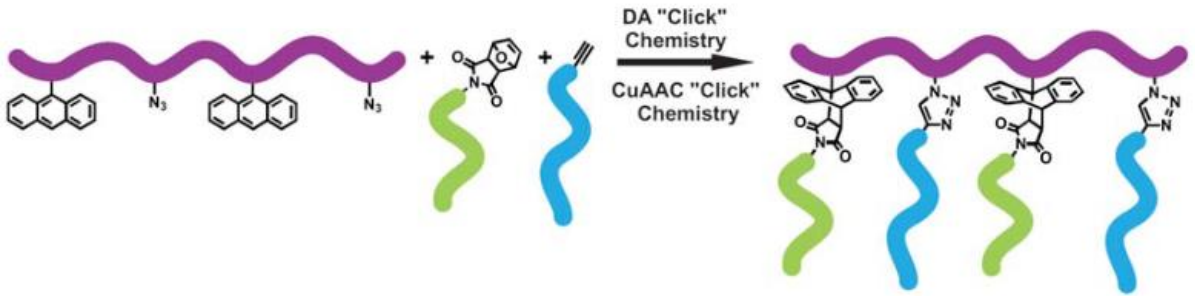

Figure 34 – Example of 'click chemistry' reactions, based on the Diels-Alder chemistry [67].

Diels-Alder chemistry classifies towards the "high temperature" side of intrinsic solutions. Chen et al. (2002) made a reversible network that is fully composed of reversible covalent bonds by polymerizing a tetra-furan with a tri-maleimide monomer in stoichiometric ratio. It was found that the polymerization process would require 23kcal/mol (or 100kJ/mol) which is little in comparison to the energetic stability of other covalent bonds [68]**.** It is claimed that heating the polymer to 150°C for 15 min would break 25% of the cross-linking reversible bonds. Those bonds were expected to be completely reformed after 1 hour at 80°C and tensile strength was estimated at 50% of its original value after a complete cut through the sample [69].

Other authors reported the same temperature range for furan-maleimide Diels-Alder reactions (about 60-90°C) and retro-Diels-Alder reactions (about 120-150°C) with variable property recovery [64], [66], [70]–[72]. Precise data is hard to compile as the wide variety of polymer nature allow for disperse results and overlapping effects.

The dissociative nature of such concepts heavily favours the flowing capabilities of the material, which is important for an effective healing opportunity when a gap is created in the material. Depending on the number and arrangement of the reversible links, one can depolymerize partially or completely the reticulated network [69], [71]. This can be a strength and a weakness, as DA reactions (towards bonding) and retro-DA reaction (towards un-bonding) are triggered by heating. The starting temperature for retro-Diels-Alder reactions can be as low as 80°C but the general range is about 120 to 150°C, making it difficult to be applied in high temperature applications where mechanical strength is still required.

On the other hand, associative CANs are designed around a competing equilibrium between chemical groups situated on the polymer chains. In order to disconnect from one end, the chain must first be bonded with another group that will keep the continuity of the network, before being able to rearrange its structure and remove the previous link, effectively conservating the average crosslink density at all times (cf. **Figure 35**).

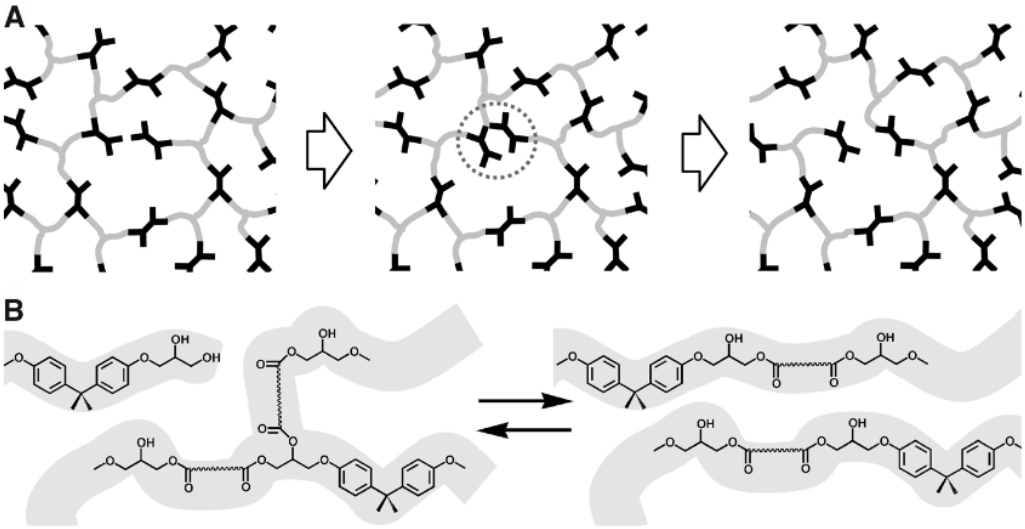

Figure 35 – Associative Covalent Adaptable Network. A) Example of the association process, dotted circle shows a metastable state between exchanges, B) Example of two polymer chains exchanging moieties [73]

Associative CANs can be based on an increasing number of chemistries, as more and more research is focussed on this concept for a growing number of applications [74]. As a general rule, the healing effect is driven by the exchange kinetics between groups, that are mostly dependant on temperature. In that regard, increasing the temperature should increase the rate of healing, without compromising entirely the mechanical stability of the network, as it can be the case with dissociative CANs. However, sufficient energy must be provided for the reaction to be noticeable at reasonable timeframes, making the healing process effective in the range of 120 to 150°C.

It is possible to obtain high stiffness self-healing materials using such concepts. Fu et al. (2018) [75] demonstrated the high flowing capabilities of their self-healing polymer, closing a 65µm gap in less than 40min at 140°C. Despite such an effective mobility, the polymer still shows elastic moduli of 5GPa below Tg and up to several hundreds of MPa above Tg.

c. Conclusion on self-healing concepts for PM reliability

Intrinsic concepts seem highly desirable compared to extrinsic concepts, as the whole material gains the ability to heal at any point within its volume. This feat allows to spread healing capabilities more evenly compared to capsules or vascular networks and enables a higher number of healing cycles, without the need of breaking a complex embedded system. Additionally, given that the healed material has conserved the intrinsic healing properties, intrinsic solutions could theoretically reach infinite cycling potential, making it a promising solution from a reliability perspective.

Among the available intrinsic solutions, reversible covalent bonds seem more aligned with the mechanical strength and thermal stability requirement, mandatory for high power module applications. The ability to create higher stiffness networks while also being able to choose from a wide range of chemistries makes it a good research base to build on.

Finally, within adaptable covalent networks, associative CANs seem more stable in the high temperature range, without ever risking complete depolymerization. This is a very big concern as most expected healing temperatures for organic systems are expected below 200°C, thus at the same operating temperature range of the new power modules. By being able to maintain a sufficient mechanical stability at such temperatures, the dielectric would therefore be able to heal at each power cycle autonomously.

Conclusion

In this chapter, the conventional module design and its limitations in terms of reliability were reviewed. The root cause of most failure was attributed to thermomechanical stress and dielectric aging, damaging the top and bottom connections and increasing the risk of dielectric breakdown during the lifetime of the device.

New designs have made their way up to full production level and using new approaches in the way to build power electronic modules. Either by using wide band gap components, changing the way interconnections are made in the package or replacing the dielectric with stiffer materials, many core aspects of power modules are changed. At the heart of these changes, PCB-embedded architectures seem to aggregate the better performances, with high integrability, high efficiency and much more effective cooling options.

However, such drastic changes bring new unknowns in terms of reliability, as the conventional materials and processes are often not suitable for the new specifications. As it is right now, silicone gel seems very limited in terms of dielectric strength for the increase of power density that comes with new components. Additionally, it cannot mechanically support the highly integrated structures that are proposed with PCB technology. On the other hand, FR4 materials traditionally manufactured for PCB applications are not designed to sustain such harsh power-cycles, resulting in mechanical failure and inducing future insulation concerns.

Trying to understand the right specifications without a clear applicative frame is quite challenging. By comparing reference materials currently used as dielectrics (FR4, silicone gels) and examining the reliability requirements of next-generation power devices, a set of material specifications is proposed that can be understood as a best expected compromise between the electrical and mechanicals properties. Of course, this set of properties should be seen as a guidance since the result of this compromise may be significantly affected by the precise application framework and module design. Yet, designing a material even with limited compromise for its properties does not guarantee to solve the mechanical failure problematic surrounding the aging of PCBs.

Therefore, investigation of novel, disruptive concepts like self-healing is proposed to address this concern. A review of self-healing concepts for polymeric materials was provided and allowed to evaluate the compatibility of each concepts with the expected specifications and operative conditions of new power modules. For this application, an intrinsic self-healing material based on reversible covalent exchanges seems like the most promising solution. Focusing on associative networks, such a new material can potentially perform its healing process autonomously without depolymerization at the operation temperature of the device, theoretically increasing the healthy lifetime of the dielectric in service.

The heart of this thesis is thus to select an appropriate chemistry for an associative Covalent Adaptable Network (CAN) and synthesize these materials to investigate their applicability and performances measure in a power electronic framework.

CHAPTER II – Selection and elaboration of a self-healing polymer for power module insulation

Chapter II: Selection and elaboration of a self-healing polymer for power module insulation.

Introduction

Amidst the numerous self-healing concepts developed in the literature, associative covalent adaptable networks are expected to be the most aligned solution with the power module application field. Different chemistries have been reported to create reversible bonds and are increasingly applied in polymer science.

At the origin of the recent interest for associative CANs, vitrimers based on the transesterification chemistry are one of the most studied concepts due to their high flowability in temperature and the easier synthesis reaction. Such vitrimers can be obtained directly from the reaction of commercial epoxy resins typically used for PCB manufacturing with carboxylic acids, making them a synthetic route of choice to be used with other PCB related processes.

Conveniently, several studies discussing the selection of the appropriate catalyst and stoichiometric ratios between the precursors have been proposed, allowing to select the most promising precursors and tune the properties of the vitrimer matrix to the desired needs. Increasing the amount of hydroxyester is favorable for faster exchange rates, while tertiary amines and metal salts seem to show the fastest relaxation times, presuming of better self-healing capabilities.

As a very first dive into vitrimer elaboration, key parameters must also be accounted for to develop a robust process. The homogeneity of the pre-polymer, the time before gelation or the temperature and reactivity of the precursor mix are all crucial parts of a successful elaboration process.

Similarly, a robust manufacturing process must also be developed to produce samples for further characterization. Using hot press-molding, it is possible to produce either films or bulk samples using customized molds, but pressure homogeneity and proper pressurization of the mold are challenges that need to be addressed in order to make repeatable and defect-free samples.

By characterizing the appropriate alcohol and ester functions in the catalysed material, one can assume that transesterification can be observed on reasonable time frames and that healing capabilities are measurable. Alternatively, demonstration of the cross-linked, unfusible nature of the polymer is also critical to ensure that the healing properties can indeed be linked to the dynamic exchanges in the network.

Self-healing properties are often rated using the reprocessability of the material, purposefully shredding and mending the material in a controlled manner, using high temperatures and pressures. However, using such an indicator for quantification of healing efficiency in a reliability perspective is rather biased, as damage is often unexpected and uncontrolled and application of a constant external force is almost never possible directly in the field. In this regard, using shape memory may be a useful strategy to generate pressure internally, thus helping the healing process autonomously.

1. Selection of an associative chemistry

1. Transesterification

The trans-esterification reaction is a renowned chemistry used in diverse fields, such as the production of polyesters, the refinement of biofuels or in analytical chemistry. This reaction is based on ester and alcohol groups exchanging their moieties and yielding new ester and alcohol groups, thus making the reaction reversible. This reaction can be catalysed by free hydroxyl groups but is usually sped up by the use of external catalysts such as tertiary amines. Transesterification is usually displayed around 150 °C with activation energies of about 80kJ/mol, but playing on the type and quantity of catalyst allows to tune the starting temperature and the activation energy of the reaction and thus the observable viscoelasticity of the network [76]–[78].

The reaction is resolved in two steps, first the nucleophilic addition of the alcohol to the sp2 Carbon takes place, then the elimination of the other alcohol through rearrangement of the electronic configuration of the carbon is achieved. Since the products are also an ester and an alcohol, the reaction can occur in reverse (cf. **Figure 36**).

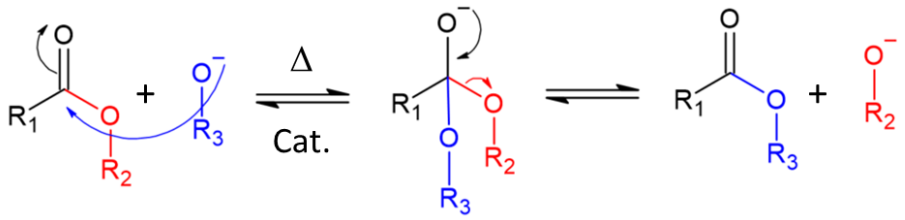

Figure 36 –Catalysed transesterification between ester and alcohol groups, showing the metastable intermediate state.

In 2011, Montarnal et al. (2011) [73] published the first article demonstrating the ability of a polymer to exhibit dynamic bonding through transesterification with the intent to create a permanently cross-linked material that remains processable. By mixing epoxy resin with multifunctional carboxylic acids, they obtained a thermoset polymer bearing both alcohol and ester groups necessary for trans-esterification. By introducing different amounts of zinc acetate as the catalyst, they could control the mechanical relaxation time constant of the vitrimeric transition, exhibiting an activation energy of 88kJ/mol. The resulting material resembled a hard epoxy resin with a Tg of 80°C and showed high mechanical properties, with a modulus of 1.8GPa and a maximum tensile stress of 55MPa, that could still flow above 100°C. Healing efficiency was not explicitly quantified but the recycled samples obtained by reprocessing samples at high temperature exhibited almost identical tensile profile compared to the pristine ones, ranging the healing efficiency on this test near or above 80%.

Following this work, several studies have been published with similar self-healing epoxies based on trans-esterification, obtained from different precursors but all showing high mechanical properties and thermal stability [79]–[82]. With the innate adequation of epoxy with PCB applications, these selected examples are encouraging for the development of transesterification-based self-healing PCBs.

2. Disulfide metathesis

Disulfide bonds are well known for their dynamic nature in a large range of biochemistries, such as protein spatial folding conformations but are also widely used for industrial vulcanized rubbers. Disulfide bonds can be used in dynamic networks with the presence of other disulfide bonds through

metathesis, or by oxidoreduction with a thiolate, generating another disulfide bond and another thiolate in the process [83], [84].

Similarly to trans-esterification, disulfide metathesis can be catalysed using tertiary amines [85], but can also occur without any catalyst. Spontaneous exchanges can also happen with the thiolate reaction by nucleophilic attack onto the disulfide bond (cf. **Figure 37**) [84].

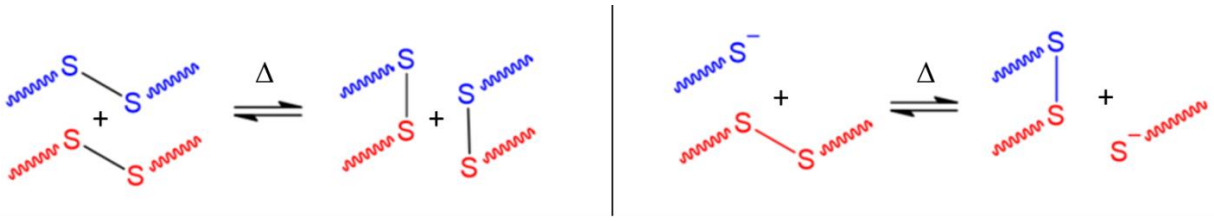

Figure 37 – Left) Disulfide metathesis; Right) Disulfide-Thiolate exchange reaction

Canadel et al. (2011) [86] proposed a self-healing epoxy containing multiple disulfide bonds in its backbone. By crosslinking the epoxy pre-polymer chains with a tetrafunctional thiol precursor, a primary cross-linked network was obtained. A reversible secondary crosslinking network was also formed through disulfide metathesis between two chains. The resulting rubber shows a glass transition of -35°C, with low stiffness (about half a Gigapascal below Tg) and could achieve a macroscopic flow near 60°C. Self-healing efficiency was assessed by breaking samples on a tensile bench. After being damaged, both parts are put back into contact for 1h at 60°C and mended samples could show a complete recovery in their elasticity and a quasi-complete recovery in their strain at break. Still, the ultimate tensile strength is lower than 0,6 MPa which shows a highly reworkable yet mechanically weak network.

Several authors have investigated disulfide healing concepts, yet, this chemistry seems to be more applicable for lower mechanical and temperature requirements (adhesives, rubbers, protective coatings, etc…) [87]–[92].

3. Transamination of vinylogous urethanes

Similarly to the disulfide chemistry, transamination reactions are less common in industrial usage and mostly found in enzymatic reactions in biosystems.

Transamination of urethanes and ureas cannot effectively create a dynamic network as is. However, through the use of vinylogous urethanes and ureas, Denissen et al. (2015) [93] managed to create a delocalized system, capable of supporting a Michael-type addition mechanism, thus creating an effective associative network that also exhibits a stronger resistance to hydrolysis compared to regular free-amine routes **Figure 38**. It was later shown that an iminium pathway is also possible [94].

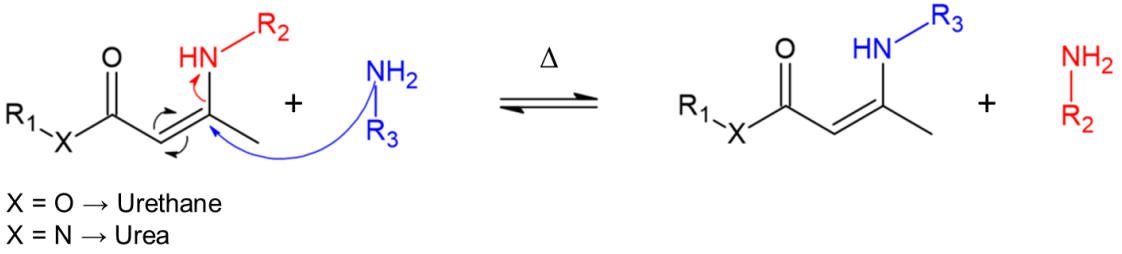

Figure 38 – Transamination of vinylogous urethanes/ureas by a Michael addition mechanism.

The obtained polymer showed interesting properties, with a storage modulus of 2.4GPa and a glass transition at 87°C. The obtained material could show relaxation times in the hundred-second range at 170°C without any catalyst, making it one of the fastest relaxation demonstrated on cross-linked polymers.

However, due to the very specific chemistry, this concept is difficult to adapt to a large range of precursors without extensive knowledge and capabilities in organic chemistry.

4. Other chemistries

Many other reversible reactions can be mentioned for creating associative dynamic networks. However, most of the chemistries reported in the literature also come with dissociative pathways, specific conditions for healing or slow exchange mechanisms. Reviews for such concepts are available, mentioning the use of transcarbamoylation, Imine/amine reactions, Siloxane-silanol reactions, transalkylation etc… [95]–[97].

Therefore, due to the limited experimental chemistry capabilities and the targeted industrial application, more in-depth or niche chemical concepts are set aside for this study.

5. Conclusion on associative concepts

Associative network concepts offer many interesting possibilities for the formulation of a new self-healing polymer. However, in the case of the reliability of new power modules insulation, mechanical strength and thermal stability are the highly critical requirements. This rules out chemistries that have clear dissociative pathways or low mechanical properties at room temperature.

Another selection criteria is the variety of precursors to choose from in order to adapt the elaboration process to the requirements of the applications.

As of now, it appears that the best chemistry would be the transesterification, which is the most aligned with the requirements of PCB manufacturing since it can be easily obtained by curing commercial epoxy resins widely used in the electronic field with carboxylic acids in the presence of the appropriate catalyst.

2. Elaboration of vitrimers based on transesterification

1. *Polymerisation reaction of epoxy resins with carboxylic acids*

Transesterification can be obtained by having alcohol and ester groups directly in the polymer chain. In the original paper presenting transesterification-based vitrimers, Montarnal et al. (2011) [73] used a stoichiometric ratio of diglycidyl ether of bisphenol A (DGEBA) resin with a mixture of dicarboxylic and tricarboxylic fatty acids (epoxy/carboxylic acid = 1) in the presence of zinc acetate, thus obtaining both of the desired groups in the form of β-hydroxyesters in the polymeric chain. To better understand the choices for this formulation, it is important to understand the dynamics of epoxy/carboxylic acids reactions.

The main reaction of epoxy rings and carboxylic acids is presented in **Figure 39** and is a chain-extending desirable reaction that will create the β-hydroxyesters responsible for the self-healing behaviour.

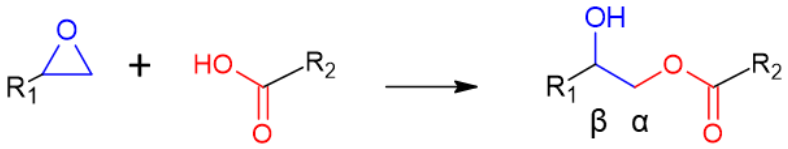

Figure 39 – Ring-opening esterification of epoxy and carboxylic acid groups, yielding a β-hydroxyester

However, side-reactions can also happen between the formed hydroxyesters and remaining epoxy or carboxylic acid groups, yielding branching/crosslinking by etherification or condensation-esterification, effectively reducing the number of ester/alcohol couples available for trans-esterification, i.e. less recombinable nodes for the network (see **Figure 40**).

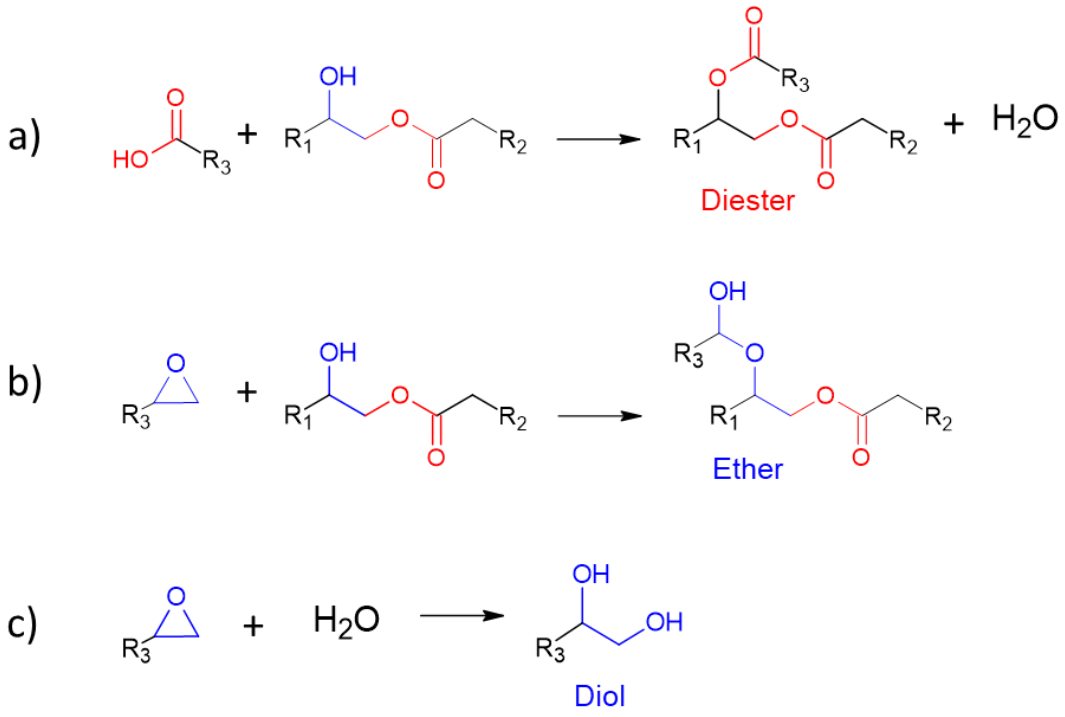

Figure 40 – a) Excess of carboxylic acid leading to condensation-esterification, b) excess of epoxy leading to etherification, c) Hydrolysis of remaining epoxy groups

By using the proper catalyst, chemists can drive the reactivity of their precursors and target a specific product from these reactions. In that case, the chosen catalyst is said to be "*selective*" and using a selective catalyst can be of great use, not only to prevent undesirable side-reactions, but also to create a non-stoichiometric mix if the formulator so desires.

Matějka et al. (1982) [98] showed that using trivalent chromium catalyst could completely inhibit the etherification of the monoester by an excess of epoxy. In this work, it is also shown that using a tertiary amine as the catalyst promotes the main esterification reaction first, while also allowing for the formation of diesters and diols in similar proportion from the formed monoesters, prefacing the transesterification reaction that two hydroxyesters could undergo together.

In conclusion, selecting a stoichiometric ratio between the two precursors ensures that minimal excess groups are available for side-reactions. And in order to promote the main reaction and prevent the eventual side-reactions that could occur, the use of a selective catalyst can be valuable, tailoring the exact desired end-product.

2. Maximizing of the exchange reaction for increased self-healing behaviour

Following on their work on vitrimers, the Leibler's research team demonstrated the role of the catalyst and the hydroxyl groups in the exchange reaction kinetics [78]. Using gas chromatography coupled with mass spectroscopy, the reactivity of model molecules bearing the hydroxyester function was studied.

By solely heating the hydroxyester mixture to 150°C, it was possible to yield new hydroxyesters through transesterification exchanges after 15h, with a conversion ratio of about 80%. When using the zinc catalyst (5mol%), the conversion approached the 100% in about 2h, showing the extensive effect of catalysis on the network dynamics. Additionally, several diesters and diols could be obtained as intermediate forms between hydroxyesters, similarly to the results shown previously by Matějka [98] **(**cf. **Figure 41)**.

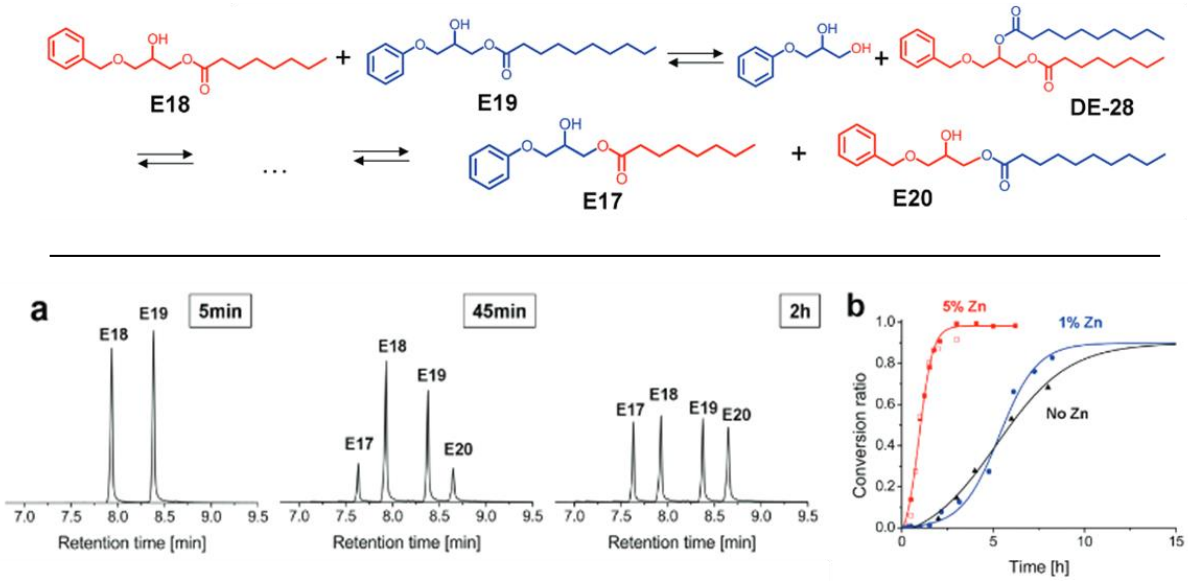

Figure 41 – Top) Hydroxyesters model molecules (E18/E19) and the resulting new esters (E17/E20). Bottom) Gas chromatography retention times (a) and the conversion ratio depending on catalyst content (b) [78].

When analysing the reactivity of two hydroxyester molecules together, the conversion ratio reaches full conversion in about 2h, whereas reacting a diester with a hydroxyester group will only reach

50% conversion in more than 30h for the same temperature and catalysis conditions. Trying to react two diesters together doesn't yield any new ester, showing no transesterification is happening in this case. Additionally, it was confirmed that having a higher concentration of hydroxyester functions in the final material would yield the strongest bond in a lap-shear test between two welded pieces, suggesting that a higher number of recombination was achieved for a higher hydroxyester content for a given welding time.

From these elements, it is clear that introducing an efficient catalyst while maximizing the material hydroxyester content is desirable for better self-healing properties (faster recombination process) and thus guaranteeing a high reliability of the repaired volumes (higher number of bonds recombined in a given time).

3. Synthesis of the pre-polymer resin

a. Precursor selection

(i) Epoxy resin selection

Selection of precursors for a new synthesis is never an easy task, especially given the environmental concerns that new materials may represent.

Most of the epoxy vitrimers developed in the literature are based on diglycidyl ether of bisphenol A (DGEBA) resin for their epoxy precursor, which is created from the reaction of epichlorohydrin and bisphenol A. While the epichlorohydrin can be made from environment-friendly sources such as glycerol, bisphenol A is a rather controversial precursor that tends to be replaced with other bisphenols, due to the fact that the ether bonds can be hydrolysed and liberate phenol groups in water. At the moment, DGEBA is still one of the most industrially used epoxy resin in the world, especially in the field of PCB manufacturing, due to its excellent mechanical and thermal properties.

In the frame of this work, with regard to the available literature focused on this resin and its adequation with the PCB application, DGEBA will be used. However, it is important to consider that this work is an opening towards new materials and that replacement of the DGEBA is very well on its way, with new competing bio-based resin that could be widely produced in the future [99].

(ii) Carboxylic acid selection

Fatty acids are typically used in the literature to make vitrimers and depending on their structure, one can expect to tune the properties of the material.

Several authors have proposed fatty acid blends to modify the network properties. Chen et al. (2018) [81] used a mix of sebacic acid and cyclohexane-diacid (CHDA) to create vitrimers with tuneable glass transition temperatures and mechanical properties (cf. **Figure 42**). In this work, they could show that the glass transition temperature can be empirically linked to the acid blend content using a mixing law and that mechanical properties are linked to the flexibility of the fatty acid used for the network. Increasing the content of CHDA, which is a short cyclic diacid, tightens the network and improves the mechanical properties but also lowers the ability to relax stress in short timeframes.

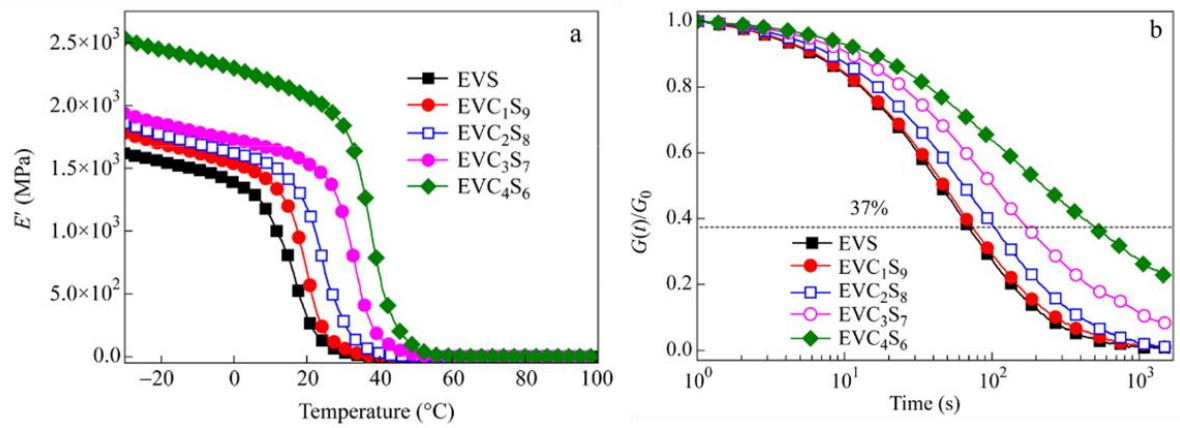

Figure 42 – Left) Storage modulus of blended vitrimers with various content of C= CHDA and S= Sebacic acid. Right) Isothermal stress relaxation of the blended vitrimers at 170°C [81].

Interestingly, the vitrimer made with sebacic acid alone presents a slightly lower storage modulus and a lower glass transition temperature (25°C lower) than the most rigid formulation (EVC_4S_6) but shows similar values of modulus above Tg and a stress relaxation that happens 10 times faster. According to the authors, increasing the rigidity of the polymer backbone with CHDA not only increased the glass transition temperature but also embrittled the material. However all of vitrimers showed excellent recyclability, which is encouraging for trying out these precursors.

Altuna et al. (2016) [79] also managed to tune vitrimer properties using blends from sebacic acid, glutaric acid and citric acid, but also by changing the epoxy/acid ratio (cf. **Figure 43**). With very similar results compared to Chen et al. (2018) [81], it was demonstrated that increasing the hydroxyl content through the use of citric acid can help to obtain higher mechanical properties, while still exhibiting the fastest stress-relaxation. Here, sebacic acid is used as a solvation medium for citric acid, making its incorporation to the network easier. Additionally, by using such carboxylic acids, the authors propose a blend that is entirely bio-sourced, since citric acid is industrially produced from fungus digestion of sugars and that sebacic acid is made from ricinoleic acid, extracted from castor oil [100].

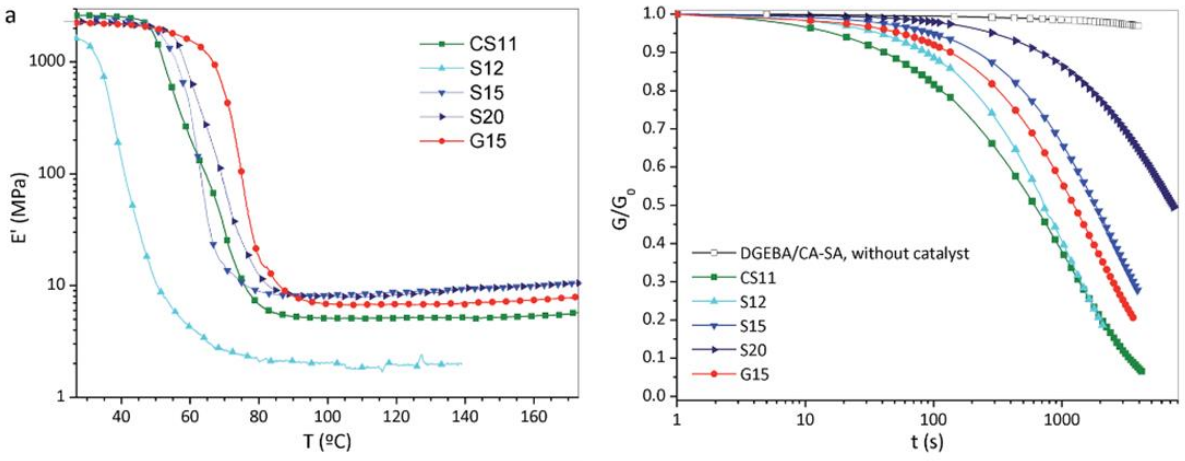

Figure 43 – Left) Mechanical properties of blended vitrimers of C= Citric Acid, S=Sebacic Acid, G=Glutaric Acid (the number is function of the epoxy/acid ratio). Right) Isothermal stress relaxation of the blended vitrimers at 160°C [79].

From these studies, it seems like sebacic acid is well aligned with the current need for flexibility, both in terms of design and in properties. Not only this precursor can be blended with many different

carboxylic acid, but it also provides a rather fast relaxation process amongst most vitrimers reported in the literature.

(iii) Catalyst selection

A good catalyst for this elaboration must serve several purposes. As mentioned before, a selective catalyst can be used to favor one product of reaction, yielding more hydroxyesters by inhibiting unwanted side-reactions. A good catalyst should also allow to increase the kinetics of the two main reactions of interest : polymerization by esterification and recombination of the network by trans-esterification.

Blank et al. studied the epoxy-carboxyl esterification using an extensive variety of catalysts. In their study, it was demonstrated that amines and metal salts are especially efficient to catalyse the polymerization of the epoxy with carboxylic acids. Imidazole are described as particularly efficient for this and depending on the basicity of the catalyst, the kinetics of the reaction can be controlled [101].

Capelot et al. (2012) [77] reviewed the different ways to catalyse the transesterification reaction and interestingly, similar compounds can be used for both the polymerization and the recombination reaction. Depending on the choice of catalyst, viscoelastic properties are changed profoundly, Zinc acetate and triazabicyclodecene (TBD) offer similar fast exchanges with a strong dependency in temperature (high activation energy) while triphenylphosphine showed slower time constants with a lower dependency to temperature (lower activation energy). Additionally, they showed that increasing the catalyst content decreases the time constant of the exchange reaction at all temperatures, but also that the activation energy is not changed (cf. **Figure 44**).

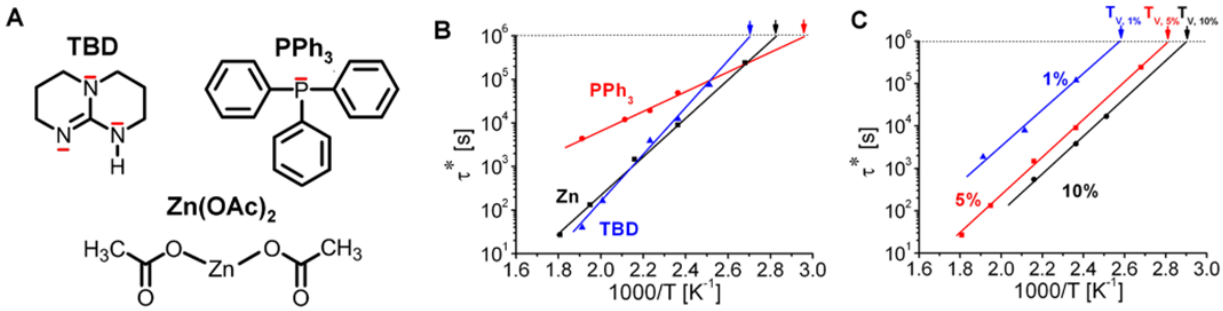

Figure 44 – A) Catalysts used in the study. B) Effect of different catalysts on the relaxation time constant. C) Impact of catalyst content on viscoelastic properties [77].

From the previous explored references, tertiary amines like TBD and methylimidazole seem efficient for all the tasks required for the catalyst (selectivity and kinetics of both reactions). Metal salts like Zinc(II)-based compounds also seem very efficient but providing a clear ionic charge on the catalyst may be in contradiction with the insulation requirement of the polymer under high voltages. Additionally, the use of tertiary amines have been identified as a valid path to homopolymerization of excess epoxy after the main esterification reaction [102]. For these reasons, tertiary amines like TBD or 1-methylimidazole are favored for this study while metal-based catalysts are set aside.

(iv) Summary

The final selection for the precursors of this study is presented in **Figure 45**.

As the main reagents for the network formation, the DGEBA/Sebacic Acid system shows a fast recombination and is compatible with many acid blends that can be later introduced to tune the properties. DGEBA is recognized as a mechanical/thermal enhancer for epoxy networks and should

pair interestingly with the long flexible chain composing the fatty sebacic acid. One concern surrounding this formulation resides in the low Tg that is not typically favored for power electronic systems, due to the expected increase of CTE above Tg. However, having a large elastic modulus drop and a fast relaxation may be a reasonable strategy to mitigate the expected rise of thermal stress from a higher CTE.

In accordance with the aforementioned references and in order to guarantee complete conversion of carboxyl groups, a 10% excess of epoxy groups will be used. In the case of side-reactions occurring during the polymerization, an excess of epoxy would increase the cross-link density by etherification, raising Tg in the process, and would still generate hydroxyl groups. Contrarily, if acid groups remained, diesters would be generated, consuming valuable hydroxyls and generating water that could prove problematic for manufacturing (bubbles, water uptake, corrosion etc…). Additionally, excess epoxy rings would react with water if generated to create dihydroxyl groups (diols) which are now identified as crucial for fast exchanges.

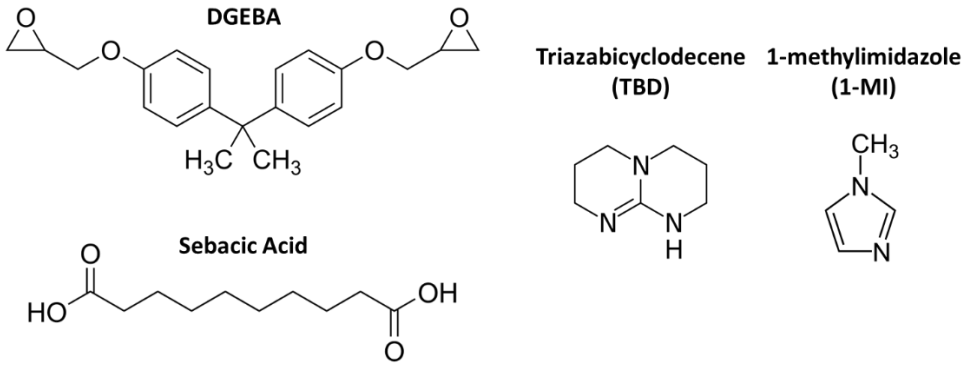

Figure 45 – Epoxy-acid and catalysts precursors selected for this study.

For catalysis, Triazabicyclodecene (TBD) and 1-methylimidazole (1-MI) have been selected as kinetic enhancers and selective catalysts for their organic nature, the fast recombination provided and the ability to homopolymerize excess epoxy. Since both the epoxy and the carboxylic acid precursors are bi-functional, the main cross-link formation path should be governed by the transesterification mechanism.

A moderate catalyst content of 5%mol should be sufficient to increase all kinetics to reasonable timeframes. This ratio will be based on the number of acid groups introduced in the material, matching the carbonyl content of the network, siege of the transesterification nucleophilic addition.

Finally, the base formulation for this study can be described as follow:

DGEBA epoxy (1,1 to acid groups) + Sebacic Acid (1) + Tertiary amine (0,05 to acid groups)

b. Polymerization process

(i) Working with multifunctional precursors

In order to prepare the pre-polymer resin with accurate stoichiometry, it is important to consider the functionality of the precursors in regard to their molar mass. Indeed, since our epoxy and acid precursors are both bi-functional, each mole of the precursors will add two moles of their respective functions to the materials. To accurately account for the right number of chemical groups introduced, it is important to divide the molar mass M of each compound by its equivalent functionality (f_{eq}), which is roughly two for both precursors in that case. The resulting number is called equivalent weight and is noted M_{eq} (g/eq) as shown in the dimensional **equation (2).**

$$M_{eq}(g.eq^{-1}) = \frac{M(g.mol^{-1})}{f_{eq}(eq.mol^{-1})} \quad (2)$$

In the case of epoxy resin, the exact equivalent weight is given directly by the manufacturer. This is because it is very unlikely for those resins to be 100% identical to the theoretical chemical formula and often display a small degree of homopolymerization, consuming a few epoxy groups compared to an ideal compound. With the highest quality resins, the practical equivalent weight tends towards the theoretical one. While calculating the equivalent weight may seem to have a rather low impact, since both precursors have their molar mass roughly halved, accurately considering the equivalent weight does play a role during the introduction of the catalyst since its concentration is a function of the accurate number of acid groups in the material. More generally, this may also be used to mix precursors with different functionality accurately, making it easier to tune the formulations.

In order to ease the elaboration process, the equivalent weight ratios between precursors are worked out in mass ratios. This way, manipulation of masses for solid/viscous precursors is possible while liquid precursors can be measured by volume, using their absolute density (mass/density = volume). For any reaction between two reagents A/B introduced in their respective stoichiometric ratio a/b, one can write the following equality **(3)**:

$$\frac{n_A}{a} = \frac{n_B}{b} \quad (3)$$

$$\frac{m_A}{a.M_{eq,A}} = \frac{m_B}{b.M_{eq,B}} \quad (3')$$

$$m_A = \frac{a}{b} * \frac{M_{eq,A}}{M_{eq,B}} * m_B \quad (3'')$$

(ii) First approach to uncatalyzed epoxy-acid systems

This elaboration process was based on Altuna et al.'s procedure since the formulations are very close [79]. Both precursors are introduced in liquid phase and allowed to react for a few minutes before addition of the catalyst and subsequent casting of the pre-polymer.

Diglycidyl ether of bisphenol A (DGEBA, D.E.R. 332 – Epoxy equivalent = 178g.eq^{-1}), sebacic acid (SA 99% purity – Acid equivalent = 101,13g.eq^{-1}), 1-Methylimidazole (1-MI 99% purity) and 1,5,7-Triazabicyclo[4.4.0]dec-5-ene (TBD – 98% purity) were used in this study. All reagents were purchased from Sigma-Aldrich and used without further purification. A summary of the molecular and equivalent weight of each precursor and the appropriate mass ratios for the selected formulation can be found in **Table 3**.

As a first experimental step to the elaboration of vitrimers, the epoxy-acid reaction was first tested without catalysis. This process allowed to fine-tune the setup required for the elaboration as well as familiarizing with the tangible aspects of the synthesis (precursor viscosities, effective melting temperatures, solvation speeds etc…).

Table 3 – Molecular and Equivalent weight for the different precursors and their mass ratios according to the selected stoichiometry.

	DGEBA (D.E.R 332)	**Sebacic Acid (SA)**	**1-methylimidazole (1-MI)**	**Triazabicyclodecene (TBD)**
Molar Mass (g/mol)	340,41	202,25	82,1	139,2
Equivalent weight (g/eq)	178*	101,13	N/A	N/A
For epoxy/acid = **1,1**	$m_{Acid} = \mathbf{0,5165}\, m_{Epoxy}$			
For catalyst/acid = **0,05**	[1-MI] → $m_{Catalyst} = \mathbf{0,0406}\, m_{Acid}$ / [TBD] → $m_{Catalyst} = \mathbf{0,0688}\, m_{Acid}$			

**provided by the resin manufacturer*

The sebacic acid is a white solid resembling a granular powder that melts near 133-137°C (according to the supplier). In order obtain both precursors in the liquid state, the elaboration process takes place at 150°C. The epoxy resin is already liquid at room temperature, but heating of the resin will help drying it and lowers its viscosity for better mixing. Pre-heating the resin also prevents cooling down the liquid acid during the introduction of the epoxy.

The epoxy is weighted first as it is more tedious to accurately target a specific mass with the viscous resin. It is gathered in a heat resistant cup and put in a convection oven at 150°C until needed. The acid is then weighted in an aluminium pan and placed on a heating plate at 150°C until melted. Once both precursors are liquid and at the designated temperature, the epoxy resin is added to the aluminium pan as a low viscosity liquid and the mixture is agitated by gently moving the liquid around (cf. **Figure 46**). At this point, the viscosity would be low enough to mix with a tool like a spoon without incorporation of bubbles but this may not be advisable as the viscosity will only increase from there. Since the miscibility of both reagents is high enough, mixing without using a external tool was possible by tilting the pan around and activating diffusion. This ensured that no bubbles or contaminants were introduced and that the entirety of the pre-polymer stayed in the aluminium pan.

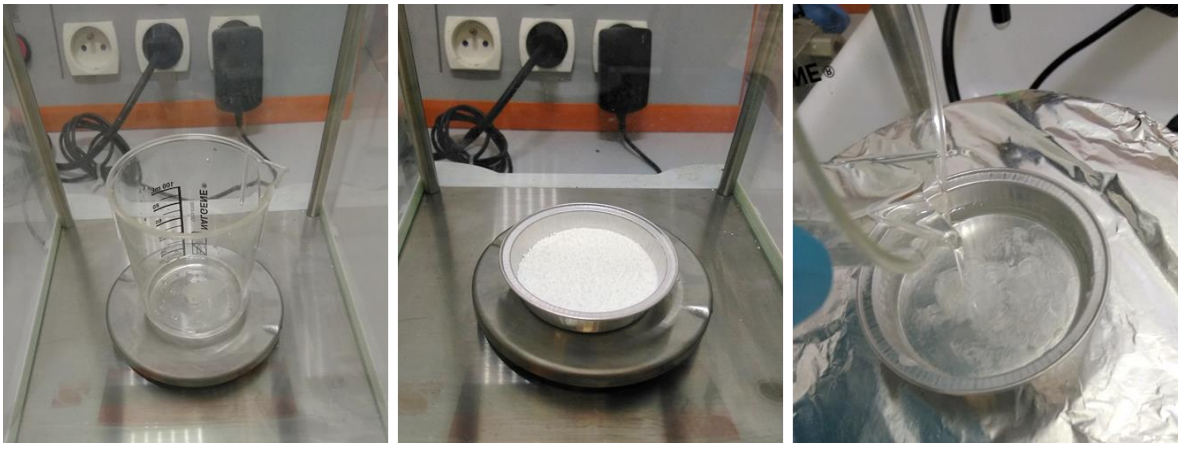

Figure 46 – Incorporation of hot DGEBA resin into melted sebacic acid.

At this point, the elaboration could be considered finished, the pre-polymer's viscosity will increase with time and temperature until gelation and ultimately complete curing. However, this process may take a long time without catalysis and apparent curing was roughly achieved after more than 12 hours at 150°C. By quenching the polymer resin and thus stopping the reaction before this time, several polymerization states can be described experimentally (see **Figure 47**)

If the reaction is stopped right after homogeneity is obtained, a phase-separated product is obtained with the acid precipitating into solid crystals while the epoxy forms a loose wax around it. This state is very similar to what Hoppe et al. (2005) [102] described in their hot-melt adhesive applicative case.

After 1-hour, a homogeneous milky wax with no distinguishable phases is obtained. By experimenting with this state, it was found that the pre-polymer is still able to melt and that weighting the wax as a two-in-one precursor may be practical for future industrial processes. However, one must keep in mind that segregation of precursors can still happen and that the full volume of the prepared wax should be used to guarantee the appropriate stoichiometric ratio.

After 2h of reaction time, the pre-polymer gradually turns transparent with very little cloudy domains remaining, showing that the free polymer chains start forming a coherent network and that the acid is not available for crystallization anymore. Past the 3h mark, the network is almost completely gelled and the only way forward after this time will be curing in this shape for the rest of the duration (excluding reprocessing of the network).

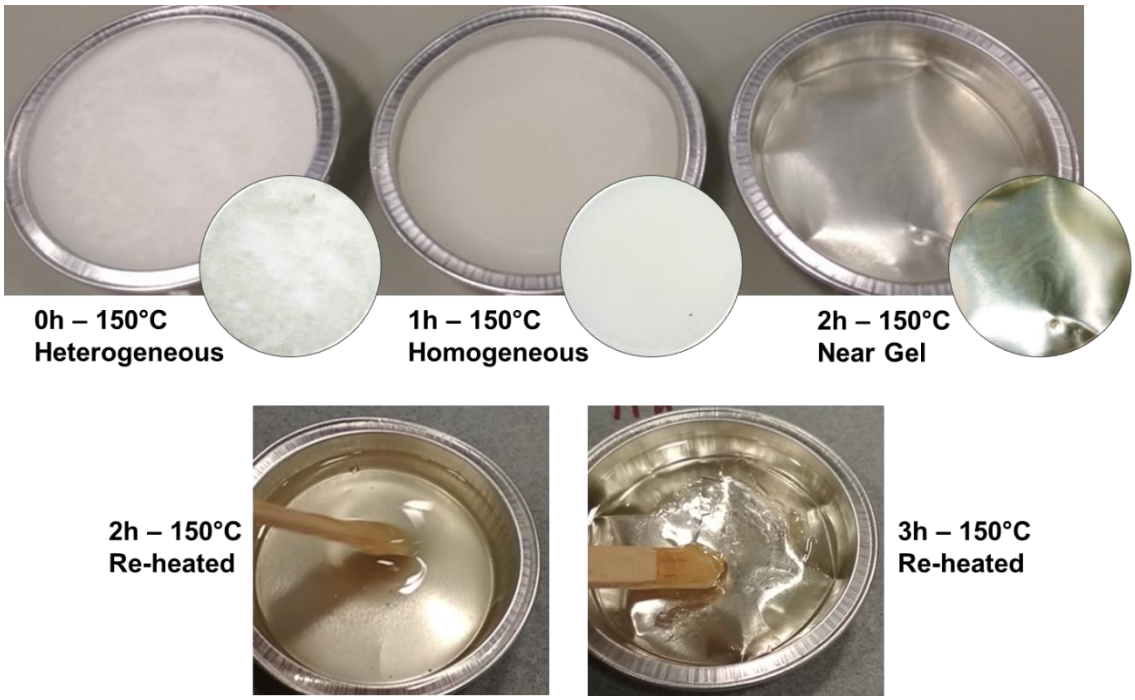

Figure 47 – Observation of different polymerization states following increasing curing time. Re-heated pictures were taken at 150°C.

(iii) Addition of the catalyst

With the prior gathered knowledge, it is now possible to include the selected catalysts in the elaboration process.

Before the introduction of the catalyst, it is important to bear in mind that the rate of reaction will strongly increase, and that polymerization can release a lot of heat quickly. There is a risk of thermal runaway in the earlier stages of the reaction that can lead to extreme temperatures, carbonizing and wasting the end-product. It is important to emphasize the violence of this heat runaway, as it can reach several hundred degrees and totally burn the content of the pan in a matter of seconds. To prevent such problems, it is therefore crucial to control the temperature rise in the pre-polymer. This can be done actively with a cooling/heating system or passively by removing the pan from the hot

plate and making smaller manageable amounts that can radiate the heat more efficiently before reaching an unstable point.

Another way to control the heat release is to allow the mixture of epoxy and acid to cool down from 150°C to a lower temperature, re-crystallizing part of the acid that precipitates in the solution. When the catalyst is added, extra heat is generated and is not dissipated fast enough, the temperature rises again and crystals will absorb this extra heat to melt again. In a way, we borrow heat dissipation capabilities during a time when temperature control is not an issue, and trigger heat absorption precisely when control becomes an issue. One advantage of this method is that the crystallizing point of pure compounds is quite precise so that it can be used by the experimenter as a reliable temperature plateau to control the reaction temperature. Pure sebacic acid normally crystallizes below 137°C, but as it starts to intimately mix and react with the epoxy this temperature can be expected to be a bit lower. If too many crystals precipitated, it is still possible to remelt them by carefully rising the temperature again. However, once the catalyst is added, the gel point will be reached in a few minutes depending on the exact temperature and catalyst used. Doing this by hand with no control apparatus requires a constant balance between rising temperature and advancing the reaction or lowering it so it remains manageable (time, viscosity, thermal accumulation).

Following the mixing of precursors in their liquid state until homogeneity, and with care for exothermal runaway, the addition of the catalyst can now be done.

TBD is a soft rubbery solid with a strong yellow color that is soluble within the organic mix. This made the incorporation somewhat difficult as the TBD had to be dissolved while reacting with the hot pre-polymer, resulting in an uneven local distribution of the catalyst, until complete homogenization was reached. Manual stirring helped to dissolve and disperse the catalyst, however this proved to be an unreliable way of proceeding as continuous mixing combined with a very fast increase in viscosity only resulted in an agglomerated polymer bulk that was unusable as is (cf. **Figure 48**). Reducing the temperature would help to decrease the reaction rate, but the sebacic acid would return to solid form which is not desirable for a proper reaction in liquid state.

Figure 48 – Left) TBD catalyst as a yellow rubbery solid. Middle) TBD catalysed vitrimer following stirring. Right) Piece of a TBD-catalysed vitrimer including many bubbles trapped during stirring.

On the contrary, 1-methylimidazole proved to be easier to work with. 1-MI is a colorless liquid at room temperature and was rapidly mixed with the rest of the precursors, again by gently tilting the pan to activate diffusion. In addition, the gelation occurred later, allowing up to 10-15 minutes of working time before casting.

As mentioned before, the chain extension leading to an increase in viscosity is governed by the esterification while the gelation of solely bi-functional reagents is governed by the transesterification reaction. It was also mentioned that the efficiency of imidazoles at catalysing the esterification reaction depends on their alkalinity in part **2.3.a(iii)**. By looking at the dissociation constant of the conjugated acid for each catalyst (pKa), it is possible to hypothesize that the same

effect is ongoing here. TBD associated pKa in water is rated as 14.5 whereas the pKa associated with 1-MI in water is evaluated at 7.25, showing that TBD is much more alkaline than 1-MI [103], [104].

With the easier working conditions, following the process using 1-MI seems like the more robust solution. At the end of a successful elaboration, the pre-polymer should take a faint yellow hue, and exhibit a very low viscosity (close to a thin oil) and true clarity (fully transparent, with no bubbles or heterogeneities). Lowering the temperature should not yield a biphasic product anymore but only a thick white or transparent wax that is re-heatable for a small time before total gelation occurs. Casting of the low viscosity pre-polymer can be performed in any desired container for later curing.

To monitor this final process, the curing of the cooled pre-polymer was separately followed by Differential Scanning Calorimetry (DSC) and the obtained thermogram is presented in **Figure 49**. Passed the first heat regulation artefacts, the pre-polymer was heated from 10°C to 150°C with a fast-heating ramp of 14°C/min. This ramp was selected according to the heat ramp available on the hot-press that will be later used for manufacturing. The first endothermic peak was attributed to the melting of the pre-polymer wax and was quickly followed by a strong exothermic peak, attributed to the polymerization reaction. No other thermal events could be recorded after 25 minutes and a complete return to baseline heat flow values from there and up until 2 hours can be observed. This indicates that the majority of the reagents have reacted and that seldom modifications of the network should happen afterwards. This time is consistent with Hoppe et al.'s [102] observed curing time, with most epoxy rings consumed in 10min at 90°C, as well as with the additional content provided by Montarnal et al.'s [73] in their original publication, showing a complete reaction time rated at 30 min at 130°C.

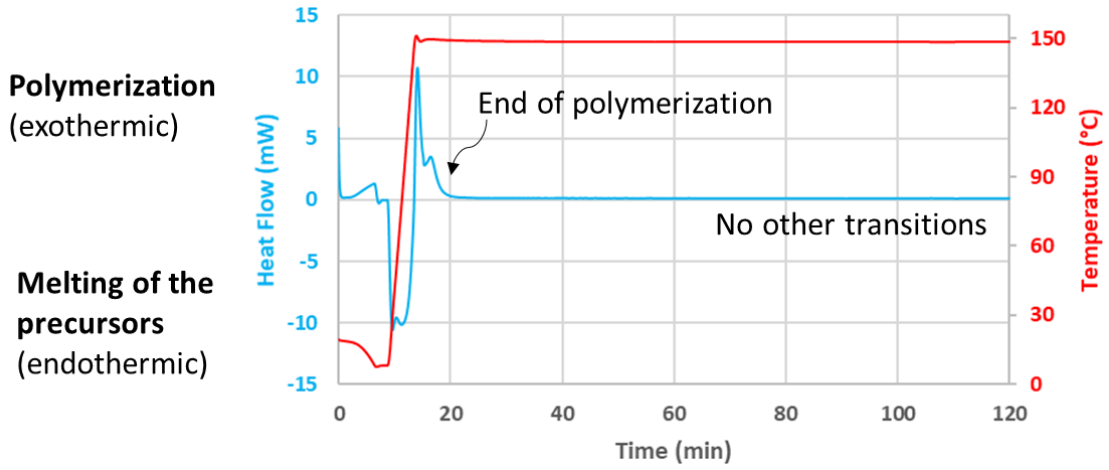

Figure 49 – DSC thermograms of the polymerization process of the cooled pre-polymer.

Final curing can therefore be appropriately achieved within 1h at 150°C, the obtained material should now be a smooth glassy solid colored in a vivid translucent orange. The resulting piece should exhibit a high toughness with a low glass transition temperature and no apparent defects. With the elaboration process completed, manufacturing of repeatable samples for characterization can be done.

The final elaboration process is summarized in **Figure 50** and shows both controlled and uncontrolled heat generation results. In the latter case, the polymerization started earlier where heat was concentrated, creating these reddish domains and leading to an unsuitable heterogeneous resin.

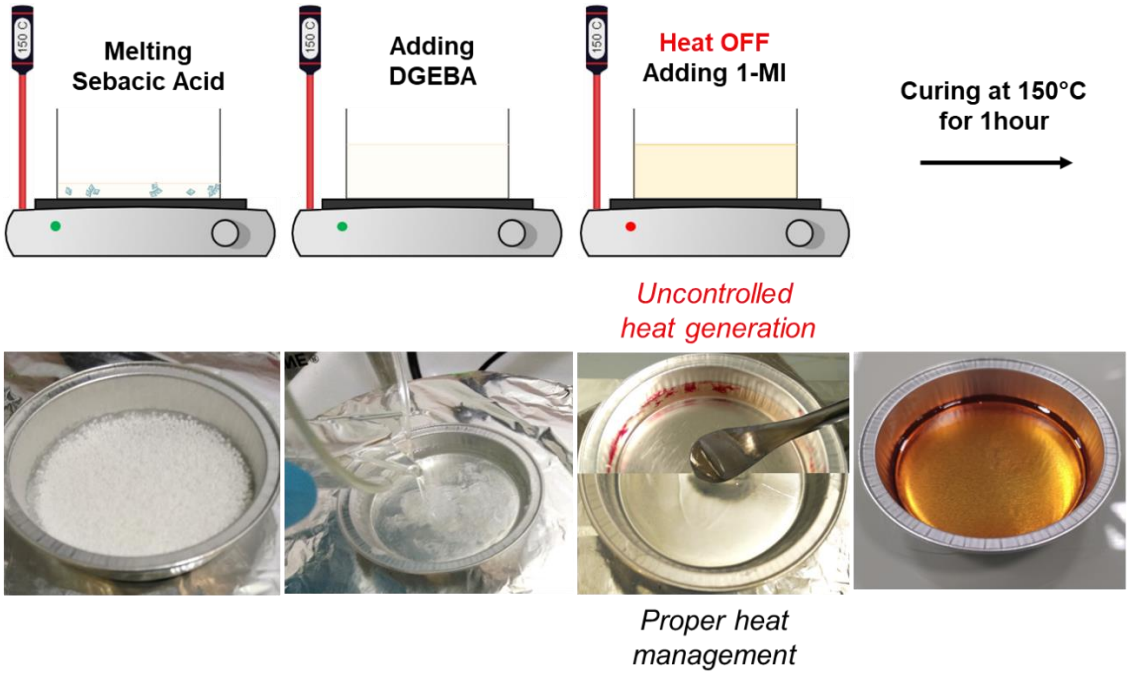

Figure 50 – Complete elaboration procedure of the studied vitrimer. The third picture shows both the degraded (top) and normal (bottom) state of the resin in case of un/controlled heat generation

c. *Hot Press-molding manufacturing*

Manufacturing of the ready-to-cast resin is performed by hot press-molding, using a *LPKF Multi-Press S*. The pressure vessel is made of a symmetrical layering of thick aluminium slabs on the outside for heat repartition, thin yet rigid steel plates on the inside to spread pressure more evenly and four vertical pins keeping the layers aligned together (cf. **Figure 51**). By placing a mold filled with the pre-polymer inside this pressure vessel, it is possible to heat up and press the curing resin to the desired shape.

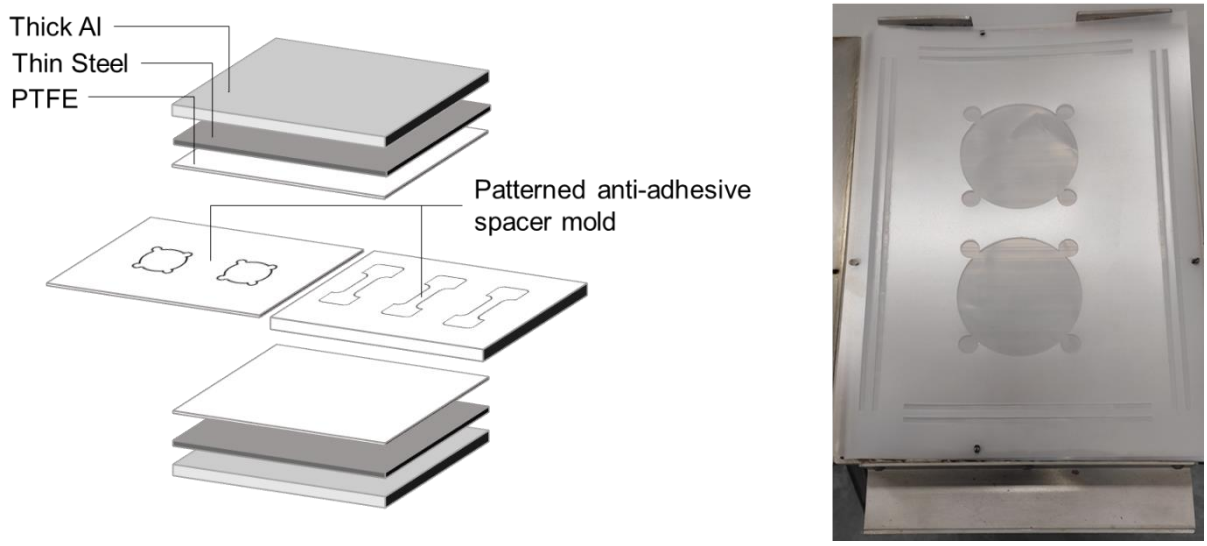

Figure 51 – Left) Complete press setup showing the stacking of the pressing vessel (Al + Steel) and the sacrificial mold (top/bottom PTFE + patterned spacer). Right) Actual picture of a stack up from bottom up to the spacer.

To receive the pre-polymer, a sacrificial mold was designed using commercial fluorinated unmolding sheets for top and bottom covers and a 300µm thick spacer for the sides of the mold. The spacer is made of a heat-resistant polymer, that has pressure repartition properties and can be

cut precisely with a CO2 laser, making it versatile for molds design and prototyping. However, the resulting vitrimer showed extreme adhesion to the commercial unmolding top/bottom sheets, making it impossible to recover the samples. This issue was solved by replacing the fluorinated unmolding material by actual 150µm thick pure PTFE sheets. Using thinner sheets resulted in warped and plied samples, also unsuitable for characterization, making the use of thicker sheets mandatory (cf. **Figure 52**).

Figure 52 – Left) Adherent samples in the fluorinated unmolding material. Right) Unmolded but deformed samples obtained with 75µm thin PTFE unmolding sheets.

Another issue that can arise in the hot-press is the vacuuming of the mold cavity. Indeed, given the very low viscosity of the hot pre-polymer, the resin flows out of the cavity through the gap between the mold layers without allowing air to enter, resulting in a decrease of the cavity volume. To counteract this effect, the press was pre-heated to 100°C and pressure was applied right away, pressing down on the deformable mold and reducing the interstice. The temperature was then allowed to increase again up to the desired 150°C before increasing pression and continuing the curing process.

Using an in-excess amount of resin is also helpful to ensure proper pressurization of the cavity, even if some of it flows out in the earlier stages. Practice helps with this method, as the shape and thickness of the mold cavity impacts the amount of resin that can flow out. After several trials, an optimum mass of resin to mold volume ratio was found at 1.25g.cm-3, which should be slightly above the true density of the resin, and overall a preparation of 1.5g.cm^{-3} was preferred to account for lost resin on the surface of the aluminium pan and other instruments. To prevent spillage of the excess resin, additional overflow volumes were added to the side of the mold and the entire pressing vessel was sealed using a heat-resistant adhesive tape. As a routine design habit, four “ears” were also added to the design of each individual mold to receive eventual trapped bubbles. This proved to be unnecessary as the resin flowed extremely well in the hot press and filled these volumes easily. However, these additional volumes were kept as they provided easily breakable pieces for additional characterization. The final pressing setup with an example of mold design is shown in **Figure 51**.

The final hot-press process profile was validated as follow:

- Pre-heat up of the entire mold to 100°C at 14°C/min to soften/melt the cooled pre-polymer
- Increase the pressure to 0,3MPa to start closing the mold and continue to pre-heat up to 150°C
- Fully apply the pressure up to 1MPa and maintain the heat at 150°C for 1h
- Remove the pressure and cool down the entire mold before removal and unmolding the samples

At the end of the hot-press manufacturing clean, defect-free and repeatable samples of about 300-350µm thickness were obtained (cf. **Figure 53**). Using this procedure it is possible to change the

shape and thickness of the mold and produce any type of samples, from 75µm films up to millimetric bulk samples.

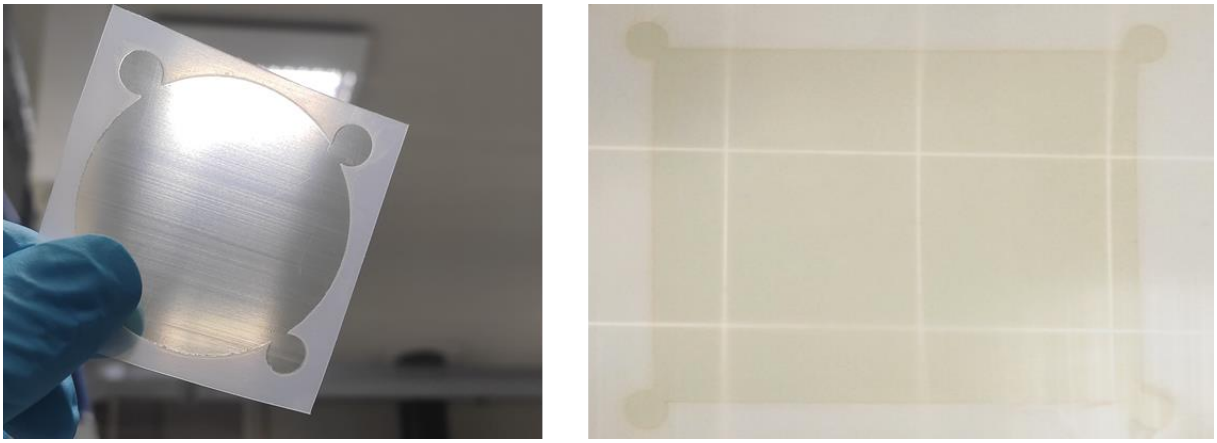

Figure 53 – Two defect-free film samples using two different spacer-mold designs.

4. Characterization of the elaborated vitrimer

The final vitrimer and its uncatalyzed counterpart were analysed by Fourier-Transform InfraRed (FTIR) spectroscopy to assess the chemical nature of the end-product. The spectrometer was set in Attenuated Total Reflectance (ATR) mode to allow the analysis of the liquid DGEBA resin, and the solid sebacic acid and resulting polymer using the exact same setup. In this mode, free-standing samples are not particularly required and solely necessitate to be in contact with the reflecting crystal.

All the following spectra have been gathered in ATR mode, scanning from 400 to 4000 cm^{-1} and averaging 20 scans with a resolution of 4 cm^{-1}. An automatic baseline correction was applied systematically and the stretch vibration band from the sp^2 carbons of the phenyl group ($\nu_{c=c(Ph)}$=1608 cm^{-1}) was used to normalize the compared spectra [105].

To confirm the consumption of the relevant reagents (epoxy and carboxylic acid) and the presence of the desired groups for transesterification (alcohol and ester), spectra of the main precursors and the resulting vitrimers obtained after the elaboration process have been gathered and are shown in **Figure 54**. The main peaks of interest have been identified in the precursors as the vibrational band from the carbonyl function of the acid ($\nu_{(C=O)}$= 1690 cm^{-1}) and the vibrational band from the oxirane ring of the epoxy ($\nu_{(C-O)}$=914 cm^{-1}). When analysing the spectrum obtained for the elaborated vitrimer, it is clear that both of these functions have been consumed.

Additionally, new absorption bands have appeared and two of them could clearly be attributed to the carbonyl of the newly formed ester that slightly shifted ($\nu_{(C=O)}$= 1732 cm^{-1}) and the broad stretch of the hydrogen in the alcohol functions ($\nu_{(O-H)}$=3200-3600 cm^{-1}). However, uncatalyzed samples showed a lower alcohol peak intensity, which indicates that side reactions probably have consumed some of the hydroxyl groups. This is consistent with previous analysis on the role of the catalyst as homopolymerization of excess epoxy cannot occur spontaneously, therefore possibly leading to a consumption of hydroxyls in a ring-opening etherification side reaction.

Overall, this test further confirmed that the entirety of the reagents had been consumed and that the appropriate chemical groups necessary for trans-esterification have indeed been created.

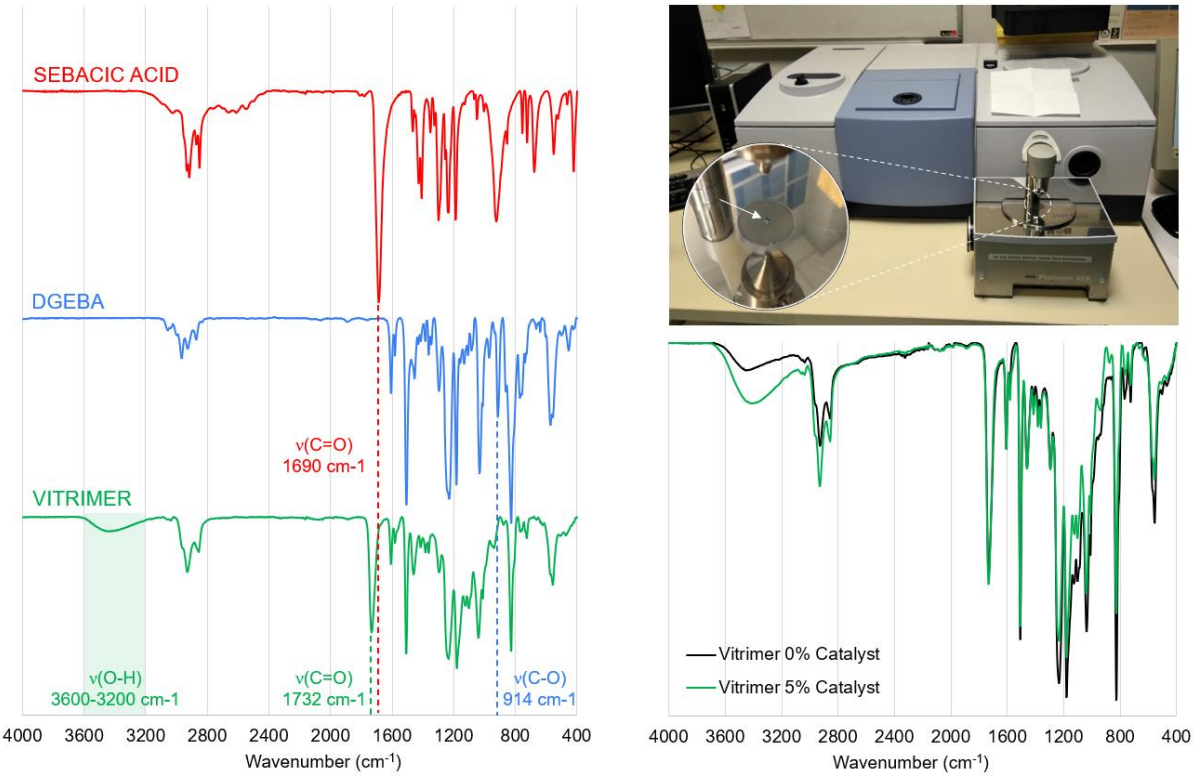

Figure 54 – Left) Precursors and vitrimer FTIR spectra. Top Right) ATR-FTIR VERTEX 60 apparatus, the insert shows the crystal window. Bottom Right) Comparison between catalysed and uncatalyzed normalized spectra.

In order to verify the crosslinked nature of the elaborated vitrimer, a differential scanning calorimetry (DSC) analysis was performed. Using a *TA-DSC 2010* with a heating rate of 5°C/min from 0 to 200°C on films of 300µm in thickness with a total mass of about 10 mg.

The thermograms presented in **Figure 55** confirmed the reticulated nature of the vitrimer, as no fusion events could be detected up to 200°C. The maximum temperature was set at 200°C to avoid thermal degradation that may occur in this range and above for most polymers. These results provided insight on the glass transition temperature (Tg), evaluated in this case near 32°C.

During the heating ramp, one can observe an endothermic peak (downwards) attributed to recovery of physical aging as Tg is very close to the ambient temperature (see insert on the Tg region). Polymers tend to relax the frozen out-of-equilibrium configuration when near Tg and increase their thermodynamic order by reducing their overall volume. When trying to get out of this relaxed state during heating up, an additional energy requirement must be provided. Once this energy has been provided to the system however, the thermal history is erased, showing a clear glass transition during the cooling portion.

According to these results, the elaborated material is chemically stable and should experience minimal structural change during its life cycles regardless of heat generation of power devices, usually capped below 200°C for most power applications.

Overall, a good adequation of the apparent and measured properties with what can be found in the literature for typical vitrimers was observed during this elaboration.

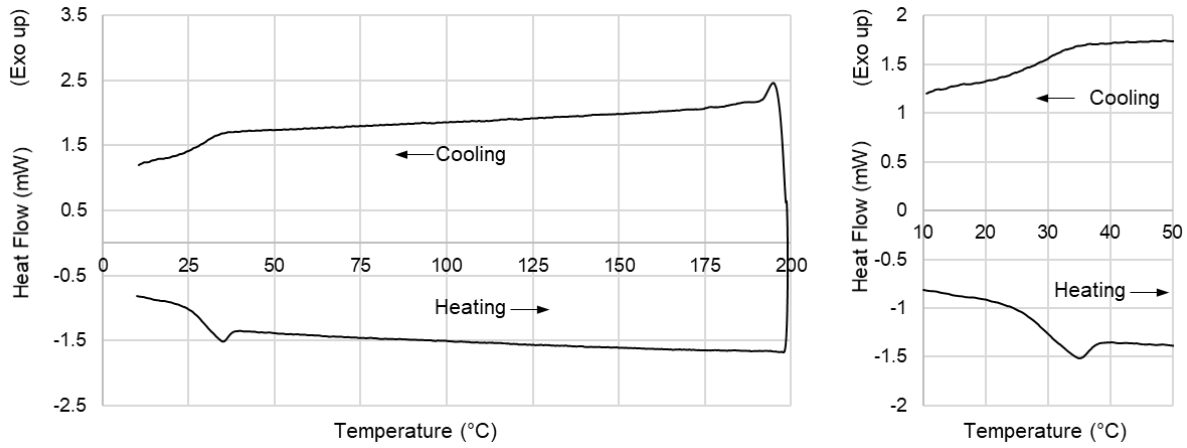

Figure 55 – DSC thermogram of the elaborated vitrimer up to 200°C showing physical aging and its rejuvenation on the cooling side. Right) Zoom on the Tg region for both heating and cooling parts.

3. Characterization of the dynamic network

1. Observation of recombinable network behaviour

a. Initial proof of healing capabilities

Since the elaborated vitrimer contains the necessary chemical functions for transesterification, the resulting material piece should also exhibit a recombinable network that can display self-healing properties. Unlike other non-dynamic polymeric networks, vitrimers exhibit two important temperature domains that controls their physico-chemical properties: The glass transition temperature (Tg) and the vitrimeric temperature (Tv).

Like Tg which governs the physical mobility of chains, Tv is a rather abstract temperature with a value that depends on the measurement method and is better represented as a range of temperature at which the several physico-chemical changes can occur. Below Tg, chains are kinetically frozen and cannot relax at relevant timescales whereas above Tg, chains regain mobility and can exhibit new physical properties. Similarly below Tv, the recombination of bonds is too slow to be relevant macroscopically resulting in a fixed network whereas above Tv, transesterification can occur more rapidly and thus the material can also exhibit new physico-chemical properties like self-healing. For transesterification, a reasonably fast exchange is often expected near 120-150°C.

To test the healing efficiency of vitrimers, most authors from the literature demonstrate their ability to reprocess the material entirely, effectively damaging voluntarily the material several times (cutting, milling etc…) and activating the healing process with high temperatures (above Tv) and under moderate to high pressures until a new solid piece is obtained. The reprocessed material can later be tested again and properties from the pristine and recycled samples can be compared.

However, when trying to implement self-healing as a reliability improvement, it is important to consider the state in which the material is receiving the damage as well as the state of the material after the damage occurrence. In the specific case of power modules, heat is readily available by the sheer power dissipation of the embedded semiconductor. However high pressures cannot be easily implemented without external intervention, risking more harm than good in terms of reliability. To assess the extent of recovery obtainable without any external pressure, a simple test was designed.

A 2 mm thick bulk sample was manufactured following the elaboration and manufacturing procedure presented in sections **2.3.b** and **2.3.c**. At room temperature, the vitrimer is hard and glassy yet very tough material, which made the damaging step rather tedious at room temperature. To help in the damaging process, the sample and a steel scalpel were heated at 150°C in the convection oven, which allowed to manually obtain a clean cut on the warm and flexible sample. The sample was then openly separated in two pieces to make sure that the cut was indeed complete and to allow air to enter the fracture plane. Finally the sample was put back into contact and maintained in this position using the same mold that was used for its manufacturing (confined but not pressed on). Surprisingly, after spending only 1hour at 150°C in the oven, the sample had already recovered its integrity as a single piece and exhibited an almost complete recovery of optical properties between both pieces (cf. **Figure 56**). This shows that diffusion of chains and recombination of bonds at this temperature can be quite significant (T > Tg and Tv) and that application of continuous external pressure may not be mandatory for retrieving a reasonable portion of the mechanical integrity.

However, one side showed a bad welding quality due to a bad alignment between the pieces in the mold, resulting in a "*failed*" healing. This emphasized the importance of having a very tight conformation between fracture planes in order to properly heal the pieces. As such, new strategies had to be found to guarantee the best conditions before trying to evaluate a healing efficiency.

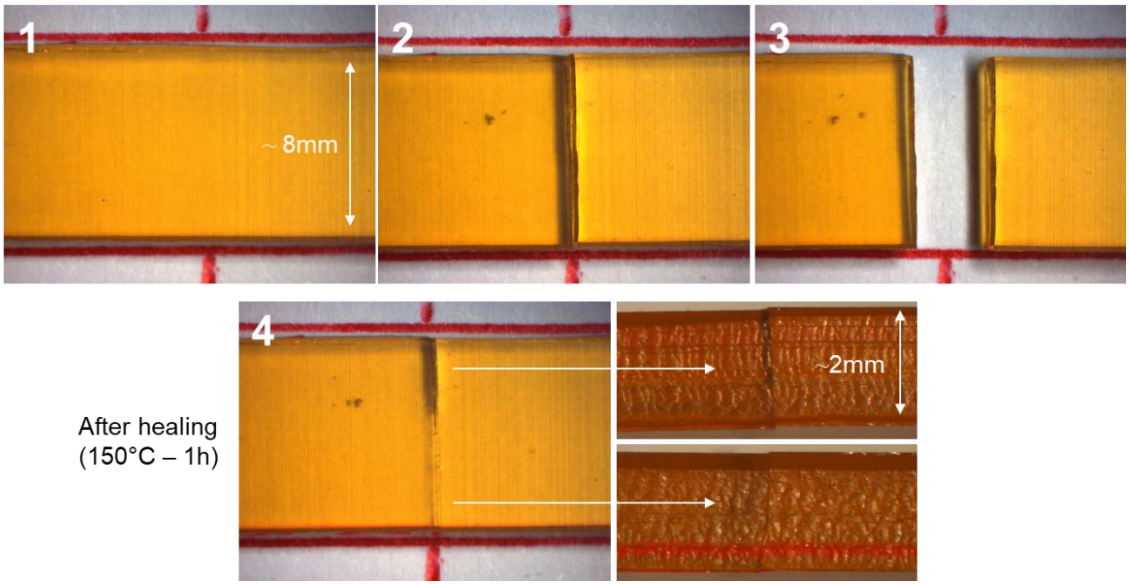

Figure 56 – 1) Pristine bulk vitrimer sample. 2-3) Cut sample and separated pieces. 4) Healed bulk sample after 1h at 150°C without external pressure, the bottom part shows better healing than the top part.

b. Shape-memory assisted healing

Shape memory is another interesting property vitrimers usually display [80], [106]–[108]. Typically, a polymer heated above its glass transition temperature can be deformed due to the increased mobility and free volume of its structural chains. Assuming that there is no relaxation in between, quenching the material following this deformation usually locks the chains in this thermodynamically unbalanced state, leading to a new temporary shape. By re-heating the polymer above its glass transition temperature, the chains are free to move again and the stored elastic energy as well as plastic entropic energy accumulated in the material helps to recover the original shape.

In the case of dynamic networks however, recombination of bonds can occur in the material when heated, leading to a new stable conformation of lower stress and thus a new relaxed shape. In that case, this shape is not temporary and can be considered as "*reprogrammed*" in the sense that the material "*learned*" this new permanent shape by changing its network configuration. As mentioned before, this process has an energy-requirement to sufficiently increase the mobility and can only occur above both Tg and the vitrimeric temperature Tv, above which the recombination is sufficiently rapid to be observable at a macroscopic scale.

Once a new shape is "reprogrammed", the material will behave as if this was its original shape, displaying regular shape memory effects when deformation from below Tg is relaxed above Tg. Altuna et al. (2016) [79] provided a demonstration for this effect, allowing the vitrimer to be deformed above Tg alone, or above Tg and Tv, thus reprogramming several times the permanent shape of the vitrimer.

In order to verify that the elaborated polymer possessed such reprogramming properties, a rod-like piece of vitrimer was maintained bended (stressed) at 150°C (over Tv) for 1h. The hot bended piece was manually straightened back to a rod-like piece before cooling it down below Tg (quench), thus yielding a rigid rod-like piece again. By re-heating it, a strong shape memory effect did indeed trigger in the sample, buckling and lifting its own weight up before re-assuming the bended form imparted in the previous heat-treatment, all in a matter of seconds, thus confirming the successful change of permanent shape (cf. **Figure 57**).

This is a very interesting feature, as it means that vitrimers can set a new permanent shape at high temperature by relaxing the previously stressed or damaged volumes, which is interesting for mitigating thermal stress aging during power cycling. But additionally, it means that shape memory may be used to recover from plastic deformations that occurred when damaging the matrix, providing a form of internal pressure in between partially connected pieces.

Figure 57 – New permanent shape memory imparted to a previously straight vitrimer piece.

To further test these hypotheses, a small piece of vitrimer film was bent repeatedly (±180°) until noticeable whitening could be seen, presuming mechanical fatigue occurred to its manufactured original shape. Optical observation showed a deep crack network in the film, barely holding by tiny pieces of material. By re-heating the partially damaged material at 150°C (above Tg and Tv) for only 30 min, the damage disappeared completely and its previous existence could only be noticed by looking at the defects in the film that moved during the recovery of plastic deformation compared to the initial image (cf. **Figure 58**). During the warming of the sample, a very fast shape memory effect was observed, presumably by crossing Tg, visually contracting the piece back together. Afterwards, the contacted pieces welded together and resulted in a completely healed film.

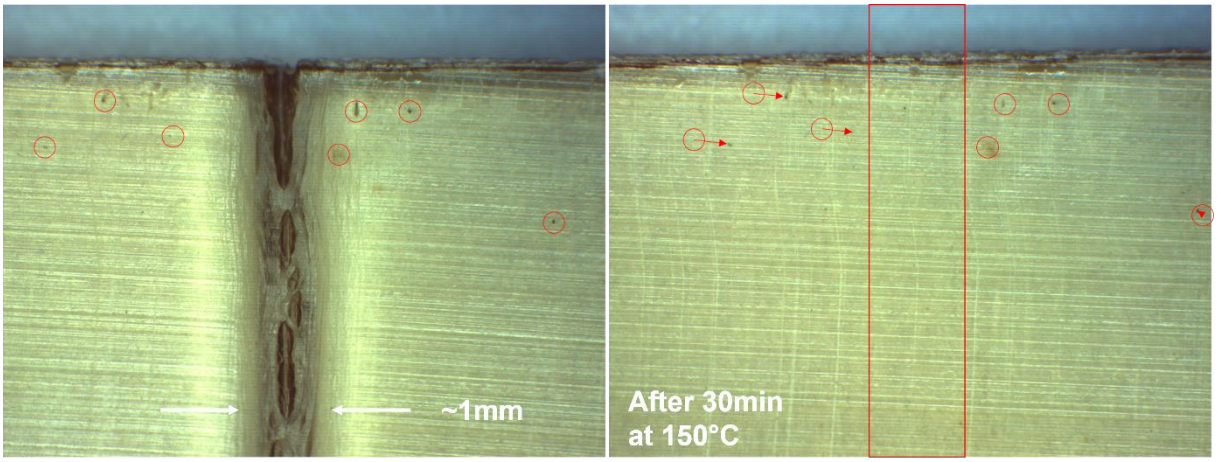

Figure 58 – Left) Partially damaged vitrimer film after multiple ±180° bending, noticeable defects are circled in red. Right) Healed vitrimer after 30min at 150°C, displacement of defects can be observed.

Montano et al. (2022) [109] recently studied the effect of shape-memory as a driving force for autogenous healing of scratches in a self-healing polymer. A direct correlation could be established between the amount of plastic deformation that a sample can receive, in the form of locally stored entropic energy, with the efficiency of the subsequent healing. Indeed, by heating the deformed samples, relaxation of the material and release of the stored entropic energy can trigger a displacement leading to autonomous gap closure. One thing to keep in mind, is that closing the gap and healing the material are not the same process, and that self-healing only benefits from gap

closure in order to be initiated. Still, this test demonstrates that having an effective closure undoubtably helps in the healing process and can be used advantageously.

Such promising results show that pressure-induced mobility is key in the healing process, but also that creating a moving force without external intervention is possible, in this case provided by shape memory effects. For a confined material, it is also possible to imagine thermal expansion as an autonomous source of internal pressure, displacing unconnected pieces towards each other or increase interdiffusion of the broken chains.

2. Evaluation of the mechanical recovery efficiency

a. Preparation and damage of the samples

Following the preliminary evaluations, an actual mechanical recovery test was prepared. The objective of this test is to break samples in a controlled manner and evaluate the ability of the material to recover from the damage by undergoing the same test again, thus testing the efficiency of the welding between two vitrimer parts. To do this, tensile testing was selected as it is common and easy to setup while still being harsh for joint strength evaluation.

Tensile testing is a simple method that is widely used in materials science to access mechanical information. The test consists in the application of a pulling force onto a sample to generate stress. The material is deformed, first elastically then plastically until failure. Typical dumbbell shaped samples are used for tensile testing as the reduced section will experience the highest stress, which is approximated as uniformly distributed in this section. The larger parts of the sample are designed to receive less stress and therefore prevent most of their participation to the results. Additionally, larger parts help getting a better grip in the tensile bench jaws. As a first approach to tensile testing, a rather simple geometry was designed without too many considerations for the final stress profile, which will be described as the "*simple design*" in the rest of this study. However, a more optimized version was re-drawn after the first tests by scaling down the type IV design proposed in the ASTM D638-14 standard to 85mm length, which will be described as the "*standard design*". Both design types can be seen as mold cavities in **Figure 59**, which were machined out of 2mm thick PTFE slabs.

Figure 59 – Left) Thick PTFE mold with 8 dumbbell samples using the simple design. Right) A similar mold using six samples using the standard design. Both designs exhibit protective overflow empty volumes at the edges.

This change of design improved the production of accurate results since the reduced section had to be better correlated to the initial length of the sample. A good indicator for parallelepipedal shapes is the use of the ratio n as :

$$n = \frac{L_0}{\sqrt{S_0}} \quad (4)$$

With L_0 and S_0, the length and surface of the reduced section at the start of the test.

When n increases, the relative length to the reduced section increases, rendering a thinner and slenderer sample. When n decreases, the shape factor changes toward a thicker, more spread-out sample. In principle, the higher n is the better the measurement will be, as a more even distribution of stress throughout the small section should be obtained. However, in practice it is better to have a slightly lower n, providing less flexible samples and therefore less errors on the measurement.

Since this material is tough and that its Tg is close to ambient temperatures, having a thicker sample meant that tests ran for longer since the material is able to relax part of the received stress while resisting crack propagation. Extreme elongations (> 100%) were obtained in controlled strain-rate experiments and tests had to be stopped before breaking the sample. By having a thinner section for the same length, less material was available for elongation, reaching the necking state and failure faster. This effect has been observed before and seem to be an important part of tensile testing of metals, where precise elongation values are critical [110], [111].

Regardless of the design, both the simple and standard type were manufactured without issue using the previously stated manufacturing protocol. Occasionally air pockets remained trapped during the pressing, but overall very clean, defect-free transparent pieces were obtained consistently (cf. **Figure 60**).

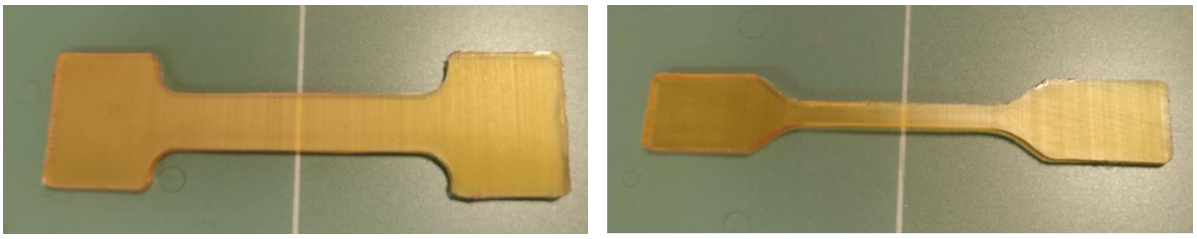

Figure 60 – Simple and Standard designs manufactured with the elaborated vitrimer. Pictures are not on the same scale.

b. Healing protocol for tensile tests

With the elaboration of several samples suitable for tensile testing, and in accordance with the previous early results, a repeatable healing protocol was imagined to test the actual healing efficiency of the broken interface, including a plastic deformation recovery step (using shape memory) and the actual healing step (using transesterification).

During the tensile test, the samples are deformed with a constant strain-rate until plastic deformation and total failure occur. In order to produce the highest efficiency without using external pressure, it is critical to be able to match the broken surfaces perfectly, granting the most surface area for the transesterification exchanges to occur. Since the samples undergo plastic deformation under Tg during this test, taking advantage of the strong shape memory of the material can help to recover the actual shape of the fractured surfaces. As mentioned before, the shape memory of this material is very strong and happens very quickly to the observer. To allow a reasonable thermalization time and a high mobility, a plastic deformation recovery step was set at 150°C for 1 min.

After obtaining samples pieces with matching surfaces, both parts of each sample need to enter into contact. Since the sample is entirely severed, using the minimal amount of force necessary, the

broken parts are pushed towards each other, aligning the pieces as best as possible by hand. Once the contact is obtained between the two pieces, no additional force is used and all of the now "in contact" samples are left free in the convection oven at 150°C for 1h before being cooled down to room temperature (RT) again. After this step, the samples are ready to go back to the tensile bench for a new test.

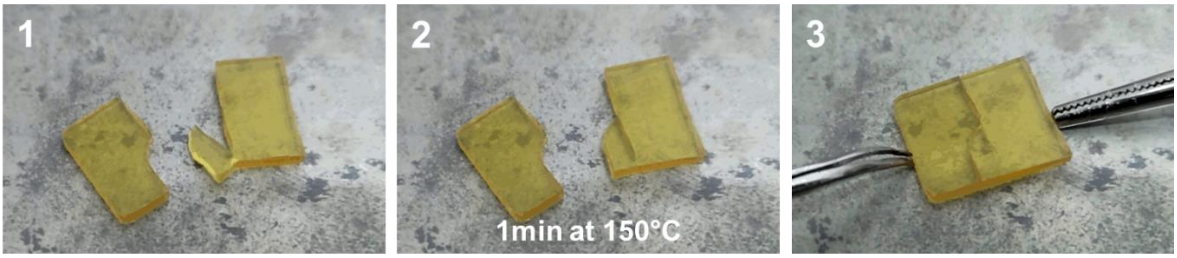

Figure 61 – 1) Deformed and severed sample. 2) Shape-memory assisted recovery. 3) Contact between severed pieces. Later the assembled sample will be set free to heal for 1h at 150°C.

c. Tensile test

In this first test, a *simple design sample* was used. Mechanical properties were assessed using a *Mecmesin Multitest-i* in tensile configuration, performed at a strain rate of 20mm/min at 20°C (thermalized room) to reduce the viscoelastic effects of the low-Tg vitrimer (Tg ≈ 32°C). To reset the thermal history, all samples were first heated for 10 min at 150°C before being cooled down to room temperature.

Figure 62 shows the different curves obtained during this test. In the first section of the initial curve (black curve), the elastic properties can be observed as the stress is correlated to the strain linearly by the elastic modulus. A typical artefact can be observed at the very start, where the jaws from the bench bite into the material resulting in a "toe region" in the first seconds of loading. At the end of the elastic region, the stress overcomes the strength of the network, that yields abruptly and relaxes stress by plastic deformation. As the elongation continues, the material integrity is expected to degrade until failure occurs. However in that case, a permanent plastic flow could be observed, allowing the material to continue its elongation without changing its stress level. Past the 40% elongation mark, the test was stopped and the plastic deformation recovery protocol was followed (1min – 150°C) before another loading was performed to fatigue the material to failure (red curve). Interestingly, the elastic modulus and strength at yield drastically diminished between the two tests and failure could finally be obtained. This shows that plastic deformation rightly damaged the network, resulting in less storable elastic energy and a lower strength overall.

Following the designed healing protocol, the sample shape was recovered by heating both parts at 150°C for 1 min, before putting them into contact and letting them free in the convection oven for 1 hour at 150°C (actual healing protocol). Afterwards, the tensile test was run again and showed impressive results. The elastic modulus was entirely recovered, with a perfect superposition of the curves, additionally the strength at yield was also recovered entirely. However, the failure mechanism changed from a plastic to a fragile failure, which confirms that the test was indeed measuring the strength of the adhesive joint that yielded abruptly when plastic deformation started.

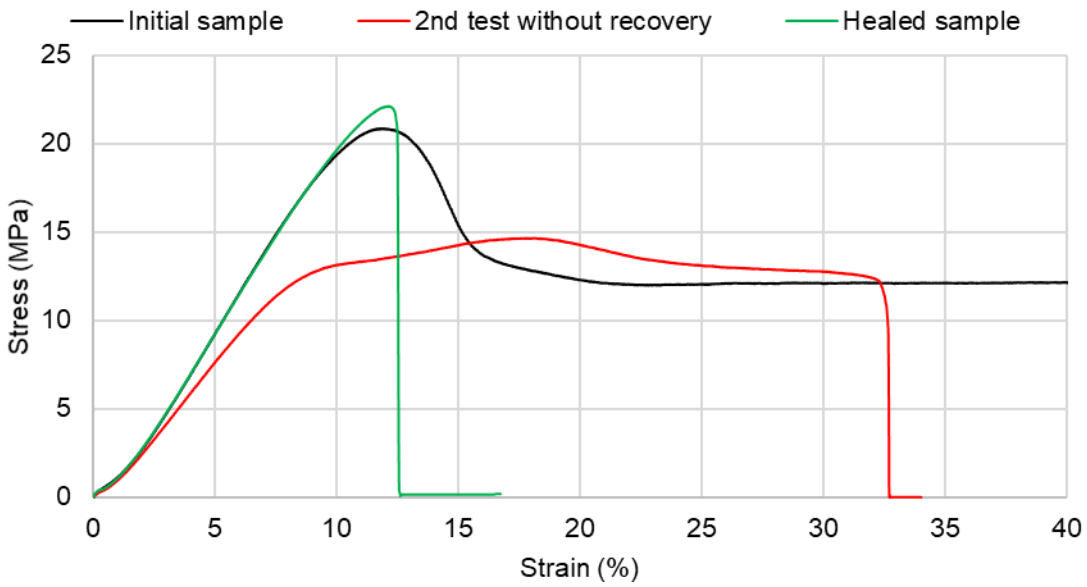

Figure 62 – First test showing the damages to elastic properties provoked during plastic deformation and recovery following the healing protocol

To better understand the effect of the plastic deformation and its recovery on the elastic properties of the material, a second test using the *simple sample design* was prepared. A new sample was deformed in the same way as the first one, until reaching yielding and thus plastic deformation, before undergoing an **extended plastic deformation recovery** process (10 min at 150°C) and going back to the tensile bench (cf. **Figure 63**).

In the first run, the initial pristine sample is deformed up to yielding and the test is stopped right at the beginning of the plastic deformation. Following a first recovery cycle, the same sample was tested again but instead of showing decreased elastic properties, the same elastic modulus as well as a slightly reduced strength at yield were measured. In comparison with the first test, it appears that the network either wasn't damaged enough or that the quick shape recovery already healed the few broken bonds.

Recovery was performed anew and the sample was put back on the bench, however this time the deformation was allowed to continue up to 40% to try triggering more damages. Unsurprisingly, a good alignment of elastic modulus is obtained compared to the previous test and yielding occurs in the same region, as the two previous runs were stopped right at yielding. After a third recovery cycle, the material was tested again and surprisingly showed a very similar profile, even with the large deformation received previously. Looking at these results, it appears that heating the material for this short period (10min – 150°C) is largely sufficient to recover the main elastic properties of the material and yield strength, regardless of the plastic deformation that occurred previously.

This provides information on the type of bonds that may be broken during plastic deformation. Indeed, in the case where no recovery is performed, the network appears as damaged, but when recovery at high temperature is done, the network appears as healed. The only covalent bonds that are effectively able to re-bind at high temperatures are the ester bonds formed by transesterification. Thus it is possible that a quick heating combined with a strong shape memory force would rapidly heal the unitary damages provoked by plastic deformation within the material in the same way as it can heal completely broken samples.

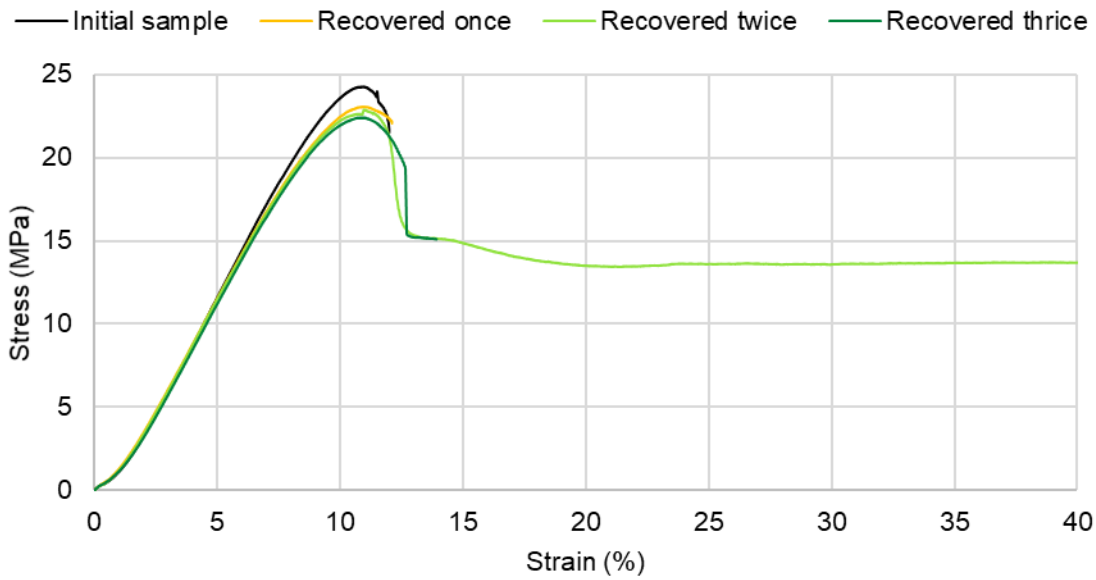

Figure 63 – Second test showing the recovery of elastic properties regardless of the previous plastic deformation.

By applying these large deformations (up to the yielding stress plateau) and extended recovery cycles (10min at 150°C) repeatedly, samples eventually broke, which indicates that the time of healing for plastic deformation recovery is probably too short. However, a decent number of cycles could be performed before actual failure and even then, it was possible to heal the completely severed sample (1h – 150°C) and continue the cycles. In a singular case, the material did not break at the adhesive joint but rather yielded at the other side of the sample, meaning that the healing procedure resulted in a tougher joint that the rest of the matrix. While this is not statistically significant, it shows that adapting the healing conditions might even give better results. As a side note, significant browning was observed on the samples during the last healing steps, which is expected for epoxies exposed to hot oxidative environments [112].

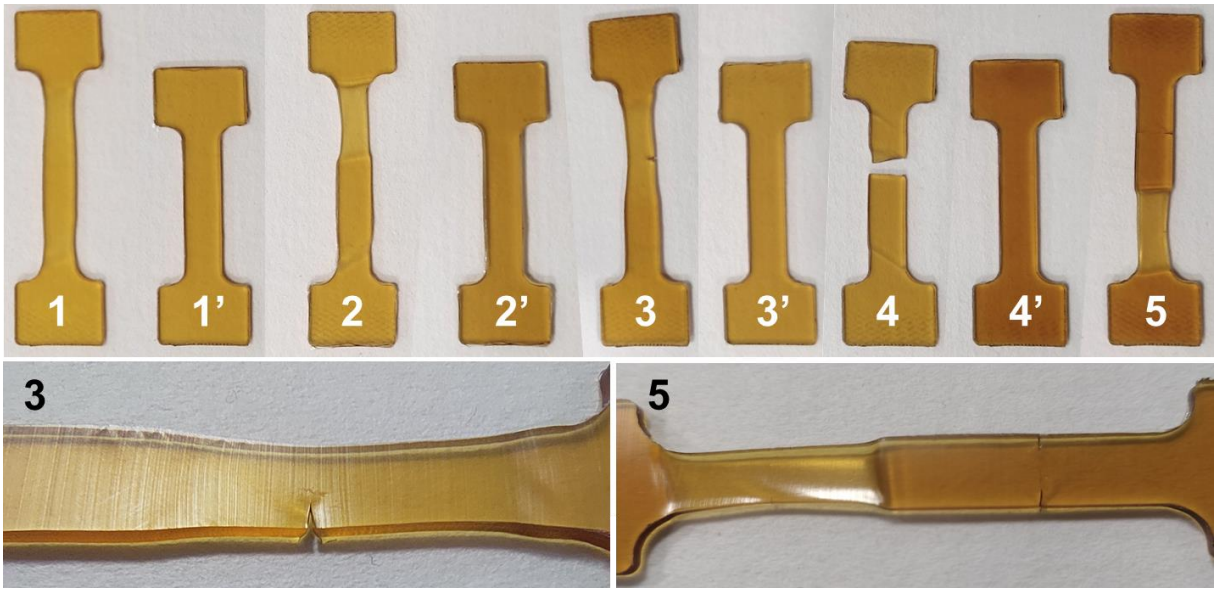

Figure 64 – (1-5) Same vitrimer sample plastically deformed five times, (1'-4') intermediate recovery states. Bottom 3) Signs of fatigue crack propagation at the third deformation cycle, Bottom 5) Yielding away from the healed region

As a final proof of mechanical recovery without the use of external pressure, a third test was performed. This time, the *standard sample design* was used to limit the very long elongations observed with the simpler design as well as to better focus the stress at the middle of the samples. This way, a better correlation between the initial and healed tensile curves can be provided, as no other degradations occurred between the two tests (cf. **Figure 65**).

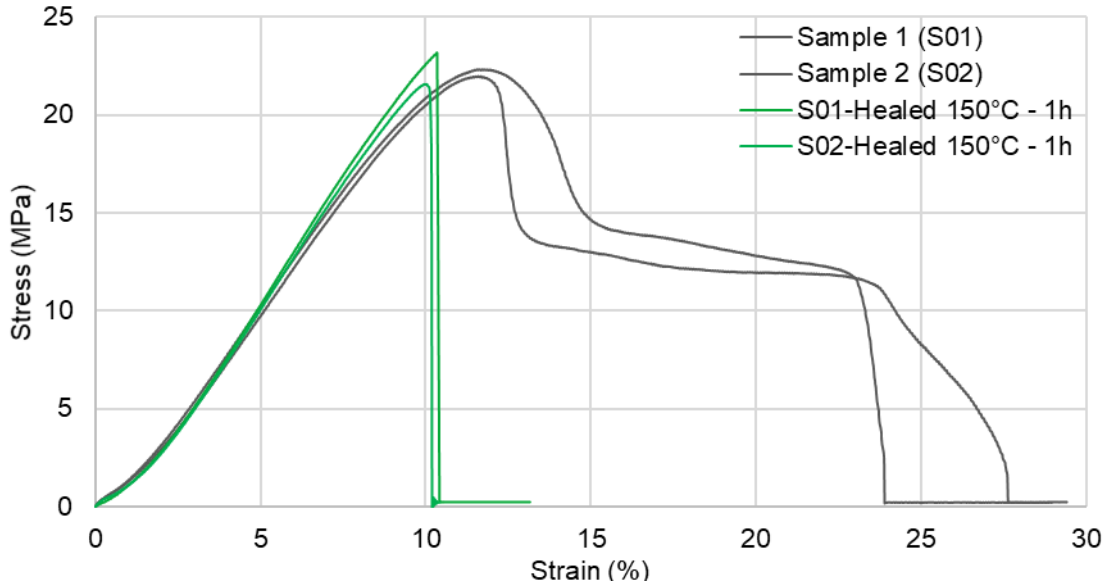

Figure 65 – Third test showing similar failure and recovery of two samples.

In this third test, two samples were prepared, damaged and healed in the same way as previously shown. Both samples exhibited similar elastic domains, with a toe region at the beginning and linear portion up until yielding. Similar strengths at yield were recorded and plastic deformation quickly led to the ultimate failure in both cases. After the healing protocol (plastic recovery + welding of the parts), both samples showed a high recovery of the elastic modulus and strength at yield before failing in a fragile manner near the 10% elongation mark.

From all of these results, healing of this material looks very efficient. Microscopic damages formed during plastic deformation can be healed in a few minutes and large macroscopic damages can be recovered entirely on elastic mechanical indicators in 1 hour. Additionally, the degree of mechanical strength and apparent toughness of the material were quite impressive, which seems very appropriate in comparison of the specifications enumerated in **Chapter I**.

Conclusion

In this chapter, an overview of the different concepts surrounding covalent adaptable networks has been proposed. By relying on the transesterification chemistry, it is possible to create self-healing materials directly from commercial precursors that are used in the PCB industry. Since these materials are based on associative exchanges, there is no depolymerization at high temperature and therefore a higher mechanical and thermal stability can be expected.

Easily produced from epoxy resins and carboxylic acids, the elaboration process was developed using the DGEBA resin as it is the most used epoxy resin for industrial applications and sebacic acid, as it seemed widely compatible with other acid precursors for property tuning. Two tertiary amines were selected as catalysts, the TBD and 1-MI, both well represented in the literature and able to selectively catalyse the polymerization (esterification) and healing (transesterification) reactions, increasing the kinetics to observable timeframes.

The elaboration process was more successful using the 1-MI catalyst, as it gave more time to process the resin in liquid state due to its lower alkalinity/reactivity compared to TBD, and a castable lightly yellow liquorish pre-polymer was obtained. Curing the castable liquid at 150°C for 1 hour yielded a nicely orange colored, transparent polymer.

Hot press-molding was selected as the main manufacturing technique and a customizable mold design was proposed, using top and bottom unmolding PTFE sheets and a patterned middle spacer. Creating defect-free samples using the spacer mold required to properly manage the pressurization of the cavities, which was achieved by adapting the top and bottom sheet thicknesses as well as introducing the resin in excess as its viscosity at high temperature was rather low.

After the production of repeatable samples, characterization of the material could be performed. FTIR spectroscopy revealed the disappearance of the epoxy and carboxylic acid functions, replaced by the new ester and alcohol functions desired for transesterification. Despite being elaborated from only bi-functional precursors, the crosslinked nature of the polymer was demonstrated, as it is expected for a vitrimer with transesterification-based crosslinking.

Finally, the self-healing capabilities of the elaborated and manufactured material were validated. Early demonstrations of recovery and shape memory were provided and this helped developing a self-healing protocol that does not involve complete reprocessing of the material, nor the usage of constant external pressure onto the fractured sample. Several tensile tests allowed to describe more precisely the mechanical profile expected from these materials and mechanical healing of several severed samples could be demonstrated, showing the entire recovery of elastic properties and yield strength on fractured and non-fractured samples.

Additionally, insight on the plastic deformation mechanisms have been proposed, leading to the idea that the material can heal damages at very different scales efficiently.

As a final consideration, it seems like performing the healing steps at 150°C for 1 hour is sufficient to obtain good healing results, that would be relevant for the application objective.

Chapter III – Compatibility of the vitrimer with power electronics applications

Chapter III: Compatibility of the vitrimer with power electronics applications

Introduction

In the first chapter of this work, the limitations of standard materials when applied to new power module architectures were listed. The replacement of silicone gel used in conventional modules by stiffer materials with a higher dielectric strength was proposed. On the other hand, FR4 materials needed to be less prone to mechanical failures, regardless of their origin, motivating the development of self-healing materials in the first place.

In order to explore the compatibility of the elaborated material with power applications, it is important to first validate key properties required for its implementation. Be it for embedded devices or regular power modules, the material must satisfy the required performances in operational conditions but must also be suited to the devices manufacturing.

Therefore, key properties necessary for the use of this vitrimer in power electronic applications have been rated. The thermal stability was evaluated following procedures close to industrial standards and the cycling thermal stability in the usage temperature domain was assessed. The elastic mechanical properties were explored as a function of temperature and electrical properties were measured to provide an insight on the applicability of the material for the manufacturing of power boards and highly integrated devices.

As a simple way of testing the compatibility of the vitrimer with PCB manufacturing, a complete procedure to create an entirely customizable PCB from the vitrimer resin is demonstrated. By using typical processes and equipment, the possibility of making these PCBs using conventional methods is demonstrated.

With the ability to create composite boards with the desired copper tracks geometry, novel tests can be designed to assess the healing efficiency of the material through electrical indicators, and for the first time, vitrimers recovery will be tested for their electrical insulation properties. Entirely new specimens were designed to replicate conditions that occur inside a failing PCB and explore the associated recovery critically. The healing efficiency was rated based on the breakdown strength and the partial discharge inception voltages (PDIV) of mechanically degraded composites.

Finally, the vitrimer was confronted to an actual power cycling test, by embedding a commercial power module of classical architecture and subjecting it to the AQG 324 automotive standardized tests. Additional measurements typically performed in the industry will be provided, rating the efficiency of this vitrimer solution on actual power modules.

1. Basic required properties for power electronics

1. Stability in temperature

a. Thermal stability

As mentioned in **Chapter I**, the thermal stability of the epoxy matrix is crucial for PCB materials since they will be subjected to possibly multiple soldering steps during manufacturing, with temperatures as high as 270°C for Lead-free processes. Other thermal tests, such as time-to-delamination tests, are typically performed at 260°C or 288°C but can go as high as 300°C [35].

To assess the thermal stability of the material, thermogravimetric analysis (TGA) was performed. This experiment involves heating two crucibles, one empty and one filled with the sample, which are simultaneously weighted precisely to account for changes in mass. By measuring the mass loss as a function of the temperature, it is possible to determine a temperature at which the material lost 5% of its total mass. From Table 2 – Chapter I, a 5% mass loss of an ideal dielectric for PCB-applications should be registered above 320°C, preferably close to 350°C.

To better reflect the standardized tests that materials are subjected to in industrial environment, a protocol was designed around the ASTM D3850 and the IPC-TM-650 2.4.24.1 standards. Using a NETZSCH TG209 TGA/DTA analyser, the thermal stability test was performed from room temperature to 700°C, following a ramp of 10°C/min, with a drying step introduced at 150°C for 15min before continuing the heating ramp. Measurements were achieved both in pure nitrogen and in dry air to discriminate the effect of an oxidative environment onto the material.

Additionally, differential thermal analysis (DTA) can be performed at the same time, since both crucibles are connected to thermocouples that can register the difference of temperature between them as a specific difference of potential (in µV/mg). By analysing both the mass loss and the DTA signals during the early stage of the test, it is possible to conclude that no water was present in the samples prior to the test (cf. **Figure 66**).

The first increase on the DTA signal can be attributed to the heat capacity of the sample, making it longer to heat up than the empty crucible used for comparison. Later, the DTA signal becomes constant despite the steady temperature increase showing this heat capacity is now filled and that the same amount of energy is required at every degree to maintain the right temperature. Reaching the start of the 150°C plateau used for drying, the signal falls as both crucible are at the same temperature and no thermal peaks could be detected from the start and up until the end of the 150°C plateau.

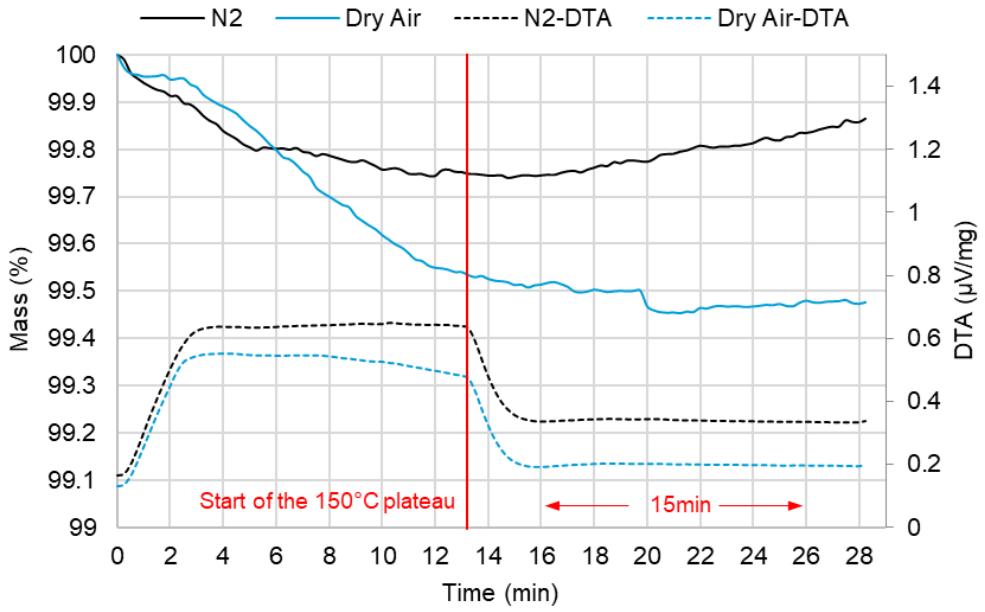

Figure 66 – Continuous Mass loss (solid lines) and DTA signals (dashed lines) until the end of the drying step, for nitrogen and dry air atmospheres, no significant water desorption is observed.

Since no clear endothermic/exothermic reaction occurred, it is difficult to attribute the observed slight mass variations to an actual mass loss. Most likely, the variations of mass are linked to buoyancy effects in the early stages where mass variations are actually null. A plausible explanation for apparent mass loss would be the increase of volume of the sample with heating, generating an increased upward force from Archimedes' principle. For the test ran in nitrogen, the mass increase starting at the beginning of the 150°C plateau could be attributed to a decrease of density of the gas, leading to less supporting force on the sample, thus appearing heavier. In that regard, the mass variations occurring before the end of the drying step are considered unsignificant. However, the mass values were not corrected and all mass losses shown later include these slight variations as normally occurring during a thermal stability test.

The data shown in **Figure 67** were obtained continuously after the drying step at 150°C and can attest of the high thermal stability of the network. With a recorded 5% mass loss at the temperature of 373°C in pure nitrogen and 362°C in dry air, the elaborated vitrimer is well aligned with the expected requirements of the PCB and power electronic applications . Since the mass loss is almost linear up to 350°C, values were gathered by directly intersecting the 95% ordinate of the curves (no onset). Considering the intermediate temperature of 288°C used for delamination tests, a mass loss of about 1% was registered in dry air.

One can notice the absence of impact of the Oxygen partial pressure (pO_2) in the first 400-450°C. This is probably due to the fact that phenolic-like polymers start to degrade by auto-oxidation, as several mechanistic pathways have been proposed in that direction [113], [114]. One likely mechanism would be the oxidation of the methylene by the hydroxyl groups present in the material, removing the need for external oxygen supply. However, it is difficult to have a more precise analysis, as additional means of chemical characterization would be necessary.

In the final segment, between 450 and 700°C, two different behaviours can be seen, with a final remaining mass of about 10% and 0% respectively for pure nitrogen and dry air tests. Indeed, without any oxygen a black thick tar remains at the bottom of the crucible, probably composed of the remaining unburnt aromatic carbon chains since aromatisation of phenols occurs near 600°C. Complementarily, when pO_2 is increased (dry air case), a more stable step can be observed between

450°C and 550°C, which can be due to the creation of more stable oxidized compounds from the early broken chains, before finally reaching 600°C and beyond where the entire network is vaporized under oxidation leaving an apparent clean white crucible [114].

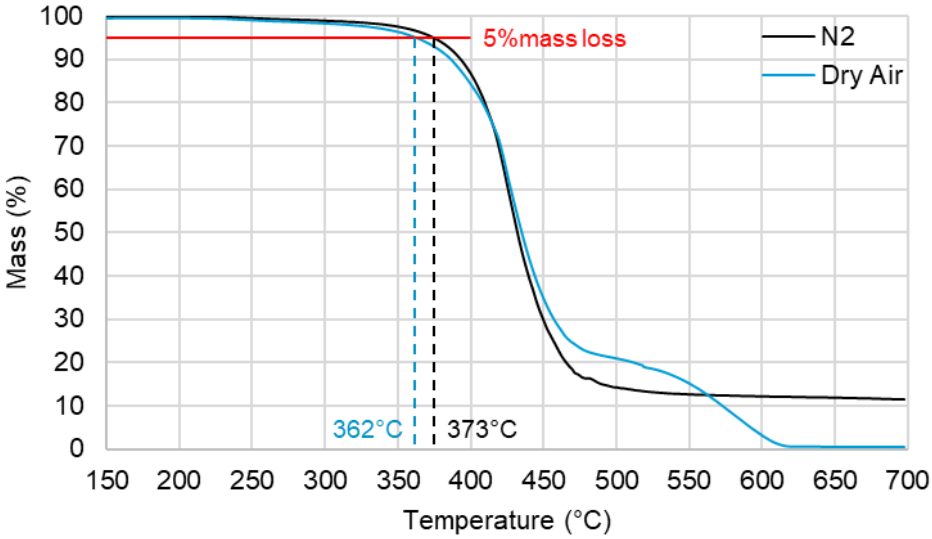

Figure 67 – Vitrimer mass loss measurement associated with thermal degradations in pure nitrogen and dry air.

b. Temperature cycling stability

The polymer stability to cyclic heat treatments was tested to make sure that the polymer can be exposed several times to high temperatures without large modifications of its physico-chemical properties, as it is expected for PCB manufacturing. The polymer response temperature cycle was monitored by Differential Scanning Calorimetry (DSC), using a TA DSC 2010 with a heating rate of 5°C/min from 0 to 300°C for a total of 4 successive cycles (cf. **Figure 68**).

On the first crossing of the glass transition temperature, one can observe the endothermic peak (downwards) at the heat flow step, attributed to recovery of physical aging and previously observed (cf. **Chapter II**). Following the glass transition, two other endothermic events can be observed, with the first one spanning between 40 and 140°C and the second one beginning right after the 150°C mark. For the first event, it is possible that water was present in this sample, drawing energy during the desorption and escaping the sealed but not hermetic sample pan. No accurate interpretation of the second could be proposed, as further cross-linking should exhibit an exothermic signature. A reasonable assumption would be that this transitions is either tied to physical events such as structural relaxations or caused by measurements artefacts, as no similar events were observed in the following cycles.

Provided the first heat ramp is passed, a good superposition of curves was obtained. However, by looking more precisely at the glass transition region (see zoom to the right of **Figure 68**), one can notice a slight increase of the Tg after each cycle, showing that additional crosslinking is occurring despite not exhibiting any exothermic peak. The main hypothesis is that it could be due to a slight thermal degradation of the material passed the 300°C mark. As mentioned in 1.1.a, the first degradations should occur near 300°C by auto-oxidation, which could lead to a more crosslinked structure [113], [114]. Given the inversion of heat flow at 300°C, it is unlikely that degradation peaks can be observed in that range. Regardless of the exact mechanism, the small evolution of Tg shows that several incursions at 300°C are acceptable for this material.

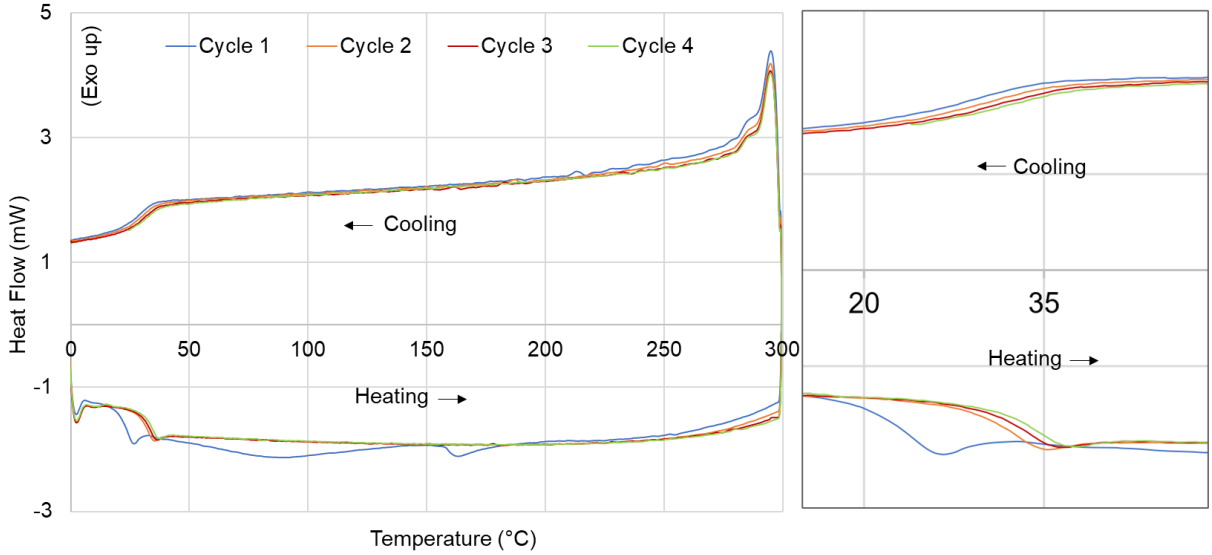

Figure 68 – Left) DSC thermogram of the elaborated vitrimer showing four consecutive heat cycles up to 300°C. Right) Zoom on the Tg region for both heating and cooling curves.

2. *Elastic properties*

Vitrimers have initially been reported for their interesting viscoelastic properties, which are linked to the choice of catalyst and its concentration [73], [77]. Instead of focusing on the dynamic properties, investigating the base elastic properties of the elaborated material and understanding the variations of elastic properties with temperature might be of interest for the formulator intending to create a reasonably rigid PCB.

In order to measure the elastic properties of the material with temperature, a Dynamic Mechanical Analysis (DMA) was performed in tensile configuration on parallelepipedal vitrimer bulk samples. Similarly to a static tensile test, this dynamic method measures the complex mechanical response to an applied sinusoidal force of small amplitude and allows to do so on a wide temperature range. Using a Mettler-Toledo DMA1, the scan was performed at 10Hz with a temperature ramp of 2°C/min from 0 to 120°C and are presented in **Figure 69**.

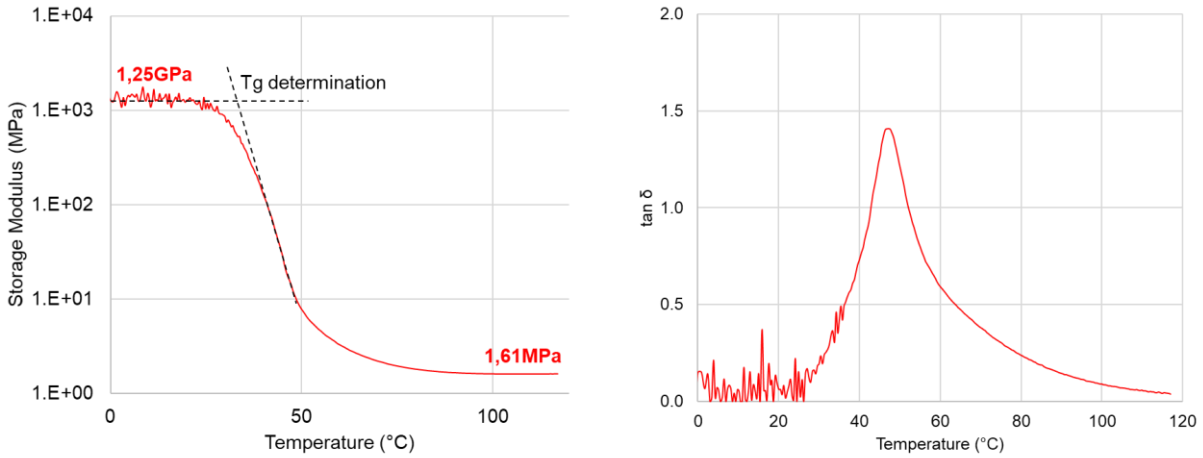

Figure 69 – Left) Storage Modulus of vitrimers with temperature. Right) Associated loss factor.

According to these results, the elaborated vitrimer exhibits a storage modulus of 1.25GPa below Tg, which is high for most polymers but common for epoxy compounds. However, a significant

difference can be observed above Tg, showing a much lower storage modulus of 1.61MPa. Decreasing the modulus by a factor of 10^2 when crossing Tg is not unusual for epoxies. However a drop of 10^3 becomes quite significant and describes a material that changes from a hard glassy material to a soft rubber. Looking at the loss factor values, the maximum mechanical damping can be found at 46°C, however the loss factor is severely skewed towards high temperatures.

Accurate determination of Tg could not be provided due to the noisy signal on the modulus plateau but could still be evaluated graphically by tracing tangent lines to the storage plateau and the linear portion at the modulus drop (onset), showing a Tg of about 32°C which is consistent with the values found in DSC.

According to the high modulus below Tg, manipulation of vitrimers to manufacture power boards is reasonable and should be on par with other composite materials once reinforced. Although, the matrix becomes quite soft above Tg, closer to what can be expected from silicone gels (still orders of magnitude above the stiffness of most gels, ranging in the 10-100kPa). Thus, the material can exhibit both interests related to its standards materials, being stiff as a substrate and allowing manipulation to create power boards, but becoming compliant and accommodating stress when heated, which could be beneficial to reduce or prevent cracking and delamination.

This effect could even play a role dynamically inside an embedded module since an important gradient of temperature can be present close to the chip, diminishing stress in high-stress areas while maintaining rigidity away from the power switches.

3. Dielectric strength

a. Experimental setup

The ability of the polymer to withstand high electrical fields is important for its use in new high-power devices. To measure the dielectric strength of the material, several breakdown tests were conducted using a Baur DPA-75C tester on thin films. A sphere-to sphere configuration (1/2”diameter spheres) was selected so that the field could be considered uniform in the material (cf. **Figure 70**). Based on preliminary tests, an AC voltage (50Hz) with a ramp of 2kV/s was selected to obtain breakdowns between 10 and 20 seconds, thus limiting the electrical aging of the material under high electrical fields.

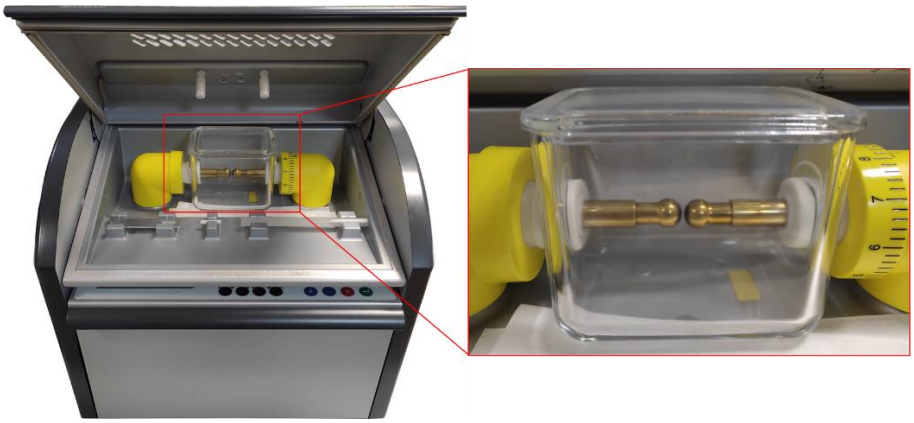

Figure 70 - Baur DPA-75C test showing the sphere-to-sphere electrode geometry and dielectric oil tank.

Film samples were selected for this test, as it is easy to control the thickness accurately with the selected manufacturing process. The uniformity and thickness of the films are crucial for accurate measurements. Samples with uneven thicknesses are likely to fail in thinner parts where the field is

more concentrated, but having a thicker uniform sample also comprise more defects per volume unit, resulting in a statistically decreased dielectric strength. By selecting an appropriate thickness and obtaining uniformly shaped samples, one can expect to gather representative values of the dielectric strength for the expected application. For this test, repeatable 350µm films were selected as it is in the same thickness range as wafers used for semiconductor chips.

Finally, to prevent arcing due to the high voltages, the film samples were immersed in a fluorinated dielectric liquid (Galden HT55), presenting a dielectric strength of about 15kV/mm. The large area of the film sample also prevents any possibility of flashover, ensuring no short circuits before the actual breakdown.

As a side note, the tests were performed in an unthermalized room, thus requiring all measurements to be performed on the same day in a short timeframe to remain comparable.

b. Data treatment

Dielectric breakdown is a destructive event and the measured breakdown voltage value depends on several parameters, such as the voltage ramp rate, the quality of the samples, the thickness homogeneity etc… It is unlikely that a single sample shows multiple breakdown results that are statistically consistent and most of the time, breakdown values can vary widely within the same sample.

Weibull statistical analysis has been favored to compare results for breakdown failures. Initially based on empirical studies of failing systems, it helps describing a statistical rate of failure depending of time. When a linear voltage ramp is applied to a material, an assumption can be made on the correlation between time-to-failure and voltage-to-failure that can be used to describe breakdown events as a function of the electrical field statistically.

In a system obeying a two-element Weibull distribution, the cumulative probability of failure P as a function of the electrical field E (from the time-to-voltage linear assumption) must obey the following equation :

$$P(E) = 1 - exp\left[-\frac{E}{\alpha}\right]^{\beta} \quad (5)$$

Where α and β are respectively the scale and shape parameters of the distribution, with α expressing the field obtained at a breakdown cumulative probability of 63.2% and β being a measure of the dispersion, increasing with the decreasing scattering of results.

By ranking the breakdown values obtained during the test by increasing order, it is possible to approximate the cumulative probability of failure [115]. According to Fothergill (1990) [116], the best approximation can be obtained using the median rank F of the i^{th} data point, calculated from the total number of measurements N:

$$F(i, N) = \frac{i - 0{,}3}{N + 0{,}4} \quad (6)$$

By assuming the equality between the cumulative probability of failure P and the median rank F, one can use the expressions (5) and (6) to plot the experimental data as a linear function and determine the two parameters α and β as follow :

$$F = 1 - exp\left[-\frac{E}{\alpha}\right]^{\beta} \quad (7)$$

$$Ln\left(\frac{1}{1-F}\right) = \left(\frac{E}{\alpha}\right)^{\beta} \quad (7')$$

$$Log\left[Ln\left(\frac{1}{1-F}\right)\right] = \beta \log(E) - \beta \log(\alpha) \quad (7'')$$

c. *Results and discussion*

Figure 71 shows the Weibull plot obtained for 28 data points and the determination of the Weibull coefficient by fitting of the associated linear function. By analysing the data, it appears that the material has a high dielectric strength at the chosen application-relevant thickness, with the lowest breakdown value being above 60kV/mm and the highest being above 70kV/mm. Focusing on the Weibull parameters, the data can indeed be represented as a two-parameter Weibull distribution and the high beta values show a narrow distribution of results. With an alpha value above 68kV/mm, this material shows high breakdown strength capabilities at room temperature on a statistically relevant indicator.

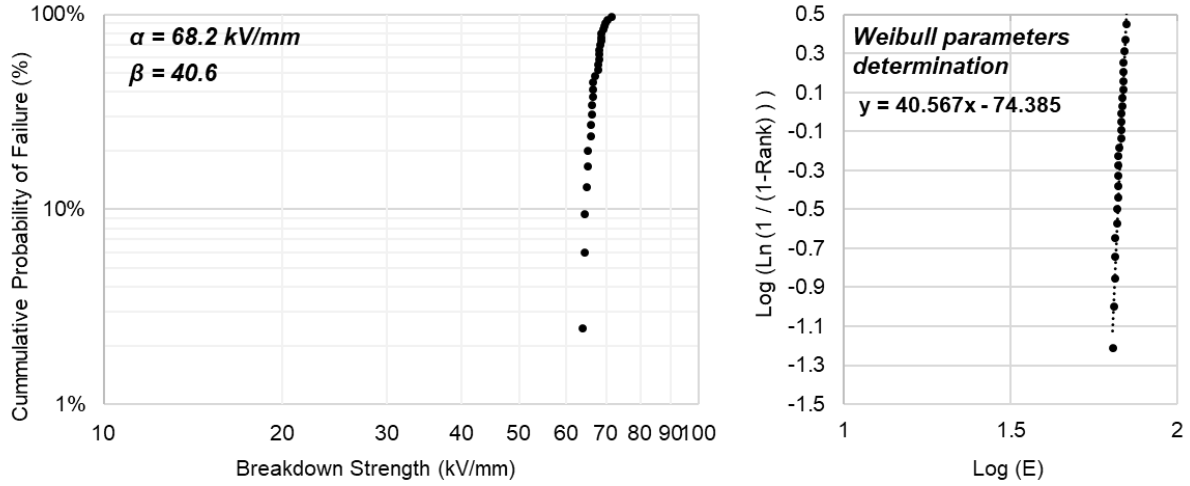

Figure 71 – Left) Weibull plot of the breakdown strength for the elaborated vitrimer. Right) Linear assumption and determination of the Weibull parameters from the trendline equation

Compared to silicone gel that exhibits a dielectric strength of about 15-20kV/mm, this is a significant increase, comparable with the expected values for hard epoxy resin. Additionally, given the high dielectric strength of this material, all measurements happened above 20kV, which is superior to the dielectric strength of the insulating oil surrounding the samples. This means that breakdowns all occurred under a sustained partial discharge regime, with the fluorinated dielectric oil generating numerous high energy sparks onto the sample surface for several seconds before finally reaching values sufficient to break the tested material (cf. **Figure 72**). Very similar conditions have been explored by Bjellheim and Helgee, testing the AC (50Hz) breakdown strength of aromatic polymers under partial discharge regime [117]. This study showed the negative impact

of partial discharges on breakdown values, suggesting that the "*true"* dielectric strength for the elaborated vitrimers is probably higher than what was measured.

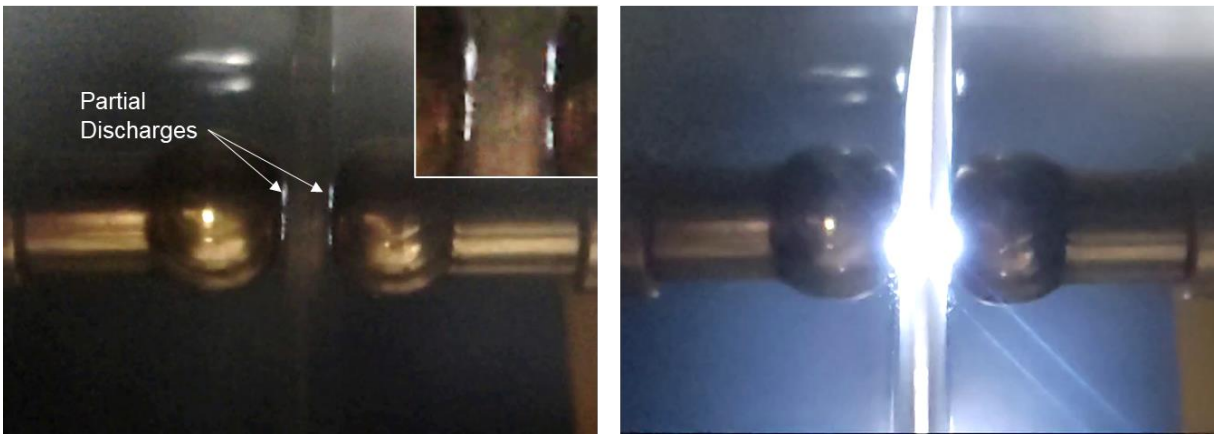

Figure 72 – Left) Electrodes in contact with the sample showing sustained arcing near the surface. Insert shows a zoom of the arcing region. Right) Actual breakdown occurring in the sample shortly after

In comparison, new WBG power modules module voltages are expected in the range of 10kV with thinner dielectric layers around the side of the chip (> 10kV/mm), but also thinner insulation on top of the component compared to Si-chip devices [20]. Looking at maximum values expected for this technology, WBG chips with a maximum blocking voltage above 20kV could be used in the future [118]. In addition, new design geometries[119], field-grading materials [120] and tuning the permittivity of the insulation [20] can also be developed to alleviate the high fields in the most stressed regions.

In that regard, the dielectric strength of the vitrimer developed in this work is well aligned with the requirements of wide band gap technology and could possibly be employed in ultra-high voltage applications in the future.

4. Conclusion on the applicability of the material

According to the high thermal stability, up to 360°C and the low degradation shown in thermal cycling up to 300°C, the designed network is well suited for high-temperature operations expected for high-power devices.

With reasonably high elastic properties below Tg, guaranteeing dimensional stability and stiffness during manipulations, this material is compatible with power boards manufacturing. In accordance with other epoxy resins used to make PCBs, the addition of reinforcing fibers should improve the mechanical properties of the material up to values comparable with that of commercial reinforced composites.

Above Tg however, a large drop in modulus can be expected and indicates that mechanical strength at high temperatures is not guaranteed, which requires specific care when planning for an actual production workflow. Tuning of the Tg is probably necessary to exploit the thermomechanical profile of these materials and make handling the material more convenient since the actual Tg is close to room temperatures. Despite the low elastic behaviour, the material already shows interesting damping properties that could be used to relax stresses, making it an interesting hybrid solution between a hard FR4 material that shows cracks in thermal cycling and a soft gel that lets wire bonds deform freely.

Finally, with a high dielectric strength at room temperature, the material is well aligned with the requirements of future modules, even in the highest voltages proposed so far. However, evaluation the breakdown strength in temperature should be performed to guarantee a high insulation level on the entire temperature range of the device. Appropriate management of the field concentration and careful design of insulation distances should also be addressed to alleviate part of the electrical stress received by the insulation material.

Overall, these measurements show that the material is compatible with power electronic applications and PCB manufacturing.

2. Manufacturing of a self-healing PCB

1. Preparation of PCB base materials

a. Resin Coated Copper (RCC) manufacturing protocol

Resin Coated Copper (RCC) is usually produced as a first stage element for PCB production. Typically composed of a single layer of copper onto which epoxy resin is coated and pre-cured, it serves as a stackable layer that can be finally cured to obtained a layered "*pre-PCB*". The actual PCB will be obtained after etching the unwanted copper into conductive tracks and drilling/etching conductive vias between the selected layers.

To make a RCC using press-molding, copper sheets were used instead of the unmolding sheets to close the top and bottom side of a rectangle mold of the desired dimensions, resulting in a dual-sided RCC. The idea behind this is that the resin will coat the copper as a viscous liquid, penetrating in the surface rugosity, before curing and strongly bonding itself to the copper sheets. In that case, the copper acts both as a confinement medium for the mold but also as a part of the final product. The entire mold will therefore be destroyed at the end of the process, cutting away the unnecessary spacer and only leaving the middle where the RCC remains.

Figure 73 and **Figure 74** show the entire RCC manufacturing process. First the bottom press plate made of layered aluminium and steel is placed on the table, the copper sheet (35µm thick here) is aligned on top of the press-plates with its treated surface side facing up, using the alignment pins. The desired sacrificial mold is placed on top of the bottom copper to create the main cavity. The top copper sheet and press-plate are reserved aside for closing the mold later.

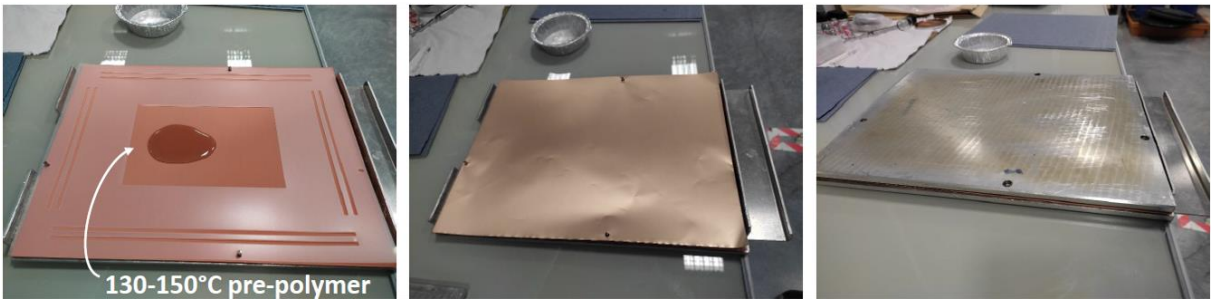

Figure 73 – Layering of the mold system. Left) Press-plates / Copper foil / Mold layer / hot pre-polymer, Middle) Addition of the top copper foil, Right) Entire pressing vessel closed

As mentioned before, the main difficulty with press-molding of large objects using this resin is being able to keep the thickness constant, by managing the relationship between the quantity and viscosity of the pre-polymer introduced, in regard with the mold volume and sealing ability. Depending on the pre-curing time, higher viscosity resins can be obtained and tend to result in a good pressurization. On the other hand, working with lower viscosities allows for a better spreading/penetrating ability in the copper roughness and accommodate the evacuation of air bubbles more easily. Thus, the prospect of better-quality product makes it desirable to work with lower viscosities, right after their mixing, as long as their confinement during the pressing remains manageable. By experimenting with these parameters, the final product should have a well distributed thickness over large distances.

For a cavity of 10x15 cm² and about 300µm thickness, about 7g of prepolymer is prepared (guideline of 1,5g.cm^{-3} accounting for resin loss in the pan). This amount should not overflow out of the press-plates as the copper sheet outside of the mold cavity has many rugosities accepting the

overflow. Regardless, overflow volumes and heat-resistant adhesive tape were still used as preventive measures, ensuring complete hermeticity.

Once the adequate quantity of pre-polymer is prepared, it is poured onto the bottom copper sheet (see **Figure 73**). Due to the low viscosity, no bubbles should be seen, and the resin should wet the copper rapidly wherever it flows. Afterwards, the top copper sheet is placed onto the still liquid pre-polymer with its surface treated side directed towards it. Angling the copper sheet and slowly applicating from one side to another allows the air to escape, preventing bubbles trapping in the middle of the RCC. Once the copper sheet is fully in contact with the resin, the top press-plates are finally added, pressing the layers together and spreading the thickening pre-polymer. After this last step, the RCC can be pressed for 1h at 150°C under 1MPa of pressure, using the same pre-heat and pre-press protocol detailed in Chapter II.

To obtain the final product, the press-plates are opened and the layered mold system is removed to cut the RCC out of the mold (see **Figure 74**). Once freed from the mold, the RCC can be observed in cross-section, revealing a very consistent polymer thickness across the entire length of the board, with an average thickness of 349.1µm over a millimetre span and no apparent voids. Compared to the 300µm thick mold used to confine the polymer on the sides and accounting the added rugosity of both copper sheets, this result is acceptable and consistent with a proper pressurization of the mold.

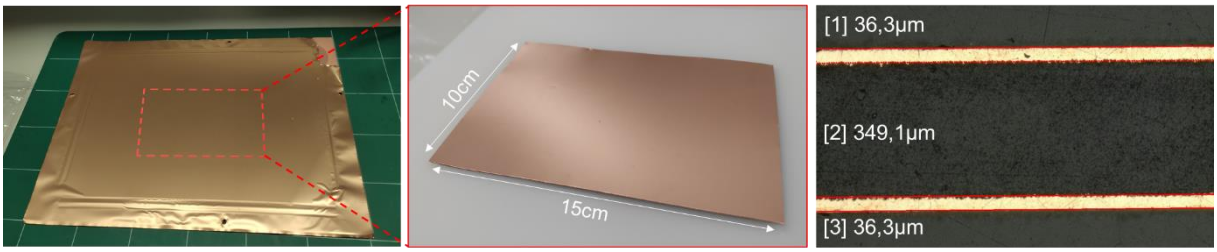

Figure 74 – Left) Raw RCC + Mold with cut lines, Middle) Cut-out RCC, Right) RCC cross-section

Using this liquid approach, power chips could be sintered onto the copper sheets and buried in a batch of liquid resin, which should create the hydrostatic pressure necessary for accurate insulation thicknesses if the mold pressurization is achieved correctly. This allows to produce any insulation thickness depending on the spacer used for the mold, which is reminiscent of injection or transfer molding processes and occurs at a similar pressure range.

On the other hand with pre-cured RCC layers, it is not easy to scale the insulation thickness to different dimensions than what is directly provided by RCC manufacturers. Transitioning from RCCs to fabric-reinforced prepregs may be a satisfying solution to stack any desired number of dielectric layer but removes the possibility of using neat resins or unwoven reinforcements without pre-curing and requires much higher pressures. Using solid dielectric layers also leads to variable insulation thicknesses depending on the pressure used during curing [121].

Overall, this method is effective to create semi-finished products of satisfying quality for future PCB manufacturing and could be used to embed power electronics systems or create pre-packaging for dies before their implementation into custom systems. However, the actual efficiency of the latter and actual the throughput still need to be evaluated. The material should also be compatible with existing processes like potting and transfer molding, given the low viscosity and apparent high wettability of the liquid resin.

b. Addition of reinforcing fibers

A similar process can be followed for the addition of reinforcing fibers, leading to a final product that resembles more of a Copper Clad Laminate (CCL), which is a commercial base material used directly for PCB production.

Fiberglass cloths for re quite diverse (types of glass, number of threads, density etc…) and for electrical applications, Electrical glasses (or E-Glass) are typically favoured. In this study, a 1080 E-glass fabric was selected as the fibers are arranged in a simple alternating pattern while also opened to resin penetration (see **Figure 75**) but manufacturers often tend to use a higher glass content, like in the 2116 or 7628 cloth as it requires less resin to produce classical PCBs, representing an economic gain.

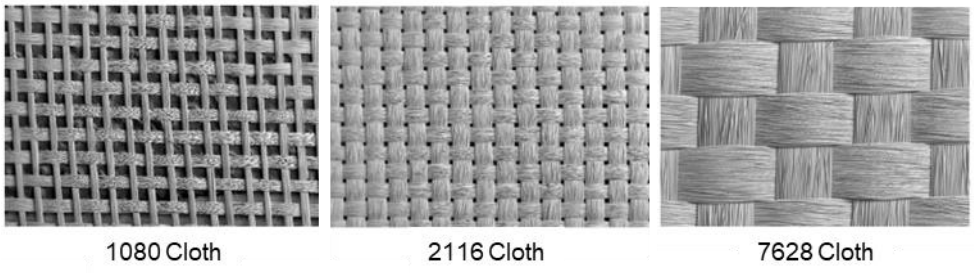

Figure 75 – Common fiberglass cloth types used for printed circuits boards [35]

Handling glass cloth by hand is quite difficult as the bundled fibers can move significantly, leading to gaps with less fibers and domains where the fibers are pressed together. Cutting the fibers to accurate tolerances is challenging by mechanical means, thus the use of a CO_2 laser was especially efficient not only for cutting precisely without manipulating the cloth but also because the melted fibers tended to lock in place and kept the appropriate shape for the mold (cf. **Figure 76**).

Figure 76 – Left) Cutting process using a CO_2 laser. Middle) Repeatable cut of glass fibers. Right) A fiberglass cloth deposited onto the bottom copper sheet and filling the mold cavity.

Similarly to the RCC process, the hot pre-polymer was directly poured on top of the dry glass fabric, resting on the bottom copper sheet. Right away, a great wettability of the fibers could be observed, with the optical disappearance of the fabric in the liquid resin due to similar refractive indexes. Once all the resin was poured, the mold was closed and subjected to the same hot-press protocol as detailed in **Chapter II**. After 1 hour at 150°C, the Copper Clad Laminate was cut out of the mold and cross-sections were performed.

Figure 77 shows the cross-section of the CCL, revealing a good distribution of the fabric inside of the board. The fibers are reasonably centred and are effectively coated with resin from the top and the bottom, despite the initial placement of the dry fibers, and this over large distances. The thickness of the board once again is well respected with a rather constant value of 330µm across the cross section of several millimetres and is assumed similar over the entirety of the board. In

addition, the fibers seem to be infused with resin as no bubbles or voids can be seen inside fibre bundles with optical microscopy. Finally, the fibers cannot be observed in their length as the fabric was purposefully cut and placed at a 45° angle with respect to the side of the CCL for later tests (detailed in part 3.3.a(iv)).

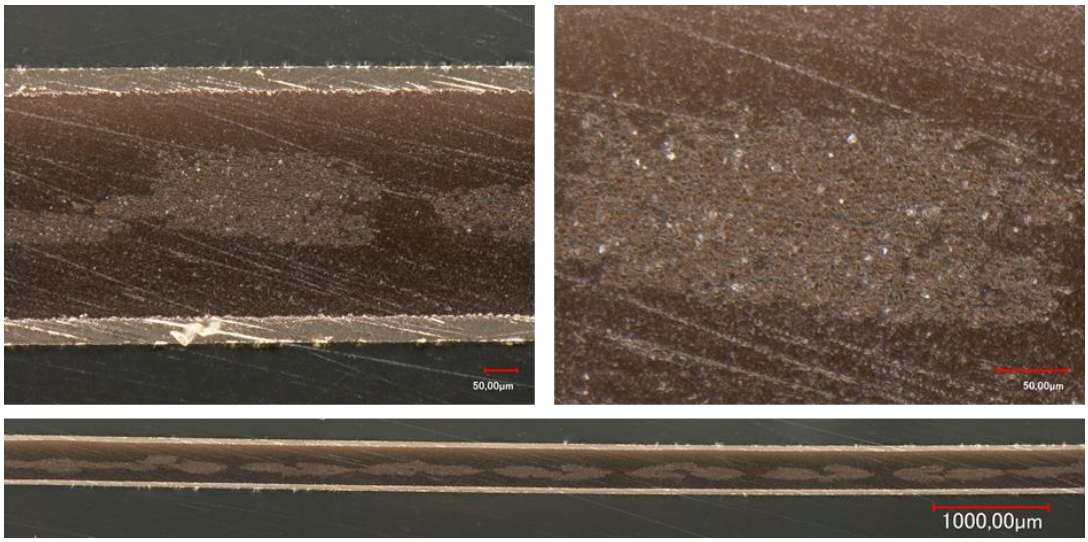

Figure 77 – Cross-sections of a self-healing CCL manufactured by hot-press molding. Different magnifications are provided, showing the infusion of glass fibre bundles and the regularity of the board thickness.

As a conclusion the use of this resin with press-molding process gives suitable results to go further into the replication of a proper PCB through the creation of copper tracks.

2. Copper etching protocol

The etching process allows to remove part of the copper from the base material to obtain the desired conductive tracks of a PCB. This process can be performed on both RCCs or CCLs regardless of the internal reinforcement, but the most critical test was to use no reinforcements and see if the board would be fit to survive all the required manipulations. The compatibility to the etching process typically used for PCB manufacturing was therefore assessed starting from a cured unreinforced RCC with copper on both sides (as presented in **2.1.a, Figure 74**).

Selective removal of the copper is achieved by following a precise protocol, involving the protection of the desired areas and exposure of the unwanted ones to chemical baths. To do so, a photosensitive dry film is laminated onto the board and will act as the main mean of protection of the copper. The lamination process was achieved using Eurolam M300 laminator that slowly heats up two rolls of the dry film and feeds the board in between them. Once finished, the RCC is completely wrapped in the film and no bubbles should be present over the entire surface.

Depending on the desired track pattern, a suitable mask is printed and taped onto the dry film to allow or prevent selectively the passage of light. Indeed, the dry film polymerizes under UV light, which makes it impervious to the chemicals used for etching, thus protecting the copper underneath. The negative pattern must therefore let the UV light pass where copper needs to remain and prevent it from polymerizing the dry film where it needs to be removed.

After a couple of minutes under a UV lamp, the board can be removed and the pattern can be seen directly as the exposed film has darken significantly. Removal of the lighter, unexposed film is achieved by immersion in a commercial revelator solution and light scratching using a very soft

brush, thus exposing the soon to be etched copper. The resulting protected board is shown in **Figure 78**.

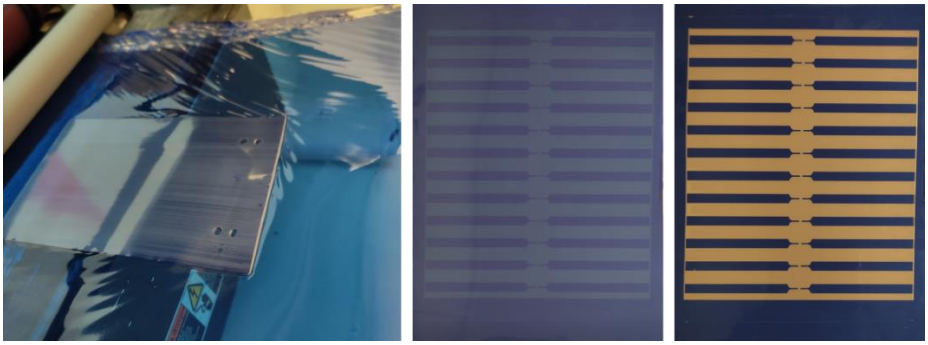

Figure 78 – Left) Lamination of the dry film onto a RCC. Middle) Dry Film after UV exposure appears darker. Left) Revealed pattern showing the unwanted copper

Etching of the now exposed copper can be done in a concentrated iron perchloride solution, using a Sprint 3000 Bungard etcher (cf. **Figure 79**). The boards are passed through several chambers projecting the hot iron perchloride solution from all sides, before being rinsed and wiped several times with absorbent rollers. Depending on the temperature of the iron perchloride bath, the speed of the rollers and the thickness of the copper that requires etching, multiple passes can be done until reaching a satisfying state. If the dry film was correctly laminated and revealed, it should remain bonded to the board.

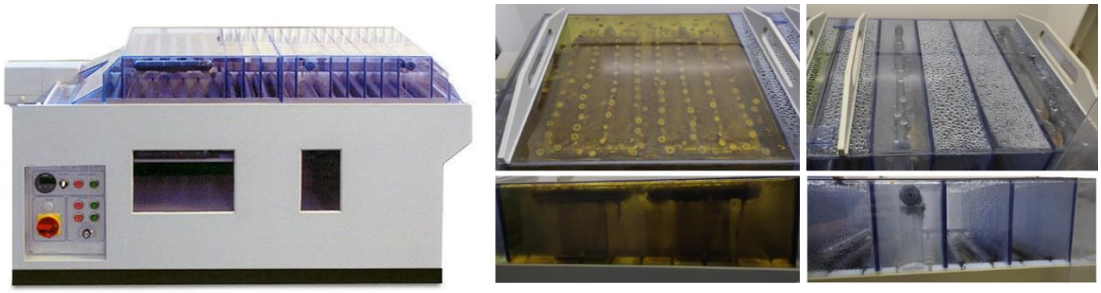

Figure 79 – Left) Sprint 3000 Bungard etcher. Right) Treatment chambers showing the yellow iron perchloride and the following rinsing compartments

To finally strip the polymerized dry film off of the etched board, the now called PCB is dipped in a dilute solution of sodium hydroxide until complete removal. The final product is obtained after rinsing in water and drying. The result can be seen in **Figure 80**, showing twenty-four large tracks per board, which are arranged in twelve mirrored couples and thinning down to a small tip. The mirrored tracks are spaced with a precise 1mm gap separating the thin tips and will be used for later testing, yielding numerous repeatable samples in one go.

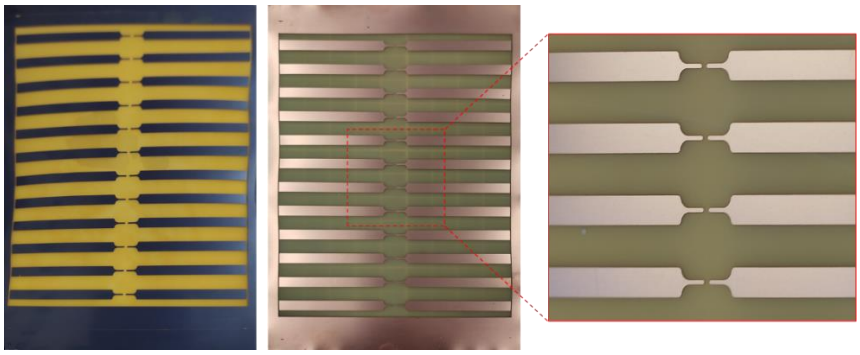

Figure 80 – Left) Etched PCB before stripping. Middle) Stripping of the dry film and exposure of the protected copper. Right) Zoom on the track design

Visual conformity was assessed, the polymer didn't seem to suffer any degradation following the procedure and its apparent adhesion to copper remained strong despite the numerous chemical baths and manipulations. A slight roughness can be seen on the vitrimer surface since the resin replicated the topography of the surface-treated copper sheets, giving it this opaque aspect. Comparison of the FTIR spectra of a fresh vitrimer film and the vitrimer exposed after the etching process showed no modification in the chemical nature of the material, which ensured conservation of self-healing properties of the printed circuit board throughout the whole manufacturing process.

3. Conclusion on the manufacturability of vitrimer-based PCBs

The adequation of the vitrimer resin with the production process of PCBs was demonstrated. The manufacturing of several high-quality semi-finished and final products was shown, using conventional manufacturing techniques and machines.

Large surfaces RCCs and CCLs, with entirely customizable elements were obtained with uniform insulation thicknesses from the commercial copper sheets and fiberglass cloth, using the developed resin. Demonstration of a complete etching protocol was provided using the worst mechanically stable material (no reinforcements) without needing additional handling care compared to a classical PCB.

While via drilling, metallization and soldering operations are not shown in this work, the potential of these vitrimeric resins for PCB manufacturing is promising.

3. Self-healing efficiency based on electrical indicators

1. Concept of electrical insulation recovery tests

Evaluation of self-healing efficiency is still a new concept that does not benefit from many previous studies and accurate testing methods are still not clearly described. Especially under high electric fields, where vitrimers are not often represented and even less so for their insulating properties. Indeed, most authors using vitrimers in electrical applications tend to create conductive composites where the conduction is mostly ensured by carbon nanostructures and where the role of the matrix is solely to provide a healable mechanical support.

To evaluate the recovery of electrical insulation properties, it was therefore necessary to imagine and create entirely novel tests that could replicate relatable damages occurring in the applicative domain, degrade the insulation properties and be able to repair those damages in order to rate the recovery.

As a reminder, the damage occurrences and the rated property do not have to exist in the same domain necessarily. In the case of power electronics, most often the damage comes from the mechanical domain and is translated into an electrical failure. Thus, mechanically damaging samples and trying to rate electrical properties prior, during and after the damaged state is the main objective for this study.

2. Breakdown recovery tests

a. Sample design process

(i) Requirements for PCB breakdown recovery tests

Breakdown events rarely occur in new, uncycled electrical systems that were properly designed. Insulation thicknesses are calculated to provide sufficient margin for the expected electrical fields and failures are most likely related to manufacturing defects or unfit design. More realistically, breakdown occurs once the healthy insulating PCB material is damaged, usually from thermomechanical stress generating cracks, thus changing the electrical field distribution and effective insulation thicknesses.

Additionally, once breakdown occurs, the system cannot be repaired anymore, as the chemistry of the material changes drastically, turning most of the useful hydroxyester functions into carbon and water. Evaluating the breakdown strength of a sample is therefore mutually exclusive with further healing steps.

With these elements in mind, proposing a critical evaluation of the breakdown strength recovery requires to degrade the insulation thickness of a PCB by creating a mechanical damage between conductor tracks, and then to be able to repair it in a way that emulates what could happen within a PCB. The healing efficiency is thus rated as the extent of breakdown recovery with reference to healthy samples. Thus, the proposed method allows to assess how well the repaired material can resist new high voltage spikes that would have provoked a breakdown without healing, compared to a pristine volume of insulation.

As a more practical consideration, a breakdown test is destructive and requires a sufficient number of measurements to provide a reliable estimation of the breakdown strength. As a single PCB board can be time consuming to produce, 12 samples were manufactured simultaneously on the same board, allowing to increase the statistical significance of the study. Also, having a complete batch of samples on the same board guaranteed that the exact same materials and treatments were used

and thus, that batch-to-batch variations would not have affected the variance in the statistical analysis.

(ii) Electrical stress concentration

The PCB manufacturing process of section **2.2** was designed specifically to answer several key requirements for breakdown voltage recovery tests. A suitable conductive material (Cu) was etched into several couples of electrodes with a precisely controlled insulation gap for the breakdown to occur in. Given the high dielectric strength of the vitrimer (> 50kV/mm) and the practical complications associated with the manipulation of tens or hundreds of kilovolts, only a thin insulation distance could be selected and was set at 1mm. Additionally, to avoid larger energy densities and to guide the electrical field toward the middle of the sample, field-enhancing tip geometries were produced, reducing the nominal voltage to more reasonable levels easier to implement experimentally (previously shown in **Figure 80**).

The etching process used to create the electrodes also removed copper in between them. To obtain a well-insulated system, the entire board was re-embedded in a new batch of vitrimer, using the same developed press-molding process. Surprisingly, doing so allowed to retrieve the transparency of the vitrimer, as new unpolymerized resin penetrated inside the surface roughness and bonded on a molecular level with the previous batch. The final test vehicle looks as a single piece with no optically visible interfaces between the two batches. Finally, to allow the connection of the electrodes to the high voltage power supply, the larger portions of the copper electrodes were exposed using a CO_2 laser that could etch selectively the vitrimer without damaging the copper (cf. **Figure 81**).

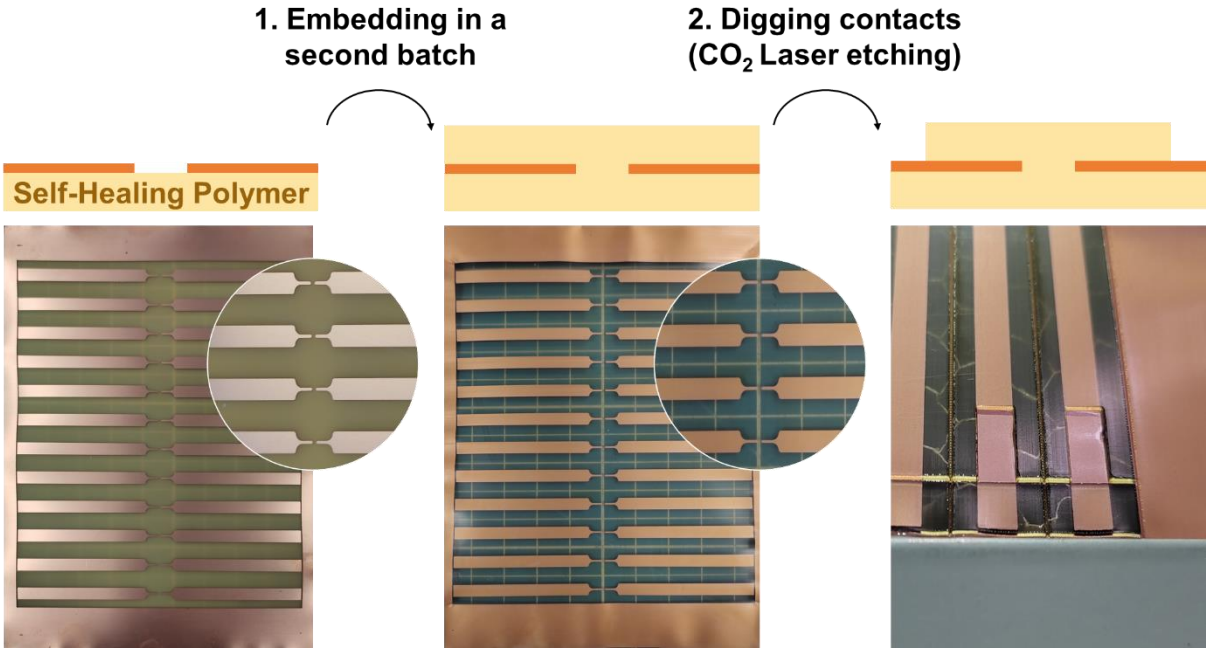

Figure 81 – Insulation of the bare electrodes in a second batch of vitrimer, before laser etching of the electrical contacts required for the breakdown test

(iii) Mechanical stress concentration

Create a crack in a tough and stretchable material, while controlling its propagation between 1mm spaced embedded copper electrode is quite challenging. The main strategy for controlling the mechanical damage was to use an open notch to direct and enhance the mechanical stress, using a CO_2 laser to cut the material precisely. By using a tensile test bench, a pulling force can be applied on both sides of the notch. This stress configuration favours a Mode I opening of the crack, that

should initiate at the notch and propagate in a straight line through the homogeneous insulating material. However, this is a rather theoretical description to of fracture mechanics for softer materials, as many polymers tend to deform extensively before actually starting to shred. To reduce the plastic deformation that relaxes some of the applied force and thus increase the stress level at the fracture tip, the test room was thermalized to 20°C and samples were quenched after thermalization at 150°C for 1min by sudden exposition to air at room temperature.

In addition, a second notch was designed as a closed cavity to receive the forming crack and stop it before complete separation of the sample. This step is important, since keeping this small interconnecting piece at the bottom allowed to benefit from the shape memory effect of the polymer to pull the sample back together and realign the electrode tips together more precisely. This is critical to guarantee a repeatable insulation distance in between the pristine and healed state.

Figure 82 shows the final samples after the electrical contacts and notches are made, yielding a dual stress-concentration geometry.

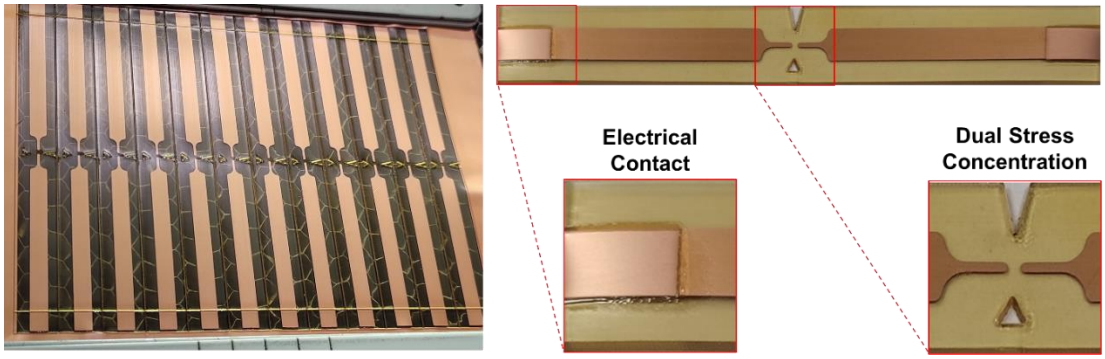

Figure 82 – Left) An embedded-PCB on the laser honeycomb cutting bed. Right) Final individual sample after complete processing showing the dual stress concentration geometry.

b. Breakdown recovery test

To evaluate the rate of recovery, reference samples were subjected to a breakdown "*as is*", asserting the baseline for "healthy" samples. Other samples were instead damaged mechanically with a *Deben Microtest tensile stage*, where traction was performed at 1mm/min, to the point where electrical failure would occur in a high voltage scenario, i.e. when a complete air gap is obtained between the electrodes (cf. **Figure 83**). The test is stopped as the crack reaches the closed notch, before the complete rupture of the bottom connective piece to take advantage of the shape memory assisting the healing process.

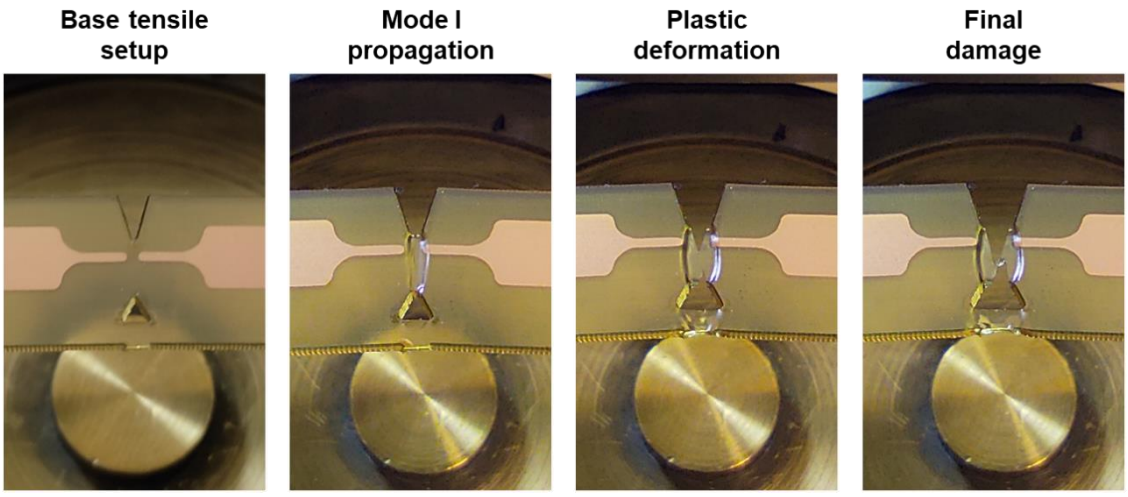

Figure 83 – Damage process using the mechanical stress concentration geometry. The bottom connective piece is plastically deformed but remains unbroken.

Again, for the recovery protocol to remain representative of what could happen spontaneously inside of a confined damaged board, no external pressure was used during the healing process. In some cases, the work provided by this small, connected part was sufficient to even weld back the fracture sides, but due to the much larger/heavier pieces lightly sticking to the oven surface, manual help was provided when necessary to put surfaces back into contact. Afterwards, the samples were healed for increasing time durations (5min, 30min, 1h) at 150°C in a convection oven. Once welded for their respective times and cooled down, the now repaired samples were subjected to the breakdown test and their dielectric strength was compared to the references value. A complete overview of the sample degradations and recovery for this test can be found in **Figure 84**.

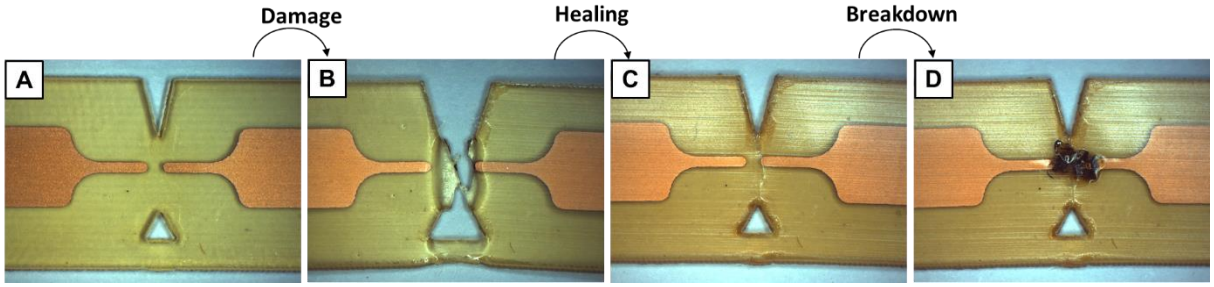

Figure 84 – A) Pristine sample showing the dual stress-concentration geometry. B) Damaged sample after crack propagation, stopped by the closed notch cavity now plastically deformed. C) Healed sample exhibiting a small surface scar. D) Tested sample after breakdown rating the quality of the welded volume.

For the breakdown tests, the pristine and healed samples were supported using a PMMA frame to avoid mechanically damaging the healed portion during manipulations. The electrical contacts were connected to a 300kV AC 50Hz ultra-high voltage supply using alligator clips and the voltage was raised linearly with a ramp of 2kV/s until breakdown. The entire setup was immersed in dielectric oil to further prevent dangerous arcing, even though the electrodes are surrounded by at least 300µm thick vitrimer from top and bottom. Given the electrode configuration and insulation conditions, no circumvention was observed as the current crossed directly in between the vitrimer gap.

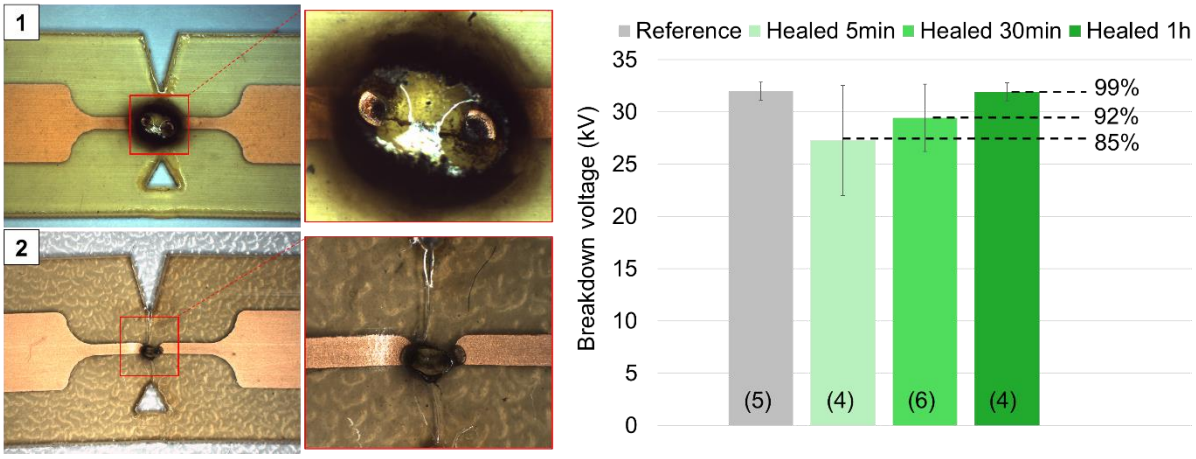

Figure 85 – Left 1) Pristine sample after breakdown. Left 2) Healed sample after breakdown. Right) Breakdown voltages of damaged samples after increasing healing durations compared to the reference. Numbers in bracket indicate the number of tested samples for each condition.

Results for the recovery of the breakdown strength of healed samples compared to the unbroken references are presented in **Figure 85**. For reference samples, the measured breakdown was repeatable with an average value of 32 ± 0.9kV for a 1mm insulation gap. Compared to the intrinsic dielectric strength measured in the appropriate conditions (> 60kV/mm), this breakdown value remains high given the concentrated field configuration.

Analysing the healed sample data, the recovery of breakdown strength starts early in the healing process with an average of 85% of the reference average breakdown voltage after only 5min of recovery at 150°C. By analogy with mechanical stress, one would assume that the networks of both fractured pieces are required to merge deeply to recover a high fraction of the initial strength and that simple reconnection of the pieces would not be significant for high stress conditions. However, since the electrical stress is very localized, it is possible that simple network reconnection is sufficient to recover a large portion of the breakdown strength. Also, for the 5 minutes healing duration, dispersion of the result is quite significant (±5.3kV) meaning that not all samples were healed as efficiently in this short time or that manipulating these barely mechanically healed samples has possibly degraded the new weld, leading to more deviation in the results.

In comparison after 30min and for longer periods of healing time, the recovery increases up to virtually 100%, with an average of 92% of the breakdown voltage of references and a decreased standard deviation of ±3.2kV, resulting in samples almost as endurant as the references against dielectric breakdown. After 1 hour in the oven, samples showed an average rated recovery above 99% and even exhibited the same dispersion as pristine samples (±0.9kV), showing that the impact of the past mechanical damage on those samples is not significant anymore compared to the variability of the breakdown value between samples.

These results are therefore very promising for designing self-healing insulation materials that can prevent catastrophic failures like breakdown by pre-emptively repairing mechanical damages that reduce the insulation thickness, thus recovering the insulating function of the original material.

3. Partial Discharge Inception Voltage recovery

a. Sample design

(i) Requirements for PDIV recovery measurements

Having a mechanical crack propagating in between conductor tracks is quite representative of damages described in the literature after thermal cycling of PCBs intended for application in the field of power electronic. However the crack itself does not always result directly in a breakdown: most of the time, partial discharges trigger in the newly formed void, slowly eroding the material until reaching the required thickness for breakdown.

To test the recovery abilities of the vitrimer material in the field of application, a reinforced self-healing PCB was manufactured with the intention of generating damages between the fibers and the matrix, suitable for partial discharge initiation. By measuring the inception voltage at which partial discharges start to occur, coupled with imagery of the damages, one can estimate a reference Partial Discharge Inception Voltage (PDIV) and rate the degradation and recovery of this indicator along the healing process. Thus, the PDIV is used here as an indicator of the health status of the sample, with an expected lower PDIV when damages readily generate discharges and a higher PDIV when those damages are repaired.

One key consideration for this test is that the PDIV and other partial discharges indicators are not directly related to an intrinsic property of the material but rather relate to the entire system. It is important to correlate the variations of PDIV with actual observations or complementary measurements that can provide an explanation for these changes. One of the simplest way to do that is to observe the damages in the material and ensure that a correlation exist between the damage and the initiation of partial discharges.

Similarly to the design process in section **3.2.a**, a new type of sample was designed and manufactured to answer the requirements of this test, making it possible to impose two types of stresses (mechanical and electrical) while still getting close to a realistic applicative scenario.

(ii) Electrode design

The main idea for the electrode design is rather simple, with two parallel conductive planes on both sides of the sample that can be connected to a high-voltage power supply in order to generate an electrical field across the material thickness, effectively probing a large volume of material. As mentioned above, later steps require to damage the samples and observe these degradations which required a see-through electrode. That way, if a cavity is present in the volume between the electrodes, the increasingly high electrical field should trigger partial discharges that should be measurable by the test bench and the see-through electrode would allow to follow the repair of the damage during the healing protocol, with the intent to correlate to the measured PDIV.

To prevent a short-circuit between the electrodes, a side insulation of about 2mm was kept around the sample and the electrodes were extended in opposite directions so that each electrode could be pinched without also connecting the conductive plane underneath. The first idea was therefore to etch a grid-like electrode on top and at the bottom, providing an average potential plane on each side but still allowing light to pass through, before damaging the samples on a tensile test bench. But by doing so, a stronger cross-section was obtained in between electrodes, precisely where damages needed to occur to be detectable, which is not suitable for further testing (cf. **Figure 86**).

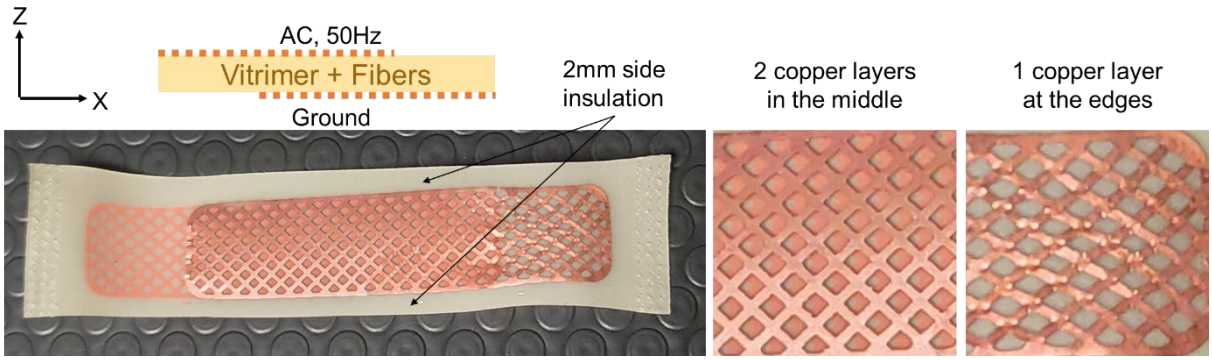

Figure 86 – Left) Electrode design on a prototype sample. Right) Observations of the copper grid after the damage showing that less deformation occurred in the test area.

To solve this problem and remove most of the mechanical contribution from the electrode, a simple reinforced PCB-like material was manufactured with the same resin and fibers but without the copper. Instead, a gold electrode was sputtered onto the material, using a custom mask system to create electrodes with a highly conductive surface, capable of accommodating the electrical needs of the test, while also remaining transparent and deformable. According to the sputtering parameters and prior evaluations done on the sputtering system, a layer of about 50nm of gold was deposited on both sides of the reinforced vitrimer sample, with both electrodes covering the middle section of the sample (cf. **Figure 87**).

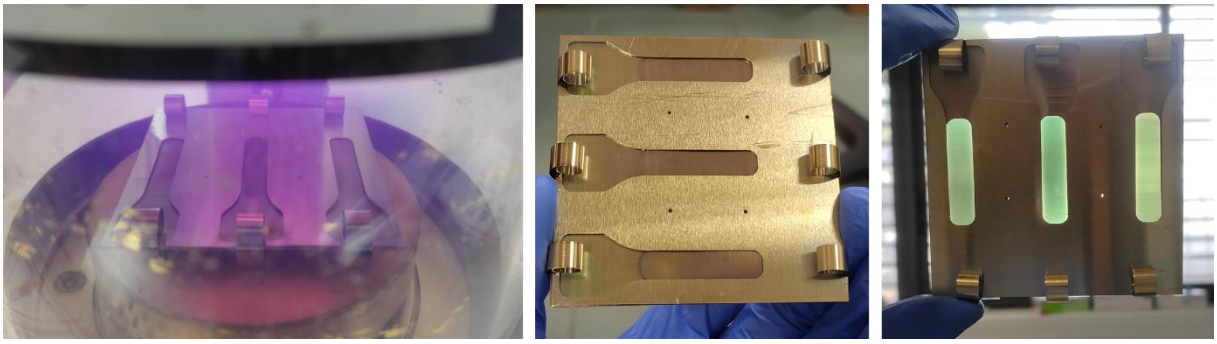

Figure 87 – Left) Steel mask with 3 samples inside the sputtering chamber. Middle) Geometry of the gold electrodes on one side of three samples. Right) Transparent middle section with the two top/bottom electrodes.

(iii) Electrical connection design

Given the system-related nature of partial discharges, a special care must also be provided to the test bench and sample connection points, to avoid triggering discharges outside of the sample. The available PD bench can already provide quality measurements up to 40kV without initiation of partial discharges but channelling such high voltages to the sample without generating parasitic PDs requires an appropriate sample holder.

A two-part custom sample holder was designed with round edges on the outside, and necessary sharp geometries hidden inside. A screw was implemented to electrically connect both parts of the holder and provided a pinching force to hold the samples. Inside of the holder, a high-performance cable is crimped by a lug that remained connected to the holder at all times via a spring, ensuring the entirety of the assembly remains at the same voltage (cf. **Figure 88**).

Manufacturing two of these holders allowed to obtain a suitable testing system for PD detection. A couple of PTFE holders were made to ensure that no electrical arcs could "*jump*" from one part of the sample to the opposite holder. After several tests, this proved to be unnecessary since the PDIV

was sufficiently low and the entire system including the sample was also immersed in fluorinated dielectric oil to prevent corona discharges.

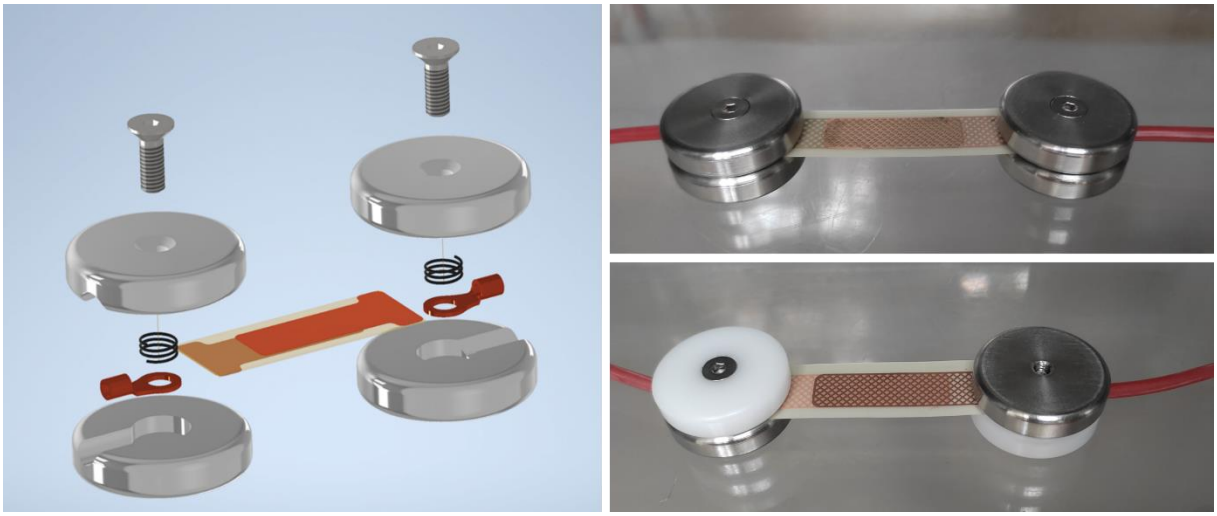

Figure 88 – Left) 3D model of the designed sample and the associated holder. Right) Both Steel/Steel and PTFE/Steel holders with a sample prototype.

(iv) Mechanical damage theory

As a first approach to generate internal mechanical damages within the composite material, reinforced vitrimer samples were subjected to a tensile test. Despite the thermalized room (20°C), the resin still exhibited a much larger elongation potential than the glass fibers, resulting in the breakage of fibers that would not be repairable regardless of the surrounding matrix.

In order to create damages in the matrix without destruction of the emulated PCB reinforcements, the fiberglass cloth was placed at a 45° angle compared to the tensile axis during the manufacturing of the samples. By doing so, pulling on inclined fibers will generate shear forces as the fibers try to align with the solicitation. Since the vitrimer is so compliant, fibers should be able to move inside the sample, thus heavily damaging the interface of each fibre with its embedding matrix (cf. **Figure 89**).

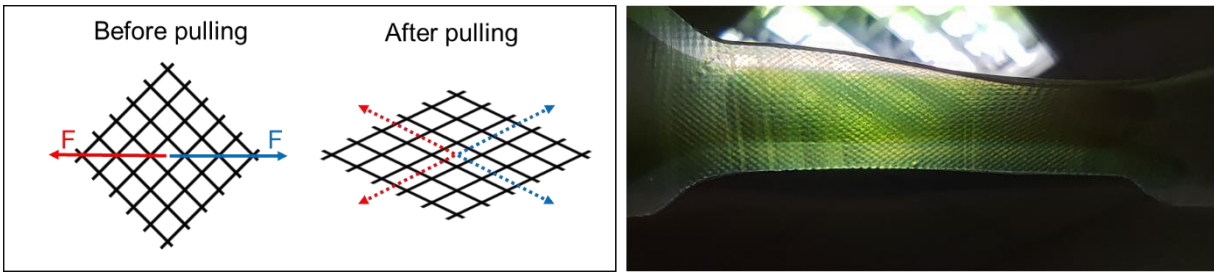

Figure 89 – Left) Concept for generating shear forces inside the reinforced material. Right) Observation of a sample with 45° inclined reinforcements, showing the deformed reinforcement in the network.

Since the fibers should not break before reaching a fully tensile position, it is possible to deform the composite significantly more, creating very large displacements. While this type of solicitation and its associated damages would not normally occur inside of a real PCB, there isn't really another representative way to create interfacial damages in a static test. Similarly, using a periodic stress test is not guaranteed to provoke the fatigue of a polymeric material and takes a very long time to perform [122]. Finally, thermal shocks most likely use temperatures ranges that include healing compatible temperatures to remain practical (without having to go to very low temperatures), making the discrimination of healing efficiency and aging difficult.

b. Partial Discharge Inception Voltage Recovery test

(i) Measurement protocol

Measurement of partial discharges initiation voltages (PDIV) was achieved using a developed 40kV PD-free test bench, run on a lower 15kV setting to improve the step voltage resolution. The high voltages was supplied using a mechanically-operated elevator transformer from the main power grid (230V – 50Hz). The discharge events were monitored using a *Power Diagnostix ICM compact* standalone interface and voltages were reported as Root Mean Square (RMS) values. To accurately measure the intensity of the discharges, the test bench was also calibrated using a *Power Diagnostix CAL1A charge injector*, delivering a precise 1pC charge to the system (cf. **Figure 90**).

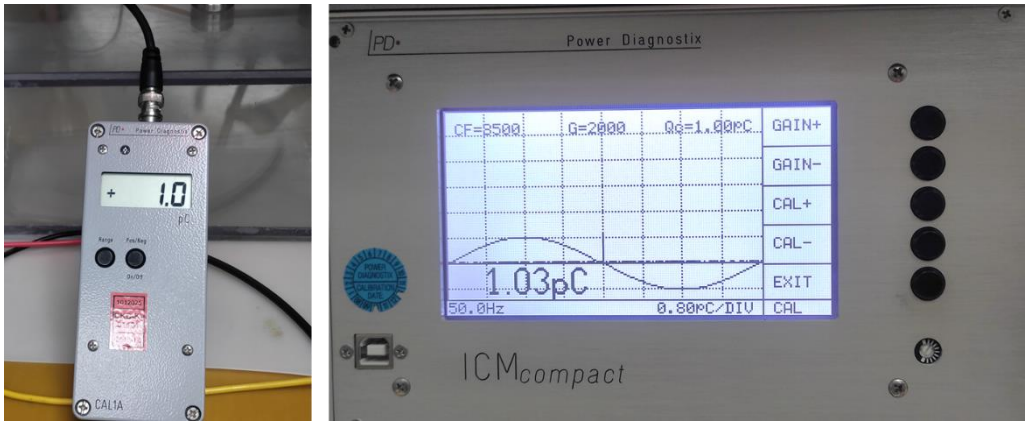

Figure 90 – Calibration of the partial discharge test bench, using a dedicated charge injector (left) producing a 1pC charge, displayed on the screen (right)

For this test, ten samples were produced and nine of them went through the entirety of the test procedure, leaving one spare undamaged sample. Each sample was tested until a sustained 4pC discharge regime was obtained, and the measurement was repeated 3 times per sample. After the nine samples have been tested, the bench was shut down until the next test phase.

The test procedure for samples regardless of their status went as follow :

- The two holders were respectively connected to the bench AC voltage supply and ground.
- Each individual sample was clamped to the sample holders and connectivity between the sample and the steel holder was verified systematically using an ohmmeter for both electrodes.
- The sample attached to the holders was placed in a tank containing a dielectric fluorinated oil (Galden HT55) preventing corona discharge.
- The bench door was closed manually and a safety electromagnet was activated, preventing further openings.
- Operating the main interface, the voltage was risen manually with 200V steps approximately until stabilization (few seconds).
- Once the PD inception criterion was reached, the voltage value (PDIV) was noted and voltage was decreased until discharge extinction.
- The voltage was increased again until reaching the criterion two more times.
- The voltage was turned off and the sample was removed until the next test.

(ii) Mechanical damage and healing protocol

After evaluation of the PDIV of pristine samples, each piece is damaged using a *Deben Microtest tensile stage* performed at 1mm/min. A maximum deformation of 15% was selected as observations

showed that the embedded cloth was deformed over most of the sample except for the thickest sections close to the clamping jaws. Deformation damages were clearly visible with the naked eye, showing optically deformed volumes where most of the pristine samples were entirely transparent.

Once all the samples had been damaged in the same way, they all underwent the same PDIV test protocol before being subjected to the healing heat treatment. According to the previous recovery results, the same treatment at 150°C for 1hour was employed. Similarly, given the extent of plastic deformation on these sample, the shape memory of the material triggered as soon as the material was heated and provided an autonomously generated internal forces that assisted the healing process, yielding samples with similar length as initially.

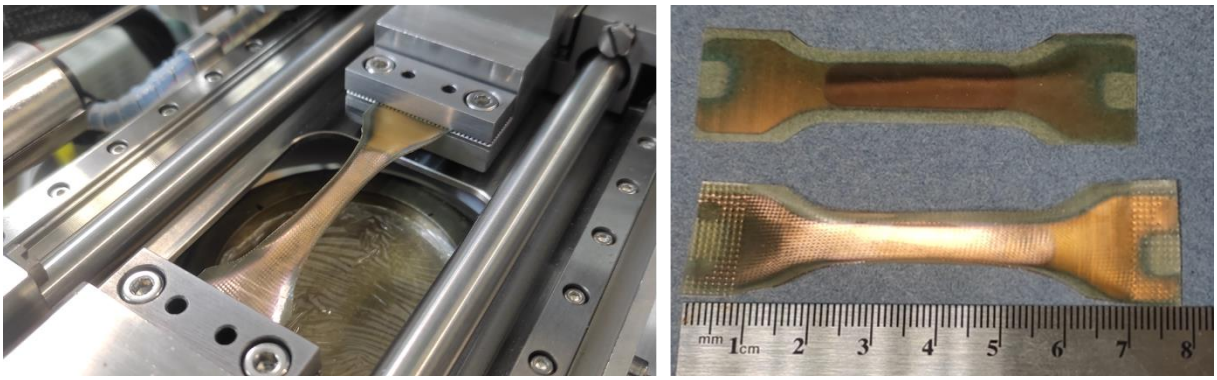

Figure 91 – Left) Tensile stage with a deforming sample. Right) Comparison between a pristine and elongated sample

When observing the surface of the healed samples (post damage and post shape-memory recovery), one can observe damages in the gold electrode, given the high deformation subjected to the samples. However, these damages were not sufficient to actually degrade the connection since connectivity was tested twice at all stage for all samples. **Figure 92** shows the topography of these samples and the appearance of cracks only in the gold-coated region. Very large cracks could be found in the gold electrode (biggest cracks in the 50µm range) with no evidence of damage on the polymer underneath. An interesting information would be to observe the state of the gold electrode directly after the damage. However, due to the low glass transition of the polymer, the heat provided by the microscope lamp was sufficient to trigger the start of shape memory, making it very difficult to access a clear optical plane right at the surface due to the sample displacement.

Figure 92 – Left) Surface observation away from the gold electrodes. Middle) Observation in the middle of a gold electrode. Right) Largest gold damage found on a sample

(iii) Results and discussion

Partial discharge measurements are inherently difficult to interpret, especially when low intensity discharges are not provoking visually appreciable arcs. Without visual confirmation of the

discharges, results can only be treated statistically and correlated to images of the most probable triggering defect to provide an insight of what might actually happen during the test. Thus, any of the following result must be regarded at a "*system level*", that can be caused by the state of the sample or not. Despite this disclaimer, the absence of partial discharge does give a clue on the healthy situation of the system and the tested sample. As shown in **Figure 93**, very high voltages (>10kV) comparable with the range of new ultra-high voltage devices can be sustained with minimal partial discharge intensity, thus demonstrating the quality of the material that can be obtained with the previously described manufacturing techniques.

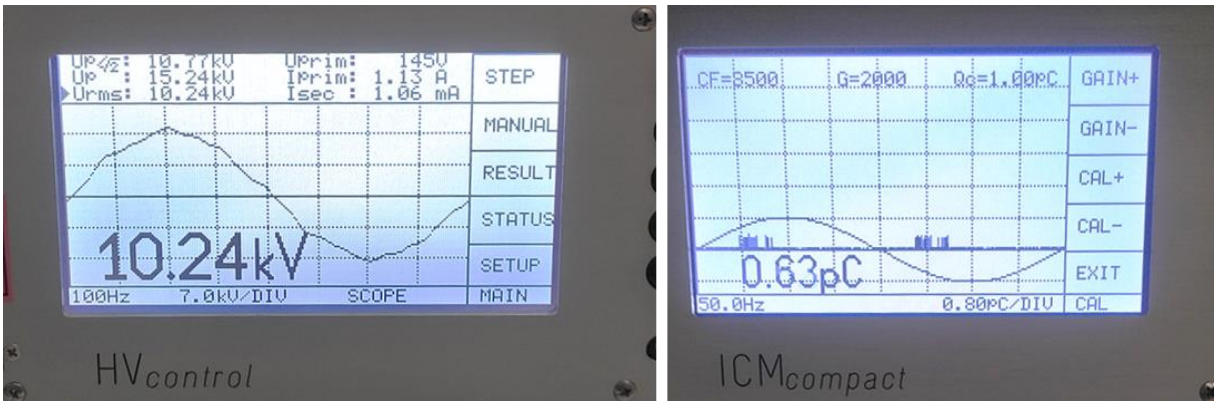

Figure 93 – Example of a very high voltage provoking very low intensity discharges on the test system including the tested sample.

All test results are provided in **Figure 94**, and show individual results obtained on the nine tested samples (3 measurements per sample) and the combined average values of PDIV obtained depending on the composite health status (27 measurements each). Interpreting the individual results, no clear trend can be found regarding the creation of damages or their recovery, on both PDIV values and deviation, with the lowest results obtained near 5kV and the highest reaching 12kV. For the latter, it appeared that 12kV was the limit of the designed system, since a clear typical ticking sound could be heard periodically (every few seconds), suggesting that charge was building up and discharging on the closest grounded surface, most probably outside of the sample.

Analysing the average values, the difference in the average PDIV for all samples at each stage of the test showed no statistical significance since averages and deviations values are very similar, with an expected voltage rating of about 8kV to attain a sustained 4pC discharge regime. To make sense of this value, it would be interesting to compare it to standard commercial PCBs, however this comparison could not be led in the timeframe of this work.

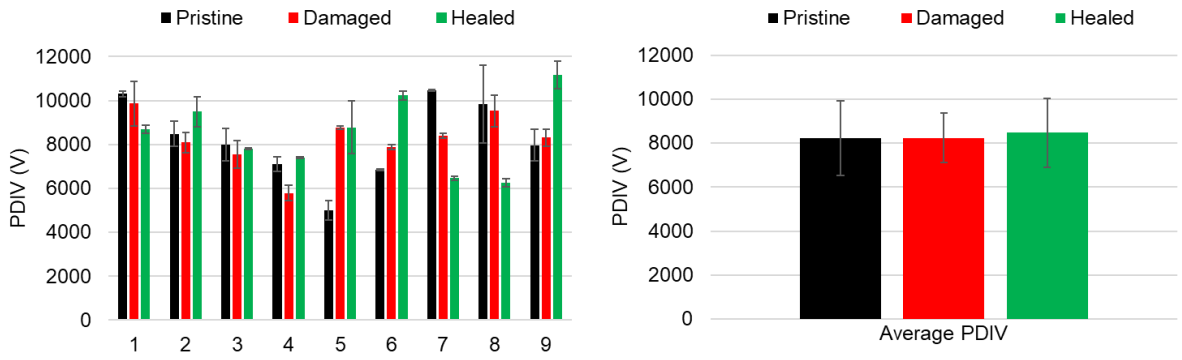

Figure 94 – Left) Individual results for all nine samples showing large deviations and no clear damage/recovery trend. Right) Average results showing no statistical difference between each step of the test.

To better understand how these results could be obtained regardless of the damage state of the samples, optical observations were performed (cf. **Figure 95**). These images were obtained by placing the microscope in a transmission configuration, thus taking advantage of the transparency of the sample to access internal defects imagery.

Figure 95 presents images of the samples at different stages of damage and recovery at the same magnification. Looking at these pictures, one can observe small spherical defects with diameters inferior to 5µm for each image but also that large interfacial damages were indeed created between fibers and the matrix, with length of several hundreds of microns an about micron-sized height. As shown in the last picture, these interfacial damages could be repaired during the healing protocol, resulting in a healed sample that exhibit similar internal defects as in the undamaged state.

The remaining defects can be attributed to microscopic bubbles that were trapped in the resin, either during its mixing or when poured onto the fiberglass cloth during the board manufacturing. Rare interfacial defects can also be seen and attributed to inappropriate wetting of the fibers or trapped air between the fibre bundles during the manufacturing of the PCB. These optical analyses suggest a good healing efficiency of the resin-fiberglass interfacial damage, however it cannot be excluded that damages not visible in the optical range exist.

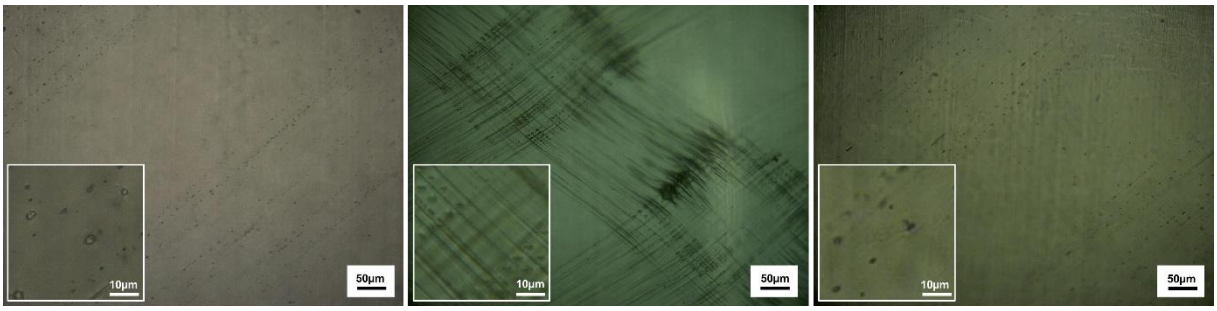

Figure 95 – Left) Undamaged sample. Middle) Damaged sample showing interfacial defects between the fibers and the matrix as dark contrast. Right) Healed sample showing complete disappearance of the damages. All inserts show 5x close-up

Thus, internal damages can indeed be generated and healed in the vitrimer composites, however these damage do not have an effect on the PDIV values measured in this test.

As a possible explanation for these results, Burgener and Fröhlich (2001) [123] modelled the probability of partial discharge inception in small voids, depending on several geometrical parameters that are quite relevant with this experimental study. Focusing on the influence of void geometry for fibre-reinforced resins in high electrical fields (twice the inception field), decreasing the height of a slender defect increases the time lag for a given probability of a discharge to occur (cf. **Figure 96 – left**). In the case of these vitrimer composites, most defects are in the range of a few microns in height, which could explain the similar results for discharge initiation.

When considering multiple crack defects of several hundreds of microns in length and 5µm in height, it appears that increasing the voltage above the inception voltage drastically decrease the time to get a discharge at start, but this effect fades up to the point where increasing the electrical field should not increase the rate of apparitions of PDs anymore (cf. **Figure 96 – right**).

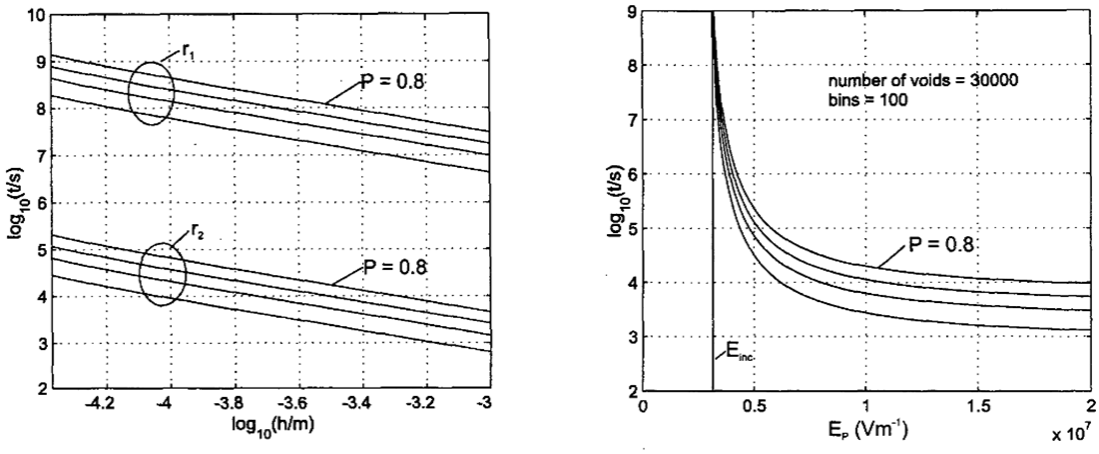

Figure 96 – Left) Impact of the crack height (h) on the time lag (t) for a given probability of PD occurrence in high electrical fields. Right) Impact of the electrical field (E_P) on the time lag (t) for a given probability of PD occurrence, E_{inc} is the inception field [123].

Since bigger damages have a lower expected time before a probabilistic discharge event occurs, and that increasing the voltage faster also drastically decreases this duration, it is probable that only the largest defects are being probed. In that regard, it is likely that these tests weren't performed with the right conditions to detect the small and slender damages created between the fibers and the matrix. Future work could focus on the effect of an increased measurement time for each voltage value and try to approach a PDIV value that could include more defects of different sizes.

As a conclusion, the healing of fiberglass-resin delamination defects was demonstrated based on optical analysis. Within the testing conditions, it was not possible to measure an effect of the mechanical damage introduced on the PDIV, and thus the healing efficiency could not be assessed quantitatively.

4. Power cycling of vitrimer-insulated modules

1. Embedding procedure

Assessing the true cycling capabilities of a new dielectric with actual power modules is challenging, since factory issued power modules usually come already encapsulated in silicone gel, requiring aggressive chemicals to be removed and risking damaging the semiconductor chips and metallizations. However, two power modules with no encapsulation could be obtained for this work, making the embedding process much more accessible and allowing to actually test the material in real conditions. These Insulated Gate Bipolar Transistor (IGBT) power modules are commercially available and are rated for 1200V and 150A, with a specified maximum junction temperature (Tj) of 175°C.

Considering the volume of an actual power module, preparing larger batches of resins also became more challenging. Heat generation must be managed very carefully as large batches accumulate more heat due to the higher number of reacting molecules and the lower heat dissipation due to the higher volume to area ratio. The encapsulation, often called "*potting"*, also requires a low viscosity during the entire process, promoting high flow of resin and easier removal of bubbles, which means maintaining a sufficiently high temperature for the resin to remain liquid. Combined, those two effects contribute to a fast curing, making it critical to work rapidly (order of minutes). Therefore, to make the potting process easier, a lower catalyst content of 2.5% is used instead of the typical 5%, making the resin gelification slower, allowing for a reasonable practical working time. Each module was also encapsulated in two batches, focusing on covering areas that are difficult to access first and filling the rest of the bulk afterwards.

To maintain a sufficiently high temperature during casting, the modules were pre-heated on a hot plate set at 130°C. To allow the resin to flow below tight wire bonds arrangements, the modules were also slightly tilted using a piece of steel (also on the hot plate). Once encapsulated in the fully transparent resin, the modules were put in a convection oven at 150°C for 1 hour before exhibiting the characteristic glassy and vivid orange (cf. **Figure 97**).

After the curing, numerous bubbles could be observed, which were not visible before casting the resin. While it is difficult to pin the exact reason for the apparition of bubbles, it seems like these defects can be seen preferentially near sharp edges and discontinued geometries, suggesting an effect of surface tension on the position of bubbles. However, it is unclear if the bubbles were generated during casting due to surface tension or if bubbles sticked to these locations instead of rising to the top. Regardless, the casting process has potential for improvements, using surface treatments and potting under vacuum to prevent any air to be incorporated in the curing resin.

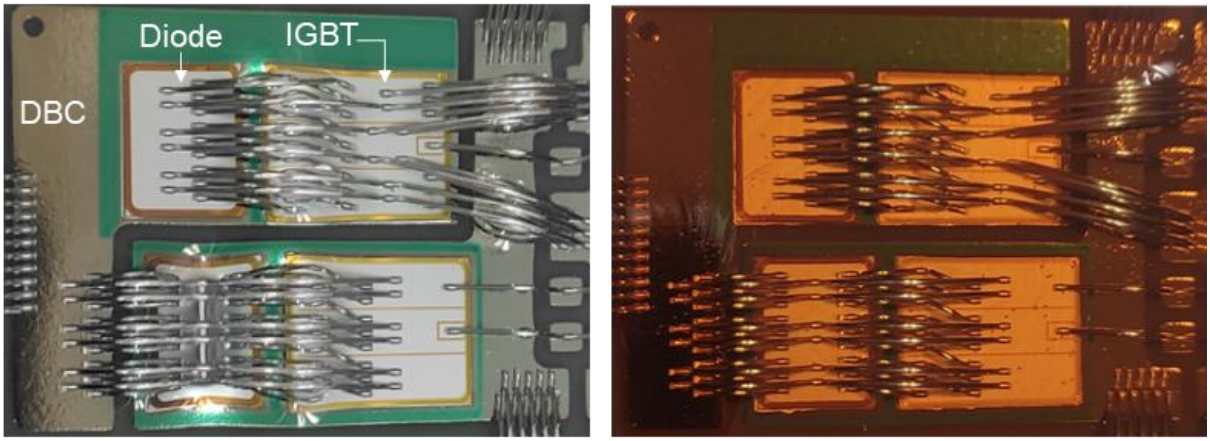

Figure 97 –Two IGBTs with the associated diodes, wire bonds and DBC substrate. Left) Embedded in uncured vitrimer resin. Right) Embedded in cured vitrimer resin

2. Power cycling test

a. Experimental setup and calibration

The encapsulated modules have been submitted to a high thermal stress during power cycling test, provoking accelerated aging. By applying a high DC current through the IGBT dies, one can actively heat up the module by Joule effect in a representative way compared to real operational work. While the conditions and thus duration of the test are not typical of normal operations, this test can give an insight on the reliability of power modules in harsh repetitive conditions and is used to qualify power devices according to the AQG 324 automotive qualification standard.

For these tests, the two vitrimer-embedded power modules were compared to four commercial references that were embedded with silicone-gel using a *Mentor Graphics MicReD Power Tester* bench. All six devices were cycled under similar conditions, alternating between an activated state that lasted 3 seconds (t_{on} = 3s) and a deactivated state that lasted for 6 seconds (t_{off} = 6s) for a total cycle time of 9 seconds, with the only difference residing in a periodic measurement of Rth for reference samples (resulting in artefact peaks on the data). An external power supply was used to activate the component by maintaining a voltage of 15V between the gate and the emitter (V_{GE} = 15V) and the test bench power supply was used to control current injection.

Accurate control of the temperature is crucial for these tests, as wider temperature swings will create more thermomechanical damages. To accurately control the temperature, the modules are placed onto a thermal interface material (TIM) and mounted on a cooling plate set to 5°C. By attaching thermocouples to the baseplate of the module, an effective temperature of 10°C was measured. By actively cooling the module, the temperature accumulated during t_{on} can be drained during the off-time before the beginning of the next cycle.

Additionally, setting an accurate junction temperature swing between on/off cycles is challenging as it depends widely on the type of module and conditions of the test and requires balancing the temperature generated by the module with the draining capabilities of the cooler. Monitoring the junction temperature can be done by measuring the voltage across the collector-emitter of the power chip (V_{CE}) and comparing it to isothermal calibrations. For two known stable temperatures, the V_{CE} is measured under low current (100mA) to prevent Joule heating, with a resulting slope that is supposed constant on the entire test interval. This allows to have an indirect measurement of the variation of Tj during cycles.

For these tests, a temperature swing of 110°C ($\Delta Tj \approx 110$ °C) was selected, thus a periodic heating current of about 180A was required and was tuned individually to obtain the same temperature variations across all modules.

The cycling end criterion was set at a 10% increase in V_{CE}, which should either be correlated to an increase in resistance due to degradation of the top connections (less current path for the same load) or an increase in junction temperature due to a decrease of the cooling efficiency. The end of life (EoL) criterion was set at a 5% V_{CE} increase.

Summary of cycling test conditions:

- Activation times : t_{on} = 3s and t_{off} = 6s
- Junction temperature : $\Delta Tj \approx 110$ °C and Tj,max = 170°C
- Test criterion : Stop at $1.1 \times V_{CE,0}$ and EoL at $1.05 \times V_{CE,0}$

3. Results and Discussions

The cycling test results are plotted in **Figure 98**, and show the evolution of the normalized V_{CE} during the on-time of the chip against the normalized number of cycles. The normalized V_{CE} values were based on the nominal $V_{CE,0}$ of each chip at the beginning of the test ($V_{CE}/V_{CE,0}$) and the normalized power cycles were based on the average cycle number at which the references (silicone-gel modules) reached the 5% V_{CE} increase EoL criteria (Survived cycles / Average $1.05 \times V_{CE}$ Cycle for references).

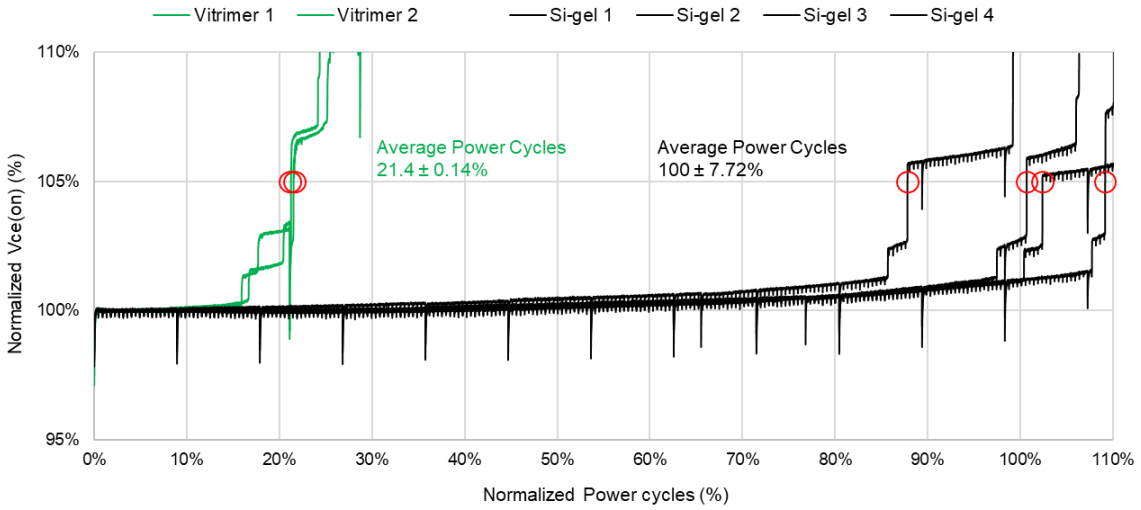

Figure 98 – Normalized power cycling tests of IGBT modules encapsulated in vitrimer and silicone gel.

By doing this, the average survived power cycles for all references is set at 100%, with some references reaching the criteria sooner and some lasting a bit longer, exhibiting a standard deviation of 7.72%. The vitrimer-encapsulated modules reached the EoL at about 21% of the cycles endured by the references for the same criterion.

The typical step increases of V_{CE} observed for the references and the vitrimer modules are typically related to wirebond lift-off from the chip due to thermomechanical stress. This hypothesis is reasonable, since the encapsulating vitrimer can still be 10 to 100 times stiffer than silicone-gel above Tg (depending on the Si-gel used), above which the entirety of the test occurred. Since thermomechanical stresses can be expressed as a product of stiffness parameters (Elastic moduli) and thermal expansions (CTEs) of the participating materials, measuring the actual CTE of these materials compared to silicone-gel and repeating the test with vitrimers filled with inorganic fillers

(lowering the CTE) could provide valuable field data on the thermomechanical impact of this new material on bonding degradation.

However, solely looking at these data is not sufficient to determine the exact failure mode. Complementary observations are required to assess the degradations mode and compare these elements to the numerical data from the cycling test. After the test, the modules were opened and the cycled chips were observed, revealing very noticeable black burnt spots that appeared on the top of the tested chips, surrounding the bond wires specifically. Large cracks can be seen in the bulk material around the burnt areas and were attributed to bursting from gas release during the thermal degradation of the material (cf. **Figure 99**).

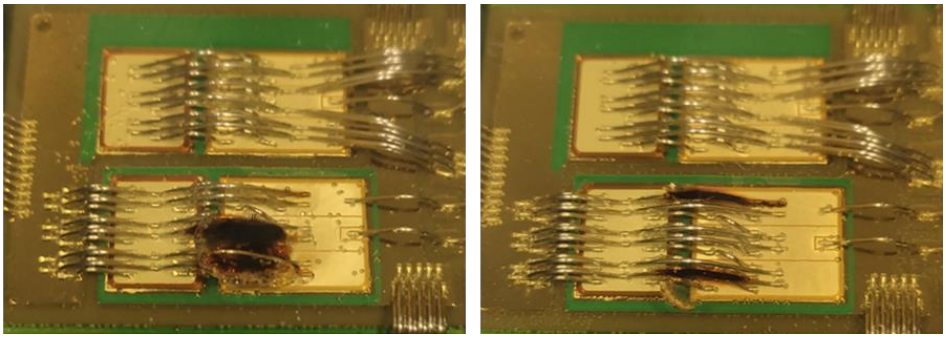

Figure 99 – Two vitrimer-encapsulated power chips after power cycling, showing carbonization and cracks in the insulation material.

These cycling test are run at a low voltage, which makes the hypothesis of a simple breakdown irrelevant. Without additional investigations, it is difficult to assert if regular burning occurred due to wire bonds heating or if high-energy arcs were generated during the failure of the wire bond. Analysing the de-bonding mechanism of the wires could provide insight on whether or not the burnt wires are still connected, which would feed the wire-heating hypothesis, or if they are typically disconnected, suggesting that high-energy sparks may have been produced during lift-offs.

Given the previous thermal characterizations showing serious thermal degradations occurring above 400°C and the obvious carbonization of the material in this case, a high temperature approaching the melting point of aluminium (660°C) may have been experienced at the failing site. Indeed, Zhao et al. (2021) [124] explored the effect of ultra-fast annealing (heating rate of 1000°C/s) on pure aluminium and showed that the microstructure should change above 400°C, with grains of increased size and significant changes on the mechanical properties in tensile tests. Future work should therefore focus on analysing the aluminium wire microstructure to clarify this hypothesis and determine the exact failure mechanism.

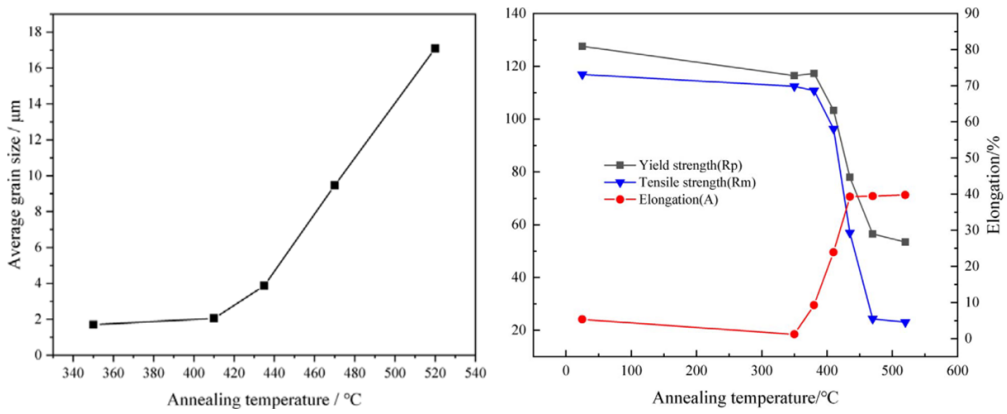

Figure 100 – Effect of ultra-fast annealing temperature of the microstructure of pure commercial aluminium. Left) Average grain sizes. Right) Mechanical properties from tensile testing [124].

4. Additional characterizations

One of the most important aspect in the electrical insulation of power components is the ability of the encapsulation to guarantee a high blocking voltage when the chip is in OFF state. To continue testing the applicability of vitrimers in regular power module architectures, the insulating performances of a vitrimer-encapsulated module compared to a silicone gel references was assessed by measuring the leakage current across the blocked semiconductor chip over the entire specified voltage range for the studied modules. Similarly to power cycling tests, the vitrimer used for encapsulation contained 2.5%mol of catalyst in regard to acid groups.

The measured leakage current is the sum of all leakage currents participating in the conduction. Thus, it is heavily dependent on the architecture and specifications of the module. In this case, the acceptable specified value for total leakage current is 1mA over the entire 0 – 1200V range.

The baseplates of both modules (Si-gel and vitrimer) were placed in contact with a heating surface and the temperature was increased from 25°C (about room temperature) to 150°C, which is the specified continuous operating limit for this package, with 25°C step increments. For each temperature step, the modules were allowed to thermalize for 10 minutes to ensure a homogeneous temperature distribution in the encapsulant. Using a *Keysight B1505A Power Device Analyzer/Curve Tracer*, the leakage current passing from the collector to the emitter ($I_{C,Off}$) of the blocked chips (V_{GE} = 0V), through the insulating material was measured and plotted (cf. **Figure 101**).

From these data, it is observed that the leakage current increases with increasing temperature at a given voltage, regardless of the encapsulation material. This is expected as polymer resistivity tends to decrease with increased mobility of charge carriers [125]. However, in the case of the silicone gel reference, an acceptable leakage current can be measured over the whole voltage range at all tested temperatures, with a maximum of 0.8mA at 150°C. On the other hand, the vitrimer insulated module could only pass the leakage current specification up to 50°C, after which a strong change in conduction behaviour could be observed with the 1mA current criterion being reached under 200V, almost behaving like a switch activated with temperature past 50°C. While this is not suitable for commercial use, these results give an insight on the electrical behaviour of vitrimers with temperature, especially on their electrical insulation properties which, to the author's knowledge have not been reported in literature so far.

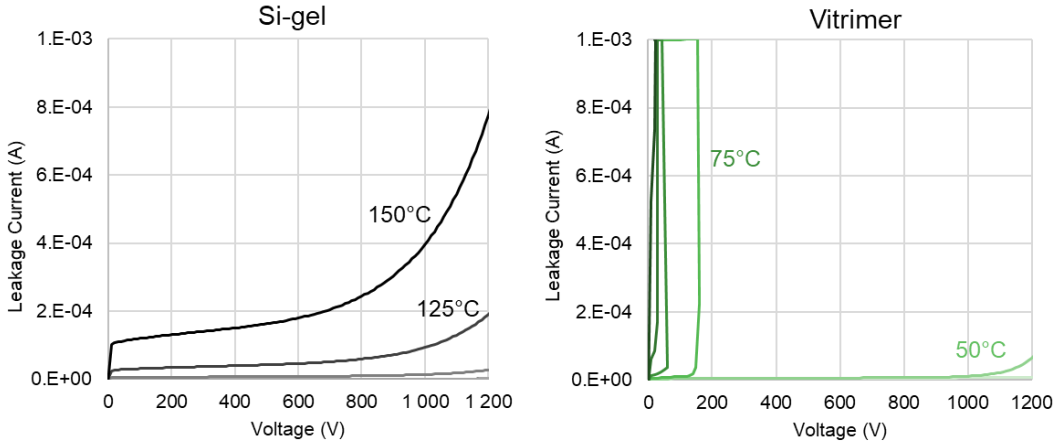

Figure 101 – Impact of temperature on the leakage currents of commercial power modules encapsulated with the reference silicone gel (left) and the elaborated vitrimer (Right).

Conclusion

Overall, the vitrimer material seem highly compatible with the thermal requirements of power applications, exhibiting a high thermal stability and showing almost no degradation up to 300°C for the current formulation, thus validating its use with typical manufacturing methods. Additionally, the high dielectric strength of the material is well aligned with the voltages and electrical fields expected for ultra-high voltage devices at thicknesses that are meaningful for the application. Given the right insulation design, this material should provide acceptable margins for compact devices. To complete this study, the impact of temperature on the breakdown strength should also be assessed. The large variation of its mechanical properties expected at Tg also makes it an interesting material for the replacement of the standard materials used today (silicone-gel and FR4) and tuning of the Tg and the elastic properties could be a promising solution to adapt the thermomechanical profile of the material to the application needs.

The production of a complete self-healing PCB showed the compatibility of the material with conventional manufacturing processes. With good spreading and wetting properties, the resin allowed to use readily available copper sheets and fiberglass fabrics, showing its compatibility with materials of the domain. Using the developed method for press-molding of liquid resin also allowed to tune the insulation layer thickness, making the creation of entirely customizable power boards possible. No changes in the chemical composition of the resin is expected during its processing, thus guaranteeing the conservation of self-healing properties. Final products displayed a high apparent quality for large surfaces comparable with typical power devices sizes.

The recovery of electrical properties following mechanical damages was evaluated, showing promising results with the entire breakdown strength being recovered after only 1h at 150°C and without the use of external pressure during the healing process. This test shows that it is possible to recover the breakdown strength in a failed insulation layer, provided that the fractured surfaces can be brought back into contact with each other. Further work could focus on using the shape memory effect or other thermally activated effects such as thermal dilation to generate self-healing in a power board spontaneously. Investigations of a failed reinforced vitrimer composite also showed promising results. Despite the lack of clear effect of the recovery on the partial discharge initiation voltages (PDIV), damages could be observed and mended with the same healing protocol. Whether or not the PDIV was set by the failed sample or another part of the system, the samples could at least withstand 5kV and up to 12kV without any meaningful sustained discharge (>4pC). This gives an insight on the quality of the fabricated board, but also on the difficulty to actually create damages in a relevant way compared to the actual conditions a power board may be subjected to.

Concerning the applicability of the selected vitrimer with conventional power module architectures, it appears that using the neat resin is not up to the standard materials used nowadays. Wire bonds are destroyed faster and carbonization was observed, although the exact damage mechanisms have not been identified. When the power module becomes hot enough (around 50-75°C) a non-negligeable leakage current can be measured, bypassing the expected blocking die, which cannot be acceptable according to the industry standards. Despite the sub-par reliability and insulation performances of these newly documented materials in comparison with highly optimized silicone-gels, these results can help defining the best course of action to provide better results with vitrimers. Inorganic fillers could be employed as a composite strategy for thermomechanical management and understanding the underlying conduction mechanisms displayed by vitrimers at high temperature could be used to tailor the desired resistive properties of new insulation materials.

Overall, the designed material is very promising and fine tuning of its properties through formulation might provide a highly reliable material for the next generation of power devices.

Chapter IV – Impact of the formulation on viscoelastic and conduction properties

Chapter IV: Impact of the formulation on viscoelastic and conduction properties

Introduction

From the previous chapters on the compatibility and applicability of the vitrimer with power applications, it appears that the material is suitable in terms of thermal stability and dielectric strength but can be improved to better match the thermomechanical properties of the material with the application needs. A decrease of the electrical conductivity at temperatures above Tg is also required as significant leakage currents appear in commercial power modules above 50°C.

Tuning of the thermomechanical properties is readily achievable by changing the types of precursors as mentioned in Chapter II. By modifying the backbone precursors to include more rigid segments, one can pilot the chain dynamics of the network and increase the temperature at which the glass transition occurs (Tg). By changing the type and concentration of catalyst, one can instead modify the dynamic viscoelastic properties of the material, thus playing on the time and temperature dependency of the vitrimeric relaxation [77], [79]. Additionally, vitrimers are known for their ability to relax stress, as part of the macroscopic consequence of their reworkable network, making the exploration of viscoelastic properties interesting for high-stress applications.

However, compared to the literature information available to tune the mechanical properties, it is more challenging to predict the impact of formulation on the electrical conductivity of a polymer. Conduction mechanism can occur through several pathways, with different charge carriers (electrons, ions) and the sum of all of these pathways result in the overall conductivity response. Classically described as governed by ion displacements from additives or impurities, the conduction of most polymers is often tied to the diffusion of the main charge carrier in regard to chain mobility, which is heavily increased when crossing Tg.

Vitrimers are particular in the way that they exhibit a second "*glass-transition-like*" domain, with the activation of the vitrimeric transition past a certain temperature (Tv). Similarly to Tg that allows chains to become more mobile by unfreezing their physical topology from a kinetic standpoint, the vitrimeric transition temperature (Tv) allows the chains to be more "*chemically*" mobile by enabling the transesterification exchanges between chain segments. Similarly to the glass transition, it is therefore possible that the vitrimeric transition plays a role in the diffusion of the dominant charge carriers responsible for conduction.

In order to investigate the variations of mechanical and electrical properties in regard to the vitrimer network structure, a formulation campaign was followed to produce several new comparable materials. Variations of the electrical insulating properties in regard to the network relaxations in temperature is also explored.

1. Elaboration of new vitrimer formulations

1. Change of the acid precursor

Variations of the type of carboxylic acid used during the elaboration was already presented as a suitable solution to tune the mechanical properties of vitrimers.

Fatty acids belong to a large family of carboxylic acids that possess an aliphatic hydrocarbon chain. Since the reactivity of these compounds in vitrimer systems is the result of the carbonyl groups, changing the length of the aliphatic chain can provide a reasonably comparative study of the properties of the resulting network. Compared to the sebacic acid precursor used for the previous studies, glutaric acid exhibit the same functionality of two carboxylic acid groups per molecule but possesses a shorter aliphatic chain, counting 5 carbons including the carbonyl functions compared to 10 carbons contained in sebacic acid molecules (cf. **Figure 102**). Apart from the difference in length, both molecules exhibit different melting temperatures, mostly due to the difference in parity of their number of carbon per chain making sebacic acid crystals more stable and thus requiring more energy to be melted.

This specificity directly impacts the elaboration process. With sebacic acid, the reaction had to take place around 140-150°C to ensure that all precursors were introduced in a liquid state. By changing to glutaric acid, the reaction could be performed at a lower temperature of approximately 110-120°C, which not only reduced the kinetics of the reaction, resulting in a more convenient manipulation time before reaching the gel point, but also reduced the risk of thermal runaway, resulting in a more robust elaboration process.

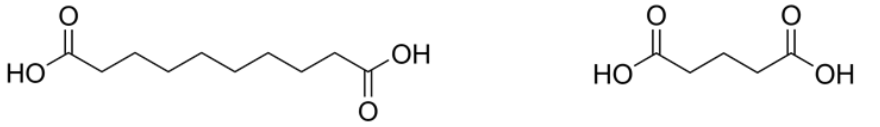

Figure 102 – Sebacic acid and Glutaric acid molecules, with their respective melting temperatures.

For the following study, comparable vitrimer network structures were produced from the bulk polymerization of DGEBA resin with either sebacic or glutaric acid, again with a 10% molar excess of epoxy groups compared to carboxylic acids for both formulations.

2. Variation of catalyst content

Changing the catalyst content also provides noticeable changes in the behaviour of the pre-polymer and even afterwards on the resulting network. As mentioned in **Chapter III**, a lower catalyst content of 2.5% with respect to acid groups was used to slow down the polymerization kinetics and make the elaboration of larger batches more manageable, effectively increasing the time before gel point. However, by decreasing the amount of catalyst, one can expect to also reduce the rate of exchanges provided by transesterification in the final material and thus observe a slower healing process.

On the other hand, the catalyst is not bound covalently to the network and could be participating to the electrical conduction when an electrical field is applied. By decreasing the amount of catalyst available for the conduction , it may also be possible to decrease the electrical conductivity of the resulting material.

The impact of catalyst content on the viscoelastic and conduction properties of the material was therefore explored, by elaborating vitrimer networks with catalyst contents of 2.5 and 5mol% in regard to acid functions (for sebacic and glutaric networks).

3. Final elaboration of the formulation matrix

The different vitrimer formulations were produced using the same technique of hot press-molding as described in **Chapter II** and cured at 150°C for 1h. The obtained samples were indistinguishable in optical aspect and perceived quality. To provide high-quality measurements, all bulk and film samples of the same formulation were created from the same resin batch simultaneously and used in the different characterization campaigns presented in this chapter.

FTIR measurements were performed in the same conditions as presented in **Chapter II**, using the ATR configuration and scanning from 4000 to 400 cm^{-1} for 20 scans with a resolution of 4cm^{-1} on film samples. Additionally, after correcting the baseline, normalization of the spectra by matching the intensity through the stretch vibration band from the sp2 carbons of the phenyl group ($\nu_{c=c(Ph)}$=1608 cm^{-1}) was performed [105].

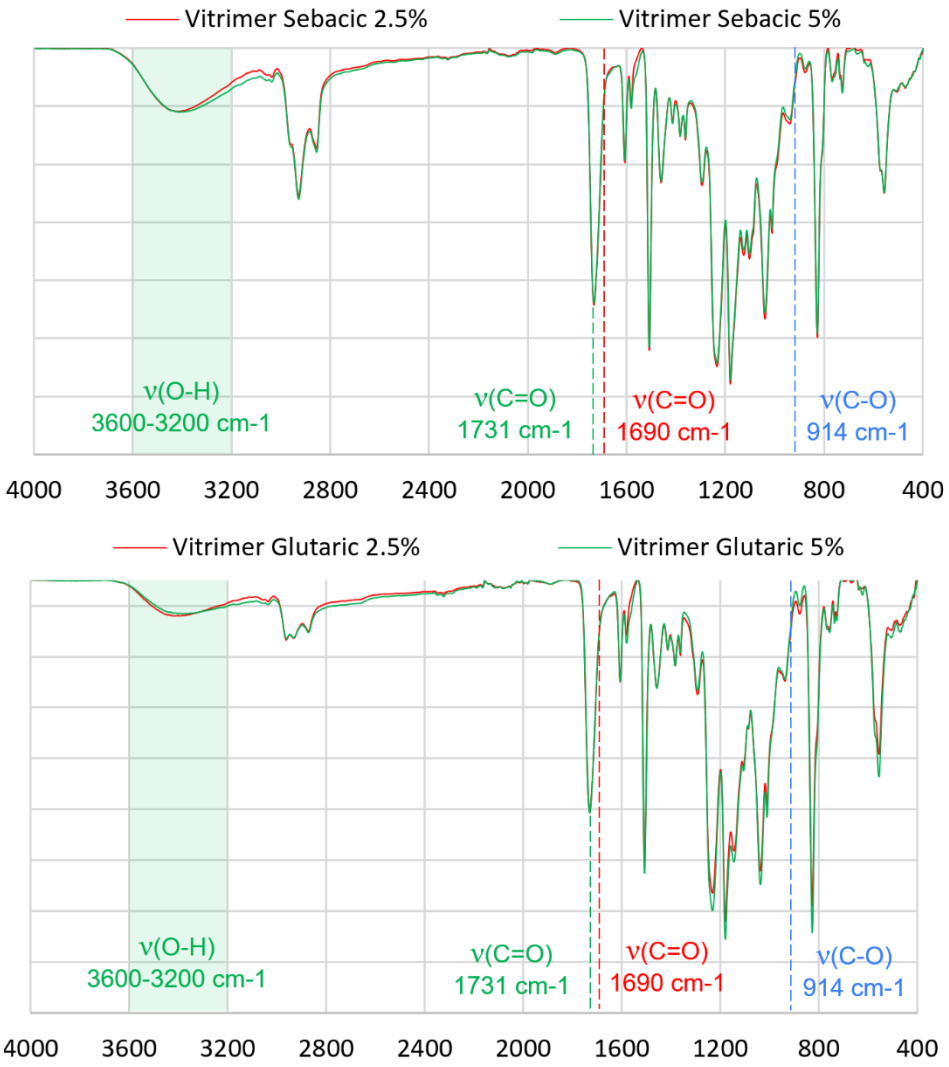

Figure 103 – FTIR spectra of the different vitrimer formulations showing similar features. Vibrational bands attributed to the epoxy (blue), the carboxylic acid (red) and the vitrimer (green) related groups are displayed.

Figure 103 shows the spectra obtained for all the elaborated vitrimers. As for the reference material elaborated in Chapter II (Sebacic based – 5% catalyst), the absence of the vibrational band from the epoxy (914cm^{-1}) and the shift of the carboxylic acid peak (1690cm^{-1}) to the ester peak (1731cm^{-1}) confirm that the reagents were indeed consumed and created the appropriate ester functions. All samples exhibited the large vibrational band of hydroxyl groups (3600-3200cm^{-1}).

Evaluation of the glass transition temperatures was achieved from graphical determination on DMA curves, yielding an average temperature of 32°C for sebacic-based vitrimers and 53°C for the glutaric-based ones.

With the successful elaboration of new formulations, it is now possible to measure the viscoelastic and electrical conductivity properties of the resulting materials.

2. Impact of formulation on viscoelastic properties

1. Maxwell's viscoelastic model

Viscoelasticity is a property that all polymers can exhibit to some extent, showing both viscous and elastic behaviours while deformed. Many authors have now measured the viscoelastic properties of vitrimers, as this is accepted as an appropriate mean to evaluate the exchange dynamics within the network, piloting the flowing capabilities of the material. Thus, measuring the variation of viscoelastic properties of the material as a function of the temperature provides valuable data on the energy necessary to trigger these exchanges, which are piloting the self-healing and shape-memory functionalities of the material.

There are several ways to model the viscoelastic behaviour of a material. One of the simplest and most popular model is the Maxwell's model used for describing stress-relaxation tests, where the material is represented as an ideal elastic spring of stiffness E following the Hooke's law, connected in series to an ideal damper of viscosity η obeying Newtonian fluid mechanics (cf. **Figure 104**).

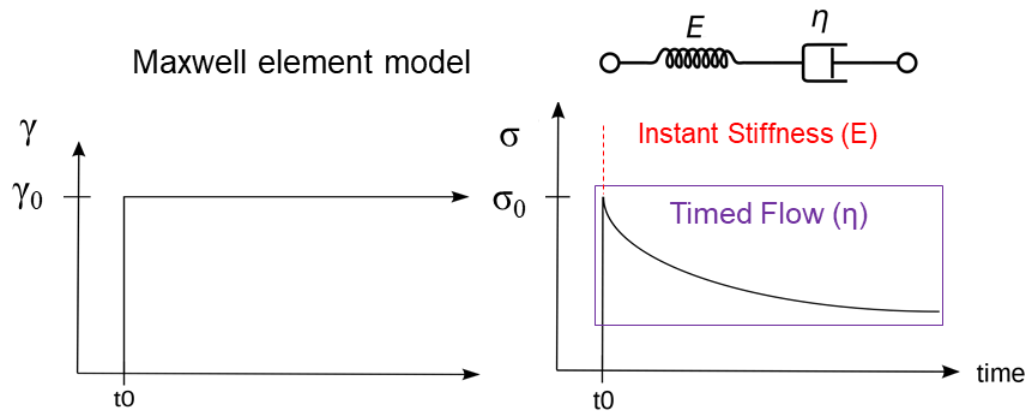

Figure 104 – Representation of a stress-relaxation experiment on a Maxwell material (displacement control). Left) A controlled displacement γ_0 is imposed at t>t0. Right) Associated stress relaxation as a function of time.

From these assumptions, it is possible to write a system of equations as follow :

Hooke's law	$\sigma_{Spring} = E\gamma$	(8)
Newtonian assumption	$\sigma_{Damper} = \eta\dot{\gamma}$	(9)
Configuration in series	$\sigma_{Tot} = \sigma_{Spring} = \sigma_{Damp}$ and $\gamma_{Tot} = \gamma_S + \gamma_D$	(10)

With γ the deformation strain and dotted variables being the time derivative of said variable.

Applying this model to experimental data to determine the values of the parameters E and η requires to set several conditions. By derivation of the total strain, one can express the deformation rate as a function of the stress and stress rate, which is a first order differential equation. Setting a constant deformation for the test results in a null deformation rate which simplifies the equation. Integration with the appropriate initial condition allows to write the following development :

Derivation of total strain	$\dot{\gamma} = \dot{\gamma_S} + \dot{\gamma_D}$ or $\dot{\gamma} = \frac{\dot{\sigma}}{E} + \frac{\sigma}{\eta}$	(11)
Constant strain	$0 = \frac{\dot{\sigma}}{E} + \frac{\sigma}{\eta}$	(11')
Initial condition	$\sigma_0 = E\gamma_0$ then integration $\frac{\sigma_t}{\sigma_0} = e^{-\frac{Et}{\eta}}$	(11")

From this development, one can setup a stress-relaxation experiment where the strain is maintained constant and the normalized stress is monitored as a function of time. At the start of the deformation of the samples, an elastic stress response can be measured in correlation with the stiffness of the spring element of the modelled material (initial condition). If the material fits Maxwell's model, the initial stress must decrease exponentially with a time coefficient depending on both the stiffness and the intrinsic viscosity of the modelled material. This coefficient is called the relaxation time τ and in this case can be written as the ratio of the viscosity over the stiffness (τ = η/E).

2. Stress-relaxation tests

a. Determination of the relaxation times and associated viscosity

To properly evaluate the relaxation time, the decreasing stress was fitted with a simple exponential function up to 63% relaxed stress. Indeed, when the elapsed time equals the relaxation time (t/τ =1), a simple decreasing exponential will have reached approximately 37% of its initial value. This ensures that the fitting is not changed due to experimental uncertainty when the measured relaxing load becomes low, which introduces the deviation from exponential behaviour (at σ/σ_0 <37%). Regardless, all relaxation times were calculated using the exponential factor of the best fit function and not by graphical reading (cf. **Figure 105**).

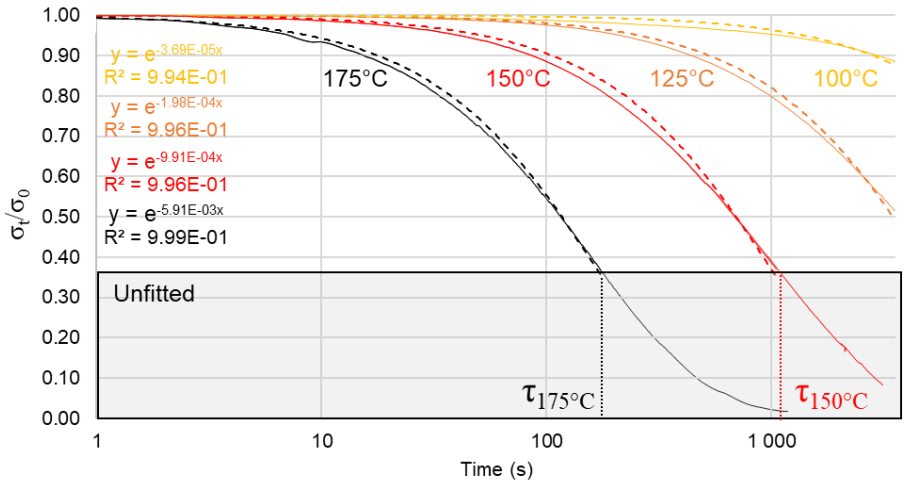

Figure 105 – Example of data treatment to obtain relaxation times showing fitted (dotted lines) and unfitted portions of the curves. Relaxation times are calculated from the exponential factor but can be identified graphically at sufficiently high temperatures using the value of τ corresponding to σ/σ_0 = 37%.

By measuring the elastic modulus E at the start of the experiment during the initial elastic response, and multiplying it with the measured relaxation time τ, one can access the intrinsic viscosity η of the material. However, it is the shear viscosity that truly represents the viscous behaviour of a material, therefore each elastic modulus measured in tensile mode will be converted in shear

modulus G, with the assumption that the Poisson's coefficient ν of the material approaches the value of natural rubber (ν = 0.5), through the following equation :

Elastic – Shear conversion

$$G = \frac{E}{2(1+\nu)} \quad (12)$$

Determination of the shear viscosity

$$\eta = G * \tau \quad (12')$$

b. *Results and discussion*

To evaluate the formulated materials flowing capabilities and determinate their intrinsic shear viscosity, several stress-relaxation tests were performed. Due to the large expected time frames for the measurement, uncatalyzed samples did not follow these tests. Using a Mettler-Toledo DMA1 operated in tensile mode, parallelepipedal samples were submitted to a constant strain of 5% in isothermal conditions and the stress response was measured as a function of time for 1 hour, which is the designated time selected for the healing protocol. To prevent other relaxation events near Tg, the thermal history of each sample was erased (1min at 150°C) and the tests were performed from 100°C and up to 175°C, following incremental steps of 25°C.

Figure 106 shows the evolution of the intrinsic shear viscosity of the catalysed materials with the inverse temperature. The X-axis was multiplied by 1000 for the sake of clarity. From these data, it is possible to confirm that increasing the catalyst content decreases the viscosity at all tested temperatures, regardless of the type of acid precursor used during the elaboration. Surprisingly when comparing between acid types, glutaric-based vitrimers show a slightly more viscous behaviour than its sebacic counterpart with 2.5% catalyst but also show a lower viscosity at 5% catalyst content.

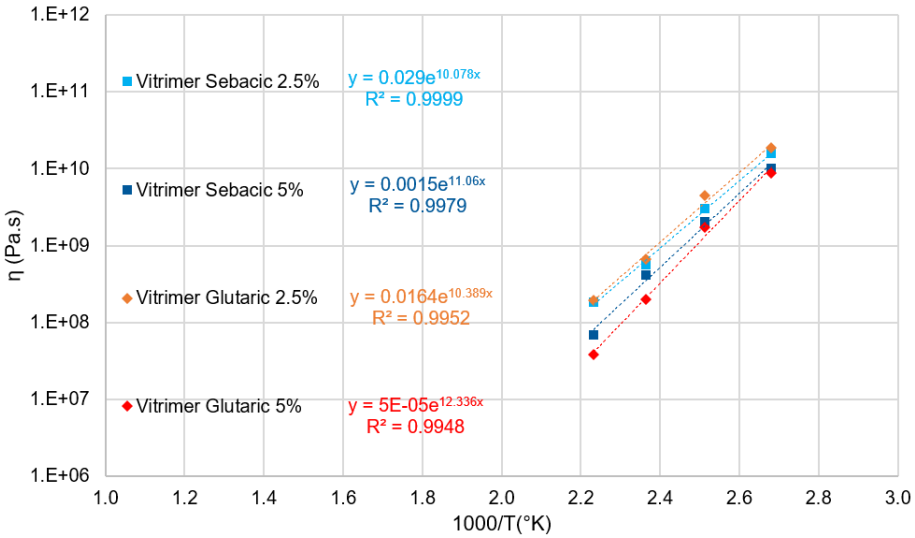

Figure 106 – Intrinsic shear viscosity of the formulated vitrimers showing an Arrhenius dependency.

All data series can be fitted appropriately with an exponential function, which is consistent with the expected flowing properties of vitrimers. Actually, vitrimer's Arrhenius-like viscoelastic properties were initially presented as one of the main interests around these materials [73]. Many polymers can exhibit viscoelastic properties to some extent, however the particularity that gave its name to vitrimers is that their dependency of the viscous behaviour follows an Arrhenius law, thus emulating the behaviour of glass (SiO_2). This behaviour is called "*strong*" and is opposed to a "*fragile*"

dependency of the viscosity in temperature of other glass-like materials where the proximity of Tg results in a strongly increased viscosity, more accurately described by Williams-Landel-Ferry (WLF) or Vogel-Fulcher-Tammann (VFT) laws (cf. **Figure 107 – Right**).

The Angell's plot in **Figure 107** shows the difference in strong or fragile viscoelastic behaviour for numerous glassy materials above Tg and demonstrates the viscoelastic limit at 10^{12} Pa.s when reaching Tg, below which no meaningful viscous behaviour can be observed on acceptable timeframes since the segmental motion of chains becomes kinetically frozen at Tg. By analogy with vitrimers, the vitrimeric transition temperature Tv should be calculated at the same viscoelastic limit since the flowing capabilities of the network are not only hampered by segmental chain motions (below Tg) but often primarily by the transesterification exchange rate (cf. **Figure 107 – Right**).

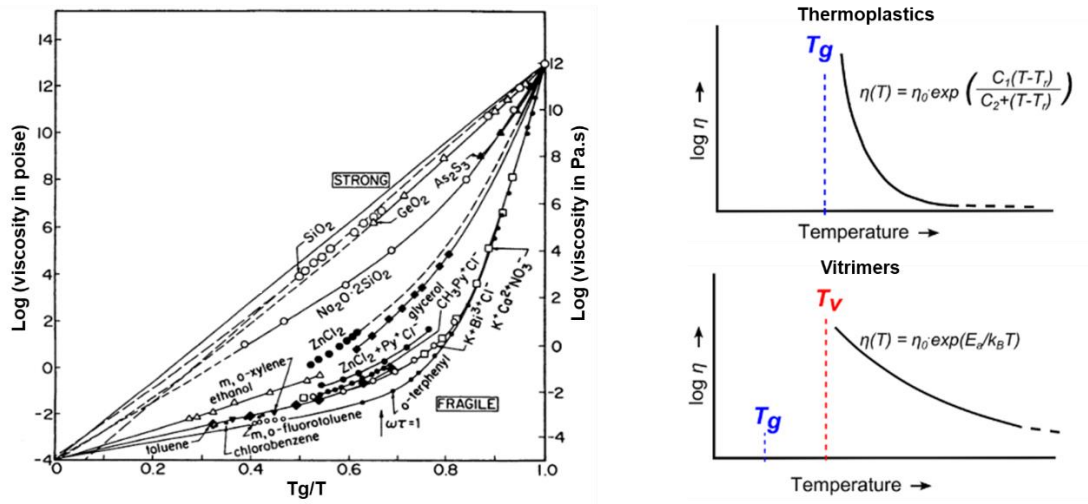

Figure 107 – Left) Angell's plot showing the strong and fragile dependency of viscosity in temperature, with the viscoelastic limit of 10^{12} Pa.s reached at Tg [126]. Right) Model laws for the variation of viscosity with temperature for thermoplastics compared to vitrimers with Tv>Tg [77]

Alternatively, other interesting behaviours can occur when Tg approaches and exceeds Tv. In the case of Tg becoming higher than Tv, it is expected that the material would exhibit a viscosity drift in the vicinity of Tg, shifting from an Arrhenius law to a Tg-driven viscosity activation (WLF or VFT law) as it is observed in thermoplastics (cf. **Figure 108**) [127]. In that case, the viscosity should be rated in respect to Tg, as it is the last transition preventing the expression of viscosity.

For Tg > Tv, the material would be considered a fully elastic solid below Tg and Tv, a kinetically frozen liquid between Tv and Tg, and a viscoelastic liquid above Tg. With careful considerations for the placement of these transitions, one could truly adapt the thermomechanical behaviour of such materials for several application needs.

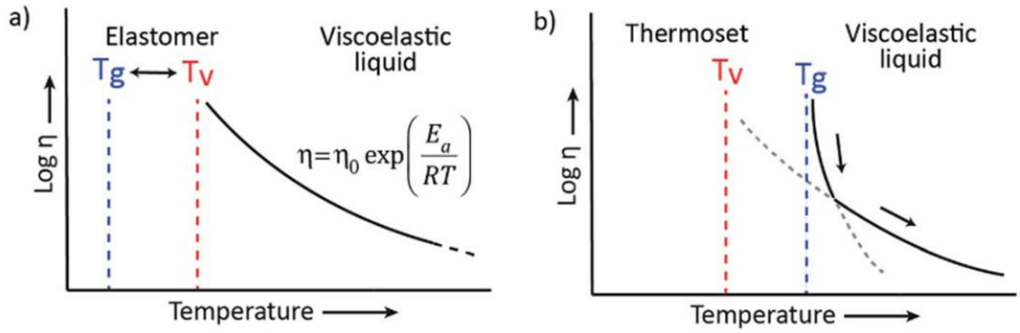

Figure 108 – Representation of the evolution of the viscosity with temperature depending on the relative position of Tv and Tg. A) When Tg < Tv, Tv drives the viscosity decrease, resulting in an Arrhenian variation (strong). B) Tg > Tv, Tg drives the viscosity decrease, resulting in a WLF-VFT kind of variation [127].

Considering the good fit of the test results in **Figure 106** and assuming continuity of this behaviour towards $\eta = 10^{12}$ Pa.s, the viscoelastic limit temperature Tv for the formulated vitrimers can be extrapolated for the sebacic-based vitrimers as 50°C and 51°C for 2.5% and 5% catalyst content respectively , and for the glutaric-based vitrimers as 54°C and 56°C for 2.5% and 5% catalyst content respectively. From the Arrhenius-like variation of viscosity, activation energies can be calculated at 84 kJ/mol (Sebacic, 2.5%) and 92 kJ/mol (Sebacic, 5%) and 86 kJ/mol (Glutaric, 2.5%) and 103 kJ/mol (Glutaric, 5%) which is consistent with values found in the literature for similar transesterification based vitrimers (about 80 – 100kJ/mol) [73], [79].

Table 4 summarizes the Tg values determined at the onset of the storage modulus on DMA scans and Tv calculated from the fitting of experimental results to an Arrhenius law and identifying Tv as the temperature for a viscosity of 10^{12} Pa.s. For sebacic-based vitrimers, Tg and Tv are close but still reasonably separated, with Tv being superior to Tg. In the case of glutaric-based networks, Tg and Tv are quite similar, considering errors in both evaluation methods.

Table 4 – Summary of the temperatures for the glass transition and the viscoelastic limit. The calculated activation energies from the fit to an Arrhenius law are also provided.

	Tg (°C)	Tv (°C)	Ea (kJ.mol^{-1})
Vitrimer Sebacic 2.5%	32	50	83.8
Vitrimer Sebacic 5%	32	51	92.0
Vitrimer Glutaric 2.5%	53	54	86.4
Vitrimer Glutaric 5%	53	56	102.6

To better discuss the different measurements, the same viscosity data were plotted with regard to the Tv of each material type (see **Figure 109**). By doing so, it is possible to show that, at similar temperature differences with their respective Tv, glutaric-based vitrimers can flow faster than the sebacic-based ones. At 2.5% catalysis, the effect of the backbone (type of acid) is barely noticeable and may not be significant, but when doubling the catalyst content up to 5%, a significant difference can be observed. Additionally, doubling the catalyst content of the glutaric networks drastically decreased the viscosity, when doing so with the sebacic base only provided a mild decrease.

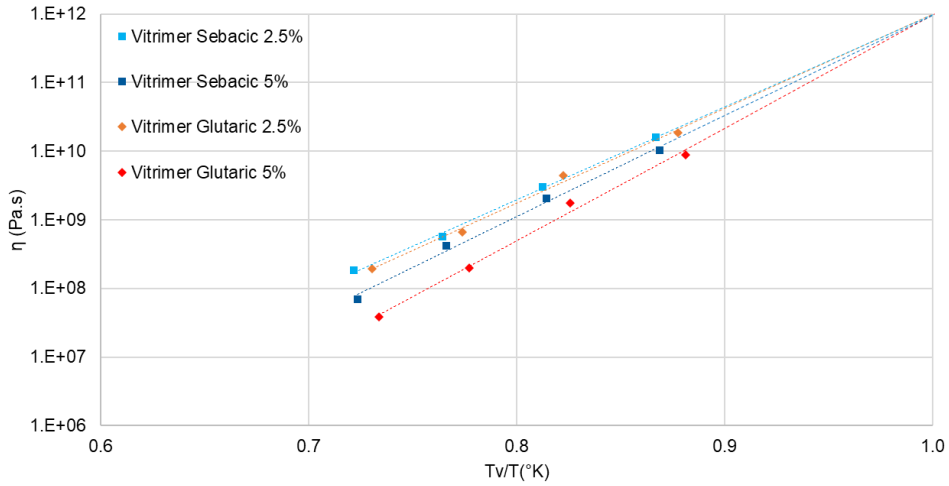

Figure 109 – Intrinsic shear viscosity of the elaborated vitrimers, plotted with inversed temperature and normalized by Tv, all reaching Tv at 10^{12} Pa.s

To explain this result, the main hypothesis is that shorter aliphatic chains make the network tighter since the distance between acid functions that will become the ester nodes is shorter. This could speed-up the transesterification exchange rate, admittedly responsible for the flowing abilities of the material, as long as enough catalysts are available to perform the exchange at this rate. In that

regard, it may be possible that a lower catalyst content represents a flow limitation in glutaric-based networks (that could go faster in theory) and this limitation may have been lifted with more catalyst molecules available, thus decreasing the viscosity values more importantly than for sebacic-based networks when subjected to the same increase in catalyst content. In that regard, testing several catalyst concentrations in larger and smaller amounts could provide interesting data about the availability of the catalyst and the limitations on the network viscoelastic properties, thus providing a formulation window for this specific catalyst.

3. Impact of the formulation on electrical properties

1. Conductivity as a function of temperature

a. Test conditions

According to the leakage current measured on the vitrimer-encapsulated power modules, the conductivity of the formulated vitrimers increase drastically at high temperature, making them unsuitable for nowadays standards above 50°C. To better understand the conduction mechanisms at play, the resistivity of the formulated vitrimers was measured as a function of temperature, using a *Novocontrol Broadband Dielectric/Impedance Analyzer,* from 0°C to 175°C. A frequency of 1Hz was selected to measure the real part of the conductivity close to the DC value while keeping a reasonably low experimental time.

Film samples of approximately 300µm in thickness were prepared by sputtering 5mm diameter gold electrodes on both sides, thus creating a planar capacitor-like geometry and standardizing the surfaces for conductivity measurements (cf. **Figure 110**). The samples were placed in the spectroscopy bench sample holder, by inserting them in between two metallic electrodes connected to the power supply and ground. To protect the sensitive piezoelectric crystal in the apparatus, a conductive disc spring is placed underneath the bench electrodes, which also limited the force applied to the sample and therefore the change of dimensions during the rise of temperature. Auto-calibration of the bench was performed without the sample before running the tests for each formulation.

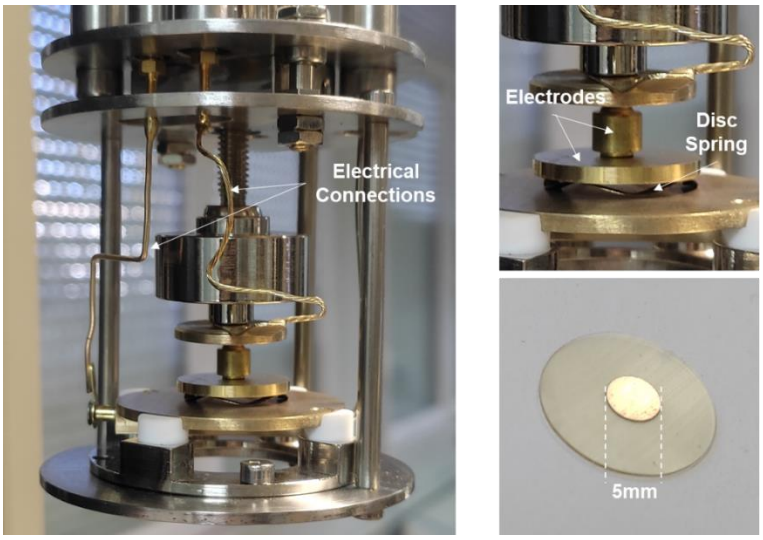

Figure 110 – Left) Sample holder with gold wire electrical connections. Right Top) Removable electrodes mounted on a disc spring. Right Bottom) Vitrimer film sample with a 5mm diameter gold electrode sputtered on each side.

b. Results and Discussion

Figure 111 presents the results of the real conductivity (σ') for the elaborated vitrimers with the inverse temperature, once again with the X-axis multiplied by 1000 for convenience. All samples have a similar conductivity at 0°C with an approximate value of $5x10^{-11}$ $S.m^{-1}$. When the temperature increases, a typical increase in conductivity can be observed in the Tg region for each polymer, which is expected as the unfreezing of the network allows for an easier diffusion of charge carriers. Given the large temperature steps for these tests and the close Tg values for both polymer backbones, an important uncertainty can be expected around the variation of conductivity in the Tg

region. Finally, upon reaching a higher temperature, all samples exhibit a linear increase in conductivity when viewed in an Arrhenius plot, reaching conductivity values between 10^{-4} and 10^{-3} $S.m^{-1}$ at 175°C. This behaviour is also expected as typical polymers will follow a Tg-driven WLF or VFT law near the glass transition, but this effect tends to decrease the further away from Tg, resulting in a mostly Arrhenian variation.

From these results, it appears that the glutaric network provides a lower conductivity than the sebacic backbone, even at higher catalyst content. However, to discriminate the effect of the glass transition (i.e. the increase of conductivity associated with the allowance of chain mobility at Tg), the data were plotted in respect to the different Tg of the vitrimer networks, showing a good overlap demonstrating that the conductivity is mostly driven by the glass transition relaxation regardless of the fatty acid used in the backbone. This is not the case with the Glutaric-5% formula however, where the conductivity is higher than the value expected near Tg, possibly showing measurement errors near Tg, since the conductivity comes back in line with other materials farther above Tg.

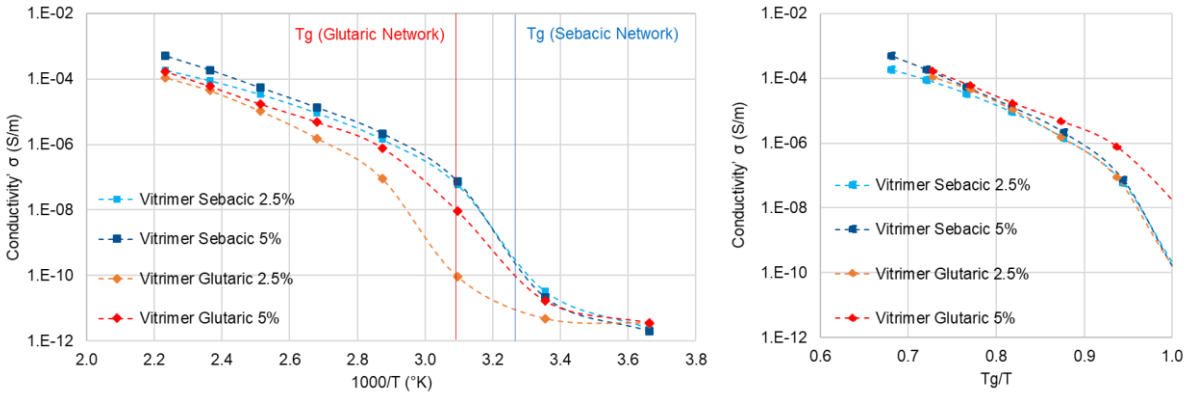

Figure 111 – Left) Conductivity of the formulated vitrimers with the inverse temperature. Vertical bars are placed at Tg values. Right) Conductivity plotted in respect to Tg/T.

Interestingly for sebacic-based vitrimers, the conductivity is almost identical through-out the entire glass transition temperature range (Tg is at about 32°C) for both catalyst contents but begins to diverge at a steady rate above Tv (about 50°C), with higher catalyst concentrations leading to higher conductivities. If the conductivity increase was solely provided by the increase in catalyst content, noticeable differences should have appeared after the passage of Tg. For the glutaric-based vitrimers, a striking difference can be observed between both samples, with a clear increase of the conductivity with higher catalyst content at most temperatures, even away from the unclear behaviour near Tg. Again, the large difference is completely negated when reaching 175°C, since the conductivity increase is steeper for the sample with 2.5% catalyst than the one with 5% catalyst.

Figure 112-Left proposes a close-up on the high temperature region where all conductivity behaviours tend to become more linear (in this representation). When looking at this portion of the curves above Tv, it appears than most vitrimers show the same dependency to temperature from 75 to 175°C, with the exception of the Glutaric-2.5% formula, which appears to be lagging behind at 75°C before reaching a similar steady increase above 100°C.

This is interesting since both glutaric backbones have similar Tg and Tv and yet show large differences in conduction past both of these transitions (up to a factor 10). While not fully understood, this effect could be due to the higher catalyst content for the Glutaric-5% formula that could allow it to go faster in this steady conductivity increase regime. Given the unexpected higher conductivity of this formulation at Tg showed in **Figure 111**, it is also likely that such differences are not significant. Additionally, glutaric networks exhibit a Tg that is right at the same temperature

as the measured Tv, making it difficult to discriminate the effect of each transition without more data points.

To try to better understand the dependency of conductivity with temperature above Tv (i.e. the increase of conductivity associated with the allowance of vitrimeric exchanges at Tv), the reduced conductivity σ/σ(Tv) is plotted against the inverse of the temperature in regard with Tv (cf. **Figure 112-Right)**. The results show that most of the vitrimers exhibit a reduced conductivity that could approximately meet the unity when the temperature tends towards Tv (Tv/T≈1), with minor variations originating from the multiple extrapolations and thus calculations errors (Tv is calculated from viscosity data).

This, to the exception of the Glutaric-2.5% formula that clearly shows a higher conductivity with respect to the calculated Tv value, showing a different behaviour with this sample and yielding a faster increase of conductivity than expected at high temperature. This might be due to measurement errors as the conductivity is calculated based on the dimension of the sample from the measured current, it is therefore possible that the pressed contact decreased the thickness of this sample, resulting in an improperly high calculated conductivity.

Focusing on the three other formulations, it appears that increasing the catalyst content also increases the conductivity at high temperature, and that tightening the network with shorter aliphatic acid precursors also provides a higher increase of conductivity in a normalized evaluation in regard to Tv.

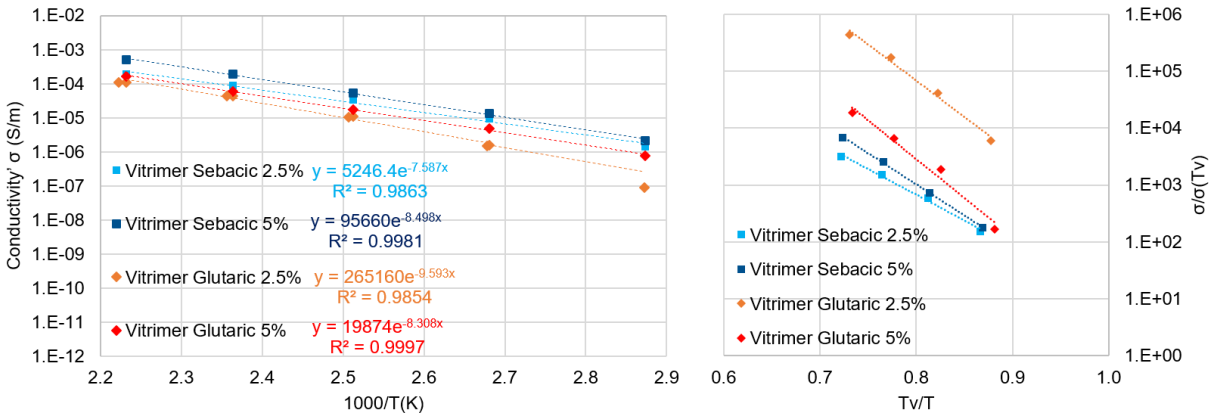

Figure 112 – Left) Close-up on the region above Tv showing an Arrhenius variation of conductivity. Right) Reduced conductivity plotted in respect to Tv/T

c. Conclusion on conductivity tests

Overall, it appears that the conductivity of these vitrimers in temperature is mostly driven by the glass transition. However, leakage current tests shown in Chapter III were performed on the Sebacic-2.5% formulation and passed the specification test until above 50°C, which is superior to its Tg value and close to its Tv value. Given the proximity of Tg and Tv it is difficult to conclude that Tv has no role in the increase of conduction. Additionally, it is widely accepted that polymer conduction in the rubber state is mostly driven by relaxation mechanisms between chains, which surely questions the role of the vitrimeric transition that is driving the chain mobility above Tv.

Also, the steady conduction increase observed above Tv spans over 3 orders of magnitude in a 100°C interval, making the understanding of above-Tv conduction an important aspect of vitrimer applicability. Indeed, promoting faster healing by increasing the temperature could potentially compromise the insulation function of the material. In that regard, further exploration of the relation between vitrimers mechanical relaxations and electrical conductivity is required.

2. Relation between conductivity and viscosity of vitrimers

Above Tg and Tv, vitrimers could be described as supercooled ionic liquids similarly to glass networks above their respective Tg. Assuming that the majority of the conduction is tied to ionic displacement above Tg (as it is often assumed for other polymers), and that the diffusion coefficient of these ionic species is inversely proportional to the viscosity (Stokes-Einstein relation), the ionic conductivity σ derived from the expression of the number of electrical charges flowing in the medium divided by their ability to diffuse inside this medium of viscosity η can be expressed as follows:

Conductivity of ionic liquids

$$\sigma = \frac{(ze)^2.N}{6\pi a\eta} \qquad (13)$$

With *z* the unitary charge number, *e* the elementary electronic charge, *N* the number of charges considered and *a* the effective radius of a considered charge. By analogy with our vitrimeric networks, assuming that the charge carrier are catalyst molecules, the conductivity provided by the catalyst (cat) can be written as a function of the catalyst concentration [Cat] (mol.m^{-3}) as follows:

$$\sigma_{cat} = \frac{(z_{cat}e)^2.N_A.[Cat]}{6\pi a_{cat}\eta} \qquad (13')$$

To investigate the variations of conductivity with the vitrimeric mechanical relaxation, an interesting lead is to plot the conductivity against the inverse of the viscosity and see if a linear relation can be obtained. Analysing **Figure 113**, one can observe that the variation of the conductivity with the inverse viscosity follows a power law ($y = k.x^n$). However, none of the formulated materials can be considered as true ionic liquids since all power exponents are inferior to 1 (n is about 0.7, except for glutaric 2.5% where a slope of 0.92 is obtained). As a hypothesis for this result, it is likely that the quantity of catalyst involved in the electrical conduction is temperature-dependent and that its interaction with the network to promote the flow of material possibly makes it less available for conduction, resulting in a power exponent for conductivity vs. viscosity inferior to 1.

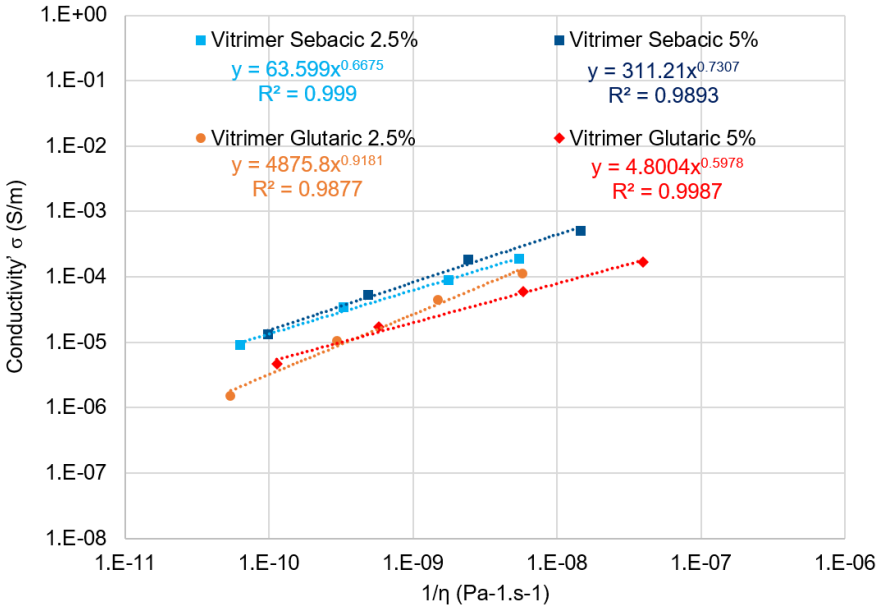

Figure 113 – Evolution of the conductivity of vitrimers at high temperature with the inverse of the intrinsic shear viscosity.

In an effort to isolate the actual effect of the catalyst over the viscosity of the material, in regard with the effect of the catalyst over the conductivity, a bi-normalized plot showing the evolution of η(T) compared to η(Tv) in regard to the evolution of σ(T) compared to σ(Tv) is proposed in **Figure 114**. Looking at the results, with again the exception of the Glutaric-2.5% formula, it appears that the change of viscosity of most of the elaborated vitrimers can be directly correlated with the change of conductivity regardless of the chain backbone, showing a quasi-linear relationship.

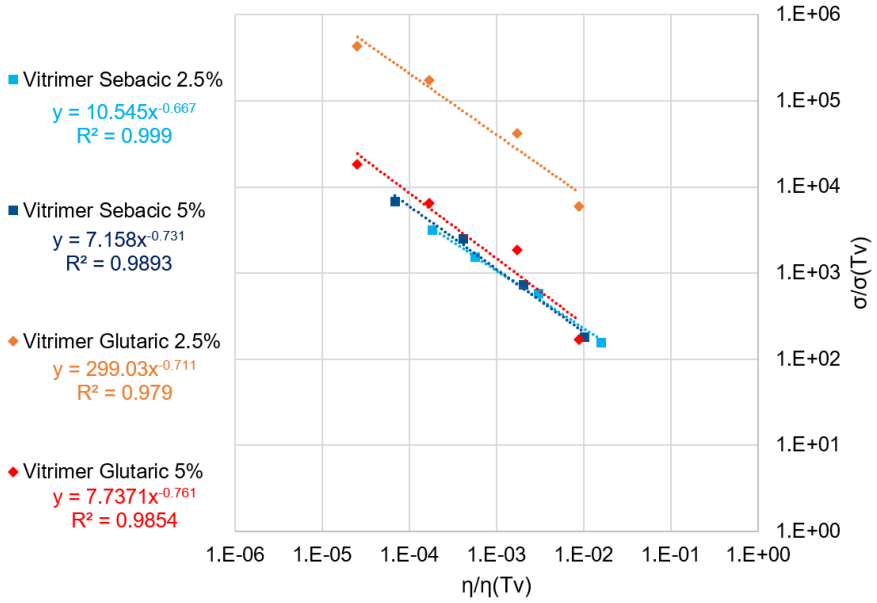

Figure 114 – Reduced conductivity against the reduced viscosity of the formulated vitrimers.

Since the catalyst is expected to control the slope for the variation of viscosity in vitrimer systems [77], it is probable that this choice of catalyst also impacts the slope for the variation of the conductivity at high temperatures (i.e. when controlled by vitrimeric relaxations). If this relation is widely verified, it could be very useful for the formulator that intends to predict the conductivity of different formulations based on the same catalyst, provided that one material of this group can be tested. This could also be useful to determine conductivity trends pre-emptively, given that the mechanical relaxation data are already available for a given catalyst.

Alternatively, this relationship implies that increasing self-healing properties through the use of an increased catalyst content also deteriorates electrical insulation properties. A trade-off is to be expected and electrical insulation designers wanting to grant self-healing properties to their materials should first take a look at the acceptable healing timeframe of their application and adjust the amount of catalyst required to reach this goal.

In any case, further exploration of this relationship with a number of vitrimers with different backbone structures, catalyst types and concentrations is still required to improve the knowledge surrounding vitrimeric materials for electrical insulation.

Conclusion

In this chapter, several new vitrimer formulations were produced and characterized. Using a shorter fatty acid, tighter networks were created, allowing to explore the effects of the polymer backbone on the electrical conductivity and on the viscosity. By modulating the amount of catalyst present in the material, it was possible to measure significant variations in the polymer's behaviours.

Vitrimers mechanical behaviour could be explored efficiently using the Maxwell viscoelastic model. By measuring the mechanical relaxation times in stress-relaxation experiment, it was possible to show that increasing the catalyst content as well as tightening the network could provide a lower viscosity as a function of temperature, thus potentially yielding higher healing efficiencies given the right healing conditions. Still, the impact of the catalyst content was greater than the one from the change on the backbone. Also, at lower catalyst content, the effect of the backbone seemed to be rather negligible, which may be related to a limitation in the catalyst availability. Exploration of catalyst-deprived networks with widely varying network densities constitutes an interesting route to test this hypothesis.

An analysis of the conduction behaviour of the formulated vitrimers was also provided. From the AC measurements, it appears that the conductivity of vitrimers is mostly aligned with the expected behaviour of any polymer around Tg. In that regard, tuning of Tg remains one of the main parameter to impact the conductivity of a vitrimer. However, when the temperature is increased above Tg, a sustained increase of the conductivity can be observed, following an Arrhenius law and representing a large portion of the total conductivity, over a moderate temperature range.

In order to guarantee sufficient insulation properties at healing temperatures, the correlation between the viscosity and the conductivity was explored. By using both data sets from the previous experiments, a clear relationship could be found for most of the tested vitrimers, demonstrating a change of viscosity that can be correlated to a change of conductivity almost linearly. Deviations were attributed to extrapolation errors and experimental uncertainty but pursuing this analysis on many other materials and trying to identify the exact relationship between these physical behaviour might prove especially useful to design new vitrimers with satisfying self-healing properties while still performing appropriately as an electrical insulator.

General conclusions

In this work, new electrical insulation materials exhibiting self-healing properties were developed and implemented with the objective to satisfy the reliability requirements of the next generation of power modules. A critical analysis of the adequation and applicability of these materials and their self-healing properties in regard to the power electronics field is proposed.

By summarizing the motives and advances leading to new power module architectures, several limitations of the conventionally used materials were demonstrated and a list of ideal specifications was proposed to guide their replacement. For conventional architectures, the main trend is to replace the soft silicone gel with stiffer materials capable of locking the embedded components in place and offering increased dielectric strength to sustain the higher voltages and resulting electrical fields that come with new Wide Band Gap (WBG) components. On the other hand, new integrated architectures with embedded chips in Printed Circuit Boards (PCBs) suffer from cracking and delamination during power cycles, requiring the development of tougher, more compliant solutions.

As an innovative solution to increase the reliability of these systems, self-healing was proposed as the main strategy to repair damages and prevent further degradations leading to insulation failures. After reviewing the different self-healing concepts, the exploration of associative covalent adaptable networks was selected as the most promising solution to increase the reliability of power devices. Indeed, these materials can possess high mechanical and thermal resistance properties, while also exhibiting sufficient mobility to heal damages without requiring depolymerization and the subsequent change of properties.

Given the novelty of these materials and even more in regard to their implementation into a highly technical application, a thorough investigation of the available chemistries and the expected final properties of the resulting materials was led. Amongst these solutions, vitrimers based on transesterification were selected as the materials most aligned with the application field, providing a wide variety of precursors and allowing the use of commercial epoxy resins used in the electronic field. Additionally, vitrimers were also expected to provide a promising base that could be tuned to the desired specifications.

A complete elaboration and manufacturing protocol was developed to produce repeatable samples for further characterization as well as quantification of the self-healing efficiency on mechanical indicators. Differential Scanning Calorimetry (DSC) and Fourier-Transformed InfraRed (FTIR) spectroscopy measurements allowed to confirm the successful elaboration of vitrimer materials and tensile testing showed that previously broken samples could be healed and recover their elastic properties entirely following a specific heat treatment (150°C, 1h), without the use of any externally applied pressure. Additionally, a strong shape memory behaviour was demonstrated, proposing an interesting lead as a more applicable strategy to provide internally applied pressure and assisting the healing process even further.

Validation of the fundamental properties for the applicability of this material to the power electronics field was provided, with the elaborated vitrimer exceeding the required dielectric strength (50kV/mm) at relevant thicknesses and showing low thermal degradations compared to the applicative standards (5% mass loss at 360°C). Following conventional manufacturing methods, entirely self-healing, high-quality PCBs were produced. Using these demonstrators, the large recovery of insulation properties was demonstrated with the entirety of the breakdown strength recovered and complete mending of interfacial defects in glass fibre composites, making these materials of high interest for the reliability of composite materials employed for high voltages.

To evaluate the reliability of the developed vitrimer in its applicative environment, successful encapsulation of commercial modules was performed, demonstrating the material compatibility with potting processes. A high stress amplitude power cycling test was subjected to these modules, sustaining only 20% of the total number of cycle endured by silicone-gel references. Additionally, leakage current tests showed a high conductivity of the material above 50°C, making this formulation incompatible with nowadays power module insulation standards. Both of these results show that using the neat self-healing matrix directly is not a sufficient solution to guarantee a reliable operation in temperature. This suggests that tuning the base matrix properties and employing fillers becomes necessary to permit further development of these vitrimer materials into effective electrical insulation products.

While it is expected that improving the mechanical properties using inorganic reinforcements can be achieved by the man of the art using existing solutions, less is currently known about how to solve the electrical insulation limitation. Therefore, to better understand the important factors related to viscoelastic effects and conduction mechanisms in vitrimers, a formulation campaign was led, changing the fatty acid used in the chains backbone and variating the catalyst content. Using Maxwell's model to precisely describe the material viscoelastic response confirmed that higher catalyst concentrations and tighter network internodes decrease the overall intrinsic shear viscosity in temperature. By measuring the AC conductivity (1Hz) of the different formulations in temperature, it was possible to show that the variation of conductivity above the vitrimeric transition Tv is tied to the variations of viscosity on the same temperature range for most samples. These results show that a trade-off exists between efficient self-healing at short time-frames and the highest acceptable conductivity at the application temperatures.

The primary intent for this work was to propose an accurate evaluation of the applicability of vitrimers and a large part of the reflexion was devoted to the critical testing of these new materials. As a major guideline, the development of tests representative of the accurate application situation was sought for, even though the vitrimer was largely different from its reference materials. Oftentimes, the material couldn't even be damaged without completely exceeding the realistic conditions of the application, making it challenging to demonstrate the ability of the material to heal itself. Overall, these vitrimers showed a high reliability of the healed volumes and an incredible toughness in most situations and are likely to provide a suitable solution for the observed PCB failure modes. On the other hand, evaluation of the dielectric strength in temperature is lacking and insufficient focus was provided on thermal aging and water uptake, all valuable properties to be rated before developing a high-temperature high voltage PCB.

Another central interest was to develop methods for formulation, elaboration and manufacturing of these new materials directed towards this technical field. With these studies, formulators can now blend different precursors more easily and be guided in the selection of a suitable catalyst, if necessary, for their targeted electrical insulation properties. Exploration of new vitrimers should be led to provide a robust basis for the formulation of highly optimized materials and help validating and modelling the physical mechanisms behind the proposed viscosity-conductivity relationship.

Finally, this work further shows the importance of the encapsulation material in a reliability mindset. As the replacement of silicone gels as known today progresses, designers should consider the encapsulation material with care and have a clear idea of the required specifications to finely tune the insulation properties accordingly. Piloting both Tg and Tv should be of great interest for managing thermomechanical stresses and the use of nanocomposites and field-mitigating geometries should provide longer expected lifetime, even in the harshest conditions.

References

[1] H. de Lambilly, « Failure Analysis of Power Modules: A Look at the Packaging and Reliability of Large IGBT's », *IEEE Trans*., vol. 16, n°4, p. 412-417, 1993.

[2] M. Held, P. Jacob, G. Nicoletti, et P. Scacco, M.-H. Poech « Fast Power Cycling Test for IGBT Modules in Traction Application », *Proceedings of Second International Conference on Power Electronics and Drive Systems, 0-7803-3773-5*, 1997.

[3] M. Ciappa, « Selected failure mechanisms of modern power modules », *Microelectron. Reliab.*, vol. 42, nº 4-5, p. 653-667, 2002

[4] V. Smet, F. Forest, J.-J. Huselstein, F. Richardeau, Z. Khatir, S. Lefebvre et M. Berkani, « Ageing and Failure Modes of IGBT Modules in High-Temperature Power Cycling », *IEEE Trans. Ind. Electron.*, vol. 58, nº 10, p. 4931-4941, 2011

[5] S. Arumugam, S. Gorchakov, et T. Schoenemann, « Dielectric and partial discharge investigations on high power insulated gate bipolar transistor modules », *IEEE Trans. Dielectr. Electr. Insul.*, vol. 22, nº 4, p. 1997-2007, 2015

[6] J.-H. Fabian, S. Hartmann, et A. Hamidi, « Analysis of insulation failure modes in high power IGBT modules », in *Fourtieth IAS Annual Meeting. Conference Record of the 2005 Industry Applications Conference,* vol. 2, p. 799-805, 2005

[7] G. Mitic et G. Lefranc, « Localisation of electrical-insulation- and partial-discharge failures of IGBT modules », in *Conference Record of the 1999 IEEE Industry Applications Conference. Thirty-Forth IAS Annual Meeting*, vol. 2, p. 1453-1458, 1999

[8] G. Finis, A. Claudi, et R. Bukovnik, « Silicone Gel as an Insulation Material for HV-Insulation Applications », 2005.

[9] Y. P. Varshni, « Temperature dependence of the energy gap in semiconductors», Physica 34, p149-154, 1967.

[10] H. Lee, V. Smet, et R. Tummala, « A Review of SiC Power Module Packaging Technologies: Challenges, Advances, and Emerging Issues », *IEEE J. Emerg. Sel. Top. Power Electron.*, vol. 8, nº 1, p. 239-255, 2020

[11] J. Millan, P. Godignon, X. Perpina, A. Perez-Tomas, et J. Rebollo, « A Survey of Wide Bandgap Power Semiconductor Devices », *IEEE Trans. Power Electron.*, vol. 29, nº 5, p. 2155-2163, 2014

[12] M. G. H. Aghdam et T. Thiringer, « Comparison of SiC and Si power semiconductor devices to be used in 2.5 kW DC/DC converter », in *2009 International Conference on Power Electronics and Drive Systems (PEDS)*, p. 1035-1040, 2009

[13] T. Stockmeier, « From Packaging to "Un"-Packaging - Trends in Power Semiconductor Modules », *Proceedings of the 20th International Symposium on Power Semiconductor Devices & IC's*, 2008

[14] Y. Zhao *et al.*, « Silver sintering die attach process for IGBT power module production », in *2017 IEEE Applied Power Electronics Conference and Exposition (APEC)*, Tampa, FL, USA, mars 2017, p. 3091-3094. doi: 10.1109/APEC.2017.7931138.

[15] F. Hou *et al.*, « Review of Packaging Schemes for Power Module », *IEEE J. Emerg. Sel. Top. Power Electron.*, vol. 8, nº 1, p. 223-238, 2020

[16] R. Simpson, A. Plumpton, M. Varley, C. Tonner, P. Taylor, et X. Dai, « Press-pack IGBTs for HVDC and FACTS », *CSEE J. Power Energy Syst.*, vol. 3, nº 3, p. 9, 2017

[17] F. Hou *et al.*, « High Power-Density 3D Integrated Power Supply Module Based on Panel-Level PCB Embedded Technology », in *2018 IEEE 68th Electronic Components and Technology Conference (ECTC)*, p. 1365-1370, 2018

[18] F. Hou *et al.*, « Fan-Out Panel-Level PCB-Embedded SiC Power MOSFETs Packaging », *IEEE J. Emerg. Sel. Top. Power Electron.*, vol. 8, nº 1, p. 367-380, 2020

[19] C. Buttay, C. Martin, F. Morel, R. Caillaud, J. Le Leslé, et al. « Application of the PCB-Embedding Technology in Power Electronics – State of the Art and Proposed Development ». 3D-PEIM, 2018

[20] J. Schuderer, U. Vemulapati, et F. Traub, « Packaging SiC power semiconductors – Challenges, technologies and strategies », *IEEE Workshop on Wide Bandgap Power Devices and Applications*, p. 18-23, 2014

[21] Z. Li, K. Okamoto, Y. Ohki, et T. Tanaka, « Effects of nano-filler addition on partial discharge resistance and dielectric breakdown strength of Micro-Al_2O_3 Epoxy composite », *IEEE Trans. Dielectr. Electr. Insul.*, vol. 17, nº 3, p. 653-661, 2010

[22] T. Seldrum et E. Vanlathem, « High Temperature Silicone Gels for Power Module Protection », *The Dow Chemical Company, PCB and Systems Assembly*, S90777/E89548, 2019

[23] Wacker Chemie AG, « Silicone Gel Solutions » 2015
[24] F. Wagner *et al.*, « Simulative Comparison of Polymer and Ceramic Encapsulation on SiC-MOSFET Power Modules under Thermomechanical Load », *20th International Conference on Thermal, Mechanical and Multi-Physics Simulation and Experiments in Microelectronics and Microsystems (EuroSimE)*, p. 1-8, 2019
[25] B. Boettge *et al.*, « Material Characterization of Advanced Cement-Based Encapsulation Systems for Efficient Power Electronics with Increased Power Density », *IEEE 68th Electronic Components and Technology Conference (ECTC)*, p. 1258-1269, 2018
[26] M. F. Naumann, B. Boettge, M. S. Behrendt, R. Eisele, et S. Klengel, « Numerical material design for reliable power electronics with cement-based encapsulation », *CIPS 2020 VDE Verlag GMBH*, ISBN 978-3-8007-5225-6, 2020.
[27] R. Randoll, W. Wondrak, et A. Schletz, « Dielectric strength and thermal performance of PCB-embedded power electronics », *Microelectron. Reliab.*, vol. 54, nº 9-10, p. 1872-1876, 2014
[28] R. Randoll, M. Asef, W. Wondrak, L. Böttcher, et A. Schletz, « Characteristics and aging of PCB embedded power electronics », *Microelectron. Reliab.*, vol. 55, nº 9-10, p. 1634-1639, 2015
[29] Q. Peng *et al.*, « The reliability investigation of capacitors embedded PCB », in *2011 International Symposium on Advanced Packaging Materials (APM)*, Xiamen, China, p. 428-432, 2011
[30] C. Feger et C. Feger, « Selection Criteria for Multichip Module Dielectrics », in *Multichip Module Technologies and Alternatives: The Basics*, D. A. Doane et P. D. Franzon, *Éd. Boston, MA: Springer US*, p. 311-348, 1993
[31] Y. Chen et P. Li, « The popcorn effect of plastic encapsulated microelectronic devices and the typical cases study », *International Conference on Quality, Reliability, Risk, Maintenance, and Safety Engineering*, p. 482-485, 2011.
[32] Dong Kil Shin, Young Hee Song, et J. Im, « Effect of PCB Surface Modifications on the EMC-to-PCB Adhesion in Electronic Packages », *IEEE Trans. Compon. Packag. Technol.*, vol. 33, nº 2, p. 498-508, 2010.
[33] T. Huesgen, « Printed circuit board embedded power semiconductors: A technology review », *Power Electron. Devices Compon.*, vol. 3, 100017, p.1-15, 2022
[34] P. Garrou, « Polymer dielectrics for multichip module packaging », *Proc. IEEE*, vol. 80, nº 12, p. 1942-1954, 1992
[35] C. F. Coombs, « *Printed circuits handbook* », 6th ed. New York: McGraw-Hill, 2008.
[36] « 3-4190 Dielectric Silicone Gel ». Dow Corning Corporation, 2008
[37] « FR-4-86PY Datasheet ». Nan Ya Plastic Corporation, 2008
[38] « FR-4-VT42 Datasheet ». VentecUSA, 2011
[39] « Typical properties data sheet of FR4 ». Cyclex Engineering Plastic Ltd.
[40] « SYLGARD 527 Silicone Dielectric Gel », *Dow Chem. Co.*, nº 11, p. 3, 2017
[41] P. Lall, K. Dornala, J. Deep, et R. Lowe, « Measurement and Prediction of Interface Crack Growth at the PCB-Epoxy Interfaces Under High-G Mechanical Shock », *17th IEEE Intersociety Conference on Thermal and Thermomechanical Phenomena in Electronic Systems (ITherm)*, p. 1097-1105, 2018
[42] F. Wagner *et al.*, « Simulative Comparison of Polymer and Ceramic Encapsulation on SiC-MOSFET Power Modules under Thermomechanical Load », *20th International Conference on Thermal, Mechanical and Multi-Physics Simulation and Experiments in Microelectronics and Microsystems (EuroSimE)*, p. 1-8, 2019
[43] X. Fan, K. T. Aung, et X. Li, « Investigation of Thermal Performance of Various Power-Device Packages », *9th. Int. Conf. on Thermal, Mechanical and Multiphysics Simulation and Experiments in Micro-Electronics and Micro-Systems (EuroSimE)*, 2008
[44] C. L. Soles et A. F. Yee, « A discussion of the molecular mechanisms of moisture transport in epoxy resins », *Journal of Polymer Science: Part B: Polymer Physics,* Vol. 38, 792– 802, 2000
[45] C. L. Soles, F. T. Chang, B. A. Bolan, H. A. Hristov, D. W. Gidley, et A. F. Yee, « Contributions of the nanovoid structure to the moisture absorption properties of epoxy resins », p. 14, 1998
[46] A. J. Kinloch, *Adhesion and Adhesives*, Springer Netherlands, 1987
[47] T. P. Ferguson et Jianmin Qu, « Predictive Model for Adhesion Loss of Molding Compounds from Exposure to Humid Environments », *56th Electronic Components and Technology Conference*, p. 1408-1414, 2006
[48] K. Cho et E. C. Cho, « Effect of the microstructure of copper oxide on the adhesion behavior of epoxy/copper leadframe joints », *J. Adhes. Sci. Technol.*, vol. 14, nº 11, p. 1333-1353, 2000
[49] M. D. Hager, « Handbook of Solid State Chemistry – Self-Healing Materials ». *Wiley-VCH Verlag GmbH & Co*. KGaA, 2017

[50] S. R. White *et al.*, « Autonomic healing of polymer composites », *Nature*, vol. 409, nº 6822, p. 794-797, 2001
[51] X. K. D. Hillewaere et F. E. Du Prez, « Fifteen chemistries for autonomous external self-healing polymers and composites », *Prog. Polym. Sci.*, vol. 49-50, p. 121-153, 2015
[52] K. S. Toohey, N. R. Sottos, J. A. Lewis, J. S. Moore, et S. R. White, « Self-healing materials with microvascular networks », *Nat. Mater.*, vol. 6, nº 8, p. 581-585, 2007
[53] Y. Chen, A. M. Kushner, G. A. Williams, et Z. Guan, « Multiphase design of autonomic self-healing thermoplastic elastomers », *Nat. Chem.*, vol. 4, nº 6, p. 467-472, 2012
[54] Y. Chen et Z. Guan, « Multivalent hydrogen bonding block copolymers self-assemble into strong and tough self-healing materials », *Chem Commun*, vol. 50, nº 74, p. 10868-10870, 2014
[55] P. Cordier, F. Tournilhac, C. Soulié-Ziakovic, et L. Leibler, « Self-healing and thermoreversible rubber from supramolecular assembly », *Nature*, vol. 451, nº 7181, p. 977-980, 2008
[56] J. Cui et A. del Campo, « Multivalent H-bonds for self-healing hydrogels », *Chem. Commun.*, vol. 48, nº 74, p. 9302, 2012
[57] A. Phadke *et al.*, « Rapid self-healing hydrogels », *Proc. Natl. Acad. Sci.*, vol. 109, nº 12, p. 4383-4388, 2012
[58] R. Zhang *et al.*, « Heterogeneity, Segmental and Hydrogen Bond Dynamics, and Aging of Supramolecular Self-Healing Rubber », *Macromolecules*, vol. 46, nº 5, p. 1841-1850, 2013
[59] X. Xing, L. Li, T. Wang, Y. Ding, G. Liu, et G. Zhang, « A self-healing polymeric material: from gel to plastic », *J. Mater. Chem. A*, vol. 2, nº 29, p. 11049-11053, 2014
[60] El Choufi, N.; Mustapha, S.; Tehrani-Bagha, A.R.; Grady, B.P. Self-Healability of Poly(Ethylene-coMethacrylic Acid): Effect of Ionic Content and Neutralization. *Polymers*, 14, 3575, 2022
[61] J.-F. Mei *et al.*, « A Highly Stretchable and Autonomous Self-Healing Polymer Based on combination of Pt···Pt and π–π Interactions ». *Macromolecular Rapid Communications*, 2016
[62] M. Nakahata, Y. Takashima, H. Yamaguchi, et A. Harada, « Redox-responsive self-healing materials formed from host–guest polymers », *Nat. Commun.*, vol. 2, nº 1, p. 511, 2011
[63] C. J. Kloxin, T. F. Scott, B. J. Adzima, et C. N. Bowman, « Covalent Adaptable Networks (CANs): A Unique Paradigm in Cross-Linked Polymers », *Macromolecules*, vol. 43, nº 6, p. 2643-2653, 2010
[64] E. Amendola, S. D. Iacono, A. Pastore, M. Curcio, et A. Iadonisi, « Epoxy Thermosets with Self-Healing Ability », *J. Mater. Sci. Chem. Eng.*, vol. 03, nº 07, p. 162-167, 2015
[65] D. Montarnal, F. Tournilhac, M. Hidalgo, et L. Leibler, « Epoxy-based networks combining chemical and supramolecular hydrogen-bonding crosslinks: Epoxy-Based Networks », *J. Polym. Sci. Part Polym. Chem.*, vol. 48, nº 5, p. 1133-1141, 2010
[66] T. S. Coope, D. H. Turkenburg, H. R. Fischer, R. Luterbacher, H. van Bracht, et I. P. Bond, « Novel Diels-Alder based self-healing epoxies for aerospace composites », *Smart Mater. Struct.*, vol. 25, nº 8, p. 084010, 2016
[67] M. A. Tasdelen, « Diels–Alder “click” reactions: recent applications in polymer and material science », *Polym. Chem.*, vol. 2, nº 10, p. 2133, 2011
[68] J. E. Huheey, E. A. Keiter, et R. L. Keiter, « Inorganic Chemistry, 4th ed. », 1993.
[69] X. Chen, « A Thermally Re-mendable Cross-Linked Polymeric Material », *Science*, vol. 295, nº 5560, p. 1698-1702, 2002
[70] J. Brancart, G. Scheltjens, T. Muselle, B. Van Mele, H. Terryn, et G. Van Assche, « Atomic force microscopy–based study of self-healing coatings based on reversible polymer network systems », *J. Intell. Mater. Syst. Struct.*, vol. 25, nº 1, p. 40-46, 2014
[71] Z. Karami, M. J. Zohuriaan-Mehr, et A. Rostami, « Bio-based thermo-healable non-isocyanate polyurethane DA network in comparison with its epoxy counterpart », *J. CO2 Util.*, vol. 18, p. 294-302, 2017
[72] S. Schäfer et G. Kickelbick, « Self-healing polymer nanocomposites based on Diels-Alder-reactions with silica nanoparticles: The role of the polymer matrix », *Polymer*, vol. 69, p. 357-368, 2015
[73] D. Montarnal, M. Capelot, F. Tournilhac, et L. Leibler, « Silica-Like Malleable Materials from Permanent Organic Networks », *Science*, vol. 334, nº 6058, p. 965-968, 2011
[74] B. Krishnakumar, R. V. S. P. Sanka, W. H. Binder, V. Parthasarthy, S. Rana, et N. Karak, « Vitrimers: Associative dynamic covalent adaptive networks in thermoset polymers », *Chem. Eng. J.*, vol. 385, p. 123820, 2020
[75] F. Fu, M. Huang, W. Zhang, Y. Zhao, et X. Liu, « Thermally assisted self-healing behavior of anhydride modified polybenzoxazines based on transesterification », *Sci. Rep.*, vol. 8, nº 1, p. 10325, 2018

[76] M. Guerre, C. Taplan, J. M. Winne, et F. E. Du Prez, « Vitrimers: directing chemical reactivity to control material properties », *Chem. Sci.*, vol. 11, nº 19, p. 4855-4870, 2020
[77] M. Capelot, M. M. Unterlass, F. Tournilhac, et L. Leibler, « Catalytic Control of the Vitrimer Glass Transition », *ACS Macro Lett.*, vol. 1, nº 7, p. 789-792, 2012
[78] M. Capelot, D. Montarnal, F. Tournilhac, et L. Leibler, « Metal-Catalyzed Transesterification for Healing and Assembling of Thermosets », *J. Am. Chem. Soc.*, vol. 134, nº 18, p. 7664-7667, 2012
[79] F. I. Altuna, C. E. Hoppe, et R. J. J. Williams, « Shape memory epoxy vitrimers based on DGEBA crosslinked with dicarboxylic acids and their blends with citric acid », *RSC Adv.*, vol. 6, nº 91, p. 88647-88655, 2016
[80] L. Lu, J. Fan, et G. Li, « Intrinsic healable and recyclable thermoset epoxy based on shape memory effect and transesterification reaction », *Polymer*, vol. 105, p. 10-18, 2016
[81] J.-H. Chen, X.-P. An, Y.-D. Li, M. Wang, et J.-B. Zeng, « Reprocessible Epoxy Networks with Tunable Physical Properties: Synthesis, Stress Relaxation and Recyclability », *Chin. J. Polym. Sci.*, vol. 36, nº 5, p. 641-648, 2018
[82] Z. Ding, L. Yuan, Q. Guan, A. Gu, et G. Liang, « A reconfiguring and self-healing thermoset epoxy/chain-extended bismaleimide resin system with thermally dynamic covalent bonds », *Polymer*, vol. 147, p. 170-182, 2018
[83] A. Rekondo, R. Martin, A. Ruiz de Luzuriaga, G. Cabañero, H. J. Grande, et I. Odriozola, « Catalyst-free room-temperature self-healing elastomers based on aromatic disulfide metathesis », *Mater Horiz*, vol. 1, nº 2, p. 237-240, 2014
[84] M. Pepels, I. Filot, B. Klumperman, et H. Goossens, « Self-healing systems based on disulfide–thiol exchange reactions », *Polym. Chem.*, vol. 4, nº 18, p. 4955, 2013
[85] A. M. Belenguer, T. Friščić, G. M. Day, et J. K. M. Sanders, « Solid-state dynamic combinatorial chemistry: reversibility and thermodynamic product selection in covalent mechanosynthesis », *Chem. Sci.*, vol. 2, nº 4, p. 696, 2011
[86] J. Canadell, H. Goossens, et B. Klumperman, « Self-Healing Materials Based on Disulfide Links », *Macromolecules*, vol. 44, nº 8, p. 2536-2541, 2011
[87] U. Lafont, H. van Zeijl, et S. van der Zwaag, « Influence of Cross-linkers on the Cohesive and Adhesive Self-Healing Ability of Polysulfide-Based Thermosets », *ACS Appl. Mater. Interfaces*, vol. 4, nº 11, p. 6280-6288, 2012
[88] M. Hernández, A. M. Grande, W. Dierkes, J. Bijleveld, S. van der Zwaag, et S. J. García, « Turning Vulcanized Natural Rubber into a Self-Healing Polymer: Effect of the Disulfide/Polysulfide Ratio », *ACS Sustain. Chem. Eng.*, vol. 4, nº 10, p. 5776-5784, 2016
[89] Y. Xu et D. Chen, « A Novel Self-Healing Polyurethane Based on Disulfide Bonds », *Macromol. Chem. Phys.*, vol. 217, nº 10, p. 1191-1196, 2016
[90] X. Jian, Y. Hu, W. Zhou, et L. Xiao, « Self-healing polyurethane based on disulfide bond and hydrogen bond », *Polym. Adv. Technol.*, vol. 29, nº 1, p. 463-469, 2018
[91] L. Ling, J. Li, G. Zhang, R. Sun, et C.-P. Wong, « Self-Healing and Shape Memory Linear Polyurethane Based on Disulfide Linkages with Excellent Mechanical Property », *Macromol. Res.*, vol. 26, nº 4, p. 365-373, 2018
[92] K. Chang, H. Jia, et S.-Y. Gu, « A transparent, highly stretchable, self-healing polyurethane based on disulfide bonds », *Eur. Polym. J.*, vol. 112, p. 822-831, 2019
[93] W. Denissen, G. Rivero, R. Nicolaÿ, L. Leibler, J. M. Winne, et F. E. Du Prez, « Vinylogous Urethane Vitrimers », *Adv. Funct. Mater.*, vol. 25, nº 16, p. 2451-2457, 2015
[94] C. Taplan, M. Guerre, J. M. Winne, et F. E. Du Prez, « Fast processing of highly crosslinked, low-viscosity vitrimers », *Mater. Horiz.*, vol. 7, nº 1, p. 104-110, 2020
[95] W. Alabiso, « The Impact of Vitrimers on the Industry of the Future: Chemistry, Properties and Sustainable Forward-Looking Applications», *MDPI Polymers*, 12, 1660, 2020
[96] V. Schenk, K. Labastie, M. Destarac, P. Olivier, et M. Guerre, « Vitrimer composites: current status and future challenges », *Mater. Adv.*, vol. 3, nº 22, p. 8012-8029, 2022
[97] J. M. Winne, L. Leibler, et F. E. Du Prez, « Dynamic covalent chemistry in polymer networks: a mechanistic perspective », *Polym. Chem.*, vol. 10, nº 45, p. 6091-6108, 2019
[98] L. Matějka, S. Pokomy, et K. Dusiek, « Network Formation Involving Epoxide and Carboxyl groups ». *Polymer Bulletin Springer-Verlag*, 7, p.123-128, 1982
[99] E. Savonnet, E. Grau, S. Grelier, B. Defoort, et H. Cramail, « Divanillin-Based Epoxy Precursors as DGEBA Substitutes for Biobased Epoxy Thermosets », *ACS Sustain. Chem. Eng.*, vol. 6, nº 8, p. 11008-11017, 2018

[100] W. Lotfy, K. Ghanem, et E. Elhelow, « Citric acid production by a novel Aspergillus niger isolate: II. Optimization of process parameters through statistical experimental designs », *Bioresour. Technol.*, vol. 98, nº 18, p. 3470-3477, 2007
[101] W. J. Blank, Z. A. He, et M. Picci, « Catalysis of the epoxy-carboxyl reaction », *J. Coat. Technol.*, vol. 74, nº 3, p. 33-41, 2002
[102] C. E. Hoppe, M. J. Galante, P. A. Oyanguren, et R. J. J. Williams, « Epoxies Modified by Palmitic Acid: From Hot-Melt Adhesives to Plasticized Networks », *Macromol. Mater. Eng.*, vol. 290, nº 5, p. 456-462, 2005
[103] G. G. Gallo, C. R. Pasqualucci, P. Radaelli, et G. C. Lancini, « The Ionization Constants of Some Imidazoles », *J. Org. Chem.*, vol. 29, nº 4, p. 862-865, 1964.
[104] K. Kaupmees, A. Trummal, et I. Leito, « Basicities of Strong Bases in Water: A Computational Study », *Croat. Chem. Acta*, vol. 87, nº 4, p. 385-395, 2014
[105] M. G. González, J. C. Cabanelas, et J. Baselga, « Applications of FTIR on Epoxy Resins - Identification, Monitoring the Curing Process, Phase Separation and Water Uptake », in *Infrared Spectroscopy - Materials Science, Engineering and Technology*, Éd. InTech, 2012
[106] X. Yang, L. Guo, X. Xu, S. Shang, et H. Liu, « A fully bio-based epoxy vitrimer: Self-healing, triple-shape memory and reprocessing triggered by dynamic covalent bond exchange », *Mater. Des.*, vol. 186, p. 108248, 2020
[107] Z. Pei, Y. Yang, Q. Chen, Y. Wei, et Y. Ji, « Regional Shape Control of Strategically Assembled Multishape Memory Vitrimers », *Adv. Mater.*, vol. 28, nº 1, p. 156-160, 2016
[108] J. Puig *et al.*, « Superparamagnetic Nanocomposites Based on the Dispersion of Oleic Acid-Stabilized Magnetite Nanoparticles in a Diglycidylether of Bisphenol A-Based Epoxy Matrix: Magnetic Hyperthermia and Shape Memory », *J. Phys. Chem. C*, vol. 116, nº 24, p. 13421-13428, 2012
[109] V. Montano, M. W. Urban, S. van der Zwaag, et S. J. Garcia, « Local strain-induced energy storage as driving force for autogenous scratch closure », *J. Mater. Chem. A*, vol. 10, nº 13, p. 7073-7081, 2022
[110] Y. Zhao *et al.*, « Influence of specimen dimensions on the tensile behavior of ultrafine-grained Cu », *Scr. Mater.*, vol. 59, nº 6, p. 627-630, 2008
[111] Y. Takeda, C. Kiattisaksri, M. Aramaki, S. Munetoh, et O. Furukimi, « Effects of Specimen Thickness in Tensile Tests on Elongation and Deformation Energy for Industrially Pure Iron », *ISIJ Int.*, vol. 57, nº 6, p. 1129-1137, 2017
[112] C. Wu, B. C. Meng, L. Tam, et L. He, « Yellowing mechanisms of epoxy and vinyl ester resins under thermal, UV and natural aging conditions and protection methods », *Polym. Test.*, vol. 114, p. 107708, 2022
[113] H. Jiang *et al.*, « The pyrolysis mechanism of phenol formaldehyde resin », *Polym. Degrad. Stab.*, vol. 97, nº 8, p. 1527-1533, 2012
[114] L. Costa, L. R. di Montelera, G. Camino, E. D. Weil, et E. M. Pearce, « Structure-charring relationship in phenol-formaldehyde type resins », *Polym. Degrad. Stab.*, vol. 56, nº 1, p. 23-35, 1997
[115] ANSI et IEEE, « IEEE Guide for the statistical analysis of electrical insulation voltage endurance data », 1987.
[116] J. C. Fothergill, « Estimating the cumulative probability of failure data points to be plotted on Weibull and other probability paper », *IEEE Trans. Electr. Insul.*, vol. 25, nº 3, p. 489-492, 1990
[117] P. Bjellheim et B. Helgee, « AC breakdown strength of aromatic polymers under partial discharge reducing conditions », *IEEE Trans. Dielectr. Electr. Insul.*, vol. 1, nº 1, p. 89-96, 1994
[118] D. A. Marckx, « Breakthrough in Power Electronics from SiC: May 25, 2004 - May 31, 2005 », NREL/SR-500-38515, 881313, 2006
[119] M. M. Tousi et M. Ghassemi, « Characterization of Nonlinear Field-Dependent Conductivity Layer Coupled With Protruding Substrate to Address High Electric Field Issue Within High-Voltage High-Density Wide Bandgap Power Modules », *IEEE J. Emerg. Sel. Top. Power Electron.*, vol. 8, nº 1, p. 343-350, 2020
[120] M. M. Tousi et M. Ghassemi, « Nonlinear Resistive Electric Field Grading in High-Voltage, High-Power Wide Bandgap Power Module Packaging », in *2019 IEEE Energy Conversion Congress and Exposition (ECCE)*, 2019, p. 7124-7129
[121] D. Manessis, S.-F. Yen, A. Ostmann, R. Aschenbrenner, et H. Reichl, « Technical Understanding of Resin-Coated-Copper (RCC) Lamination Processes for Realization of Reliable Chip Embedding Technologies », in *2007 Proceedings 57th Electronic Components and Technology Conference*, Sparks, NV, USA, p. 278-285, 2007

[122] G. J. Lake et P. B. Lindley, « The mechanical fatigue limit for rubber », *J. Appl. Polym. Sci.*, vol. 9, nº 4, p. 1233-1251, 1965
[123] H.-P. Burgener et K. Frohlich, « Probability of partial discharge inception in small voids », in *2001 Annual Report Conference on Electrical Insulation and Dielectric Phenomena (Cat. No.01CH37225)*, p. 298-302, 2001
[124] Y. Zhao *et al.*, « The effect of annealing temperature on the recrystallization and mechanical properties of severe plastic deformed commercial pure aluminium during ultra-fast annealing », *Mater. Res. Express*, vol. 8, nº 4, p. 046515, 2021
[125] H. Kiess et W. Rehwald, « Electric conduction in amorphous polymers », *Colloid Polym. Sci.*, vol. 258, nº 3, p. 241-251, 1980.
[126] C. A. Angell, « Formation of Glasses from Liquids and Biopolymers », *Science*, vol. 267, nº 5206, p. 1924-1935, 1995
[127] W. Denissen, J. M. Winne, et F. E. Du Prez, « Vitrimers: permanent organic networks with glass-like fluidity », *Chem. Sci.*, vol. 7, nº 1, p. 30-38, 2016